The role of cholangiocytes in the prediction and detection of drug-induced liver injury

Thesis submitted in accordance with the requirements of the University of Liverpool for the degree of Doctor in Philosophy

By

Lawrence Scott Howell

September 2019

DECLARATION

This thesis is the result of my own work. The material contained within this thesis has not been presented, nor is currently being presented, either wholly or in part for any other degree or qualification.

Lawrence Scott Howell

This research was carried out in the Department of Molecular and Clinical Pharmacology, University of Liverpool, UK.

CONTENTS

ACKNOWLEDGEMENTS

First and foremost, a massive thank you to my primary supervisor Prof. Chris Goldring for his scientific discussion and advice, but most importantly, for the personal support and encouragement he has given me throughout my PhD. I would also like to extend thanks to my secondary supervisors, Dr. Ian Copple and Prof. Kevin Park for their scientific and personal input over the last 4 years. I am grateful to all the external collaborators and colleagues at the BSU and Proteomics Department for all their assistance in helping to put this work together. I would also like to acknowledge the MRC for the financial support which made this project possible.

A huge thank you to everyone in the LiverTox group (past and present!) who has inevitably helped me at some point in designing and running an experiment. Honourable mentions to Chris, Lucia and Shiva who have been willing to get hands on with *in vivo* work (especially those 12 h time points..sorry!). A massive appreciation to everyone who has made my time at Liverpool as fun as possible. Special mentions to Chris, Lucia, Amy, Joel, Sammy, James, Ben and Georgia. Whether it is just talking about absolute rubbish in the office, or with a drink and a Costco pizza, thank you!

The biggest thanks of all go to Lucy, my absolute superstar fiancé. For every western blot, qPCR, IF, organoid and *in vivo* that did not work, you have been my first port of call for (A) a shoulder to cry on and then (B) troubleshooting and getting it right. Thank you so much for all the daily support that extended well beyond the working hours of 9-5 and being there through all the troughs and peaks.

Last but certainly not least, a large heartfelt thank you to my Mum, Zand and Dom, my family who have supported me all along the way, even though I think they still do not fully understand what I have been doing for the last 4 years! Most important of all, this thesis and all the work leading up to it is dedicated to my late Dad, without whose advice, guidance and drive I would not be in the position that I am today. I hope I have made you all proud.

PUBLICATIONS

- Proteomic profiling of murine biliary-derived hepatic organoids and their capacity for drug disposition, bio-activation and detoxification
  Howell LS, Jenkins RE, Goldring CE, Park BK, *manuscript in preparation,* September 2019

- Gastric toxicity associated with pre-clinical models dosed with ANIT by oral gavage
  Howell LS, Ressel L, Goldring CE, Park BK, *manuscript in preparation,* September 2019

- Circulating levels of miR-122 increase post-mortem, particularly following lethal dosing with pentobarbital sodium: implications for pre-clinical liver injury studies
  Clarke JI, Forootan S, Lea J, **Howell LS**, Monne JR, Kipar A, Goldring CE, Park BK, Copple IM, Antoine DJ, *Toxicol. Research.* 2017 Apr; 6, 406 DOI: 10.1039/c6tx00442c

- MiR-122 and other microRNAs as potential circulating biomarkers of drug-induced liver injury
  Howell LS, Ireland L, Park BK, Goldring CE, *Expert Review of Molecular Diagnostics.* 2017 Dec 18:1, 47-54, DOI: 10.1080/14737159.2018.1415145

- Leading-Edge Approaches for In Vitro Hepatotoxicity Evaluation
  LeCluyse EL, Norona LM, Akingbasote JA, **Howell LS**, Woodhead JL, Cross MJ, Roth AB, Goldring CE, *Comprehensive Toxicology (3rd Edition)*. 2018, 2:651-712, DOI: 10.1016/B978-0-12-801238-3.64267-8

- Potential use of miRNAs as biomarkers of cholangiocyte drug-induced liver injury
  Howell LS, Goldring CE, Park BK, *Toxicology Letters*. 2017 Oct 280:1, S134-135, DOI: 10.1016/j.toxlet.2017.07.375

ABSTRACT

Drug-induced liver injury (DILI) is a leading cause of drug attrition throughout all stages of the drug discovery process and is a frequent adverse drug reaction (ADR) with significant clinical burden. Therefore, a concerted effort to predict the onset of DILI before clinical manifestation is paramount. Nevertheless, currently available models to predict DILI are often lacking, due to their poor physiological relevancy to the *in vivo* hepatic phenotype. Furthermore, the current gold standard biomarkers for diagnosing DILI, such as alkaline phosphatase (ALP), have inadequate sensitivity and specificity. Whilst circulating levels of miR-122 have shown improved clinical utility in diagnosing hepatocellular DILI, miRNAs signatures for other hepatic cell types have not yet been elucidated.

Cholangiocytes are epithelial cells that line the hepatic bile ducts and are primarily responsible for altering the composition of canalicular bile. Cholangiocytes are targeted by both mixed and cholestatic DILI, which without proper diagnosis and clinical intervention, can cause bile duct degeneration and destruction. Cholangiocyte DILI is typically diagnosed by elevations in circulating ALP, though it is not known if a panel of cholangiocyte-derived miRNAs could aid a more effective diagnosis. Recent research has identified that cholangiocytes can be reprogrammed *in vitro* into a bi-phenotypic hepatic organoids. This novel liver model has demonstrated a degree of Drug-Metabolizing Enzymes and Transporter (DMET) activity, which may make them viable *in vitro* tools for predicting DILI. However, their proteome remains poorly characterised.

Therefore, the aims of this thesis were threefold. 1) To characterise global miRNA expression in murine cholangiocytes and hepatocytes in order to identify novel circulating biomarkers. 2) Induce cell-specific toxicity *in vivo* to assess the detection of putative circulating biomarkers in pre-clinical models. 3) Characterise the proteome of biliary-derived organoids to assess their phenotype relative to donor-derived liver tissue.

In order to identify the global miRNA profiles of hepatocytes and cholangiocytes, both cell types were isolated from CD-1 mice with a purity of ≥97 % and ≥94 %, respectively. Global miRNA expression was assessed by microarray, which revealed 93 miRNAs uniquely expressed in cholangiocytes and 178 miRNAs co-expressed between cholangiocytes and hepatocytes. This data was further triaged by SAM statistical analysis and publicly available database searching. Ultimately, 50 uniquely expressed and 13 enriched cholangiocyte miRNAs were identified as candidate miRNA biomarkers of cholangiocyte DILI. Although these 63 miRNAs of interest were all translational into human, their tissue expression is not solely liver specific. The expression of all five members of the miR-200 family (miR-141, -200a, -200b, -200c and -429) were found to be enriched or unique to cholangiocytes. These miRNAs have previously been implemented as circulating biomarkers for various biliary diseases, although their role in cholangiocyte DILI is yet to be assessed. Cholangiocyte injury was therefore induced in CD-1 and C57BL/6J mice and Sprague Dawley rats with α-napthylisothiocyanate (ANIT) and 4,4′-Diaminodiphenylmethane (DAPM). Although these miRNAs were elevated in the serum of hepatotoxin-dosed animals, there was a highly variable degree of liver injury. In ANIT-dosed animals, significant enlargement and toxicity of the stomach was observed, which has not been previously reported. Further work is therefore required to induce a more consistent liver injury and to fully elucidate if the detection of these circulating miRNAs in the serum was caused by hepatic or gastric toxicity.

Hepatic organoids are a recent innovation in *in vitro* modelling. Initial research suggests organoids better recapitulate the liver phenotype *in vitro* compared to pre-

existing proliferative cell models. However, they remain poorly characterised. A global proteomic profiling of undifferentiated and differentiated hepatic organoids and donor-matched livers was therefore performed to assess both their similarity to liver tissue and DMET expression. iTRAQ analysis revealed 4,405 proteins commonly detected in all sample types. Differentiation of organoids significantly increased the expression of multiple CYP450s, phase II enzymes, liver biomarkers and some hepatic transporters. While the final phenotype of differentiated organoids is distinct from liver tissue, they contain multiple DMET proteins necessary for liver function and drug metabolism, such as CYP450 3A, GSTA and MDR1A. Further experimentation, optimisation and characterisation of biliary-derived hepatic organoids is needed relative to pre-existing models to fully contextualise their use as a putative *in vitro* model of DILI.

In summary, this work has utilised cholangiocytes as both diagnostic and predictive tools of DILI. A selection of translational candidate miRNAs that could be used as circulating biomarkers of cholangiocyte injury has been identified. *In vivo* investigation of cholangiocyte injury by ANIT was highly variable and was associated with a previously unidentified stomach toxicity. However, a selection of candidate miRNAs was elevated under certain conditions. This work has also characterised the proteomic profile of biliary-derived organoids, a novel hepatic *in vitro* model.

ABBREVIATIONS

µL	Microlitre
µm	Micrometre
µM	Micromolar
A1AT	Alpha-1-antitrypsin
ADR	Adverse drug reaction
AFE	Agilent Feature Extraction
AFP	Alpha-fetoprotein
ALF	Acute liver failure
ALP	Alkaline phosphatase
ALT	Alanine aminotransferase
ANIT	α-napthylisothiocyanate
ANOVA	Analysis of variance
APAP	Acetaminophen
AST	Aspartate aminotransferase
BCA	Bicinchoninic acid
BCRP	ATP-binding cassette sub-family G member 2
BDL	Bile duct ligation
BEC	Cholangiocyte/Biliary epithelial cell
BSEP	Bile salt export pump
BtPC	Biliary tree progenitor cells
°C	Centigrade
CK	Cytokeratin
cm	Centimetre
CO_2	Carbon dioxide
CYP450	Cytochrome p450
DAPM	4,4′-Diaminodiphenylmethane
DDC	3,5-diethoxycarboncyl-1,4-dihydrocollidine
dH_2O	Distilled water
DILI	Drug-induced liver injury

DMET	Drug Metabolizing Enzymes and Transporter proteins
DMSO	Dimethyl sulfoxide
DNA	Deoxyribonucleic acid
EDTA	Ethylene diamine tetraacetic acid
EpCAM	Epithelial Cell Adhesion Molecule
FBS	Fetal bovine serum
g	Relative centrifugal force
g	Grams
G	Gauge
GGT	γ-glutamyl transpeptidase
GLDH	Glutamate dehydrogenase
GSH	Glutathione
GST	Glutathione S-transferase
h	Hours
HBSS	Hank's buffered saline solution
HCC	Hepatocellular carcinoma
HEPES	4-(2-hydroxyethyl)-1-piperazineethanesulfonic acid
hESC	Human embryonic stem cell
HLA	Human Leukocyte Antigens
HMGB1	High mobility group protein B1
HNF4α	Hepatocyte nuclear factor 4 alpha
HPC	Hepatic progenitor cells
HSC	Hepatic stellate cells
H&E	Haematoxylin and eosin
ICC	Intrahepatic cholangiocarcinoma
IHL	Intrahepatic lymphocytes
i.p	Intraperitoneal
iPSC	Induced pluripotent stem
iTRAQ	Isobaric tagging for relative and absolute quantitation

KC	Kupffer cells
KEGG	Kyoto Encyclopaedia of Genes and Genomes
kg	Kilogram
L	Litre
LGR5	Leucine-rich repeat-containing G-protein coupled receptor 5
LSEC	Liver sinusoidal endothelial cells
M	Molar
MDR	Multidrug resistance protein
mg	Milligram
Min	Minutes
MIP	Maximum intensity projection
miRNA	MicroRNA
mL	Millilitre
MRP	Multidrug resistance-associated protein
NAFLD	Non-alcoholic fatty liver disease
NAPQI	N-acetyl-p-benzoquinone imine
NASH	Non-alcoholic steatohepatitis
NPC	Non-parenchymal cells
OATP	carrier organic anion transporter/transporting polypeptide
OCT1	Solute carrier family 22 member 1
o.g	Oral gavage
PBC	Primary biliary cirrhosis
PBS	Phosphate buffered saline
PCA	Principle component analysis
PFA	Paraformaldehyde
qPCR	quantitative polymerase chain reaction

RFU	Relative fluorescence units
RIN	RNA integrity number
RIPA	Radioimmunoprecipitation assay
RISC	RNA-inducing silencing complex
RNA	Ribonucleic acid
ROC	Receiver Operating Characteristic
RPM	Revolutions per minute
RT	Room temperature
RUCAM	Roussel-Uclaf Causality Assessment Method
s	seconds
SAM	Significance Analysis of Microarrays
SEM	Standard error of the mean
SOS	Sinusoidal obstruction syndrome
TBIL	Total bilirubin
TBS-T	Tris-buffered saline with Tween 20
TGS	Total gene signal
TXN-	Thioredoxin
U	Units
ULN	Upper limit of normal
VBDS	Vanishing bile duct syndrome

Designation of statistical significance:

$p \leq 0.05$ = *

$p \leq 0.01$ = **

$p \leq 0.001$ = ***

$p \leq 0.0001$ = ****

n.s = non-significant

Chapter One:
General Introduction

Contents

1.1 Anatomy and physiology of the liver

1.1.1 Microanatomy of the liver

The liver is the largest gland in the human body and is responsible for a number of key functions, such as detoxification of endogenous and exogenous compounds, lipid metabolism and bile acid synthesis. It is formed of microanatomical polygon-shaped units, termed hepatic lobules (Fig 1.1) [1]. These are characterised by a large vein, the central venule, at the heart of the lobule. Located around the lobule periphery are multiple portal triad structures, which consist of biliary ductules, hepatic arterioles and portal venules (Fig 1.1). Hepatic arterioles deliver a small volume of oxygen-rich blood from the aorta, which mixes with a larger volume of nutrient-rich, partially deoxygenated blood delivered by portal venules from the gastrointestinal tract, pancreas and spleen. Blood runs into hepatic sinusoids and flows to the terminal hepatic venule to join systemic circulation [2].

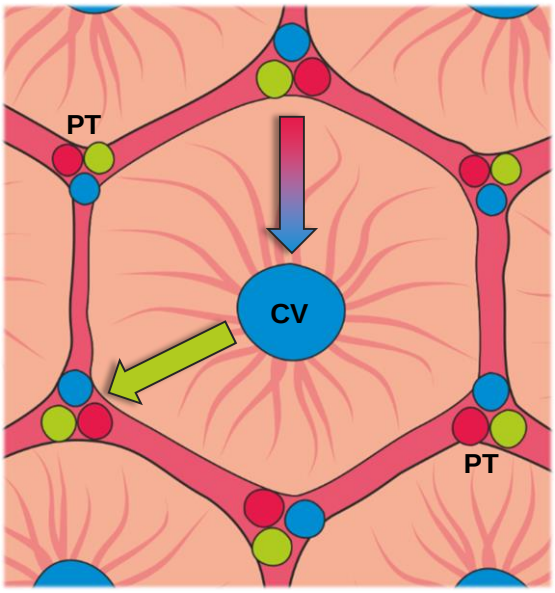

Figure 1.1- Structure of a hepatic liver lobule

The liver consists of an arrangement of hepatic lobules, which are the functional units of the liver. Each lobule consists of a central venule (CV) surrounded by multiple portal triads (PT), comprising of a hepatic arteriole, portal venule and bile duct. The red/blue arrow represents the flow of oxygenated blood from the PT to the CV, whereas the green arrows represents the flow of bile from CV to PT.

1.1.2 Microenvironments of the liver

Hepatocytes, the parenchymal cells of the liver, exist as a heterogeneous population across the lobule due to liver zonation. Areas of liver zonation can be delineated as zone I (periportal region), zone II (mid-lobular region) and zone III (perivenous region) (Fig 1.2A). The flow of blood across hepatic lobules creates a gradient of oxygen, nutrients, metabolites, hormones and cytokines. These physiological variances combined with zone specific signalling pathways, such as Wnt/β-catenin [3], hedgehog [4] and hepatocyte nuclear factor 4 alpha (HNF4α) signalling [5,6], produce zonation [7].

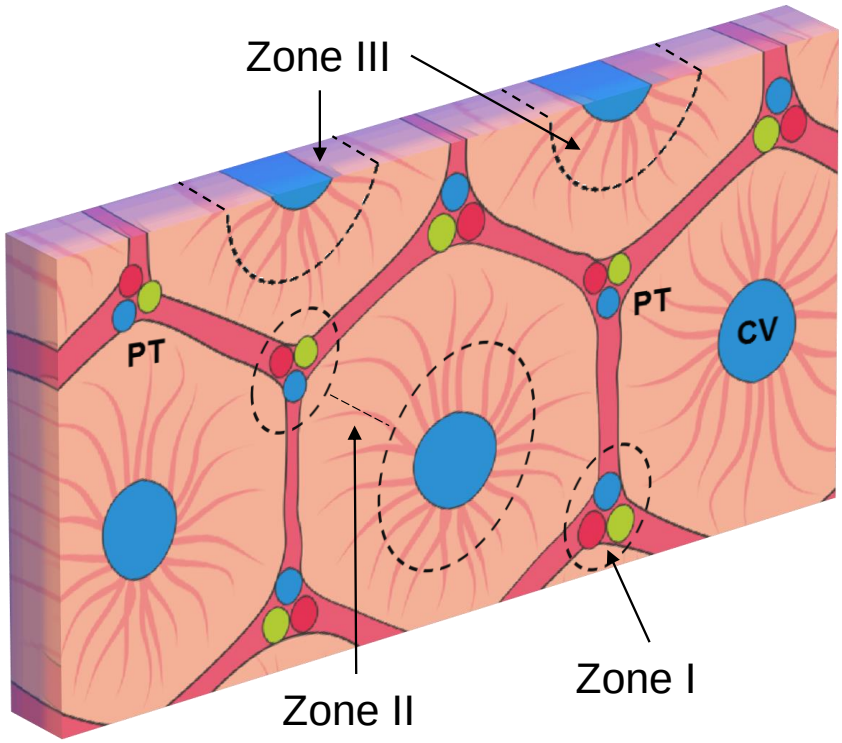

Figure 1.2A- Zonation across the hepatic lobule

Various environmental and genetic factors contribute to liver zonation. Cells within these zones are phenotypically and functionally distinct from one another. The liver acinus is described as zone I (periportal region), zone II (mid-lobular region) and zone III (perivenous region). Zones indicated by dashed lines. Central venule (CV), portal triads (PT).

There are multiple differences in the phenotype and function of hepatocytes seen within different liver zones. For example, the rate of β-oxidation and gluconeogenesis is highest in zone I, whereas lipogenesis, ketogenesis and glycolysis are highest in

zone III [8]. For pharmacological and toxicological studies, zone III is typically of interest as it expresses the highest levels of cytochrome P450 (CYP450) enzymes [9] and various hepatic transporter proteins [10]. Nevertheless, zone I has gained more attention within regenerative medicine studies following the identification of hepatic progenitor cells (HPC) within the biliary tree [11].

1.2 Cell types in the liver

The liver consists of physiologically and morphologically distinct cell types. Hepatocytes represent approximately 60 % of all cells in the liver yet occupy 80 % of the total liver volume. The remaining liver cell types are referred to as the non-parenchymal cells (NPC) and make up 40 % of the hepatic cell population, but only represents 6.5 % of the liver volume, with vasculature and ductular structures accounting for the remaining volume [12]. Of the hepatic NPC, liver sinusoidal endothelial cells (LSEC) account for 50 %, intrahepatic lymphocytes (IHL) for 25 %, kupffer cells (KC) for 20 %, cholangiocytes (also known as biliary duct epithelial cells, BEC) for 5 % and hepatic stellate cells (HSC) for <1 % [13]. Each of these cells are found in distinct areas within the liver (Fig 1.2B) and perform niche roles during hepatic homeostasis and injury, which have been extensively reviewed elsewhere [14–17]. Owing to the nature of the work in this thesis, hepatocytes, cholangiocytes and hepatic stem cells are further discussed.

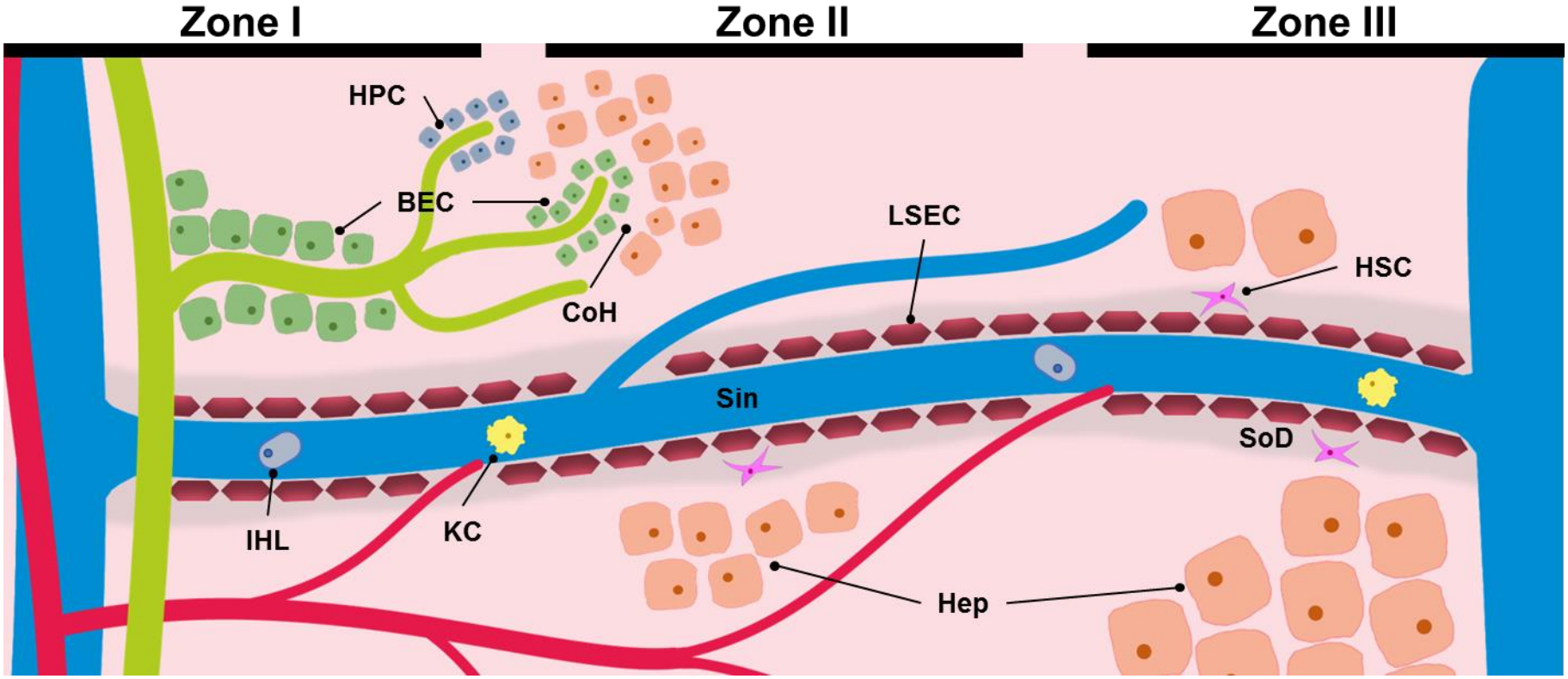

Figure 1.2B- The liver consists of heterogeneous parenchymal and non-parenchymal cells

Hepatocytes (Hep) are ubiquitously expressed throughout the liver lobule and are the functional cell type in the liver. The non-parenchymal cells (NPC) in the liver consist of liver sinusoidal endothelial cells (LSEC), intrahepatic lymphocytes (IHL), kupffer cells (KC), cholangiocytes or biliary duct epithelial cells (BEC) and hepatic stellate cells (HSC). Each of these NPC are functionally different and occupy specific niches in the liver. Sinusoid (Sin), Hepatic Progenitor cell (HPC), Canal of Hering (CoH), Space of Disse (SoD).

1.2.1 Hepatocytes

Hepatocytes are highly specialised and polarised epithelial cells and are responsible for the majority of physiological processes associated with hepatic function; in broad terms, they are responsible for metabolism of carbohydrates, proteins and lipids, storage of fat and glycogen and protein synthesis and secretion [18]. Hepatocytes are ubiquitously found across zone I-III of the liver lobule, although their gene and protein expression vary greatly between these zones. They are typically identified by the expression of α1-antitrypsin (A1AT), HNF4α and albumin [19]. Zone I hepatocytes have higher expression of carbamoylphosphate synthetase (CPS1) and zone III hepatocytes express higher levels of glutamine synthetase (GS) and most CYP450 enzymes [20,21].

A major component of the hepatocyte phenotype is the expression of Drug-Metabolizing Enzymes and Transporter (DMET) proteins. Lipophilic compounds undergo biotransformation by CYP450 enzymes in order to create a polar intermediate compound. These are further metabolised to endogenous compounds (e.g. glucuronic acid) to create a hydrophilic molecule which can be exported into plasma or bile for excretion [22].

Canalicular bile is produced by hepatocytes and deposited across their apical membranes into bile canaliculi, which connect to the finest branches of the biliary tree, named the Canals of Hering. These canals represent an anatomical and physiological intermediate between the liver parenchyma and the start of the biliary tree in the liver microarchitecture [23].

1.2.2 Cholangiocytes

Cholangiocytes (BEC) are epithelial cells which line the bile ducts. They are identified by specific protein markers, such as cytokeratin (CK) 7 and CK19 and gamma-

glutamyl transpeptidase (GGT) [24]. As biliary excretion of drugs is a major pathway of drug elimination, the roles of cholangiocytes in toxicology is an area of interest.

In humans, the intrahepatic biliary tree is made up of small ducts (ductules, interlobular, and septal) and large ducts (area and segmental) [25]. The morphology of cholangiocytes varies depending on their location within the biliary tree. In humans and rodents, small bile ducts are typically lined by 4-5 cholangiocytes (approximately 6 μm) with a flat, cuboidal morphology. Alternatively, large ducts are lined with <40 cholangiocytes in human and 15 in rodents (approximately 15 μm) with a columnar morphology [24]. Large cholangiocytes are typically described as more specialized, as they possess a higher number of organelles and smaller nucleus to cytoplasm ratio than small cholangiocytes [26]. Interspecies variation in protein expression is seen between large and small cholangiocytes, which is extensively reviewed elsewhere [27,28].

The main physiological role of cholangiocytes is to alter the composition of canalicular bile through a series of secretive and re-absorptive processes, largely regulated by hormones, neurotransmitters, nucleotides, and peptides. These processes are mediated predominantly by the large cholangiocytes though adenosine 3′,5′-cyclic monophosphate (cAMP)-dependent processes [29]. On the other hand, small cholangiocyte function is principally controlled by inositol trisphosphate (IP3)/Ca^{2+}/calmodulin-dependent protein kinase I signalling pathway [30]. Regardless of size, cholangiocytes possess primary cilia that extend into the lumen of the bile duct from the apical membrane. These primary cilia function to detect changes in bile flow, composition, and osmolality that feed back into intracellular signalling pathways within cholangiocytes [31].

The full array of physiological roles performed by cholangiocytes in biliary modification is extensive and has been reviewed elsewhere [27–29,32]. Some key examples include the Cl^-/HCO^{3-} exchange, which results in bicarbonate-rich, alkaline bile which is

important for a number of physiological processes, such as digestion [27] and cytoprotection against bile acids, which are found in mM concentrations at the luminal surface of cholangiocytes [33]. These bile acids are also moved across the cholangiocyte basolateral membrane into the local circulation, where they return to hepatocytes to be re-secreted into bile. This process is known as the cholehepatic shunt pathway and aids in total hepatobiliary transport of bile acids and the adaption of cholangiocytes to chronic cholestasis [34,35].

1.2.3 Resident hepatic stem cells

Multiple adult stem cell niches exist within the liver. Wang *et al.* recently discovered diploid Axin2$^+$ hepatocyte-like cells located proximal to the central venule that differentiate into polyploid mature hepatocytes under normal homeostatic conditions [36]. Biliary tree progenitor cells (BtPC) exist within the peribiliary glands of the large intra- and extrahepatic ducts of the liver and are able to differentiate into hepatic or pancreatic lineages [37]. BtPC are suspected to be the source of cell turnover for the entire extrahepatic biliary tree and the large intrahepatic ducts. Finally, hepatic progenitor cells (HPC, named oval cells in rodents) are bipotent progenitor cells located in the Canals of Hering and biliary ductules. They are thought to be precursor cells to hepatoblasts and capable of regenerating hepatocytes and small cholangiocytes [11,38].

Both BtPC and HPC exhibit a phenotype similar to cholangiocytes, such as CK7, CK19, SOX9, neural cell adhesion molecule (NCAM) and epithelial cell adhesion molecule (EpCAM) expression [21,39]. Unlike cholangiocytes, they both express markers such as prominin-1, forkhead box L1, Trophoblast Cell Surface Antigen-2 (TROP-2) and Leucine-rich repeat-containing G-protein coupled receptor 5 (LGR5) [40–43]. Uniquely to hepatoblasts, some mature hepatocyte attributes such as CK18 and albumin expression may also be co-expressed with the biliary phenotype [11,44].

The prevailing consensus for HPC-mediated regeneration states that when the liver is injured in such a way that negates the proliferative effects of hepatocytes and cholangiocytes, a ductular reaction occurs. This is an alternate method of cellular regeneration by the proliferation and differentiation of HPC [45]. Under normal physiological conditions, the presence of HPC is minimal, though progressive liver injury induces their prevalence over time [46]. Depending on the type of injury, HPC are suggested to rapidly differentiate into either cholangiocytes or hepatocytes [47]. Functional roles of these cells have mostly been identified in rodent studies, where the hepatobiliary cellular population is diminished, and consequential regeneration is impeded. 2-acetylaminofluorene (2-AAF) with partial hepatectomy, 3,5-diethoxycarboncyl-1,4-dihydrocollidine (DDC) or a choline-deficient, ethionine-supplemented (CDE) diet are the typically used models of progenitor cell proliferation and liver injury [48–51]. Novel genetic models have used targeted inducible depletion of E3 ubiquitin ligases to induce hepatocyte death and progenitor cell proliferation [52,53].

However, experimental validation of the roles of HPC in liver injury and regeneration have been controversial. While HPC have been isolated, expanded and partially characterised *in vitro*, multiple studies have cast doubt on the ability of these cells to differentiate and repopulate the liver *in vivo* post-injury. Lineage tracing of novel hepatocyte populations following classic HPC-inducing liver injury revealed <2 % of hepatocytes were HPC derived, and were instead replenished from pre-existing hepatocytes [54–57]. On the contrary, Raven *et al.* have recently more accurately mimicked the human *in vivo* phenotype by genetically inhibiting the proliferative ability of hepatocytes, in combination with liver injury. Lineage tracing revealed approximately 20-30 % of regenerating hepatocytes were biliary derived. The new parenchyma was CYP450 $2D^+$ and $HNF4\alpha^+$ and normally found adjacent to $CK19^+/SOX9^+$ ductal cells, with $SOX9^+/HNF4\alpha^+$ intermediate cells seen at the interface of novel hepatocytes and ductular reactions [58]. It still remains to be fully

elucidated if HPC are a defined cholangiocyte-like stem cell, or the result of a de-differentiated mature cholangiocyte [59].

1.3 Drug-induced liver injury (DILI)

Adverse drug reactions (ADR) are a major concern for healthcare systems and the pharmaceutical industry with an estimated annual cost to the UK of £ 1 billion and $ 4 billion to the USA and are responsible for approximately 5 % of hospital admissions [60]. Furthermore, the incidence of developing an ADR within hospital has been estimated between 3.2-14.7 % [61–63]. A concerning statistic is that approximately 50 % of all ADR have been classified as potentially or certainly preventable [61,64,65].

ADR are capable of causing systemic toxicity in multiple organ systems; however, the liver is especially susceptible due to its proficient metabolic turnover of xenobiotics. Although drug-induced liver injury (DILI) is an infrequent disease within the general population, it is a common ADR. The annual incidence of DILI is estimated to occur in 1 per 10,000-100,000 patients [66], though this is thought to be underestimated; European population and cohort studies over the last 16 years have refined this rate to range between 3.4 and 19.1 cases per 100,000 inhabitants [67–69]. It is the leading cause of acute liver failure (ALF) in the western world, with relatively poor prognosis [70]. Six months after initial DILI onset, 10 % of patients have died or undergone liver transplantation. Of the remaining patients, 20 % present with persistent hepatocellular injury requiring further medical attention [71]. Furthermore, it is one of the major causes of drug attrition throughout all stages of the drug discovery process. In early development, 50 % of all pre-clinical candidate drugs display effects upon the liver at supra-therapeutic doses [72]. Over a 60 year period, DILI was responsible for 18 % of all drugs retracted post-marketing which represents the largest single reason for withdrawal [73].

DILI is caused by a wide array of prescribed and over-the-counter medications, which are taken on their own, or in combination. To date, over 1,000 medications and supplements have been identified as hepatotoxic [74]. Antibiotics (in particular, amoxicillin-clavulanate), anti-infectives, non-steroidal anti-inflammatory drugs (NSAIDS), antipsychotic drugs and analgesics are the therapeutic classes of drugs most commonly associated with DILI [68,75–78]. Dietary and herbal supplements are increasingly identified to cause hepatotoxicity, being responsible for 4 %, 9 % and 16 % of identified DILI cases in the Spanish DILI registry [79], Drug-Induced Liver Injury Network (DILIN) [80] and a prospective study of the Icelandic population [67], respectively.

1.3.1 Classifications of DILI

DILI is categorised as either intrinsic or idiosyncratic. Intrinsic reactions are those which are perceived as an extension of the pharmacology of the drug. These are predictable in nature and show a clear dose-response relationship, such as liver toxicity associated with supra-therapeutic doses of acetaminophen (APAP) [81]. Idiosyncratic reactions are complex to model pre-clinically and are unpredictable. This is due to patient genetic variation, alongside complex pathophysiological mechanisms which includes both metabolic and immune-mediated responses. These reactions can be very severe in nature and are commonly undiscovered until post-marketing distribution, where the drug becomes widely available to susceptible individuals [72,82].

DILI can arise as a consequence of acute or chronic toxicity and is typically difficult to diagnose. DILI patients typically present with non-specific symptoms, such as malaise, nausea, vomiting and abdominal pain and only liver-specific symptoms, such as jaundice and ascites, in severe cases. Furthermore, biopsy samples can histologically appear similar to other acute or chronic liver disease [83]. Once a DILI diagnosis is made based upon clinical chemistry and pathological observations, the severity is classified as mild, moderate, severe or fatal, as recommended by international expert opinion guidelines [84].

The main cellular targets of DILI are hepatocytes and cholangiocytes. Consequently, the pattern of injury caused by hepatotoxins can be described as hepatocellular, cholestatic or mixed injury. This diagnosis is based on the R-ratio at patient presentation, depending upon serum and liver biopsy results (later described in section 1.5.1). Hepatocellular DILI is the most common form of injury, accounting for approximately 50 % of all injury, with cholestatic and mixed representing 30 % and 20 % respectively [85,86].

1.4 DILI of hepatocytes and cholangiocytes

If a case of DILI of the hepatocytes or cholangiocytes occurs without resolution, it can lead to a chronic pathological state. Clinically, this resembles primary liver or biliary cirrhosis with elevated levels of liver enzymes and jaundice, detectable over several months to years [87]. Persistent injury of the cholangiocytes leads to ductal sclerosis and ductopenia. Ultimately this leads to vanishing bile duct syndrome (VBDS) which is characterized by a loss of >50 % of bile ducts within the portal triad. In general, DILI without resolution leads to fibrosis and cirrhosis, liver failure, and ultimately death [88].

Early biochemical studies of freshly isolated rat hepatocytes and cholangiocytes showed that cholangiocytes have approximately 35 % of the total level of glutathione (GSH) compared to hepatocytes. The activity of glutathione S-transferase (GST) activity and the ability of cholangiocytes to reduce oxidized GSH was also significantly lower in cholangiocytes compared to hepatocytes [89]. This may offer an insight into the susceptibility of cholangiocytes to DILI.

The exact mechanisms of direct cholangiocyte and hepatocyte injury can be broadly described as a toxic effect of a parent compound or reactive metabolite. The downstream effects of toxicity manifests as distinct cellular perturbations, such as oxidative stress, endoplasmic reticulum stress and mitochondrial dysfunction [90].

1.4.1 Parent compound toxicity

Evidence of parent compound toxicity in cholangiocytes comes from the use of α-napthylisothiocyanate (ANIT) and 4,4′-diaminodiphenylmethane (DAPM), though the final toxic insult is typically mixed hepatocellular injury. Neither ANIT nor DAPM are clinically relevant compounds; the former has limited industrial use, whereas the latter is used in the production of epoxy resins, polyamides, and polyurethanes [91].

ANIT has been shown to conjugate to hepatocyte GSH which is then transported into bile ducts by the multi-resistance-associated protein 2 (MRP2, ABCC2). ANIT and GSH readily dissociate, leaving a high concentration of ANIT in the bile, which is then taken up by cholangiocytes [92–94]. The cellular mechanisms of ANIT injury are suggested to be a depletion of cholangiocyte GSH, leading to oxidative injury in combination with the release of cytotoxic and inflammatory mediators [95,96]. DAPM-associated cholangiocyte injury is also though to occur via biliary excretion of toxic compounds. Bile isolated from DAPM-treated rats has been shown to be toxic to cholangiocytes both *in vivo* and *in vitro*. The cellular mechanisms of DAPM biliary toxicity are proposed to be rapid mitochondrial dysfunction and impairment of glucose uptake [97–99].

Parent compound toxicity is also observed in hepatocytes. *In vitro* dosing of rat primary hepatocyte cultures with papaverine and its major metabolites revealed greater cytotoxicity with the parent compound [100]. Similar observations were noted when dosing with leflunomide, whereby CYP450 inhibitors enhanced toxicity and CYP450 inducers decreased toxicity [101].

1.4.2 Reactive metabolite toxicity

The most well-known reactive metabolite-mediated DILI is by APAP, a commonly taken analgesic and anti-pyretic. With APAP overdose, the glucuronidation and sulphation pathways within hepatocytes are overloaded and metabolism is

prominently mediated by CYP450 2E1 into the reactive metabolite N-acetyl-p-benzoquinone imine (NAPQI). NAPQI brings about a rapid depletion of GSH and the formation of reactive oxygen species, protein adducts and release of inflammatory cytokines. Critically, these adducts can also form within the mitochondria, disrupting the electron transport chain, which ultimately leads to necrotic cell death [102]. This CYP450-dependant metabolism is typically zone III specific. However, a similar phenomenon is also observed in cholangiocytes, whereby CYP450 2E1 expressing large cholangiocytes are damaged by carbon tetrachloride and small cholangiocytes are unaffected [103].

Specifically, for cholangiocytes, Lakehal *et al.* demonstrated that flucloxacillin is not directly toxic to human hepatocytes or gall bladder-derived cholangiocytes. However, hepatocyte-conditioned media and liver microsomes with recombinant CYP450 3A4 conditioned media triggered significant dose-dependent cell death in 58 % and 69 % of cholangiocyte cultures respectively [104].

A number of metabolites from bile duct cannulated rats treated with fenclozic acid, an NSAID withdrawn post-marketing due to hepatotoxicity, have also been associated with cholangiocyte DILI. These metabolites were capable of binding to GSH and coenzyme A, which are associated with the toxicity of other carboxylic acid containing drugs [105]. Cholangiocyte injuring GSH-conjugated reactive metabolites have also been identified in human and rat microsomes incubated with terbinafine [106].

1.5 What is a biomarker?

To help identify and accurately diagnose the onset of DILI in both pre-clinical and clinical settings, there is a need for a sensitive and specific biomarker(s) that could aid drug design and modification, as well as patient diagnosis, stratification and treatment. A biomarker is defined as, “a characteristic that is objectively measured

and evaluated as an indicator of normal biological processes, pathogenic processes or pharmacological responses to a therapeutic intervention" [107].

When evaluating candidate biomarkers for DILI, the ideal biomarker would show complete liver specificity and only elicit a response to DILI and no other hepatic injury. It should also be sufficiently sensitive that it can be detected at injury onset with the use of non-specialised equipment for rapid diagnosis and prognosis within the clinic or point-of-care environment. Early diagnosis would also be greatly facilitated by biomarkers easily obtained from bio-fluids by a non-invasive procedure, such as those found in the circulation. They should be conserved and translational, allowing the transition of candidate markers in pre-clinical studies to be clinically viable in humans.

1.5.1 Current biomarkers of DILI

Currently, there is no single biomarker that is suitable for the diagnosis of DILI, due to the multi-factorial character of its pathophysiology. Consequently, current diagnosis is one based upon exclusion of conditions that commonly mimic DILI symptoms in order to create a causal link between a drug and any potential liver injury. These causality valuations into drug-mediated hepatotoxicity are made using methods such as Roussel-Uclaf Causality Assessment Method (RUCAM) and combined expert opinion [108].

A major component of diagnosis relies on a liver function test, which examines biochemical perturbation within the patient using a panel of serum biomarkers such as alanine aminotransferase (ALT), aspartate aminotransferase (AST), alkaline phosphatase (ALP) and total bilirubin (TBIL). Elevations of ALT/AST in the serum correlate with hepatocyte necrosis and subsequent release of these markers into the circulation. Elevations in ALP reflects damage to the cholangiocytes or canalicular membrane and TBIL is indicative of whole liver function [109,110]. The criteria for determining hepatocellular, cholestatic or mixed liver injury is determined by upper limit of normal (ULN) values and the R-ratio, established by the Council for

International Organizations of Medical Sciences (CIOMS) [111]. The R-ratio is defined as R = (ALT/ALT ULN) / (ALP/ALP ULN). Liver injury is defined as: hepatocellular, ALT ≥ 3 ULN and R ≥ 5, cholestatic, ALP ≥ 2 ULN and R ≤ 2 and mixed injury, ALT ≥ 3 ULN and ALP ≥ 2 ULN and 2 < R < 5 [83,84].

These panels have been clinically relevant for many years and remain the gold standard for DILI diagnosis. As an extension of these biomarker panels, the Food and Drug Administration (FDA) endorses the use of Hy's law, which is typically used pre-clinically to identify hepatotoxicity. Hy's law is based on the observations of Dr Hyman Zimmerman and it states that "drug-induced jaundice caused by hepatocellular injury, without a significant obstructive component, leads to death or liver transplantation in >10% of cases". This has been refined to a drug which causes elevations of ALT/AST >x3 and TBIL >x2 ULN in the absence of other cholestatic/hepatic co-morbidities is likely to cause hepatotoxicity. The use of Hy's law has been validated in various DILI cohorts [78,85,112].

1.5.2 Problems with current biomarkers

The current diagnostic biomarkers of DILI are not without their limitations. None of the aforementioned markers offer true mechanistic insight into the basis of DILI and are also detectable in other forms of liver disease, such as viral hepatitis and ischaemic injury [109]. Furthermore, they are not liver-specific and injuries in other tissue types causes elevations of these markers which may cause false-positive diagnosis in patients with multiple co-morbidities. Both ALT and AST are present in skeletal muscle and have shown to be elevated in the serum of patients of polymyositis and extreme exercise [113]. This was shown by Thulin *et al*., who demonstrated that serum ALT/AST were significantly elevated in healthy volunteers after extreme exercise with fold changes of 2.5 and 5.5 respectively when compared to pre-exercise serum samples [114]. ALP is also present in bone tissue and is increased in response to osteoblast activity. Elevated serum levels have been detected in metabolic bone

disease, downstream effects of hyperthyroidism and in post-menopausal women, who incidentally represent a high-risk group for DILI [115,116]. Serum TBIL can also appear elevated by the processing of erythrocytes and subsequent degradation of haemoglobin or by alteration of bilirubin transporters [117].

Although Hy's law has relatively high sensitivity for detecting DILI, it lacks specificity as many incidences that match the criteria for hepatotoxicity will fully recover without progression to ALF [118]. This was highlighted by a recent suspension of neuregulin-1β from phase I clinical trials due to two patients meeting the criteria for Hy's law. However, following serum sampling and mathematical modelling, it was predicted that there was <13 % hepatocyte death, which would not be sufficient to raise circulating TBIL <2x ULN [119].

One of the major limitations of the aminotransferases is the relatively low sensitivity and delayed release from the cell following DILI. Furthermore, they have an extended half-life in circulation; although biomarker stability is necessary, ALT has a half-life of approximately 47 hours and AST has a half-life of 17 hours [109]. This may be undesirable as the DILI may have resolved and the liver be in repair, whereas ALT/AST measurements would not reflect this. The detection of circulating ALT/AST is purely diagnostic as these markers are released into the serum post-injury, representing a defined period of latency in the recognition of DILI following exclusion of other diseases. Relatively large elevations in ALT/AST can also be observed in response to drug treatment that do not cause overt progressive DILI, such as statins and heparins, which may only serve to remove safe candidate drugs during pre-clinical testing in the future [120,121].

Consequently, there has been recent interest in the development of novel circulating biomarkers which are able to detect mitochondrial damage (GLDH and mitochondrial DNA fragments), cell death (total HMGB1, full and caspase cleaved keratin-18) and APAP-protein adducts in APAP-DILI patient cohorts. Many of these circulating

biomarkers show improvement over the existing set in terms of specificity, prognostic and mechanism-based utility [122,123]. However, a limitation of these biomarkers is that they are not liver or disease specific. Furthermore, they are predominantly protein-derived, thus their stability and detection of low-level injury may be challenging compared to RNA-derived biomarkers [124].

1.6 microRNAs as potential biomarkers

Despite these inadequacies, the combination of ALT/AST, ALP and TBIL remain the current gold standard in DILI detection in man. Any novel biomarkers must therefore provide added value to the pre-existing ones in order to be deemed clinically useful. Novel markers would therefore have to show increased specificity and sensitivity, while demonstrating prognostic and mechanistic attributes.

MicroRNAs (miRNAs) have been shown to be a rich source of biomarkers for a wide range of pathological states across multiple organs. They are small (18-25 nucleotides long) non-coding RNA molecules that regulate post-transcriptional gene expression [125]. The biogenesis of miRNAs is a tightly regulated process, whereby the hairpin pri-miRNA structure is initially transcribed from miRNA genes (Fig 1.3). These precursor structures are subsequently cleaved into pre-miRNA by the type 3 RNAse Drosha-DGCR8 complex and translocated into the cytosol by Exportin 5 [126]. The hairpin structure is then processed into a double strand RNA molecule by another type 3 RNAse DICER-HIV-1 TAR RNA binding protein (TRBP) complex, and mature single strand miRNA is produced by association with the RNA-inducing silencing complex (RISC). Within the RISC complex, mature miRNA can associate and bind to target mRNA, preventing its translation and ultimately repressing protein expression [127].

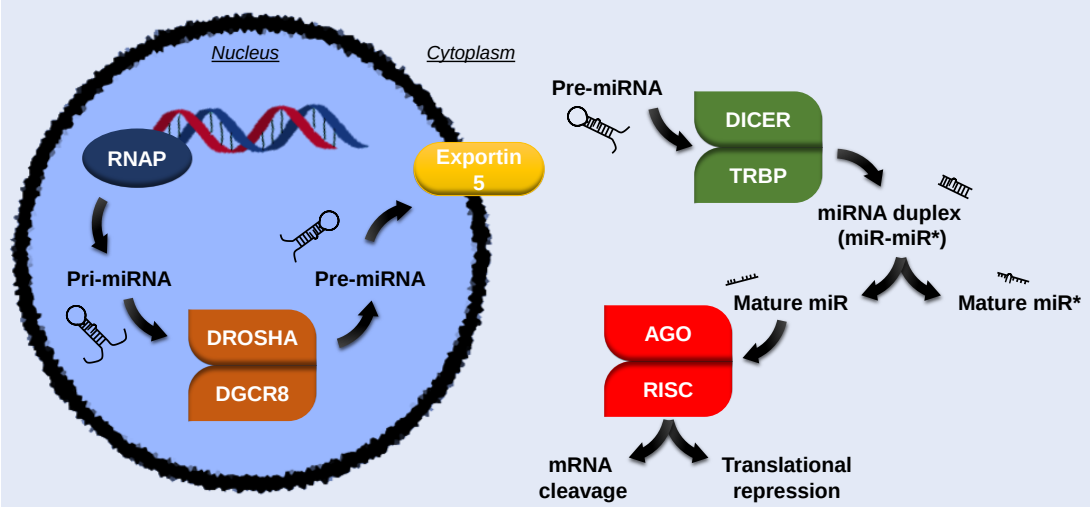

Figure 1.3 Biogenesis and processing of microRNAs

Canonical microRNA (miRNA) biogenesis consists of nuclear transcription by RNA polymerases (RNAP) and processing of intermediate stem-loop primary (pri-miRNA) and precursor (pre-miRNA) molecules. Pri-miRNA undergoes nuclear cleavage by the DROSHA-DGCR8 complex to form pre-miRNA. Pre-miRNA molecules are exported to the cytoplasm by Exportin 5 and further cleaved by the DICER-TRBP complex, into a mature miRNA duplex (miR-miR*, astericks denotes passenger strand). Finally, a mature miRNA strand associates with Argonaute (AGO) to form the RNA-induced silencing complex (RISC), which modifies gene expression.

miRNAs make for an attractive non-invasive biomarker as following organ damage, they are released from the cell into easily obtained bio-fluids, such as blood and urine. Within the bloodstream, they are incorporated into extracellular vesicles (e.g. microparticles, exosomes or apoptotic bodies) or are protein-bound (e.g. lipoproteins or argonaute2) which protects them from endogenous RNase degradation, ensuring their stability [128]. Furthermore, miRNAs are very highly conserved across mammalian genomes, which greatly aids a translational approach from pre-clinical studies to the clinic [129]. There has been emerging evidence to suggest miRNA biomarkers can be used to identify mechanistic effects upon the liver, such as inflammation [130,131] and hepatic regeneration[132,133]. Fig 1.4 details the initial cellular processing and ultimate release of miRNA and current biomarkers into the circulation following toxicity.

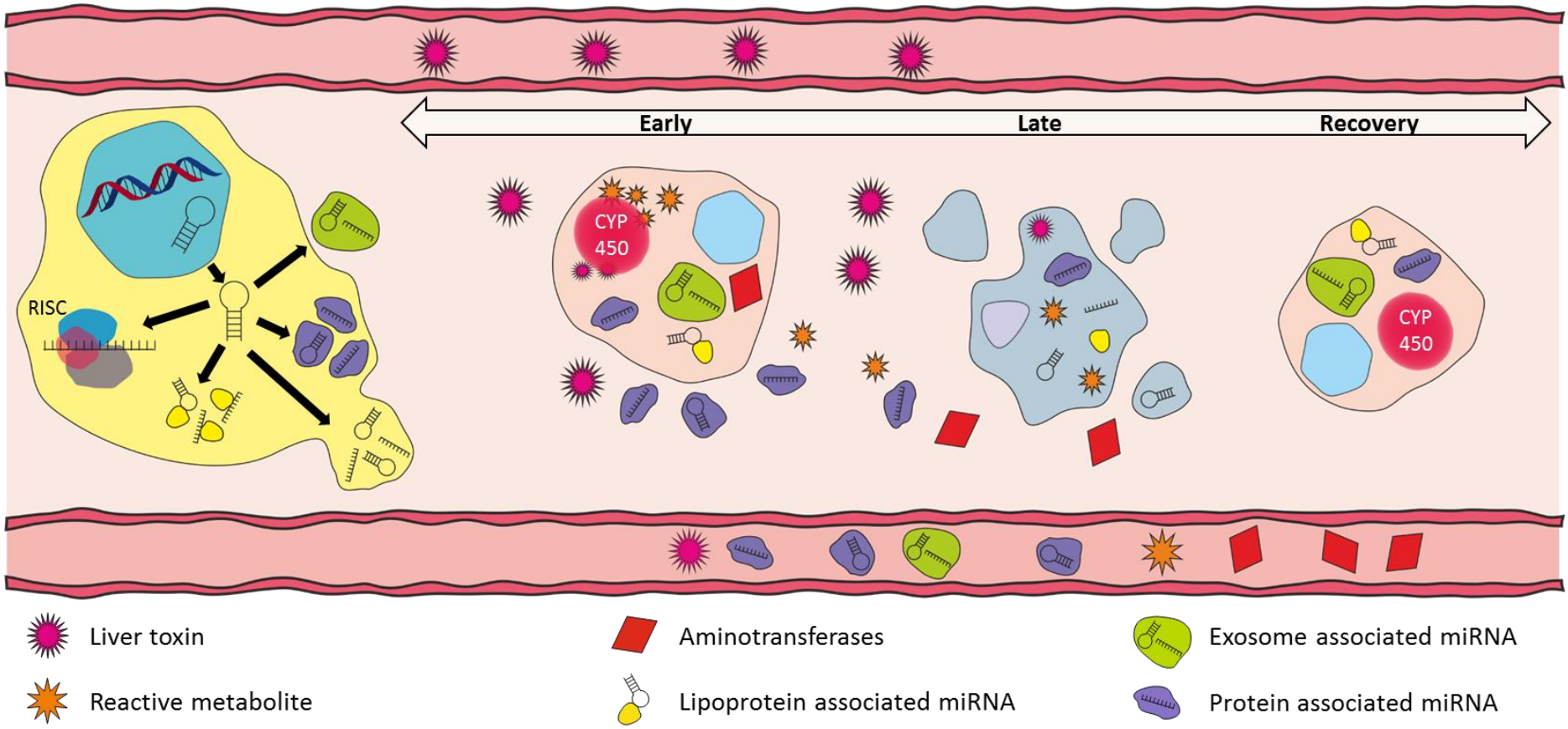

Figure 1.4- Production and processing of miRNAs in response to drug-induced liver injury

miRNAs are processed into protein complexes such as RISC. They then further associate with other proteins (e.g. lipoproteins, argonaute2) or incorporate into extracellular vesicles (e.g. microparticles, exosomes). Upon delivery to the liver, liver toxins are taken up by the cells and are processed into reactive metabolites. Both the parent compound and metabolites may cause acute toxicity to the cell, which causes the early (<4h) release of liver-enriched miRNAs into the blood stream as a detectable biomarker. As DILI progresses into later stages, miRNAs may also be detected in apoptotic bodies. Aminotransferases are the current gold standard biomarker for hepatocellular injury, but their use is limited as they are released at these later time points (8h) compared to miRNAs. They can also be detected once DILI has resolved and progressed into hepatic recovery.

1.6.1 microRNA-122

Select miRNAs have been shown to be highly tissue specific. Of those miRNAs that are liver enriched, the highlight candidate biomarker for DILI is miR-122. miR-122 is one of the most abundant adult hepatic miRNAs, accounting for approximately 70 % of the total liver miRNAome [134]. Due to its prevalence within the liver, it is of no surprise that it regulates a wide range of key gene networks such as hepatic circadian rhythm, lipid metabolism and cell differentiation [135–137].

The role of circulating miRNAs in DILI was first demonstrated back in 2009, where elevated levels of liver-enriched miRNAs, including miR-122 and miR-192, were discovered in mouse plasma following toxic APAP exposure. It was further noted that changes in the serum levels of these miRNAs could be detected significantly earlier than the aminotransferases [138]. The translational aspect of miRNAs as potential biomarkers of DILI was subsequently highlighted in a cohort of 53 APAP-overdose humans, where circulating levels of miR-122 were found to be around 100 times higher than control samples [139]. Since then, there have been several studies showing the release of liver enriched miRNAs in response to toxic injury in both human and rodents, but also in cynomolgus monkeys [140] and zebrafish [141]. The release of miRNAs into cell culture medium by *in vitro* modelling of drug-induced NAFLD has also been shown to correlate to circulating miRNAs in patient serum samples, highlighting the potential use of miRNAs at the multiple stages of pre-clinical testing [142].

It has been shown in clinical case studies that miR-122 is detectable up to 8 hours before ALT and only 4 hours after initial toxic insult, thus proving a more rapid approach in diagnosing DILI [143]. The half-life of miR-122 is also shorter than either ALT or AST, returning to baseline after 3-7 days, which may be more representative of the progression of liver injury [139]. Ultimately, this reduces clinical burden by achieving an earlier diagnosis and appropriate treatment plans. Furthermore, in

serum samples of patients with APAP toxicity with early presentation to hospital, Receiver Operating Characteristic (ROC) analysis of miR-122 showed greater sensitivity in predicting APAP toxicity compared to aminotransferases [144].

Although liver specific, miR-122 is not unique to DILI profiles. It is differentially processed and elevated in serum in response to other hepatic injury types of differing aetiology. In hepatocellular carcinoma, levels of miR-122 are significantly reduced and are associated with poor prognosis and loss of hepatocyte phenotype [145]. Circulating levels of miR-122 have been shown to increase in bile duct ligated mice [146], reperfusion injury and acute rejection of liver transplantation [147] and in NAFLD [148]. Therefore, it is important to exclude these other hepatic pathological conditions before using individual miRNAs to diagnose DILI. This has led to the idea that a panel of serum miRNA profiles may be a more accurate method to diagnose liver injury. Ward *et al.* showed that a panel of 11 miRNAs, including miR-122, could discriminate a diagnosis of APAP-induced DILI against patients with ischaemic hepatitis [149]. This work has recently been advanced by examining serum samples from 72 patients from patients with APAP-DILI, hepatitis B infection, liver cirrhosis and type II diabetes with next generation sequencing. It was found that patients of each disease group presented with elevated ALT levels, indicative of liver damage. However, each disease state presented with a specific “signature” of circulating miRNA which could be used to identify the individual underlying cause of liver injury [150].

1.6.2 Zonated and non-parenchymal derived microRNAs in liver injury

Liver zonation is the master regulator of the differential phenotype seen within the liver parenchyma, although there are contributing genetic factors, such as zone-specific miRNA regulation [151]. Though the majority of toxicology and biomarker research focuses on APAP which exerts its toxicity in the perivenous area, there are many drug classes that produce periportal DILI [152].

Identification of DILI in either zone I or zone III of the liver by a circulating biomarker would be advantageous for a number or reasons. Cholangiocytes, found within the periportal region are targets of toxicity for numerous commonly prescribed drugs, such as penicillins [104]. Serious damage of these cells may ultimately lead to VBDS, which requires liver transplantation. Diagnosis is dependent upon liver biopsies, whereas a panel of miRNA biomarkers selective for cholangiocyte or generalised periportal injury would ensure a non-invasive, early diagnosis [88]. Detection of zone-specific miRNAs in pre-clinical testing may also ultimately aid future drug design by linking the drugs chemical properties to the area of DILI.

Investigations into miRNA serum profiles of zonal hepatotoxins are in their infancy yet may prove to be very important in the future search for novel mechanistic biomarkers. Yamaura *et al.* induced zonal hepatocellular necrosis by dosing rats with APAP or methapyrilene. They noted uniquely upregulated and downregulated circulating miRNAs between the two different dosing groups, which may indicate a unique zonated biomarker [153]. It was noted in a follow-up paper that the miRNAs that are upregulated in serum do not necessarily correlate to miRNA that are downregulated in liver tissue following DILI, indicating a potentially more complex method of miRNA release than a simple deposition of highly abundant miRNA into biofluids [131]. Church *et al.* used the hepatobiliary toxins ANIT and FP004BA to cause periportal injury in rats. Several miRNAs that were consistently elevated in blood samples from the two drugs were identified, indicating possible novel and unique hepatobiliary injury markers. [154]. A recent study by Oda *et al.* is one of the first comprehensive reports of circulating miRNA biomarker discovery in NPC. LSECs are sensitive to injury following chemotherapy or radiotherapy, which can lead to vascular disease and sinusoidal obstruction syndrome (SOS). miRNA analysis of isolated LSECs revealed an enrichment of miR-511-3p compared to isolated hepatocytes. Circulating levels of

miR-511-3p were observed in rats 6 hours after dosing with monocrotaline, whereas levels of miR-122-5p were observed 34 h post-dose [155].

1.7 Modelling DILI

Although there have been improvements in the detection and diagnosis of DILI, the expression “prevention is better than cure” is applicable for hepatotoxicity. DILI modelling has evolved and improved to ultimately better reflect the human *in vivo* phenotype. However, to date there is not one cell detection system that sufficiently satisfies the wide-reaching requisites of DILI prediction.

1.7.1 *In vivo* models

In vivo pre-clinical toxicity testing is a critical component in determining drug safety. Mice and rats make up approximately 85 % of all animals used in scientific animal procedures and are the most commonly used species in evaluating toxicity of a compound [156]. *In vivo* studies are advantageous as they can model the pharmacokinetic and pharmacodynamic effects of a drug. Critically, they can reproduce the hepatic systemic organ phenotype; furthermore, it is possible to evaluate hepatocellular, vasculature, inflammatory and hyperplastic effects of a drug.

However, the main concern of animal testing is the lack of translation into human, due to species dependant differences in toxicity sensitivities and metabolism. For example, genome mining revealed mice have been shown to express 102 putatively functional CYP450 genes, whereas humans only express 57 [157].

Rodent toxicology studies are estimated to only positively predict 43 % of potentially hepatotoxic events in human [158]. A number of high profile compounds that passed pre-clinical testing have gone on to cause severe or fatal DILI in humans, such as troglitazone, lumiracoxib and bromfenac, which have been withdrawn post-marketing [159–161].

In order to reduce the number of end-stage and post-marketing withdrawals of novel compounds, more predictive *in vitro* models are therefore needed.

1.7.2 *In vitro* models

Prior to *in vivo* testing, a large catalogue of candidate drug analogues is tested *in vitro*. These models are typically human derived in order to combat species differences seen with *in vivo* modelling and vary in complexity. Cells may be cultured in 2D-monolayers or in 3D-structures, such as spheroids or extracellular matrix supported sandwich cultures. Cultures may also be static or contained within complex bioreactors and microfluidic systems [162]. Finally, *in vitro* models may be multicellular, incorporating NPC and immune cells around a hepatocyte core in order to mimic the *in vivo* phenotype [163].

A major undertaking in these systems is improving the phenotype of the central hepatocyte-like core. Table 1.1 highlights the advantages and disadvantages of commonly used hepatocyte and hepatocyte-like cells within *in vitro* toxicology. Whilst primary hepatocytes are the gold standard cell model for hepatotoxicity testing, their availability, and stability during long-term culture and high inter-individual variation limit their utility. Furthermore, their inability to proliferate make them an expensive single-use option [164]. Basic and advanced cancer-derived and immortalised cell lines, such as HepG2, HepaRG and Upcyte cells are therefore commonplace. However, these cells generally have low DMET activity, altered Nrf2 cell defence signalling pathways and poorly represent the *in vivo* organ phenotype [165,166]. There has therefore been significant investment into stem cell derived systems due to the unmet need for an *in vitro* hepatic model that shows physiological improvement over the currently used systems.

	Advantages	Disadvantages
Basic cell lines (HepG2, HuH7)	Easy, quick and inexpensive to culture, readily available, highly reproducible.	Cancer derived, low of DMET activity, prone to genetic drift.
Advanced cell lines (UpCyte, HeapRG)	Generally better DMET activity and physiological representation than cancer cell lines.	Costly proprietary media, HepaRG: Cancer derived, requires time consuming differentiation UpCyte: Donor dependant variability, limited availability.
iPSC derived cells	Phenotype of a semi-mature hepatocyte. Exhibits same phenotype as the donor. Can differentiate into any hepatic cell.	Currently invalidated for DILI testing. Time consuming and expensive culture, no universally agreed differentiation protocol.
Organoids	Long term culture possible, exhibits same phenotype as the donor. Can differentiate into a hepatocyte or biliary phenotype.	Poorly characterised and unvalidated for DILI testing. Time consuming and expensive culture, no universally agreed differentiation protocol.
Primary hepatocytes	Most physiologically representative; highest DMET expression of all currently available models.	Donor dependant variability, poor availability, single use, rapid de-differentiation in culture.

Table 1.1 Advantages and disadvantages of hepatocyte cells currently used *in vitro*

Currently used *in vitro* models of hepatotoxicity vary in their complexity and phenotypic relevancy. Different hepatocyte cell models are more suitable than others depending on the defined endpoints of hepatotoxicity testing.

1.7.3 Stem cells models

There is a significant recent interest in developing hepatocyte-like cells from human embryonic stem cells (hESC) and human induced pluripotent stem cells (iPSC). Both hESC and iPSC have been shown to demonstrate a relatively mature hepatic phenotype, being capable of fat and glycogen storage, alongside albumin production and select CYP450 activity comparable to primary hepatocytes [167–169].

Sirenko *et al*. has demonstrated that iPSC can be used in high-throughput toxicity screening against a library of 240 hepatotoxins of differing toxicity mechanisms, including steatosis, mitochondrial toxicity, reactive metabolite formation and CYP450 inactivation [170]. Patient-derived iPSC are an attractive concept as they have been shown to mimic the *in vivo* phenotype of any genetic polymorphisms, such as A1AT, which has allowed the development of novel clinical compounds to challenge the disease state [171]. A biobank of iPSC derived from patients with differing Human Leukocyte Antigens (HLA) has been created, which will potentially aid personalised drug design and prediction of genetic-mediated idiosyncratic DILI [172].

However, a major caveat in the use of iPSC is the long-term stability of the genome and relative lack of metabolic competence. Cellular reprogramming causes DNA aberrations, which affect differentiation capacity and increase tumorigenicity [173].

1.7.4 Organoid models

Organoids are a recent innovation in stem cell-derived *in vitro* modelling. They are described as a 3D cell model consisting of self-organising, organ-specific cell types that mimics the corresponding *in vivo* tissue [174]. To date, organoids from multiple tissues have been developed as a models of disease [175]. Attention has turned to resident liver stem cells, as described in section 1.2.3, as a possible source of hepatocyte-like cells for *in vitro* modelling.

Huch *et al.* identified $LGR5^+$ stem cells (HPC) near the bile ducts in damaged murine livers, which regenerated both hepatocytes and cholangiocytes *in vivo*. Isolated HPC cultured *in vitro* formed self-organising 3D structures with both biliary and hepatocyte phenotypes, termed hepatic organoids. It has been reported that approximately 5-30 % of biliary derived cells will form an organoid *in vitro* [176,177]. Hepatic organoids can be differentiated into a hepatocyte lineage by blocking Notch signalling and engrafted back into murine livers [178].

It has been further demonstrated differentiated human derived organoids were genetically stable in long term culture (90 days) by chromosomal karyotyping. Hepatic organoids were capable of glycogen and fat storage, albumin secretion, bile acid production; CYP450 3A4 activity and midazolam metabolism was also confirmed in organoids [179,180]. Organoids from patients with A1AT deficiency and Alagille syndrome have both been cultured, which successfully recapitulated the disease phenotype *in vitro*. Long term expansion (8 months) of liver organoids from canine livers has also been reported [181]. However, biliary-derived hepatic organoids have not been sufficiently characterised to the levels of pre-existing *in vitro* models.

1.8 Thesis Aims-

The role of NPC in DILI has historically been understudied relative to the liver parenchyma. Cells within the biliary network of the liver are both possible targets of DILI and potential tools in predicting toxicological outcomes. However, currently used biomarkers for hepatocellular injury have numerous limitations and putative cholangiocyte biomarkers remain to be investigated. Moreover, novel biliary derived *in vitro* organoid models may be more physiologically relevant compared to currently used systems, although they remain critically under-characterised. The work in this thesis has therefore been undertaken in an attempt to further understand the roles of biliary cells in the prediction and detection of DILI. Consequently, the aims of the research presented within this thesis were to:

- Characterise global miRNA expression in murine cholangiocytes and hepatocytes in order to identify novel circulating biomarkers.
- Induce cell-specific toxicity *in vivo* to assess the detection of putative circulating biomarkers in pre-clinical models.
- Characterise the proteome of hepatic organoids from ductal structures to assess their phenotype relative to donor-derived liver tissue

Chapter Two:

Identification of candidate miRNAs as biomarkers of cholangiocyte injury by global miRNAome analysis

Contents

2.1 Introduction

The liver is the largest gland in the body that consists of multiple cell types that mediate numerous key physiological functions, such as the detoxification of xenobiotics and the production of bile. These specific functions are directly mediated by both hepatocytes and cholangiocytes, which are examples of parenchymal and non-parenchymal cell types, respectively.

Hepatocytes are the most abundant cell type in the liver, constituting 60-80 % of the total liver cell population. They are located throughout zone I-III in the liver and are accountable for the majority of drug metabolism and clearance. Consequently, research directed at understanding the mechanisms of DILI have mostly focused on hepatocytes [13].

Cholangiocytes are epithelial cells which line the bile ducts located within zone I of the liver and typically represent 5% of the total liver cell population. These cholangiocytes, or bile duct epithelial cells (BECs), exist as a heterogeneous population of large and small cells, depending upon their microanatomy within the biliary tree [25]. Cholangiocytes primarily function to modify canalicular bile through a series of secretive and absorptive processes, largely regulated by hormones, neurotransmitters, nucleotides, and peptides [29].

More recently however, the mechanisms of damage and response of the non-parenchymal cells in response to toxic insult is being increasingly investigated. As biliary excretion of drugs is a major pathway of drug elimination, the roles of cholangiocytes in pharmacology and toxicology is of interest.

Adverse drug reactions (ADR) are a major concern for healthcare systems and the pharmaceutical industry with an estimated annual cost to the UK of £1 billion and $4 billion to the USA [60]. Drug-induced liver injury (DILI) is a common ADR and represents

the leading cause of acute liver failure in the western world, as well as being responsible for 18% of all drugs removed from the market between 1953-2013[70 73].

DILI is clinically classified as hepatocellular, cholestatic or mixed depending on the point of injury and subsequent serum biomarker analyses. Hepatocellular signifies injury to hepatocytes, cholestatic indicates cholangiocyte damage and mixed injury presents with symptoms of both. Cholestatic or mixed injury is prevalent, accounting for 50 % of all DILI cases in patient cohorts [858680]. However, when diagnosing a mixed or cholestatic injury, the current gold standard biomarkers (ALT, AST, ALP, GGT, TBIL) are collectively lacking. They are not truly liver specific, are altered with a range of other co-morbidities that are commonly observed in high-risk DILI patients, and have differing release kinetics following injury [124]. Therefore, there is a need for novel, sensitive and specific biomarkers that can aid patient diagnosis and stratification. Furthermore, they could be used to aid drug design and modification throughout pre-clinical testing.

MicroRNAs (miRNAs) are small (18-25 nucleotides long) non-coding RNA molecules that regulate post-transcriptional gene expression and have been shown to be a capable source of biomarkers for a wide range of pathological states across many organs [125]. Following organ injury, they are released from stressed or damaged cells into easily obtained bio-fluids, such as whole blood, where they remain relatively stable [182]. Furthermore, miRNAs are highly conserved across mammalian genomes, which greatly aids a translational approach from pre-clinical studies to the clinic [183].

With respect to detecting DILI, miR-122 has been the main biomarker of interest, due to the fact it is both highly expressed and liver specific [184]. However, the abundancy of miR-122 stems from its expression in hepatocytes, making it an ideal biomarker for detecting hepatocellular injury, such as paracetamol toxicity [139].

A miRNA biomarker derived from cholangiocytes could therefore inform of mechanistic cholestatic DILI, as well as offering greater sensitivity and specificity over the currently used protein biomarkers. Thus far, a comprehensive analysis of miRNA expression in cholangiocytes has yet to be undertaken.

2.1.1 Aims and hypothesis

The aims of this chapter were to:

- Optimize and utilize an isolation protocol for both cholangiocytes and hepatocytes from suitable primary tissue.
- Establish global miRNA expression in these cells by a miRNA microarray.
- Identify translational miRNAs with unique or enriched expression in cholangiocytes.

The main hypothesis within this chapter was that cholangiocytes express unique or enriched miRNAs when compared to hepatocytes when isolated from the same donor, that ultimately allow for the identification of novel candidate circulating biomarker(s).

2.2 Materials and Methods

Unless otherwise stated, all materials were purchased from Sigma Aldrich (Poole, UK).

2.2.1 Human Resection Samples

Human liver tissue was collected from surgical margins of patients undergoing liver resections at Aintree Hospital, Liverpool. Adult patients (age ≥18 years) were recruited to this study and all tissue collection was undertaken with full informed consent and ethical approval from the relevant institutional review boards (National Research Ethics Service REC reference code: 11/NW/0327).

2.2.2 Experimental animals

The protocols described were undertaken in accordance with the criteria outlined in a project licence granted under the Animals Scientific Procedures Act 1986 and approved by the University of Liverpool Animals Ethics Committee. 5-7-week-old male CD-1 mice were purchased from Charles River laboratories (Cambridge, UK) and had a 7-day acclimatisation period prior to experimentation. Animals were maintained in a 12-hour (h) light/dark cycle with free access to food and water.

2.2.3 Immunohistochemical staining of EpCAM positive cells in liver samples

Human liver samples and left median liver lobes were resected and placed in 4 % Paraformaldehyde (PFA) solution for 24-48 h for fixation. Livers were then transferred to 70 % ethanol for long term storage and transport.

Immunohistochemistry of mouse samples were performed in collaboration by Julie Haigh at The School of Veterinary Science, University of Liverpool.

Tissues were dehydrated in a rising concentration of ethanol washes, followed by incubation in xylene. Tissues were then submerged in molten paraffin to create a

tissue block. Blocks were sectioned in 4 µm slices and dried onto polylysine microscope slides. Sections were de-waxed and subjected to low pH antigen retrieval using a Dako autostainer PT link as per the manufacturer's instructions. Slides underwent a peroxidase block for 30 min at room temperature (RT), were washed in 0.1 % Tris-buffered saline with Tween 20 (TBS-T) and then blocked in 10 % horse serum for 10 minutes (min) at RT.

Slides were then incubated with the anti-EpCAM antibodies (anti-mouse G8.8 (DSHB), 1:1 dilution, anti-human HEA125 (Progen, Heidelberg, Germany), 1:10 dilution) in TBS-T for 1 h at RT, washed for 5 min in TBS-T and then incubated with the respective secondary antibody (anti-rabbit BA-4000 (Vector Laboratories Ltd, Peterborough, UK), anti-mouse K5007 (Dako, Denmark), both at a 1:100 dilution for 30 min at RT. Positive staining was detected using an avidin-biotin complex (ABC) stain with a DAB (3, 3 -diaminobenzidine) horseradish peroxidase (HRP) substrate (Vector Laboratories Ltd). Slides were washed three times in dH_2O for 5 min at RT. Slides were stained with Papanicolaou's 1b Haematoxylin for 1 min and tap water was used as a blueing solution. Slides were dehydrated in a rising concentration of ethanol, cleared with xylene and mounted with DPX mounting medium.

2.2.4 Isolation of primary murine cells

Primary mouse hepatocytes and cholangiocytes were isolated using a modified versions of the two-step collagenase methods [185] [186]. Five CD-1 mice were anesthetised by intraperitoneal (i.p) injection of sodium pentobarbital 50 mg/mL (200 mg/kg) (Merial, Lyon, France).

2.2.4.1 Isolation of primary murine hepatocytes

Upon loss of corneal and pedal reflexes, a U-shaped transverse incision was performed on the lower abdomen to the bottom of the ribcage to reveal the intestinal cavity. The intestines were then moved to the right to reveal the hepatic portal vein

and inferior vena cava. A 22 gauge (G) cannula was inserted into the vena cava and a wash buffer (Hank's buffered saline solution (HBSS) x1, 4.3 mM $NaHCO_3$, 250 µM Ethylene diamine tetraacetic acid (EDTA), 20 mM 4-(2-hydroxyethyl)-1-piperazineethanesulfonic acid (HEPES), pH 7.4) was perfused through the liver at a rate of 10 mL/min. The portal vein was immediately cut to allow the liver to clear of blood and the liver was left to perfuse for approximately 8-10 min. The perfusion was then switched to a digestion buffer (HBSS x1, 4.3 mM $NaHCO_3$, 830 µM $MgSO_4$, 5 mM $CaCl_2$, 20 mM HEPES, 0.013% collagenase IV, pH 7.4) for approximately 3-5 min, until the liver was digested.

Following the digestion, the liver was excised and washed with HBSS. The gallbladder was removed, and liver capsule was disrupted using forceps to release the digested hepatic cell mixture. The liver was gently agitated with forceps in HBSS, leaving the biliary tree and a cell suspension. The cell suspension was filtered through a 100 µm cell strainer and biliary tree was placed in HBSS on ice for sequential digestion. To isolate hepatocytes, cells were centrifuged at 50 x *g* at 4 °C for 2 min and the supernatant discarded. The pellet was washed in HBSS twice more using the previous centrifuge conditions.

2.2.4.2 Isolation of primary murine cholangiocytes

All centrifuge steps were performed at 300 x *g* at 4 °C for 5 min and all orbital shaker steps were performed at 30 RPM at 4 °C.

Biliary trees from 4-5 mice were collected as a by-product of the hepatocyte isolation and left gently agitating on an orbital shaker for 15 min to remove any contaminating cells. The tissue was then diced into 0.3-0.5 cm pieces with a scalpel and suspended in digest buffer (RPMI media with 200 µg/mL DNase I, 320 µg/mL collagenase I and 480 µg/mL hyaluronidase) and was left in an agitating water bath at 37 °C for 20 min.

The tissue was pelleted, washed in HBSS and re-pelleted. The tissue was re-suspended in another digest buffer (Phosphate buffered saline (PBS) with 200 µg/mL EDTA and 1 mg/mL trypsin) and was left in an agitating water bath at 37 °C for 5 min. The digestion was stopped by the addition of isolation buffer (RPMI media with 10 µg/mL DNase I) supplemented with 10 % foetal bovine serum (FBS) and cells were further incubated in an agitating water bath at 37 °C for 5 min. The mixture was then pelleted and resuspended in isolation buffer. Any remaining clumps were removed by passing the mixture through a 19 G needle, followed by a 22 G needle. Finally, the mixture was passed through a 100 µm cell strainer to isolate single cells. The single cell suspension was divided between 4 tubes to maximise cholangiocyte yield. The suspension was pelleted and then resuspended in isolation buffer and an anti-EpCAM hybridoma antibody (G8.8, DSHB, IA, US) at a 1:5 dilution. Cells were incubated at 4 °C with gentle agitation for 30 min before being pelleted and washed with HBSS. Cells were resuspended in isolation buffer and 1 % anti-rat immunomagnetic beads (11035, Invitrogen, Vilnius, Lithuania) that were prepared as per the manufacturer's instructions. Cells were incubated at 4 °C with gentle agitation for 30 mins. Cells were passed through a DynaMag-15 magnet (ThermoFisher, UK) and cholangiocytes were retained through positive magnetic immunoaffinity selection.

2.2.5 Immunoblotting of protein lysates

Isolated hepatocytes and cholangiocytes were homogenised in Radioimmunoprecipitation assay (RIPA) buffer for 15 min on ice with intermittent vortexing and centrifuged at 15,000 x *g* for 15 min at 4 °C. The resulting supernatant was retained, and protein concentration was determined by BCA assay. Samples were prepared for loading by mixing with NuPage sample reducing agent and NuPage LDS sample buffer (ThermoFisher) and then denatured at 90 °C for 5 min. Protein separation was performed on 4-12 % NuPage polyacrylamide gels at 170nV for 70 min in NuPage MOPS running buffer (ThermoFisher). The resolved proteins were

transferred to a nitrocellulose membrane at 230 mA for 70 min in a 20 % methanol tris-glycine buffer. Successful transfer and even loading were confirmed with Ponceau Red stain. Membranes were washed in 0.1 % TBS-T and blocked in 5 % non-fat dried milk for 1h at RT. The appropriate membranes were then probed with anti-albumin (ab207327, Abcam (Cambridge, UK), 1:2,000 in 2.5 % milk), anti-CK19 (ab52625, Abcam, 1:40,000 in 2.5 % milk), anti-α-tubulin (T6199, 1:5,000 in 2.5 % milk) and anti-β-actin (ab8227, Abcam, 1:10,000 in 2.5 % milk) overnight with gentle agitation at 4°C.

The primary antibody solutions were discarded, and the membranes were washed 5 x 5 min in 0.1 % TBS-T. The membranes were then incubated with anti-mouse IgG (A9044, 1:5,000 in 2.5 % milk) or anti-rabbit IgG (A9169, 1:5,000 in 2.5 % milk) for 1 h with gentle agitation at RT. The secondary antibody solutions were discarded, and the membranes were washed 5 x 5 min in 0.1 % TBS-T, before being treated with a chemiluminescent substrate (PerkinElmer, MA, US). Proteins were visualised by exposure to X-ray film in a dark room.

2.2.6 Suspension immunofluorescence staining

All centrifuge steps were performed at 300 x *g* at RT for 5 min, unless otherwise stated, all incubation steps were performed on an orbital shaker at 30 RPM at 4 °C.

Freshly isolated hepatocytes and cholangiocytes were washed in PBS and pelleted before being resuspended in 4 % PFA. Cells were incubated for 30 min, before being pelleted and washed twice with PBS. Cells were then incubated with permeabilising buffer (PBS with 0.5 % Triton-X and 0.2 % Tween-20) for 30 min. Cells were washed in PBS and then incubated with blocking buffer (permeabilising buffer with 10 % goat serum or 10 % casein-blocking solution) at RT for 30 min. After blocking, cells were pelleted and resuspended with blocking buffer with either anti-CK19 (ab52625, Abcam, 1:500) or anti-albumin (ab207327, Abcam, 1:200) antibodies and left to incubate overnight.

Cells were pelleted and washed with permeabilising buffer three times and resuspended in blocking buffer with anti-rabbit Alexa Fluor 488 (ab150077, Abcam, 1:500) or anti-rabbit Alexa Fluor 647 (ab150083, Abcam, 1:500) and left to incubate for 1 h. Hoechst reagent was added at a 1:5,000 dilution and cells were incubated for a further 20 min at 4 °C. Labelled cells were washed once with permeabilising buffer and once with PBS. Finally, cells were resuspended in ProLong gold (ThermoFisher) and mounted on coverslides. Maximum intensity projection (MIP) images were captured on an Axio observer Z1 microscope (Zeiss, Germany).

Purity was calculated as a percentage by counting positively stained cells (albumin or CK19) in the population of total cells (Hoechst) of three separate areas of the slide from independent isolations (n=3).

2.2.7 Total RNA extraction

Total RNA was isolated from hepatocytes and cholangiocytes by the miRNeasy mini extraction kit (Qiagen, Venlo, Netherlands) as per the manufacturer's instructions. Briefly, 700 µL of Qiazol reagent was added to the cells. Samples were vortexed and incubated for 5 min at RT to ensure complete lysis and then spiked with the exogenous miRNA cel-lin 4 to a final concentration of 10 pM (Applied Biosystems, UK). 140 µL of chloroform was added to the samples, which were vortexed and centrifuged at 12,000 x *g* at 4 °C for 15 min. Approximately 350 µL of the resulting upper aqueous solution was then transferred to a new microcentrifuge tube. The RNA extraction was automated by the Qiacube liquid handler (Qiagen), using the manufacturer's protocol, "Aqueous phase- Total RNA_V2" from their online protocol repository. RNA concentration and purity were assessed on a NanoDrop1000 (ThermoFisher).

2.2.8 Assessing differences in global miRNA expression in murine primary cells

2.2.8.1 Preparation of samples for microarray analysis

The miRNA microarray of mouse hepatocytes and cholangiocytes was performed in collaboration with Dr. Carolyn Jones at The MRC Toxicology Unit, University of Leicester.

Before proceeding with the microarray, the total RNA underwent a quality control on an Agilent 2100 Bioanalyzer using an RNA 6000 Nano kit as per the manufacturer's instructions (Agilent). Total RNA was prepared for the microarray using miRNA Complete Labelling and Hybridisation Kit, miRNA Spike-In Kit and Gene Expression Wash Buffer Kit as per the manufacturer's instructions (Agilent, CA, US).

In order to label the miRNA, 100 ng of total RNA was combined with CIP mastermix to a total of 4 µL. RNA was incubated at 37 °C for 30 min in order to dephosphorylate the samples. 2.8 µl of 100% Dimethyl sulfoxide (DMSO) was added and the samples were incubated at 100 °C for 10 min to denature the samples. Finally, the 3'-end of RNAs were labelled with pCp-Cy3 upon incubation with a T4 RNA ligation master mix for 2 h at 16 °C.

Labelled miRNAs were purified using Micro Bio-Spin 6 columns kit (Bio-Rad) as per the manufacturer's instructions and eluted RNA was formed into a dried pellet using a DNA SpeedVac (ThermoFisher). To hybridise miRNAs to the microarray chip, the pelleted RNA was resuspended in nuclease free ddH_2O and mixed with the hybridisation master mix and incubated 100 °C for 5 min. The resulting mixture was loaded onto the microarray chip (SurePrint Mouse miRNA Microarray, Release 21.0, Agilent) and placed into a hybridisation oven at 55 °C for 20 h at 20 RPM. Microarray slides were then washed twice with wash buffer, before being scanned using a G2505C microarray scanner (Agilent) and the raw microarray data extracted.

2.2.8.2 Microarray analysis

The analysis of the microarray data was performed in collaboration with Dr. Ben Francis at Biostatistics Department, University of Liverpool.

The raw dataset was analysed using the Agilent Feature Extraction (AFE) software (Agilent). The AFE algorithms estimate a quality control of the data as well as a summarised signal for each identified miRNA, termed as the total gene signal (TGS). The TGS was then further analysed in the R statistics package, using the AgiMicroRna library, an open source Bioconductor package [187]. The AgiMicroRna library allowed a further QC of the data by producing principle component analysis (PCA) and differential expression analysis of the microarray data.

The data were subject to quantile normalisation and differential expression analysis using both a t-test and Significance Analysis of Microarrays (SAM). Reported miRNA values are stated as normalised relative fluorescence units (RFU) and those miRNAs with an FDR ≤ 5 % from the SAM analysis were retained as candidate biomarkers. Fold change relative to cholangiocytes for miRNAs was calculated by $2^{(\text{Log2 cholangiocyte gene expression} - \text{Log2 hepatocyte gene expression})}$.

2.2.8.3 Triage of microarray data to identify candidate miRNA biomarkers

Each detected miRNA was initially stratified according to if their expression was unique to cholangiocytes or shared with hepatocytes. All miRNAs with inconstant expression across biological replicates were removed, along with miRNAs identified to be false positive by miRBase V.21.

All miRNAs that exhibited significantly enriched or unique expression in cholangiocytes by SAM analysis were retained. Finally, any miRNAs that were specific to mouse, without a human equivalent according to miRBase V.22, were removed from downstream analysis.

2.2.8.4 Tissue distribution of miRNAs

A publicly available miRNA high-throughput Solexa deep sequencing library of 14 different tissues in mouse was downloaded (Gene expression omnibus accession: GSE67885)[188]. The individual reads for each miRNA expressed in liver, cerebrum, spleen, stomach, kidney, oesophagus, small intestine, cerebellum, lung, ovary, uterus, heart, colon and pancreas were cross referenced against the miRNAs of interest. The total reads of each miRNA in each tissue were listed to assess total gene expression, alongside individual miRNA reads in the liver expressed as a percentage of the total reads, to assess liver specificity.

2.2.9 Quantitative polymerase chain reaction (qPCR)

Specific miRNAs of interest were measured using TaqMan qPCR. Total RNA extraction was performed on primary murine hepatocytes and cholangiocytes as outlined in section 2.2.7.

Total RNA was reverse transcribed using specific stem-loop primers for each individual miRNA species of interest (mmu-miR-200b-3p, mmu-miR-200c-3p, mmu-miR-429, cel-lin-4-5p, snoRNA202) and the TaqMan MicroRNA Reverse Transcription Kit, according to the manufacturer's instructions (Applied Biosystems).

Total extracted RNA was diluted to 2 ng/mL and combined with the reverse transcription master mix to a total volume of 15 µL. cDNA was generated on a GeneAmp PCR System 9700 (ThermoFisher) thermocycler at: 30 min at 16 °C, 30 min at 42 °C, 5 min at 85 °C and a 4 °C hold. Then, 2 µL of cDNA was added to the corresponding specific TaqMan qPCR primer and PCR mastermix according to the manufacturer's instructions. All liquid handling was automated by a QIAgility robot (Qiagen) and all samples were loaded into PCR plates in duplicate. Samples underwent the qPCR reaction in a ViiA 7 (Applied Biosystems) with the following conditions: 2 min at 50 °C, 10 min at 95 °C and then 50 cycles of 15s at 95 °C and 60

s at 60 °C. Ct values were determined using the fluorescence signal produced from the TaqMan probes. Cel-lin-4 was used as an exogenous normaliser and snoRNA-202 was used as an endogenous normaliser. Fold change in expression of miRNA was calculated by the $2^{-\Delta\Delta Ct}$ method [189].

2.3 Results

2.3.1 Identification of antibodies suitable for isolation of primary cholangiocytes

To accurately understand the global miRNA expression of cholangiocytes and hepatocytes, pure populations of each cell type needed to be isolated from whole liver tissue. As the isolation of cholangiocytes is performed by positive selection immunoaffinity purification, it was imperative to use an antibody with high specificity for a unique cholangiocyte cell surface antigen in order to minimise contamination of other cell types. Both cholangiocytes and hepatocytes are hepatic epithelial cells, although the expression of epithelial cell adhesion molecule (EpCAM) is unique to cholangiocytes. Different monoclonal anti-EpCAM antibodies positively stained bile duct structures without non-specific binding to other cell types (Fig 2.1), indicating they would be suitable for isolating primary cholangiocytes from either mouse or human livers.

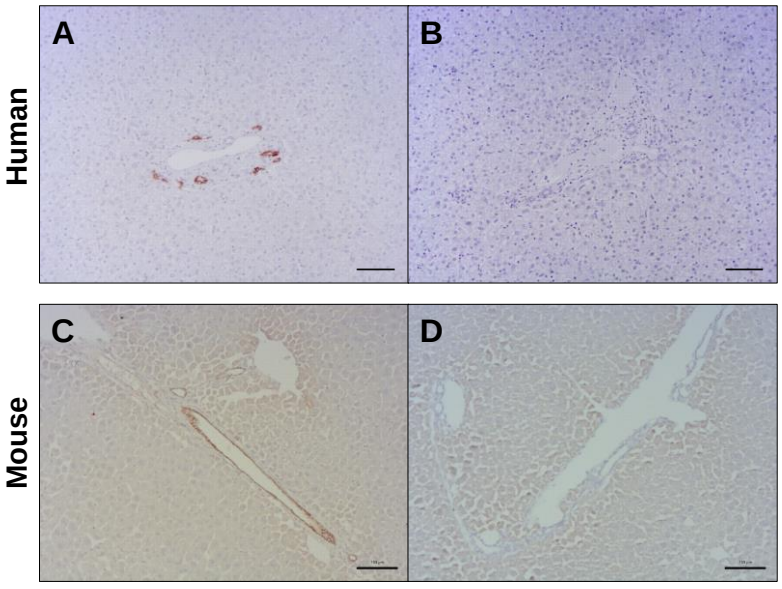

Figure 2.1- Anti-EpCAM antibodies specifically stain cholangiocytes in mouse and human livers.

Healthy tissue from resected human liver (A) and a CD-1 mouse (C) were stained for the unique cholangiocyte marker EpCAM with two different monoclonal antibodies. A negative control with no primary antibody was used for comparison (B,D). Magnification x10, scale bar 100 µm.

2.3.2 Histopathological scoring of human liver samples

It was important to ensure that miRNAs in both cholangiocytes and hepatocytes were only expressed under normal conditions in healthy tissue, as perturbations in the liver can induce differential expression in the basal miRNAome.

When assessing the quality of the anti-EpCAM antibody in human tissue, multiple human samples presented with biliary hyperplasia (Fig 2.2A) and immune infiltration (Fig 2.2B) in the periportal area. Areas of lipid deposition were also noted throughout the liver (Fig 2.2B).

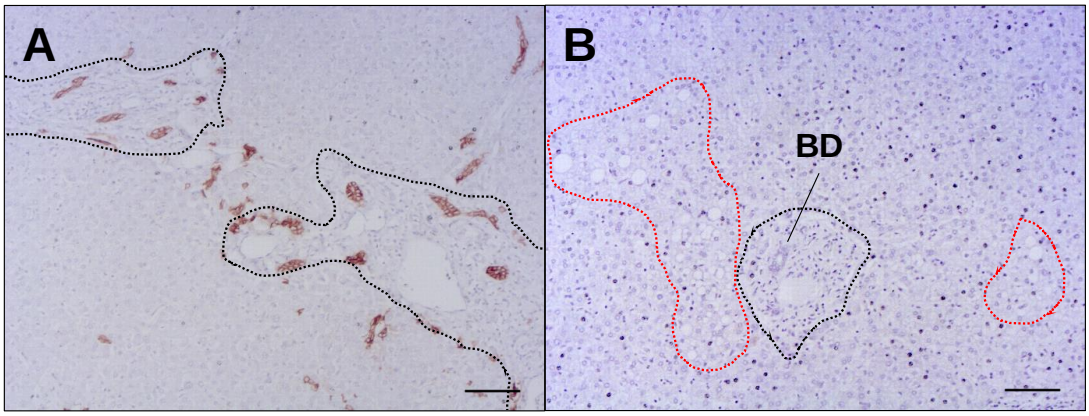

Figure 2.2- Evidence of periportal injury in representative healthy human liver samples

(A) EpCAM+ stained bile ducts in human liver reveal atypical bile duct growth and formation, throughout the periportal area. (B) Red dotted areas indicate areas of lipid deposition and black dotted areas show inflammation/fibrosis around the periportal area of the liver. BD= Bile duct. Magnification x10, scale bar 100 µm.

A total of 17 human resected liver samples were therefore collected in order to assess the quality of the tissue. Although this tissue was designated healthy by surgical margins, human liver samples typically came from elderly patients undergoing a form of cancer resection, who typically present with several comorbidities and are taking multiple medications at the time of hospital administration. Further patient histories revealed donors were diagnosed with liver cirrhosis (n=4) and undefined liver disease (n=2), secondary to the cause of resection. Details of these patients are listed in Table 2.1

	Human resected samples (n=17)	
	Male (n=12)	**Female (n=5)**
Age	61.5 ± 13.0	66.8 ± 30.5
BMI	27.6 ± 3	21.1 ± 2.5
# medications taken	5.4 ± 3.1	3.5 ± 2.6
Hypertensive		
Yes	6	1
No	6	2
N/A	0	2
Diabetic		
Yes	1	1
No	10	4
N/A	1	0
Cause for resection		
Primary liver tumour (HCC/CCA)	4	2
Liver metastasis	8	2
Bile duct stones	0	1

Table 2.1- Patient information of resected human liver samples.

Representative healthy liver samples (n=17) defined from surgical margins was collected alongside patient's medical history in order to evaluate tissue quality. Patients age, BMI and number of medications taken at time of hospital admission are presented as mean ± SD.

The human liver samples underwent histological review by a trained pathologist who assessed the tissue for fibrosis, immune cell infiltration and lipid deposition. Altogether, 17/17 patients presented with at least mild lipid deposition, mild periportal fibrosis and mild periportal inflammation (Table 2.2). Given the location of cholangiocytes in the periportal region of the liver, it was deemed that cholangiocytes isolated from human liver samples could not be truly classed as healthy cells when compared to those derived from naïve mouse livers.

Patient #	Fibrosis	Inflamation	Lipid Deposition
1	Mild, PP only	Mild, PP only	Mild
2	Mild, PP only	Mild, PP only	Moderate/ Severe
3	Moderate, PP only	Moderate, PP only	Moderate/ Severe
4	Mild, PP only	Mild, PP only	Mild
5	Mild/Moderate, PP only	Moderate, PP only, Interstitial	Moderate/ Severe
6	Mild, PP only	Mild, PP only	Mild
7	Mild, PP only	Mild, PP only	Mild
8	Mild, PP only	Mild, PP only	Mild
9	Moderate/Severe, local bridging	Moderate, PP only, Interstitial	Moderate
10	Mild, PP only	Mild, PP only	Moderate
11	Mild, PP only	Mild/Moderate, PP only, Interstitial	Mild
12	Moderate, initial bridging	Moderate, PP only	Mild
13	Mild, PP only	Mild, PP only	Mild
14	Mild, PP only	Mild, PP only	Moderate
15	Mild, PP only	Mild, PP only	Mild
16	Mild, PP only	Mild, PP only	Mild
17	Moderate, PP only	Moderate, PP only	Mild

Table 2.2- All representative healthy human liver samples show some degree of periportal injury.

Representative healthy liver samples (n=17) were scored by a trained pathologist for fibrosis, inflammation and lipid deposition as none, mild, moderate or severe. All liver samples were scored as at least mild for all criteria, with inflammation and fibrosis specifically affecting the periportal area.

2.3.3 Isolation protocols produce viable and pure populations of cells

Based on the unsuitable condition of the human tissue, the CD-1 mouse was chosen to isolate healthy cholangiocytes and hepatocytes. Optimisation of isolation procedures reported in section 2.2.4 successfully revealed biliary structures from the liver (Fig 2.3A), which allowed subsequent digestion for individual cholangiocytes.

Isolated hepatocytes and cholangiocytes had a viability of ≥85 % by trypan blue staining. To assess the initial success of an isolation, isolated hepatocytes and cholangiocytes were lysed and probed for the positive specific cell markers, albumin and CK19 respectively, by western blot (Fig 2.3B). The HepG2 hepatocellular carcinoma cell line was used as a positive control, as it expresses both albumin and CK19. Independent isolations of hepatocytes and cholangiocytes (n=3) stained positively for their respective cell markers, indicating successful isolations for each cell type.

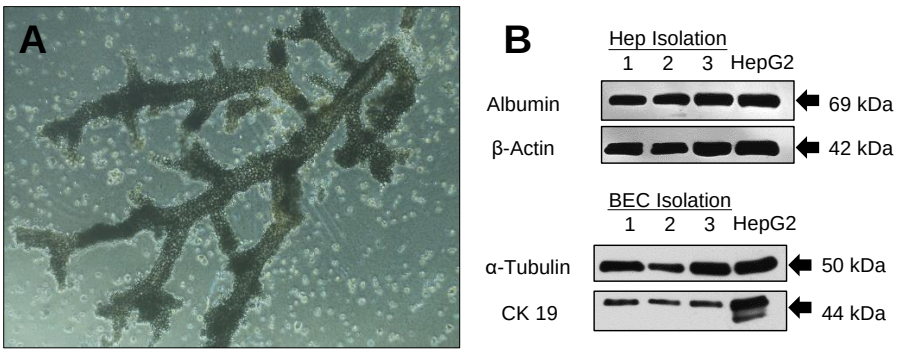

Figure 2.3- Isolated hepatocytes and cholangiocytes are positive for their respective unique cell markers.

(A) Fragments of the biliary tree, which is subsequently further digested to isolate cholangiocytes, magnification x10. (B) Isolated murine hepatocytes and cholangiocytes from independent isolations (n=3) are positive for albumin and CK19 respectively by western blotting. HepG2 was used as a positive control for both cell types.

Importantly, western blot does not reveal the purity of isolations, and as freshly isolated cell samples would be lysed immediately for microarray preparation, a suspension immunofluorescence was performed. This allowed the assessment of the purity of freshly isolated cells without the need for plating, which could cause contaminating cells to die off due to selective media. Albumin and CK19 were used to positively identify each cell type. The technique was initially validated in HepG2 cells to assess sufficient, uniform staining (Fig 2.4).

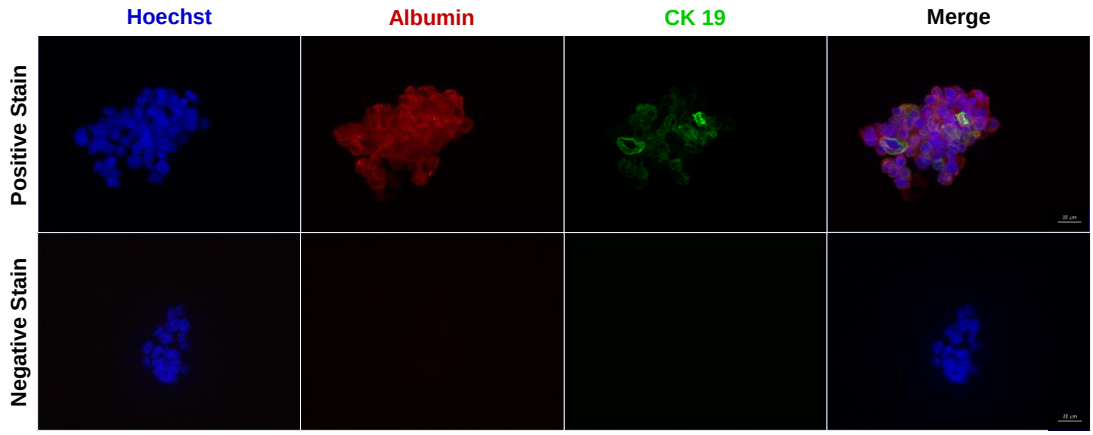

Figure 2.4- Validation of the suspension immunofluorescence technique in HepG2 cells

Adherent HepG2 cells were placed into suspension and stained for the hepatocyte marker albumin (red), the cholangiocyte marker CK19 (green) and Hoechst (blue). A negative control with no primary antibody was used for comparison. Scale bar 20 µm.

Following isolation, hepatocyte purity was calculated at ≥97 % (Fig 2.5). Other features of hepatocytes such as large cell size and binucleation aided cell identification. Cholangiocyte yield was predictably lower than hepatocytes, with a purity of ≥94 % (Fig 2.6A). Further to the CK19 stain, a brightfield channel highlighted the DynaBeads physically bound to the cholangiocytes via the anti-EpCAM antibody used in the isolation (Fig 2.6B). Therefore, the isolation protocols for hepatocytes and cholangiocytes produced effectively pure populations of each cell type to be used on the microarray.

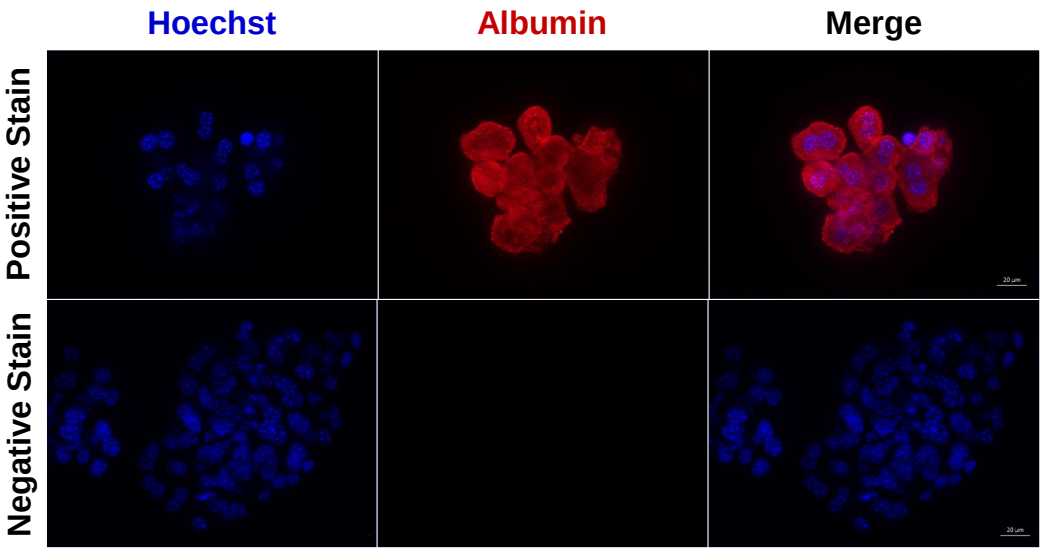

Figure 2.5- Hepatocytes isolations are shown to be highly enriched by suspension immunofluorescence.

Freshly isolated hepatocytes were stained for the hepatocyte marker albumin (red) and Hoechst (blue). Purity of the isolations was calculated as a percentage of albumin+ stained cells (red) relative to all cells (blue). A negative control with no primary antibody was used for comparison. Scale bar 20 µm.

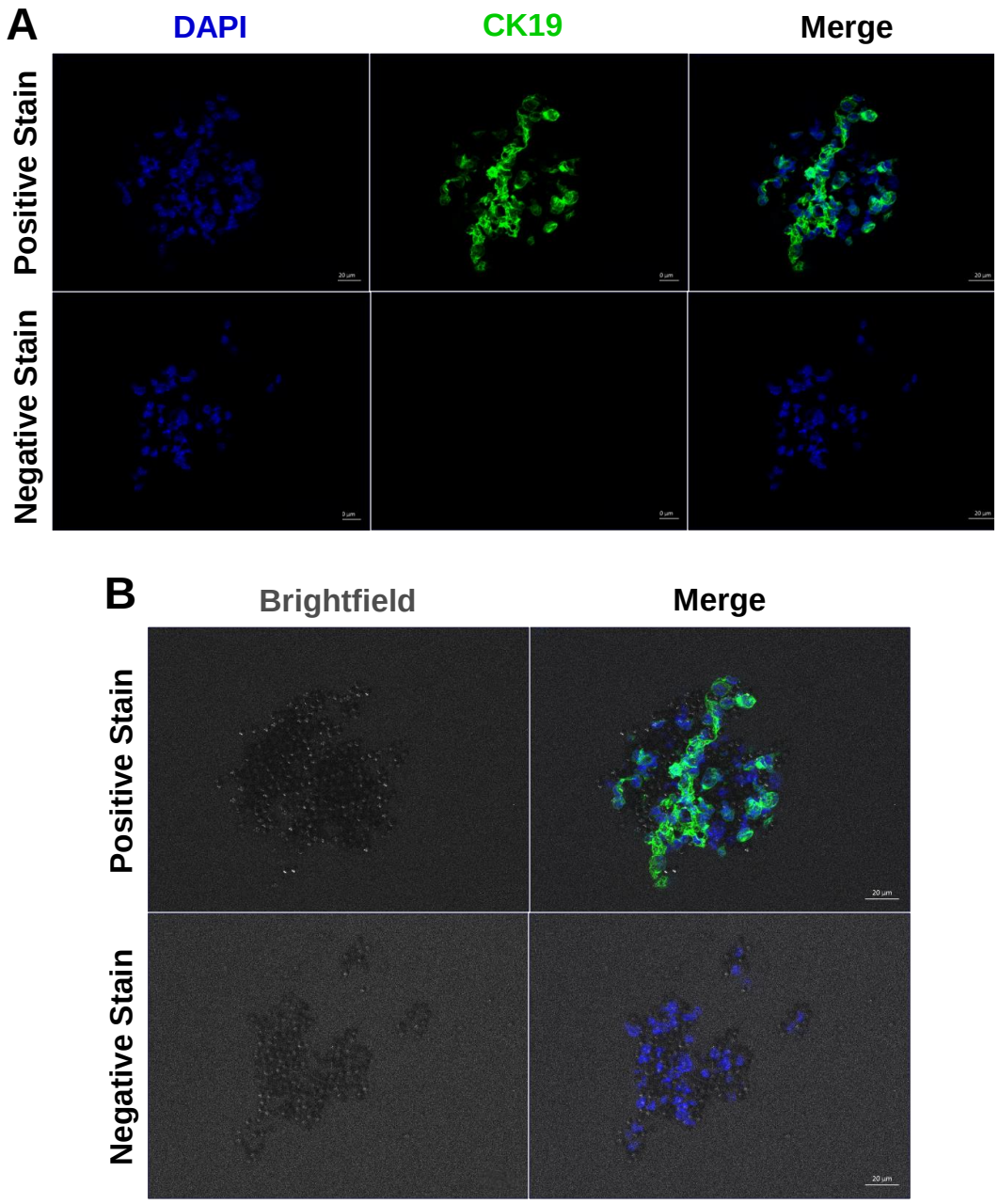

Figure 2.6- Cholangiocyte isolations are shown to be highly enriched by suspension immunofluorescence.

(A) Freshly isolated cholangiocytes were stained for the cholangiocyte marker CK19 (green) and Hoechst (blue). Purity of the isolations was calculated as a percentage of CK19+ stained cells (green) relative to all cells (blue). A negative control with no primary antibody was used for comparison. Scale bar 20 µm. (B) A brightfield view of isolated cholangiocytes reveals immunomagnetic beads used in the isolation protocol, bound to the unique cholangiocyte marker EpCAM. A negative control with no primary antibody was used for comparison. Scale bar 20 µm.

2.3.4 Isolated total RNA from hepatocytes and cholangiocytes is high quality

As RNA is prone to degradation, the accurate assessment of its integrity is one of the most critical steps for the success of any downstream analysis. Therefore, total RNA isolated from hepatocytes and cholangiocytes (n=4) was assessed on an Agilent 2100 Bioanalyzer. The bioanalyzer produces an electropherogram and gel-like image and scores an RNA integrity number (RIN) between 1-10 (severely degraded to most intact, respectively) based on a complex algorithm of the entire electrophoretic trace. It is accepted that for sensitive RNA applications, a RIN score of at least seven is required.

Total RNA from hepatocytes was determined to be high quality with strong peaks at the 28S and 18S rRNA fragment regions. There was minimal generation of shorter RNA fragments, indicating little to no degradation (Fig 2.7A, Fig 2.7C), which is reflected in the high average RIN score of 9.85 (Fig 2.7D). The total RNA from cholangiocytes displayed some degradation, shown by the increase in absorption spectra of shorter fragments (200-100 NT) when compared to hepatocytes (Fig 2.7B). This is more clearly recognised in the simulated gel image (Fig 2.7C). However, the RNA was still of sufficient quality for the microarray, with an average RIN score of 7.78 (Fig 2.7D).

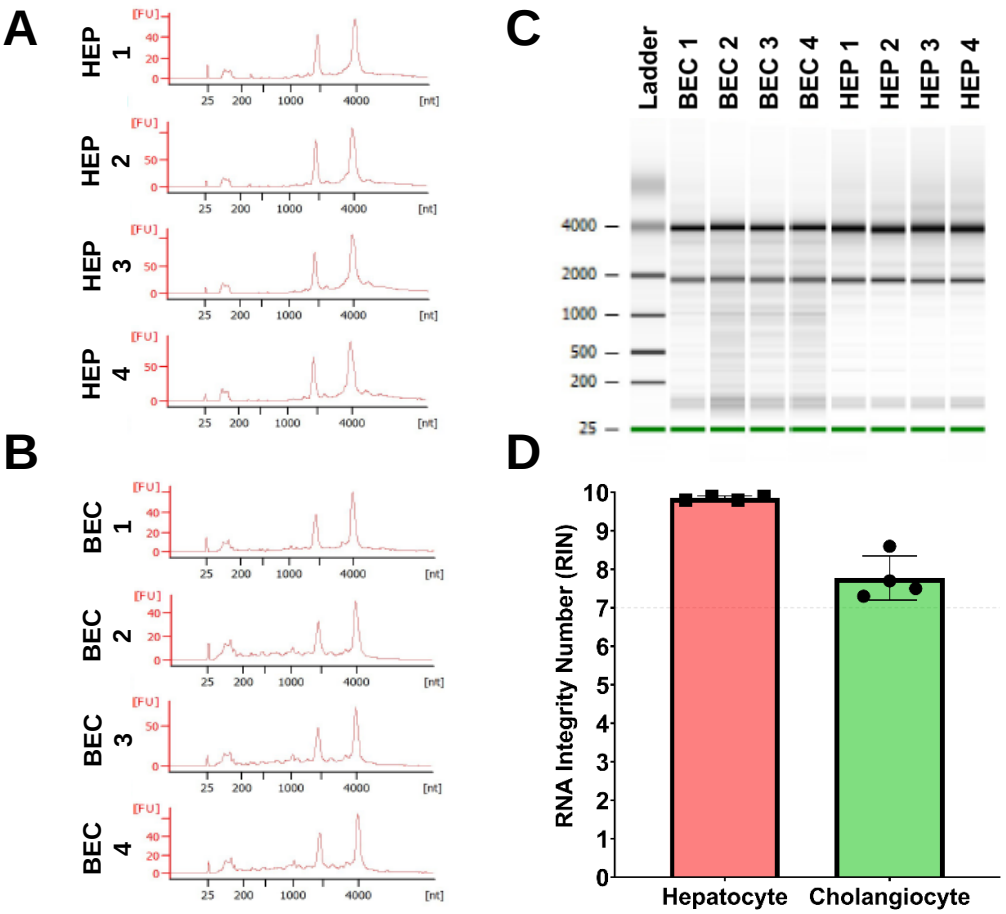

Figure 2.7- Isolated hepatocytes and cholangiocytes produce high quality total RNA.

RNA was extracted from isolated hepatocytes and cholangiocytes and assessed on an Agilent Bioanalyser. An electrophoretic trace for hepatocytes (A) and cholangiocytes (B) and gel-like image of both cell types (C) reveal minimal RNA degradation. (D) RNA Integrity Number (RIN) scores for both isolated cell types were acceptable (>7) for the microarray. Data shown as mean ± SD, n=4.

2.3.5 Initial microarray output reveals similar gene expression between hepatocytes and cholangiocytes

Global miRNA expression profiles in hepatocytes and cholangiocytes were evaluated by SurePrint Mouse miRNA Microarray (Release 21.0), which contains probes for 1,881 murine miRNAs.

The initial data from the array was subject to quality control by AFE and AgiMicroRna software packages to ensure the microarray was correctly prepared, the necessary controls were functional, and that the downstream analysis of candidate biomarkers

was accurate. Principal component analysis (PCA) of all samples revealed a hepatocyte sample that had not grouped with the other hepatocyte biological repeats, indicated by the red circle (Fig 2.8A). Consequently, this sample and its matched cholangiocyte variant were removed from all subsequent analysis.

Following quality control and normalisation of the microarray data to internal and spike-in controls, a total number of 276 miRNAs were detected in total across all samples. Of these, 178 miRNAs were shared between hepatocytes and cholangiocytes, 93 were unique to cholangiocytes and 5 unique to hepatocytes (Fig 2.8B).

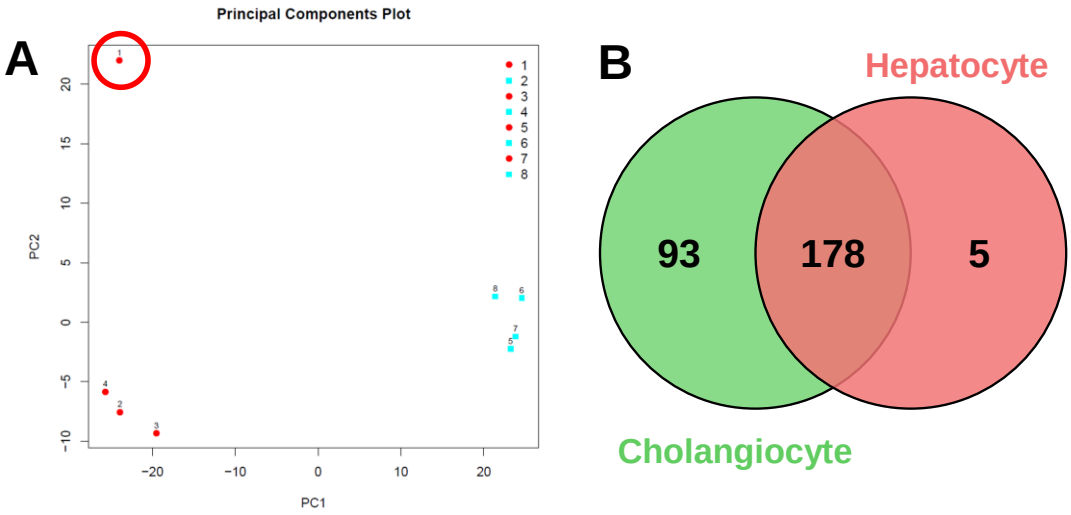

Figure 2.8- Quality control of the microarray reveals large population of uniquely expressed miRNAs in cholangiocytes

(A) Principal component analysis (PCA) revealed a hepatocyte isolation (circled in red) that did not cluster with other isolations. The sample and its matched cholangiocyte variant were removed from downstream analysis. (B) Initial analysis of the array detected 276 miRNAs (178 shared, 93 cholangiocyte unique, 5 hepatocyte unique) miRNAs in all samples.

2.3.6 Identification of unique or enriched miRNAs in cholangiocytes

As the overarching aim of this work was to identify uniquely expressed or enriched miRNAs in cholangiocytes, data from the array was triaged as outlined in section 2.2.9.1 in order to identify candidate circulating miRNA biomarkers of DILI.

Briefly, miRNAs with inconsistent detection across all biological replicates in the microarray were removed from downstream analysis as well as miRNAs identified as false positives by miRBase V.20 [190]. This resulted in 69 unique and 134 shared miRNAs expressed in cholangiocytes (Fig 2.9**)**.

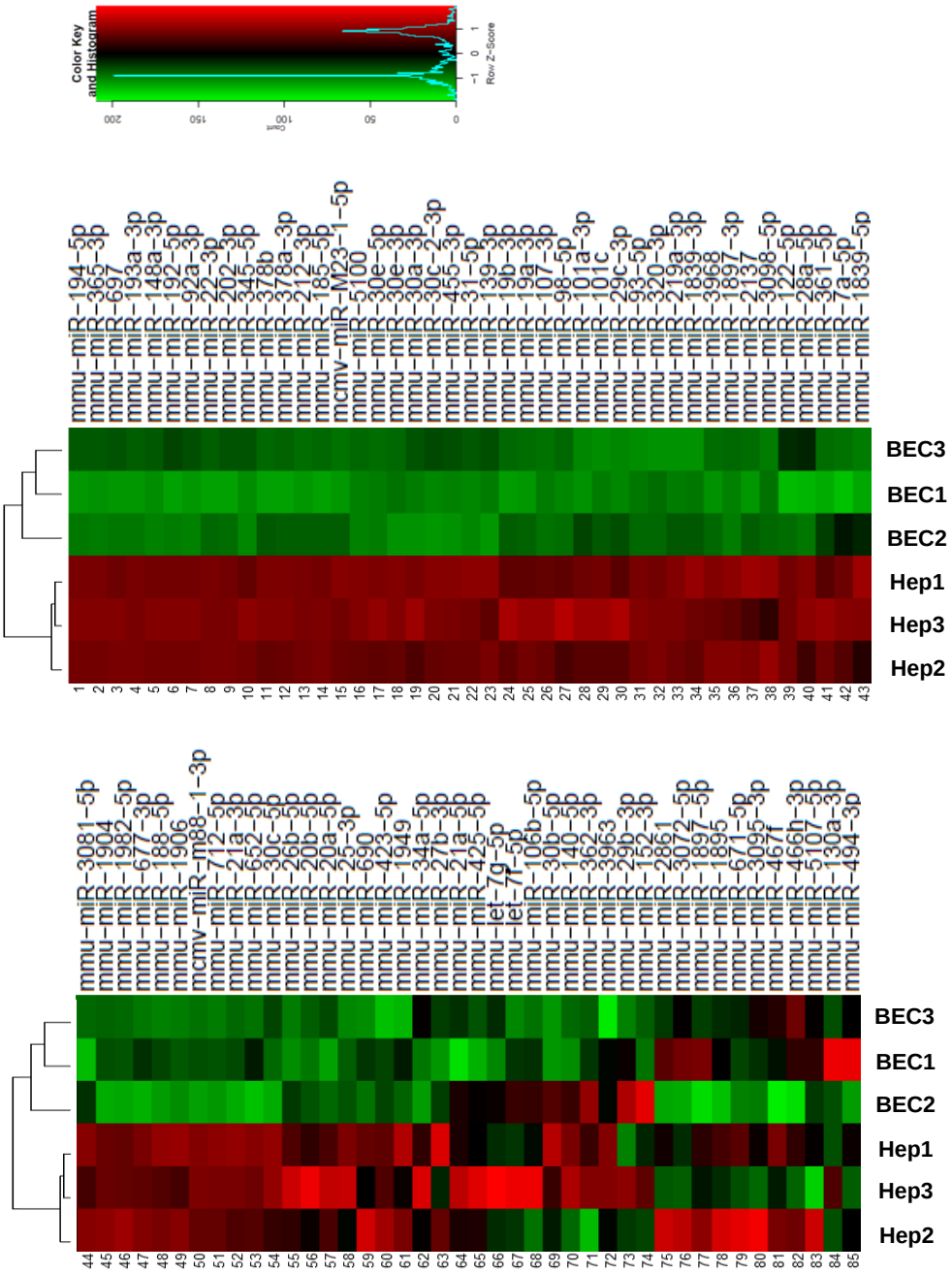

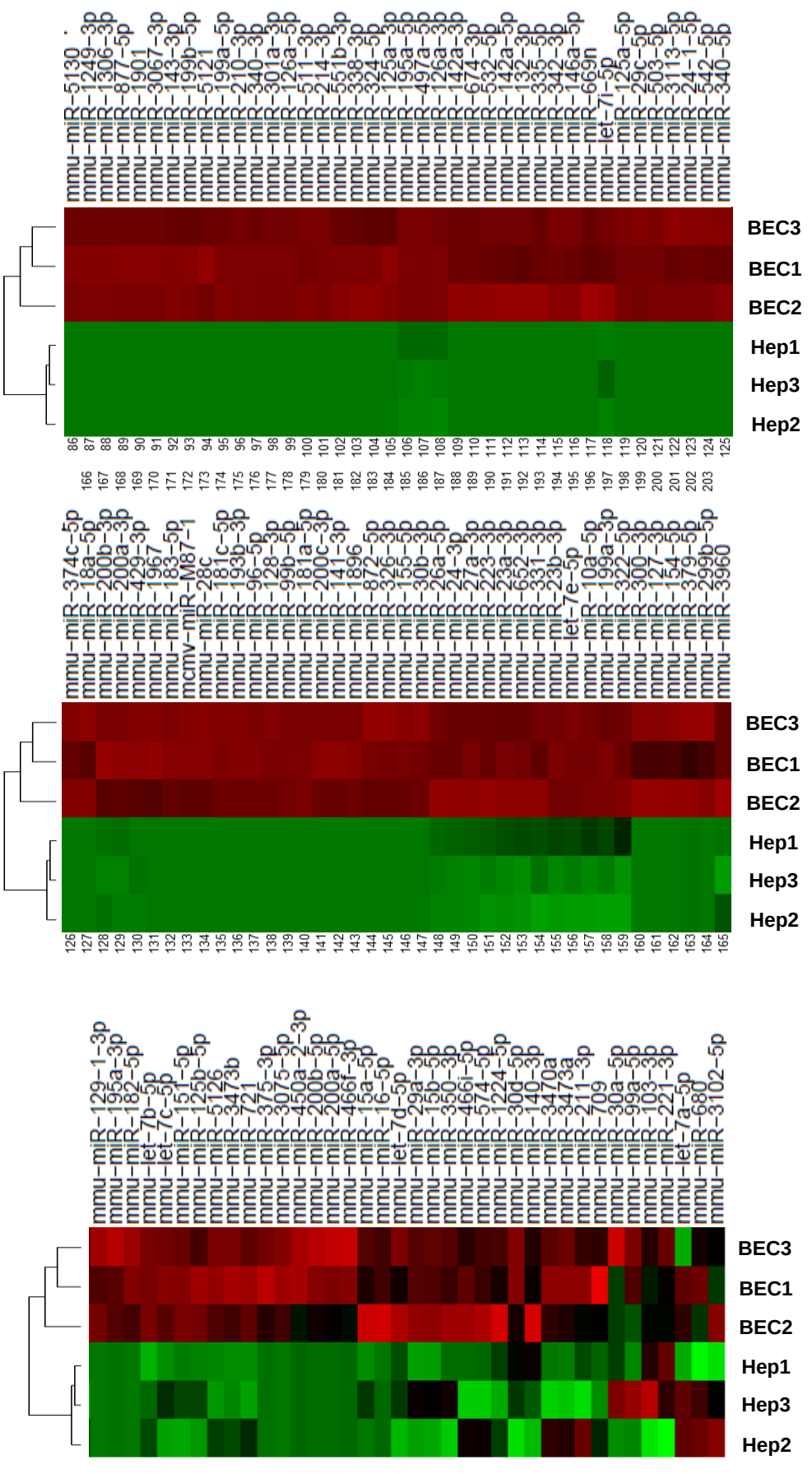

Figure 2.9- Characterisation of miRNA expression in mouse hepatocytes and cholangiocytes

A Heatmap of unique (n=69) and shared (n=134) cholangiocyte miRNAs was generated, following removal of inconsistent replicates and false positive miRNAs (n=3).

One of the reasons why miR-122 is an attractive biomarker is due to its abundance in hepatocytes, so miRNAs from both cell types were ranked in descending order of expression to determine if a cholangiocyte equivalent existed. However, a comparison of the top 25 expressed miRNAs revealed very similar expression profiles between hepatocytes and cholangiocytes (Fig 2.10). There were no uniquely expressed miRNAs in the most abundant cholangiocyte miRNAs (Fig 2.10A) and 19/25 miRNAs were also detected in the most abundant hepatocyte miRNAs (Fig 2.10B).

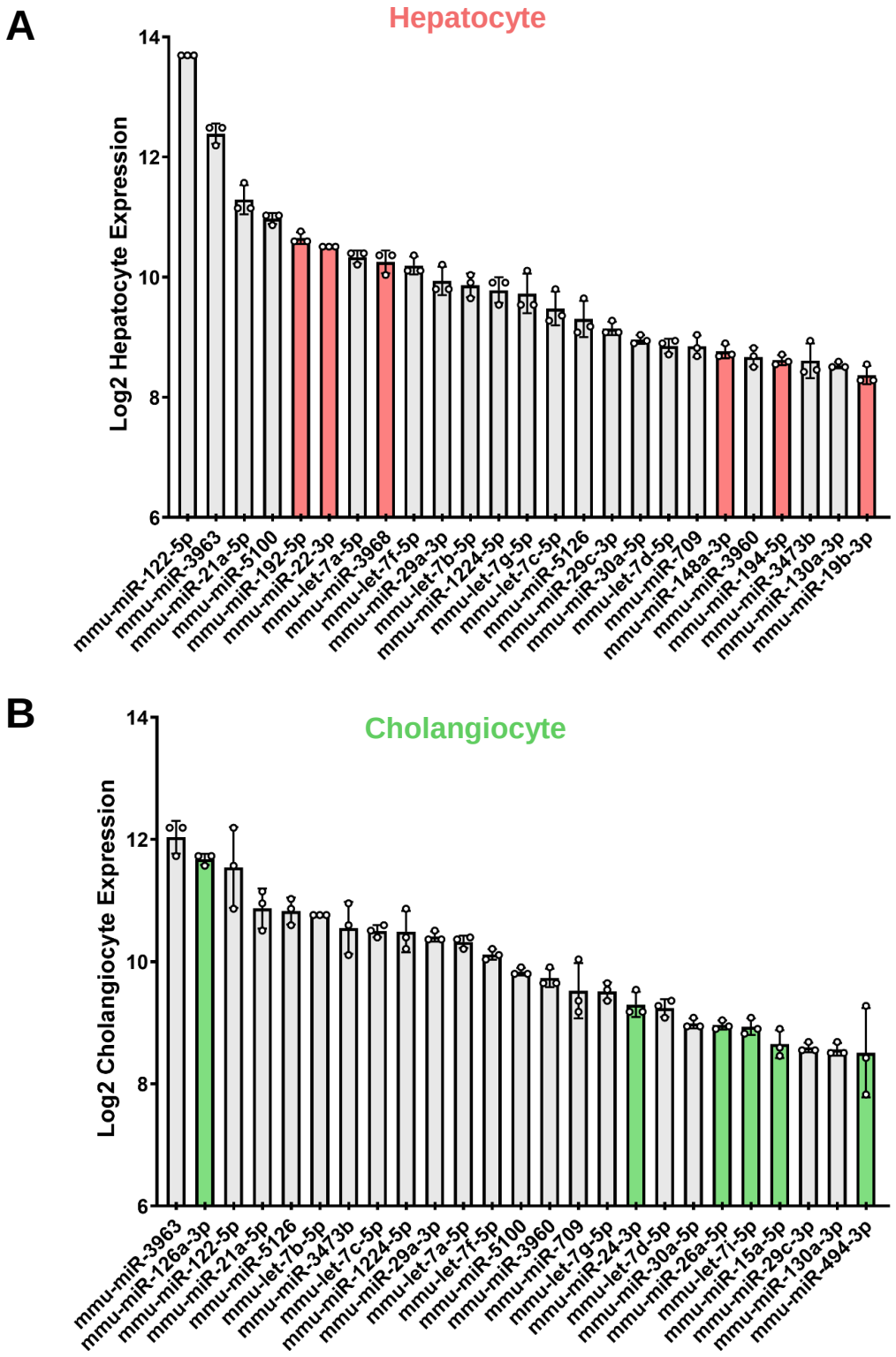

Figure 2.10- The top 25 most abundantly expressed miRNAs in each cell type are similar

The most abundant miRNAs in hepatocytes (A) and cholangiocytes (B) were ranked in decreasing order of their log2 gene expression from the microarray. 19/25 miRNAs were expressed in the most abundant miRNAs in both hepatocytes and cholangiocytes; those miRNAs not shared in the most abundant miRNAs are highlighted in red and green for hepatocytes and cholangiocytes, respectively.

Therefore, to identify desirable cholangiocyte miRNA biomarkers with high abundance, a more targeted approach was taken. The top 25 uniquely expressed miRNAs were ranked in descending order of abundance (Fig 2.11A). Also, the basal expression of cholangiocyte enriched shared miRNAs was plotted against their fold change expression over hepatocytes (Fig 2.11B). This identified miRNAs with both high basal expression and enrichment over hepatocytes.

The 69 unique and 134 shared miRNAs of interest, previously identified in section 2.3.6, were further subject to statistical analysis by SAM in order to identify miRNAs with significantly different expression in cholangiocytes over hepatocytes. The miRNAs of interest were defined as those with an FDR <5 %. A complete listing of these miRNAs, their expression and significance is listed in appendix 2.1.

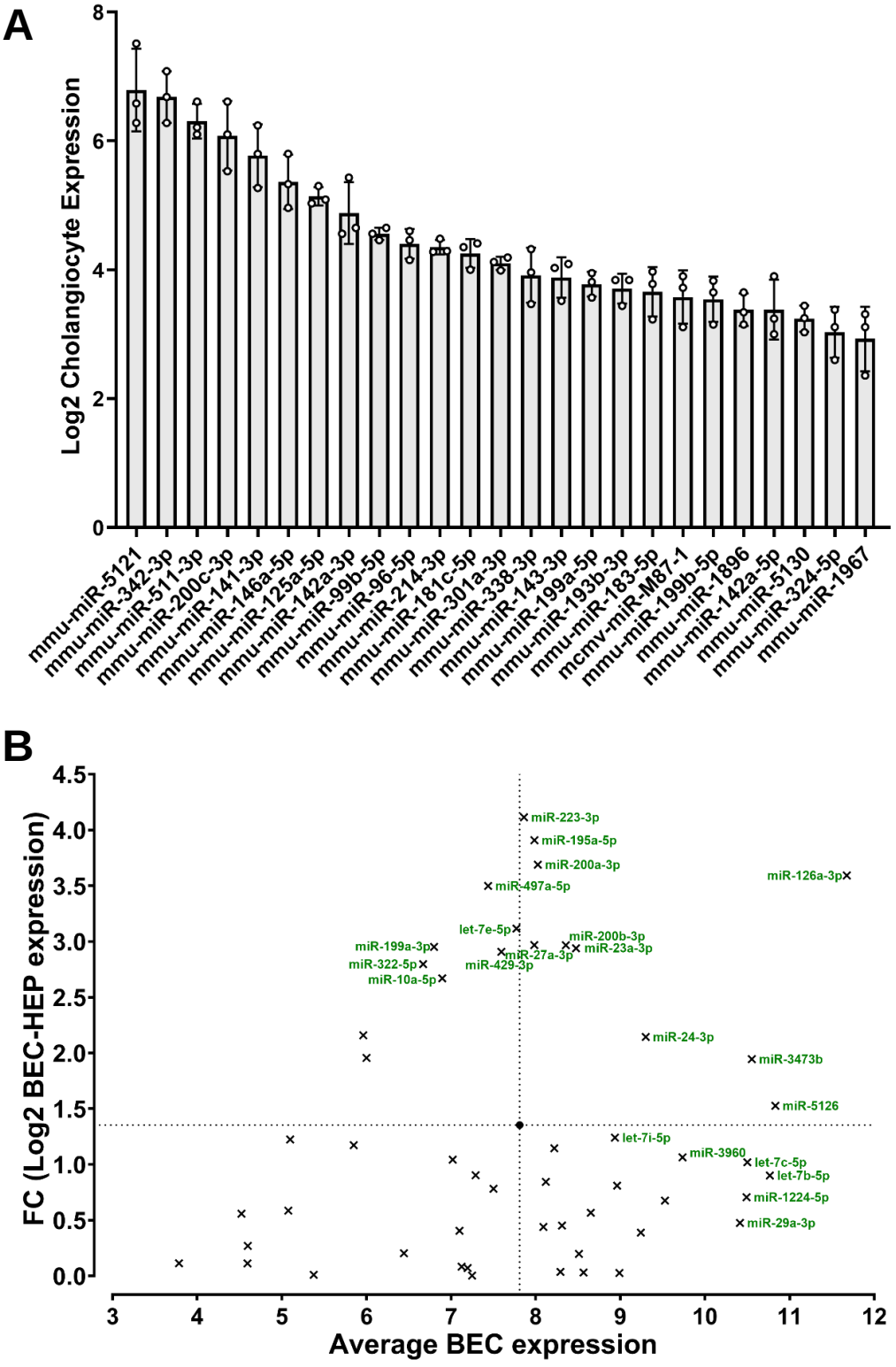

Figure 2.11- Highly abundant miRNAs make ideal biomarker candidates.

(A) The most abundant uniquely expressed miRNAs in cholangiocytes were ranked in decreasing order of their log2 gene expression from the microarray. (B) Shared miRNAs with cholangiocyte enrichment were plotted as basal gene expression against their log2 fold change expression in hepatocytes. Black dot indicated average data point, miRNAs of interest were annotated in green.

Of the 134 shared miRNAs, 13 were enriched in cholangiocytes and were significantly different by SAM analysis (Fig 2.12A). Statistical analysis of uniquely expressed cholangiocyte miRNAs was possible as the AFE software assigns an undetected miRNA in hepatocytes a Log2 expression value of -1. Of the 69 unique miRNAs, 61 were significant by SAM analysis (Fig 2.12B). The 8 insignificant miRNAs were generally low expression with high variation (average Log2 expression ± SD = 1.3 ± 0.63).

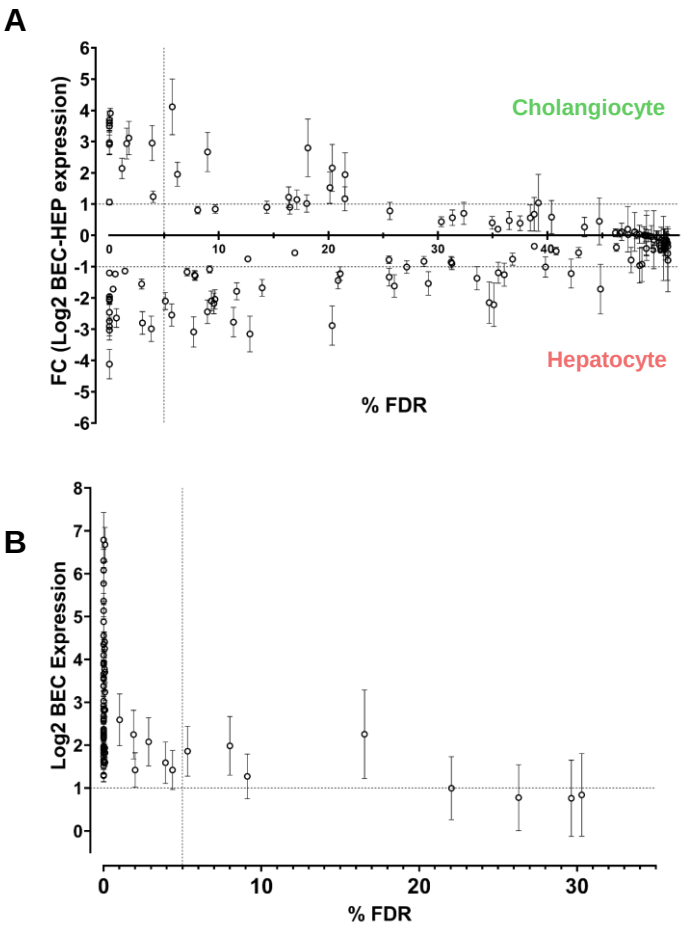

Figure 2.12- Statistical analysis of shared and unique cholangiocyte miRNAs by SAM analysis

(A) Shared and (B) unique miRNAs were assessed by SAM analysis to identify significant differentially expressed miRNAs in cholangiocytes and hepatocytes. Shared miRNAs were first divided into cholangiocyte or hepatocyte enriched expression. The threshold for statistical significance was set at 5% FDR. Data is expressed as mean log2 expression ± SD.

2.3.7 Further triage of significantly different microRNAs

Although the microarray was performed in mouse, the ultimate goal of any translational biomarker is to have clinical utility in humans. Therefore, the 61 unique and 13 cholangiocyte enriched mouse miRNAs were compared on miRBase V.22 (the most recent database at the time of searching) to attest if a human equivalent existed. All 13 cholangiocyte enriched miRNAs and the 50 of unique miRNAs were also expressed in human. Some miRNAs exhibited base additions, substitutions and nomenclature differences when comparing mouse and human equivalents, but these miRNAs were still retained (Appendix 2.2).

An ideal circulating miRNA biomarker would show tissue specificity to the injured organ, such as miR-122 in the liver. The 13 shared and 50 unique translatable miRNAs of interest were further examined using a publicly available miRNA expression dataset of 14 organs in mouse (GEO accession: GSE67885); miR-122 was included in the dataset for a comparison of a liver specific miRNA. There were 3 unique miRNAs (miR-28c, miR-299b-5p) and a single shared miRNA (miR-3960) that were not detected in the GSE67885 database. There was a wide range in the total read count of unique and shared miRNAs in the different tissues (Appendix 2.3). However, neither unique nor shared miRNAs of interest showed substantial liver specificity.

2.3.8 Validation of microarray by qPCR

In order to validate the array, a selection of promising shared (miR-200b-3p and miR-429-3p) and unique (miR-200c-3p) miRNAs were chosen to be analysed in freshly isolated hepatocytes and cholangiocytes by RT-PCR. The miRNA expression in the array relative to cholangiocytes (Fig 2.13A) was compared against a PCR normalised to the exogenous cel-lin-4 (Fig 2.13B) and endogenous snoRNA202 (Fig 2.13C). Gene expression determined by RT-PCR was shown to be very similar to the data obtained from the microarray.

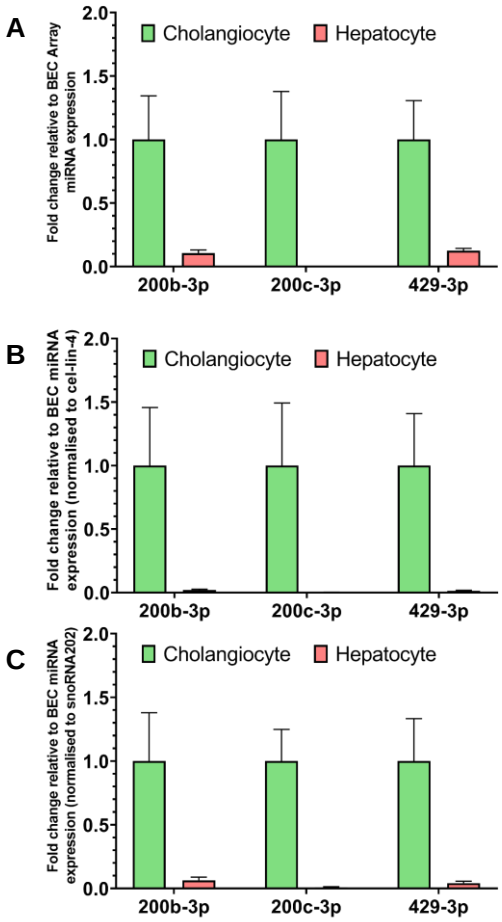

Fig 2.13 Similar miRNA gene expression is detected by both microarray and PCR

(A) The gene expression of three miRNAs of interest reported by the microarray, relative to cholangiocytes. In order to validate the microarray data, gene expression in freshly isolated hepatocytes and cholangiocytes was assessed by PCR. Data was normalised to the exogenous cel-lin-4 (B), or endogenous snoRNA202 (C). Relative gene expression detected by the microarray and PCR was comparable.

2.4 Discussion-

Over the last decade, circulating miRNAs have gained attention as a novel class of biomarker in the detection of specific organ and cell injury. Multiple studies have shown the utility of miR-122 in the detection of hepatocellular injury following APAP toxicity in both human and pre-clinical models [144,191]. However, miR-122 is also increased in response to cholestatic and mixed injury; whereas a different miRNA species derived from cholangiocytes could be better suited in detecting an injury of this nature [192]. In this study, global miRNA expression profiles in murine hepatocytes and cholangiocytes were compared with the aim of identifying candidate miRNAs as novel DILI biomarkers.

Primary human tissue is the gold standard model for cell isolations and our group has published extensively with isolated hepatocytes from resected tissues[139,193,194]. However, this study is the first to isolate cholangiocytes. As the quality of the periportal regions of the human livers were compromised, determined by pathologist scoring, it was necessary to switch to a pre-clinical model. Nevertheless, we have demonstrated that isolations of hepatocytes and cholangiocytes from murine livers produce viable and pure cell populations.

A microarray analysis of isolated populations of native hepatocytes and cholangiocytes initially revealed 69 unique and 134 enriched cholangiocyte miRNAs. The large number of shared miRNAs is unsurprising given the similarities of both cell types. During development, cholangiocytes and hepatocytes both develop from hepatoblasts, a common precursor cell [195]. There is also experimental evidence that cholangiocytes and hepatocytes can transdifferentiate to each other's phenotype when their function and regeneration is significantly impaired [196].

The evidence for the two cell type's similarities was further demonstrated by ranking expressed miRNAs in terms of abundance. Previously identified liver enriched

miRNAs such as miR-122 and miR-192 were highly expressed in hepatocytes (Fig 2.10A); this was to be expected as miR-122 reportedly constitutes 70% of all mature miRNAs in mature hepatocytes with an approximate copy number of 130,000 per cell [197] and miR-192 is one of 9 miRNAs that accounts for ~89% of the hepatic miRNAome [198]. miR-122 was also highly expressed in cholangiocytes (Fig 2.10B), though it is unclear if this is due to hepatocyte contamination, as even a small number of hepatocytes could drastically inflate perceived gene expression.

As highly abundant miRNAs were similar between the two cell types, we therefore sorted uniquely expressed miRNAs in cholangiocytes to identify candidate miRNA biomarkers (Fig 2.11A). A number of these miRNAs have been implicated in different hepatobiliary processes. For example, miR-342 has been shown to be downregulated in hepatocellular carcinoma (HCC) tissue [199], yet is upregulated in methionine/ choline-deficient (MCD) mouse models of non-alcoholic steatohepatitis (NASH) [200]. miR-200c is downregulated in both HCC and intrahepatic cholangiocarcinoma (ICC) [201] and has been detected in the serum of pre-clinical models with biliary hyperplasia [154]. miR-141 has been identified as potential circulating biomarker for primary biliary cirrhosis (PBC) [202] and its over-expression is implicated in poor prognosis of biliary tract cancers [203]. Furthermore, it has been shown to be expressed in multiple intra- and extra-hepatic cholangiocarcinoma cell lines by microarray analysis [204]. miR-146a expression is also downregulated in HCC [201] and is thought to supress liver fibrosis and stellate cell activation following chemical [205] or NASH injury [206].

Although potentially not as desirable as uniquely expressed miRNAs, those with shared expression may still be viable biomarkers. Candidate shared miRNAs were identified by examining those with high basal cholangiocyte expression, as well as high enrichment over hepatocytes (Fig 2.11B). These miRNAs are also implemented in a number of cholangiocyte disease processes: downregulation of miR-126 in resected ICC relative to healthy cholangiocyte tissue is associated with increased

survival [207]. miR-200a and miR-200b and miR-429 have been identified as a circulating marker of biliary hyperplasia [154] and biliary atresia [208] [209].

The aforementioned miRNAs were shown to be significantly different by SAM analysis and express a human equivalent; they are specifically referenced here due to their high abundance and enrichment and their defined role in biliary disease, or as a biomarker. Indeed, other significantly different miRNAs from the array are also implemented in various forms of liver physiology.

However, when we compare the tissue distribution of candidate miRNAs, it becomes apparent that a single miRNA biomarker would not be feasible to inform of cholangiocyte injury. Both unique and shared miRNAs have relatively low liver abundance compared to other tissues, thus a panel of miRNA and/or protein biomarkers would be needed to confirm specific liver injury. Many promising miRNAs (miR-141, miR-200a, miR-200b, miR-200c, miR-429) have a low individual read count in liver tissue, and therefore very low liver specificity, according to the GSE67885 tissue library. However, this could be a consequence of their unique or enriched expression in cholangiocytes, which only make up 5% of the total liver.

2.4.1 Conclusions & future work

In this chapter, miRNA expression profiles for both hepatocytes and cholangiocytes were compared, and 50 unique and 13 shared miRNAs were identified as potential candidates for circulating biomarkers of cholangiocyte DILI. It was also noted that resected human tissue typically presents with a damaged periportal area, which impedes sensitive RNA interrogation of the tissue. Consequently, optimised isolation protocols for isolating murine hepatocytes and cholangiocytes provided pure and viable hepatic cell populations

Future work should aim to characterise the finalised 50 unique and 13 shared miRNAs in an *in vivo* CD-1 mouse with cholangiocyte DILI, or in serum samples of human

patients presenting with mixed or cholestatic injury. These miRNAs should be contextualised relative to the current gold standard biomarkers in order fully compare their sensitivity and release kinetics.

2.4.2 Limitations

A potential caveat of the initial analysis was the manner in which the cells were isolated. As the cells were donor matched, the differences in isolation time may have had an effect on miRNA expression. Hepatocytes are typically isolated within 1 h of sedating the animal, whereas cholangiocytes are isolated after >4 h.

Furthermore, the GSE67885 tissue atlas used 8-week-old female C57BL/6J mice to generate their sequencing reads. Whilst these are a similar age to the mice in this study, sex status can produce differential miRNA expression [210].

Finally, SAM analysis was used to identify differentially expressed miRNAs. The data was also analysed by paired multiple t-test, which was shown to be less stringent (Appendix 2.1). Some miRNAs removed due to the more rigorous statistical exclusion criteria may still be viable biomarker candidates (e.g. miR-223-3p, Log2 BEC= 7.86, Log2 HEP= 3.75, t-test FDR= 0.03, SAM FDR= 5.75%).

Chapter Three:

Circulating miRNAs as biomarkers of cholangiocyte drug-induced liver injury

Contents

3.1 Introduction

Bile duct lesions are a feature of both mixed and cholestatic DILI, which account for approximately 50 % of all clinical DILI cases [211]. Perturbations to the cholangiocytes, the cardinal cell of the bile duct, can result in a prolonged state of cholangitis. Without proper diagnosis and clinical intervention, this can ultimately lead to bile duct degeneration and destruction, necessitating the need for liver transplantation [212].

Currently, both the diagnosis and the classification of DILI is dependent upon RUCAM and R-ratio scoring [213,214]. These scoring measurements currently utilise circulating protein biomarkers as diagnostic tools. ALP is the classical marker of cholestatic liver injury. Within the liver, it is located within cholangiocytes and on the apical membranes of hepatocytes [215]. The circulating levels of ALP in healthy patients is prone to variation and can be influenced by sex, blood group, pregnancy, old age and bone development in children [216]. Furthermore, the distribution of circulating ALP in healthy adult patients is derived from bone (approximately 58-67 %), liver (25-33.5 %), and the intestinal tract (8-9 %) [217]. Abnormal ALP serum values are therefore typically corroborated by further biomarker tests, such as 5' nucleotidase (5'NT) or γ-glutamyl transferase (GGT) in order to confirm complete liver specificity. Mild to moderate (2-3x ULN) levels of circulating ALP are typically seen in multiple types of liver disorder and significant elevations (>3x ULN) are associated with both intra- or extrahepatic cholestasis [216]. These values represent a relatively small dynamic range between healthy and diseased states.

miRNAs have been proposed as a novel family of biomarkers that may offer improved clinical utility over the current gold standard protein biomarkers. Hepatocellular enriched miRNAs, such as miR-122 and miR-192 have already showed improvement over ALT/AST in identifying DILI in both pre-clinical models and humans [139,218]. However, no such miRNAs currently exist for identifying cholangiocyte DILI. In the previous chapter, over 60 cholangiocyte enriched or unique murine miRNAs were

identified as circulating biomarker candidates. Five of these miRNAs, miR-141, -200a, -200b, -200c and -429, show promise as they have previously been detected in the serum of other biliary diseases, such as ICC [201,203], PBC [202], biliary hyperplasia [154] and biliary atresia [208,209] following a search of the literature.

Cholangiocyte DILI is clinically associated with commonly prescribed drugs, such as amoxicillin/clavulanic acid [219], flucloxacillin [220] and carbamazepine [221]. However, human cholangiocyte DILI is supposed to be predominantly idiosyncratic and mediated via T-cell hypersensitivity, opposed to direct parent compound or reactive metabolite toxicity [212]. Attempts to pre-clinically model DILI involving the adaptive immune response have largely been unsuccessful [222,223]. Therefore, the classic methodology of inducing cholangiocyte injury is bile duct ligation (BDL), though this is not translational to human DILI [224]. Consequently, toxicological studies of cholangiocytes have historically used acute dosing of ANIT and DAPM, two chemical compounds, which ultimately result in a mixed periportal injury. While these compounds are not clinically relevant, they have been shown to induce cholangiocyte DILI predominantly in rats [154,225–228], but also in mice [229–232]. The details of these studies are summarised in Table 3.1.

Species	Strain	Animal Information	Drug - Vehicle	Dose (mg/kg)	Administration route	Reference
Rat	Sprague Dawley	Male, 8 wk	ANIT - Corn Oil	50	*o.g*	154
Rat	Wistar	200-250 g	ANIT - Corn Oil	300	*o.g*	225
Rat	Wistar	Male, 220-240 g	ANIT - Olive Oil	100-200	*o.g*	227
Rat	Wistar	300-335g	ANIT - Corn Oil	20-40	*o.g*	228
Rat	Sprague Dawley	Male, 290-350 g	DAPM - 35% EtOH	50	*o.g*	226
Mouse	C57BL/6	Female, 8-9 wk	ANIT - Olive Oil	50	*o.g*	229
Mouse	C57BL/6	Male, 8-10 wk	ANIT - Corn Oil	75	*o.g*	231
Mouse	C57BL/6	Male, 8-10 wk	DAPM - N/A	50	*i.p*	230
Mouse	ICR	N/A	DAPM - N/A	10-100	*o.g*	232

Table 3.1- Experimental conditions of previous hepatobiliary toxicology studies

ANIT and DAPM, typically administered by oral gavage, have been extensively used in the past to induce cholangiocyte injury *in vivo*.

To date, the CD-1 mouse has yet to be utilised in combination with ANIT to induce biliary injury. Furthermore, the detection of miR-141, -200a, -200b, -200c and –429 in response to cholangiocyte DILI in a mouse model has not yet been elucidated. The detection of these cholangiocyte enriched and unique miRNAs coupled with analysis of their fold change relative to a vehicle control would allow a direct comparison against the currently used protein biomarkers.

3.1.1 Aims and hypothesis

The aims of this chapter were to:

- Induce cholangiocyte injury in CD-1 and C57BL/6J mice and Sprague Dawley rats with a single acute dose of hepatobiliary toxicant.
- Assess the degree of liver injury by classical serum biomarkers and histopathological scoring.
- Detect cholangiocyte enriched or unique miRNAs of interest in the serum of these animals and contextualize them relative to the type and degree of injury.

The main hypothesis within this chapter was that cholangiocytes would be injured in the CD-1 mouse following a single dose of hepatobiliary toxicant, causing previously identified cholangiocyte-enriched miRNAs to be released from the liver and be detected in serum. The degree of injury and biomarker release would be similar to C57BL/6J mice and Sprague Dawley rats, which have been previously utilised in cholangiocyte toxicology studies. Candidate miRNA biomarkers would be released at an earlier time point and show a greater dynamic range between healthy and DILI samples than the current gold standard biomarkers.

3.2 Materials and Methods

Unless otherwise stated, all materials were purchased from Sigma Aldrich (Poole, UK).

3.2.1 Experimental animals

The protocols described were undertaken in accordance with the criteria outlined in a project licence granted under the Animals Scientific Procedures Act 1986 and approved by the University of Liverpool Animals Ethics Committee. 5-7-week-old male CD-1 and C57BL/6J mice and Sprague Dawley rats were purchased from Charles River laboratories (Cambridge, UK) and had a 7-day acclimatisation period prior to experimentation. Animals were maintained in a 12 h light/dark cycle with free access to food and water.

3.2.2 Chemical exposure in experimental animals

The animal numbers, dosing and time points utilised in this study were selected, in part, based on previously published data [154,231,233,234]. For fasted animals, food was withdrawn approximately 16 h prior to dosing. All animals were dosed approximately between 09.00-10.30 a.m. On the morning of dosing, all animals were weighed and received a single dose of freshly constituted hepatobiliary toxicant. ANIT (50 mg/kg and 75 mg/kg) or corn oil and DAPM (100 mg/kg and 200 mg/kg) or polyethylene glycol 300 (PEG) were administered by oral gavage (o.g) in a volume of 10 mL/kg.

3.2.3 Sample collection and processing

Experimental animals were euthanized in a rising concentration of CO_2 and weighed post-mortem. Livers and stomachs were excised, weighed and immersed in 4 % PFA and fixed for 24-48 h at 4 °C. Animals were exsanguinated via cardiac puncture by a 20 G needle and the blood was collected and left to clot at RT for 30-60 min. The clot was separated by centrifugation at 1,500 x *g* at 4 °C for 10 min with no brake. The serum was retained without disturbing the clot, aliquoted and stored at -80 °C.

3.2.4 Haematoxylin and eosin (H&E) staining and histological scoring

H&E staining of experimental animal samples were performed in collaboration with Julie Haigh at The School of Veterinary Science, University of Liverpool.

The processing and sectioning of tissue blocks is described in Section 2.2.3. For H&E staining, liver and stomach sections underwent deparaffinisation by 3 x 5 min incubations in xylene and 5 min in 100 % ethanol. Slides were briefly submerged in decreasing concentrations of 100 %, 95 %, 80 %, 70 % and 50 % ethanol. Slides were rinsed twice in dH_2O and submerged in Mayer's haematoxylin for 5 min, followed by one wash in tap water for 5 min and one rinse in dH_2O. Slides were then submerged in Eosin Y solution for 5 min. To dehydrate the sample, slides were briefly submerged in 95 % ethanol, then twice into 100 % ethanol. Finally, slides underwent two 1 min washes in xylene.

Histological scoring of experimental animal samples was performed by Dr Lorenzo Ressel at The School of Veterinary Science, University of Liverpool.

H&E stained liver and stomach sections (n= ≥3 per experimental condition and time point) were microscopically examined by a trained veterinary pathologist and pathological changes of interest were annotated. The severity of pathological findings was graded between none, mild, moderate, marked and severe. Incidence was stratified as low, moderate or high. This was defined as present in ≤1/3 of examined samples, present in ≤2/3 of examines samples and present in all samples, respectively.

3.2.5 Quantification of serum ALT activity

Serum ALT was determined by a photometric kinetic assay using the Infinity ALT (GPT) Liquid Stable Reagent (TR71121, ThermoFisher Scientific, UK). ALT catalyses the production of pyruvate from L-alanine and 2-oxoglutarate. Pyruvate is then reduced by lactate dehydrogenase into L-lactate, whilst NADH is co-currently

oxidised into NAD. The kit measures ALT activity by the decrease in absorbance at 340 nm due to the oxidation of NADH.

To perform the assay, ALT reagent was warmed to 37 °C and the serum samples were defrosted on ice. Serum was diluted 1:10 in dH_2O and 30 µL was loaded in duplicate into a 96 well plate. 300uL of pre-warmed ALT reagent was added to the serum and the maximum rate of ALT activity was determined by the decrease of absorbance at 340 nm over a 10 min kinetic read by a Varioskan Flash plate reader (ThermoFisher Scientific). This value was then multiplied by a determined factor, which accounted for path length correction, dilution factor and the millimolar absorption coefficient of NADH at 340 nm, to produce a final ALT activity (U/L) value.

3.2.6 Quantification of serum ALP activity

Serum ALP was determined by a colorimetric kinetic assay using the Alkaline Phosphatase Assay Kit (ab83369, Abcam (Cambridge, UK). ALP catalyses the hydrolysis of phosphate esters in an alkaline buffer. The kit uses p-nitrophenyl phosphate (*p*NPP) as a phosphatase substrate, which is de-phosphorylated by ALP. This causes a colorimetric change, with a peak optical density at 405 nm.

To perform the assay, ALP assay buffer and stop solution were warmed to RT and the serum samples defrosted on ice. Murine serum samples were diluted 1:10 in dH_2O and rat serum samples were diluted 1:100 in dH_2O. The standard curve and 80 µL of diluted serum were loaded in duplicate into a 96 well plate. 50 µL of 5 mM *p*NPP solution was added to the serum samples and 10 µL of reconstituted ALP enzyme was added to the standard curve samples. The plate was incubated at 25 °C for 1 h in darkness, briefly shaken, and the optical density at 405 nm was determined by a Varioskan Flash plate reader. Final ALP activity (U/mL) in serum samples were extrapolated from the standard curve values.

3.2.7 Total RNA extraction

Total RNA was isolated from serum by the miRNeasy mini extraction kit (Qiagen, Venlo, Netherlands) with minor modifications to the manufacturer's instructions. 120 µL of serum was made up to a total volume of 200 µL with nuclease-free H_2O. 1 mL of Qiazol reagent was added to the diluted serum. Samples were vortexed and incubated for 5 min at RT to ensure complete lysis and then spiked with the exogenous miRNA, cel-lin-4, to a final concentration of 10 pM (Applied Biosystems, UK). 200 µL of chloroform was added to the samples, which were vortexed and centrifuged at 12,000 x g at 4 °C for 15 min. Approximately 600 µL of the resulting upper aqueous solution was then transferred to a new microcentrifuge tube and mixed with 900 µL of 100% ethanol. All future centrifuge steps were performed at RT.

This new mixture was loaded into a RNeasy Mini column and spun at 8,000 x g for 15 s. 700 µL of RWT buffer was added to the Mini column and spun at 8,000 x g for 15 s, followed by 500 µL of RPE buffer and another spin at 8,000 x g for 15 s. The spin columns were washed with 500 µL of RPE buffer and a spun at 8,000 x g for 2 min. 50 µL of nuclease-free H_2O was added to the Mini column and spun at 8,000 x g for 15 s in order to elute total RNA into a new microcentrifuge tube.

3.2.8 Quantitative polymerase chain reaction (qPCR)

Specific miRNAs of interest were measured using TaqMan qPCR. Total RNA was reverse transcribed using specific stem-loop primers for each individual miRNA species of interest (mmu-miR-122-5p, mmu-miR-141-3p, mmu-miR-200a-3p, mmu-miR-200b-3p, mmu-miR-200c-3p, mmu-miR-429-3p, let-7d-5p and cel-lin-4-5p,) by the TaqMan MicroRNA Reverse Transcription Kit, according to the manufacturer's instructions (Applied Biosystems).

5 µL of total RNA was combined with the specific reverse transcription primer and master mix to a total volume of 15 µL. cDNA was generated on a GeneAmp PCR

System 9700 (ThermoFisher Scientific) thermocycler at: 30 min at 16 °C, 30 min at 42 °C, 5 min at 85 °C and a 4 °C hold. The resulting cDNA was then made to a total volume of 20 µL with nuclease-free H_2O. Then, 2 µL of cDNA was added to the corresponding specific TaqMan qPCR probe and master mix according to the manufacturer's instructions.

The plating and reaction conditions of the PCR is described in Section 2.2.10. Cel-lin-4 was used as an exogenous control for extraction and reverse transcription efficiency and let-7d-5p was used as an endogenous normaliser. Fold change in expression of miRNA was calculated by the $2^{-\Delta\Delta Ct}$ method [189].

3.2.9 Statistical analysis

All statistical analysis was performed on GraphPad Prism V.8.2.0 (CA, US). The differences in total body weight pre- and post-dose were analysed by a paired two-tailed t-test. The differences in organ weight and biomarker levels between time-matched controls were analysed by unpaired two-tailed t-test. Differences in biomarker levels relative to the 0 h control was performed by one-way ANOVA with Dunnet's multiple comparison test.

3.3 Results

3.3.1 ANIT does not cause liver injury in non-fasted CD-1 mice

For physiological relevancy, the hepatobiliary toxic effects of ANIT were observed in non-fasted CD-1 mice. Throughout the study, ANIT appeared to be well tolerated by the mice. Non-fasted CD-1 mice dosed with corn oil (n=5 per time point) or 75 mg/kg ANIT (n=5 per time point) were assessed for liver injury by histopathological assessment alongside serum ALT and ALP concentrations at 0 h, 12 h, 24 h, 48 h and 72 h post-dose. A small number of animals per group exhibited hypertrophy in the perivenous area, though this was also observed in the 0 h control group (Fig 3.1A). Liver staining revealed minimal changes to liver histology at 0 h, 12 h, 24 h, 48 h and 72 h post-dose (Fig 3.1B-H).

A

CD-1, Male, 6-8 weeks old, Fed, ANIT 75 mg/kg, 10mL/kg, o.g administration

Timepoint (h)	Perivenous Effects	Incidence	Periportal Effects	Incidence
0	Hypertrophy	Incidental-Low	None	High
12	None	High	None	High
	Diffuse hypertrophy	Low	Areas of lymphocytes/EMH	Low
24	None	High	None	High
	Diffuse hypertrophy	Low	Areas of lymphocytes/EMH	Incidental-Low
48	None	High	None	High
	Hypertrophy	Low	Areas of lymphocytes/EMH	Incidental-Low
72	None	High	None	High
	Hypertrophy	Low		

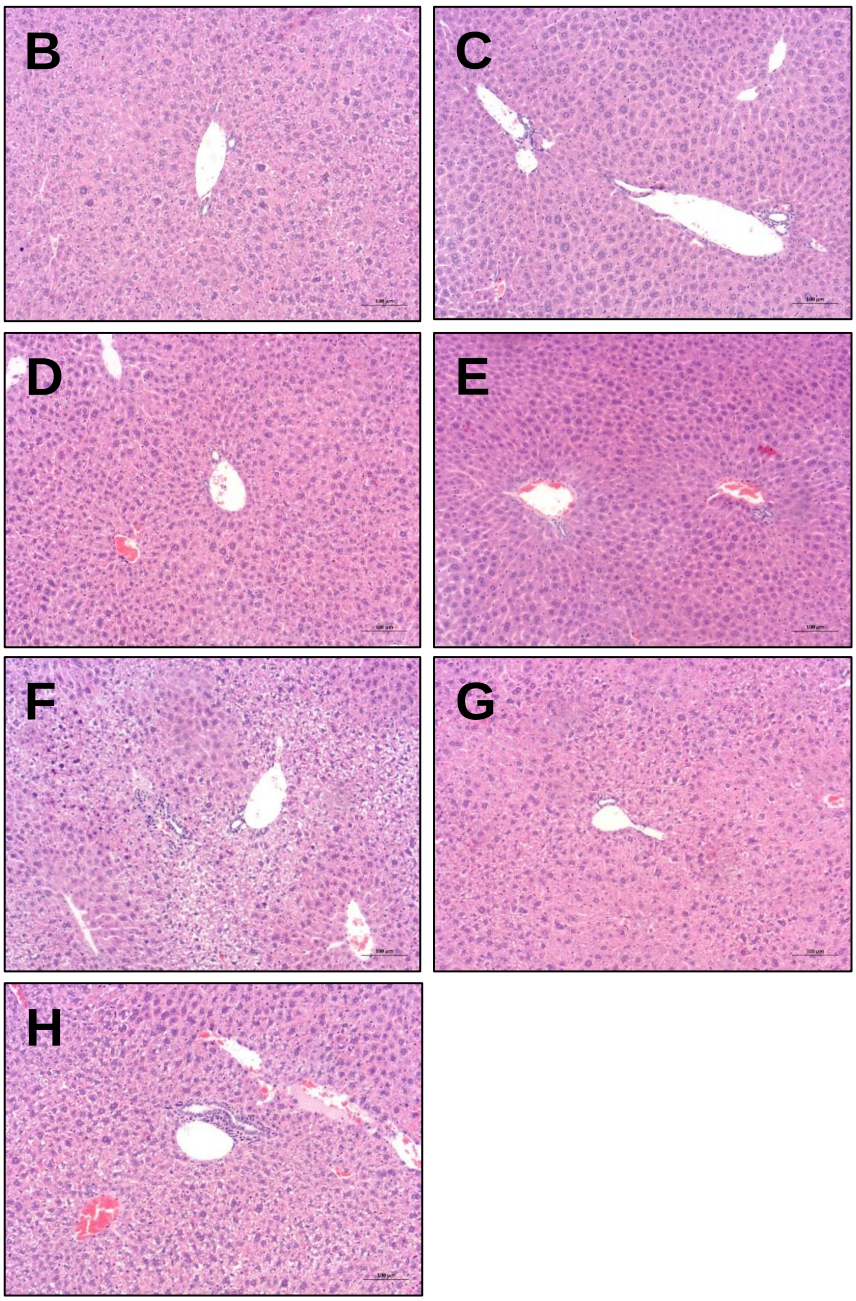

Figure 3.1- ANIT does not cause liver injury in non-fasted CD-1 mice by histological assessment

(A) Histopathological assessment and representative images of H&E stained liver sections from non-fasted CD-1 mice dosed with ANIT (75 mg/kg) at (B) 0 h, (C) 12 h, (E) 24h, (F) 48 h and (H) 72 h or corn oil at (D) 24 h and (G) 72 h post-dose. Magnification x10, scale bar 100 µm.

Circulating levels of ALT (Fig 3.2A) and ALP (Fig 3.2B) in serum from ANIT-treated animals displayed minimal elevation compared to the 0 h and time-matched controls. All time points were non-significant except for ALP in ANIT treated mice 72 h post-dose, which decreased. A relatively high intra-group variation was also observed within these groups.

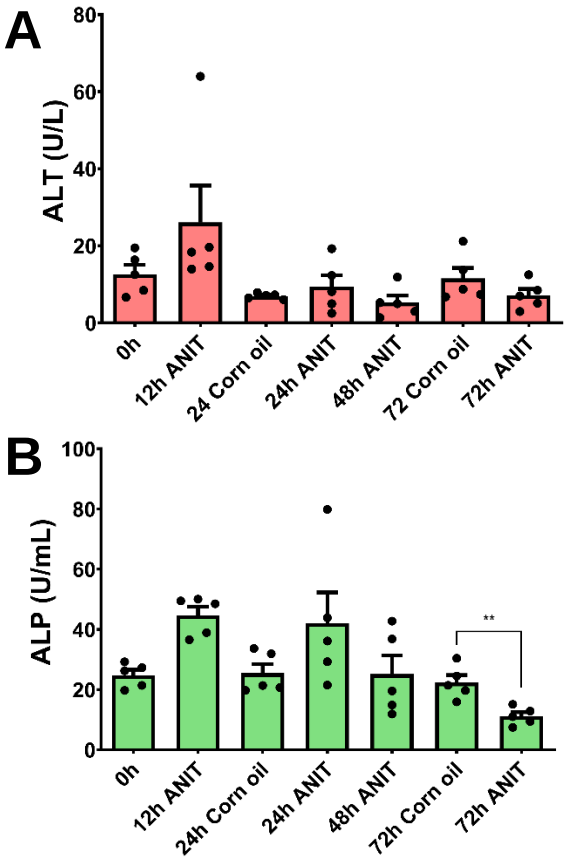

Figure 3.2- ANIT causes minimal liver injury in non-fasted CD-1 mice by serum biomarker assessment

Liver injury in non-fasted CD-1 mice dosed with corn oil or ANIT (75 mg/kg) was assessed by serum (A) ALT and (B) ALP. n=5 per group, bars represent the mean value ± SEM. ** = $p<0.01$

3.3.2 ANIT causes minimal liver injury in fasted CD-1 mice

Due to the minimal hepatotoxicity observed in non-fasted CD-1 mice, food was withdrawn from future studies. It was hypothesised that food in the stomach may be dampening the toxic effects of ANIT, possibly due to retarded gastric emptying and intestinal absorption [235] and the intra-group variability may have been caused by different nutritional states of individual animals [236].

Fasted CD-1 mice were dosed with corn oil (n=5 per time point) or 75 mg/kg ANIT (n=≥5 per time point) and sacrificed 0 h, 9 h, 24 h, 48 h and 72 h post-dose. Throughout the study, ANIT appeared to be poorly tolerated by the mice. Mice displayed a hunched posture, laboured or minimal movements and loose stools. The 12 h time point was altered to a 9 h time point in order to not exceed the project licence animal severity limitation.

H&E Liver staining revealed some hypertrophic effects in the perivenous area of a few select ANIT-treated mice (Fig 3.3A). No consistent and definitive liver injury was detected in the majority of ANIT-treated mice at 0 h, 9 h, 24 h, 48 h and 72 h (Fig 3.3B-H).

A

CD-1, Male, 6-8 weeks old, Fasted, ANIT 75 mg/kg, 10mL/kg, o.g administration

Timepoint (h)	Perivenous Effects	Incidence	Periportal Effects	Incidence
0	None	High	None	High
	Hypertrophy	Incidental-Low		
9	None	High	None	High
	Diffuse hypertrophy	Low	Immune infiltration	Low
24	None	High	None	High
	Diffuse hypertrophy	Low	Coagulative necrosis (mild)	Minimal-Low
48	None	High	None	High
	Diffuse hypertrophy	Low	Coagulative necrosis (marked)	Low
72	None	High	None	High
	Diffuse hypertrophy	Low	Coagulative necrosis (marked)	Low

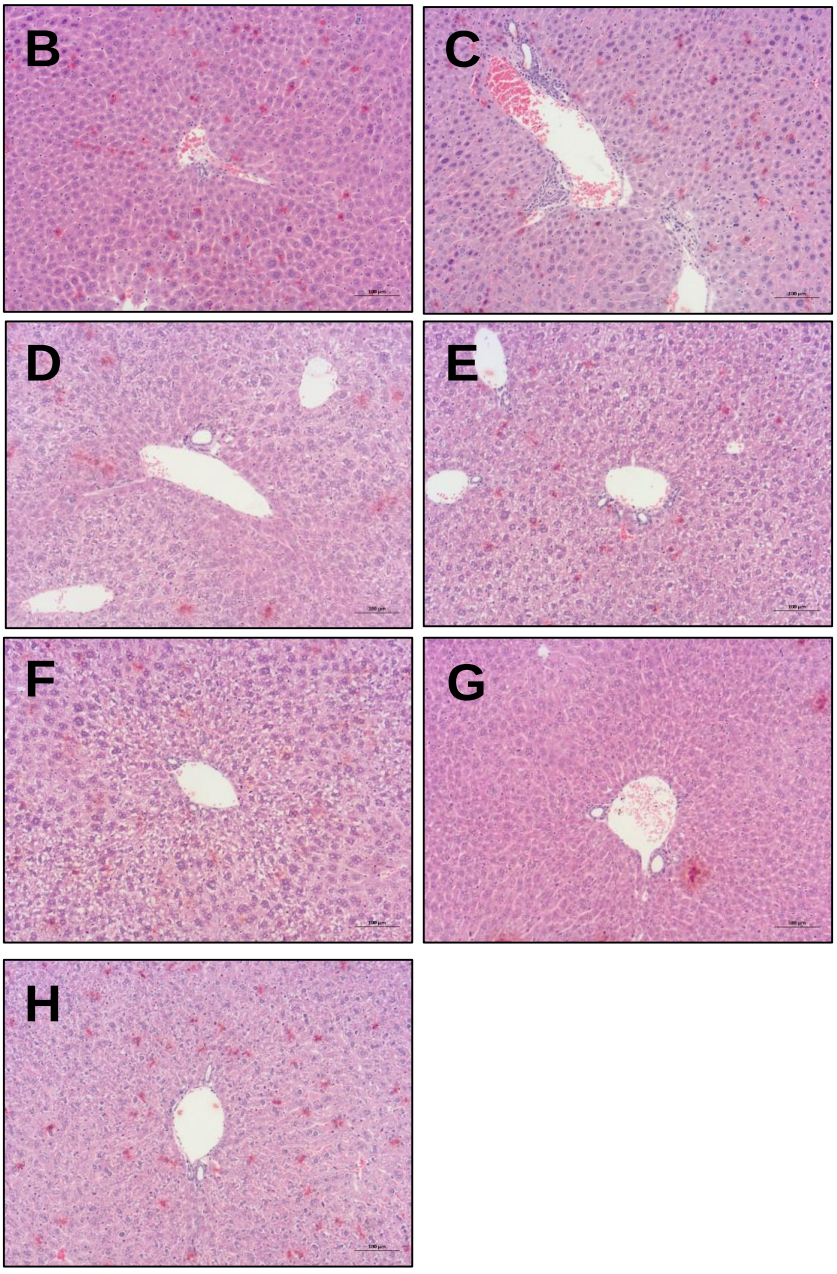

Figure 3.3- ANIT causes variable liver injury in fasted CD-1 mice by histological assessment

(A) Histopathological assessment and representative images of H&E stained liver sections from fasted CD-1 mice dosed with ANIT (75 mg/kg) at (B) 0 h, (C) 9 h, (E) 24h, (F) 48 h and (H) 72 h or corn oil at (D) 24 h and (G) 72 h post-dose. Magnification x10, scale bar 100 µm

A single mouse at both 48 h (Fig 3.4A) and 72 h (Fig 3.4B) exhibited marked liver injury consistent with ANIT toxicity, with periportal immune infiltration and necrosis.

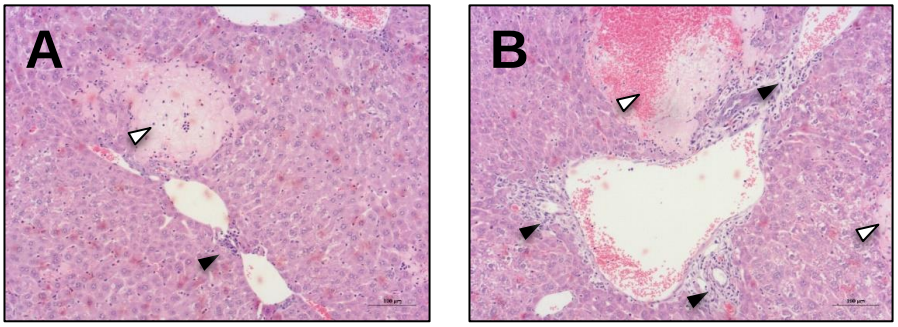

Figure 3.4- ANIT causes variable liver injury in non-fasted CD-1 mice by histological assessment

Images of H&E stained liver sections from two non-fasted CD-1 mice dosed with ANIT (75 mg/kg) at (A) 48 h and (B) 72 h post-dose. Liver injury in this model was inconsistent, though select mice did exhibit ANIT-induced periportal perturbation. White arrows indicate coagulative necrosis, black arrows indicate infiltrating immune cells. Magnification x10, scale bar 100 µm.

This same inconsistent pattern of injury was observed in the circulating levels of ALT (Fig 3.5A) and ALP (Fig 3.5B) in ANIT-treated animals. A single mouse in both the 48 h and 72 h group showed severe responses compared to all other mice at the corresponding time points. In all time points, there was an increase in biomarker concentration compared to 0 h and time-matched controls, though this effect was much more prominent in ALT than ALP. Significant differences were observed between the 24 h post-dose group for both ALT and ALP, however these changes were small. In combination with histology analysis, it was determined liver injury and cholangiocyte damage was insufficient.

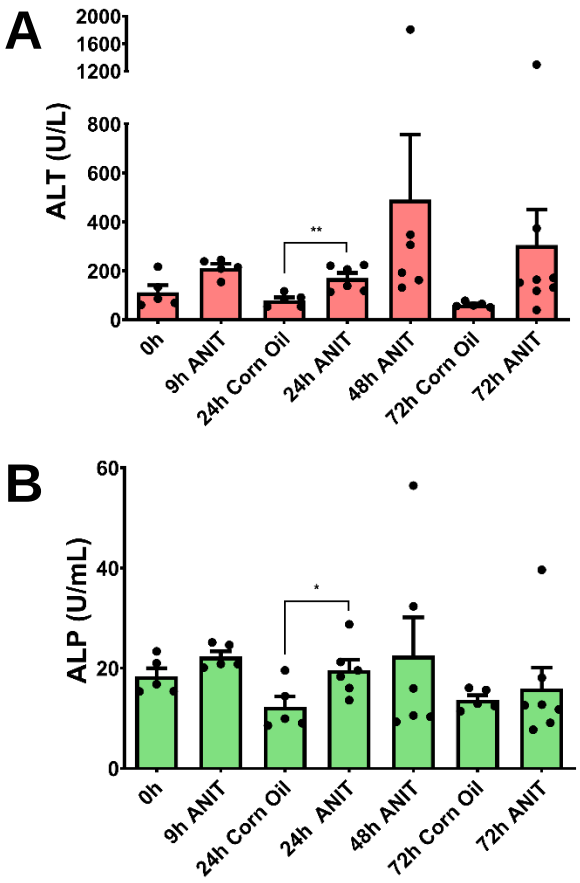

Figure 3.5- ANIT causes minimal liver injury in fasted CD-1 mice by serum biomarker assessment

Liver injury in fasted CD-1 mice dosed with corn oil or ANIT (75 mg/kg) was assessed by serum (A) ALT and (B) ALP. n=≥ 5 per group, bars represent the mean value ± SEM. * = p<0.05, ** = p<0.01

3.3.3 ANIT causes significant changes in liver and stomach weight in fasted CD-1 mice

During the fasted ANIT-treated CD-1 mouse study, it was noted that the animals displayed laboured movement. Through handling the mice and post-mortem examination, it was noted that the stomachs were enlarged and appeared to contain blood clots. A small follow-up study was therefore performed to examine this change in organ weight, whereby CD-1 mice were fasted, weighed and dosed with corn oil (n=3) or 75 mg/kg ANIT (n=3) and culled 30 h post-dose.

Upon sacrifice, corn oil-dosed mice weighed significantly more than their pre-dose weight. However, ANIT-dosed mice maintained a similar weight throughout the study (Fig 3.6A). Lack of weight gain in response to a toxic stimulus is not a rare occurrence, therefore livers and stomachs were also weighed and normalised to individual animal weight at time of sacrifice. Livers from ANIT-dosed animals weighed significantly less compared to corn oil control livers (Fig 3.6B). The stomachs from ANIT-dosed animals weighed significantly more than those of corn oil control mice (Fig 3.6C). The observed changes in liver, stomach and whole-body weight did not reflect the variability seen in the serum biomarker concentrations.

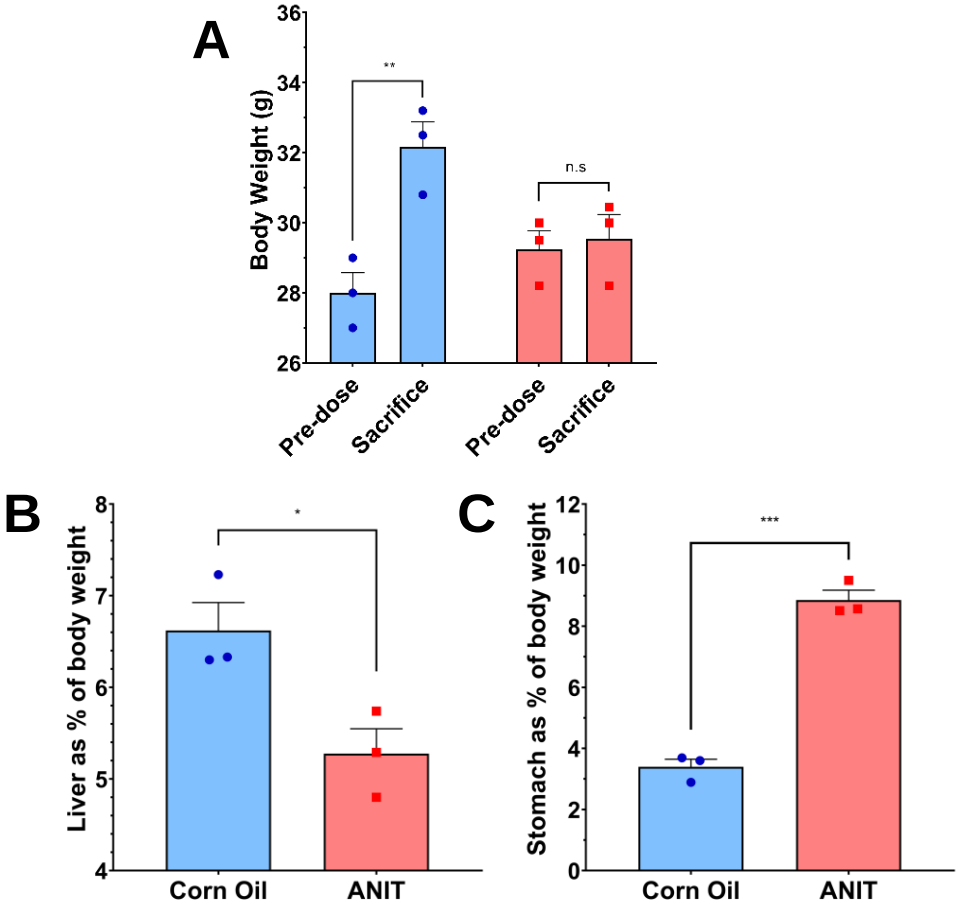

Figure 3.6- ANIT causes significant changes in liver and stomach weight in fasted CD-1 mice

Differences in the (A) total body, (B) liver and (C) stomach weights of CD-1 mice dosed with corn oil or ANIT (75 mg/kg) 30 h post-dose. Individual liver and stomach weights were calculated as a percentage of post-mortem body weight. Bars represent the mean value ± SEM. n.s= non-significant, * = p<0.05, ** = p<0.01 and *** = p<0.001.

Stomachs underwent histological assessment in order to evaluate any cellular perturbations (Fig 3.7A). Control stomachs displayed unremarkable glandular (Fig 3.7B) and non-glandular (Fig 3.7C) regions of the stomach. However, ANIT appeared to cause significant stomach toxicity in CD-1 mice. In the glandular region, a flattening and possible hyperplastic response of the epithelium was observed (Fig 3.7D), proximal to areas of haemorrhaging (Fig 3.7E). In the non-glandular area, a mild extravasation of neutrophils into the tissue was also apparent (Fig 3.7F) The size and weight difference of these stomachs, as well as visible areas of gastric bleeding is demonstrated in Fig 3.7G.

A

CD-1, Male, 6-8 weeks old, Fasted, ANIT 75 mg/kg, 10mL/kg, o.g administration, 30h Timepoint

Dose (mg/kg)	Stomach Effects	Incidence
Corn Oil	None	High
ANIT (75)	None	Low
	Neutrophil extravasation, flattening of epithelium with possible hyperplastic response, congestion/haemorrhages, possible erosion	Moderate

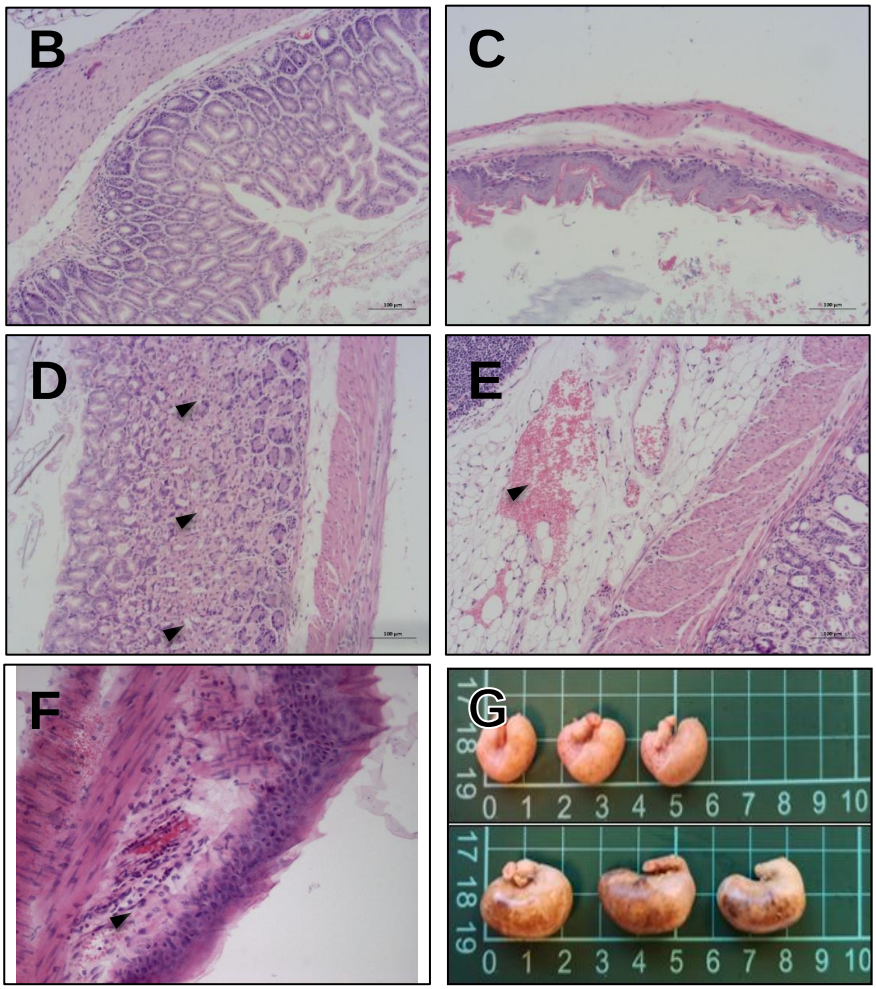

Figure 3.7- ANIT causes stomach toxicity in fasted CD-1 mice by histological assessment

(A) Histopathological assessment and representative images of H&E stained stomach sections from fasted CD-1 mice dosed with corn oil or ANIT (75 mg/kg) 30 h post-dose. (B) corn oil treated, glandular stomach, (C) corn oil treated, non-glandular stomach, (D) ANIT treated, glandular stomach, black arrows indicate flattened epithelium, (E) ANIT treated, black arrow indicates haemorrhages (E) ANIT treated, non-glandular stomach, black arrow indicates neutrophil extravasation. (A-D) magnification x10, scale bar 100 µm, (F) magnification x20. (G) Image of corn oil and ANIT treated CD-1 stomachs.

3.3.4 DAPM causes minor liver injury in fasted CD-1 mice

Due to the irregular liver toxicity observed with ANIT in the non-fasted and fasted CD-1 mouse, a small pilot study using DAPM, a secondary line biliary toxin, was performed. CD-1 were fasted and dosed with PEG (n=3), 100 mg/kg DAPM (n=3) or 200 mg/kg DAPM (n=3). Mice were culled at 30 h post-dose. Throughout the study, DAPM appeared to be well tolerated by the mice at both doses.

Liver staining revealed a mild but consistent hydropic degeneration in the periportal areas of all experimental groups (Fig 3.8A-D). Diffuse coagulative necrosis was observed in the periportal areas of DAPM-treated mice, and this severity increased with dose strength (Fig 3.9C-D). However, the pattern of necrosis was not localised entirely to the periportal area and was described as randomly scattered throughout the liver lobule by the histopathologist.

A

CD-1, Male, 6-8 weeks old, Fasted, DAPM 100/200 mg/kg, 10mL/kg, o.g administration, 30h Timepoint

Dose (mg/kg)	Perivenous Effects	Incidence	Periportal Effects	Incidence
PEG	None	High	None	High
			Hydropic degeneration (mild)	Low
DAPM (100)	None	High	None	Low
	Diffuse hypertrophy, Diffuse coagulative necrosis (mild-moderate)	Low	Diffuse coagulative necrosis (mild), Hydropic degeneration (mild)	Moderate
DAPM (200)	None	High	None	Low
	Diffuse hypertrophy, Diffuse coagulative necrosis (moderate)	Low	Diffuse Coagulative Necrosis (moderate), Hepatitis (mild)	Moderate

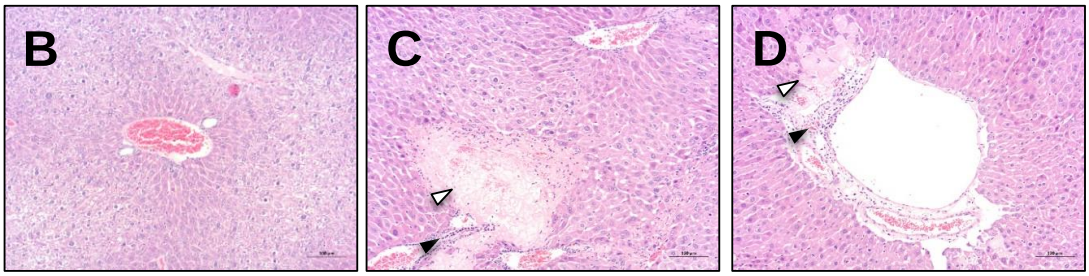

Figure 3.8- DAPM causes minor liver injury in fasted CD-1 mice by histological assessment

(A) Histopathological assessment and representative images of H&E stained liver sections from fasted CD-1 mice dosed with (A) PEG, (B) 100 mg/kg DAPM or (C) 200 mg/kg DAPM 30 h post-dose. White arrows indicate coagulative necrosis, black arrows indicate infiltrating immune cells. Magnification x10, scale bar 100 µm.

Serum biomarker analysis revealed a variable degree of liver injury. DAPM caused a non-significant concentration-dependant increase in both ALT (Fig 3.9A) and ALP (Fig 3.9B). However, there was a high degree of intra-group variability.

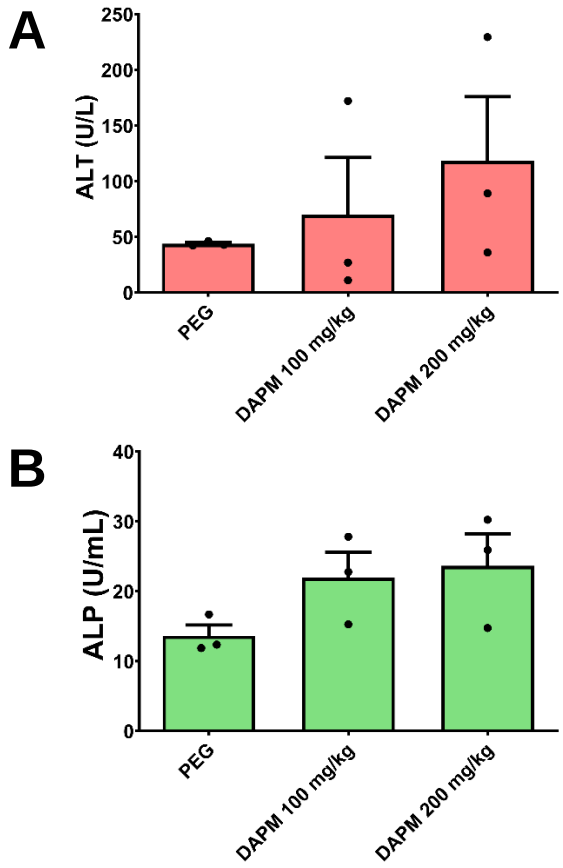

Figure 3.9- DAPM causes minor liver injury in fasted CD-1 mice by serum biomarker assessment

Liver injury in fasted CD-1 mice dosed with PEG or DAPM (100 and 200 mg/kg) was assessed by serum (A) ALT and (B) ALP. n=3 per group, bars represent the mean value ± SEM.

3.3.5 DAPM does not cause significant changes in liver and stomach weight in fasted CD-1 mice

As both ANIT and DAPM were administered by o.g, whole body, liver and stomach weights of DAPM-treated mice were recorded to see if similar discrepancies also occurred. Upon sacrifice, all experimental mice weighed significantly more than their pre-dose weight (Fig 3.10A). No significant difference was observed in the weights of livers between all dosed animals (Fig 3.10B). While there was a concentration-

dependant increase in the stomach weights in animals dosed with DAPM, the overall change was relatively small and non-significant (Fig 3.10C).

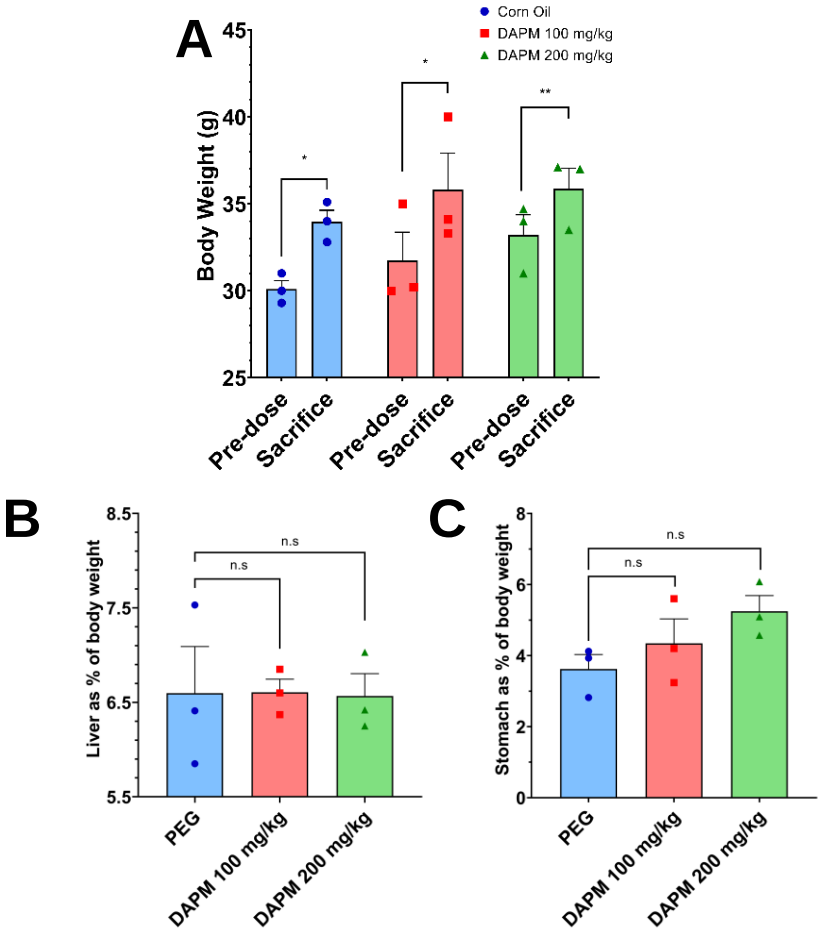

Figure 3.10- DAPM does not cause significant changes in liver and stomach weight in fasted CD-1 mice

Differences in the (A) total body, (B) liver and (C) stomach weights of CD-1 mice dosed with PEG or DAPM (100 and 200 mg/kg) 30 h post-dose. Individual liver and stomach weights were calculated as a percentage of post-mortem body weight. Bars represent the mean value ± SEM. n.s= non-significant, * = p<0.05 and ** = p<0.01

3.3.6 ANIT causes moderate liver injury in fasted C57BL/6J mice

Histological analysis revealed the pattern of liver injury in DAPM-treated CD-1 mice to be random and not confined completely to cholangiocytes (Fig 3.8A). This limited its utility as a consistent periportal toxin.

Though ANIT displayed minimal and unreliable liver toxicity in CD-1 mice, published work has demonstrated its hepatobiliary toxicity in C57BL/6J mice. Therefore, a small

time-matched study of ANIT in C57BL/6J mice was performed. Mice were dosed with corn oil (n=3 per time point) or 75 mg/kg ANIT (n=3 per time point) and were culled 24 h, 48 h and 72 h post-dose. Throughout the study, ANIT appeared to be well tolerated by the mice. No issues arose regarding exceeding the animal severity limit in the first 12 h in this study, unlike in the CD-1 experiment, although movement was lethargic up to 48 h post-dose.

H&E liver staining revealed no changes to the perivenous area of ANIT-dosed mice (Fig 3.11A). However, in the periportal areas, mild hepatitis was observed at 24h (Fig 3.11D), which progressed to infiltrating immune cells localised to the bile ducts at 48 h (Fig 3.11F) and 72h (Fig 3.11H), with marked coagulative necrosis.

A

C57, Male, 6-8 weeks old, Fasted, ANIT 75 mg/kg, 10mL/kg, o.g administration

Timepoint (h)	Perivenous Effects	Incidence	Periportal Effects	Incidence
0	None	High	None Fatty degeneration (mild)	High Incidental-Low
24	None	High	None Hepatitis (mild), Fatty degeneration (moderate)	Moderate Low
48	None	High	None Coagulative necrosis (marked), Inflammation associated to bile duct	Low Moderate
72	None	High	None Coagulative necrosis (marked), Inflammation associated to bile duct	Low Moderate

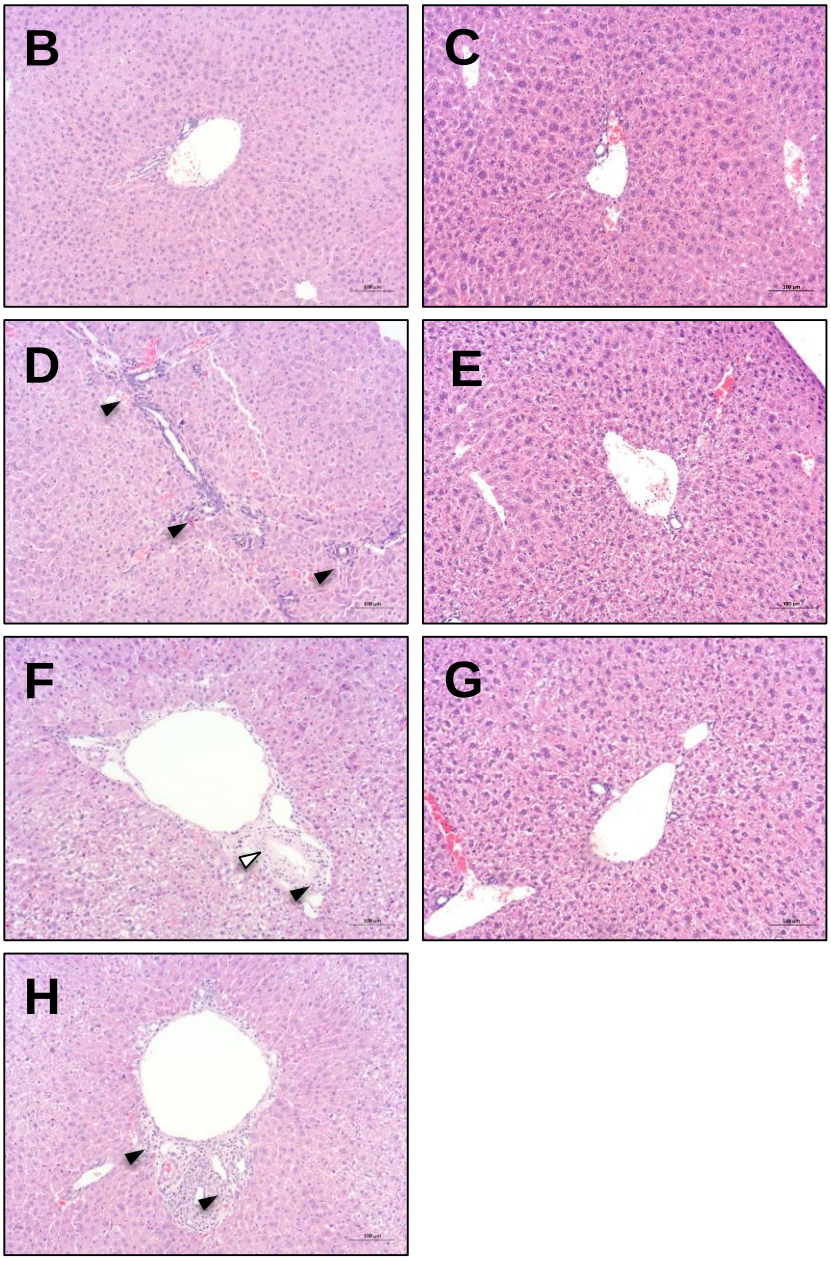

Figure 3.11- A time course of ANIT causes liver injury in fasted C57BL/6J mice by histological assessment

(A) Histopathological assessment and representative images of H&E stained liver sections from fasted C57BL/6J mice dosed with ANIT (75 mg/kg) at (B) 0 h, (D) 24 h, (F) 48 h and (H) 72 h, or corn oil at (C) 24 h, (E) 48 h and (G) 72 h post-dose. White arrows indicate coagulative necrosis, black arrows indicate infiltrating immune cells. Magnification x10, scale bar 100 µm

Serum biomarker analysis represented a more comprehensive and reproducible profile of liver injury than compared to previous CD-1 mouse studies. Peak ALT injury was observed at 48 h post-dose, though all time points were significantly elevated compared to the corn oil-treated mice. Furthermore, ALT was significantly higher at 48 h and 72 h post-dose compared to the 0 h control (Fig 3.12A). Similar to ALT, the serum levels of ALP were all elevated in dosed animals compared to their time-matched controls. This effect was significant at 24 h and 48 h post-dose. ALP levels appeared to peak at 24 h post-dose, with the exception of one mouse at 72 h (Fig 3.12B).

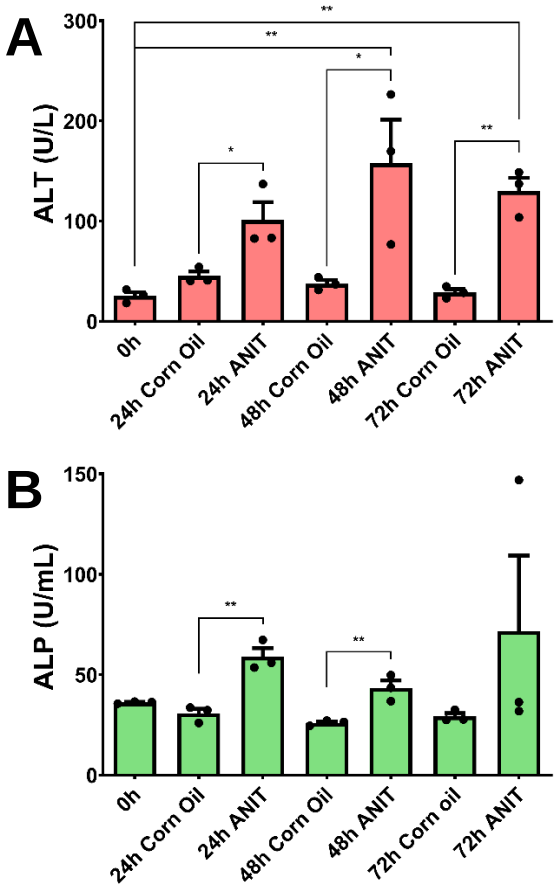

Figure 3.12- A time course of ANIT causes moderate liver injury in fasted C57BL/6J mice by serum biomarker assessment

Liver injury in fasted C57BL/6J mice dosed with corn oil or ANIT (75 mg/kg) was assessed by serum (A) ALT and (B) ALP. n=3 per group, bars represent the mean value ± SEM. * = p<0.05 and ** = p<0.01

3.3.7 ANIT causes significant changes in liver and stomach weight in fasted C57BL/6J mice

Although ANIT appeared to be better tolerated in C57BL/6J mice than in the CD-1 strain, an enlargement of the stomach was still apparent post-mortem. Measurements of total body, liver and stomach weight were therefore recorded.

Similar to the CD-1 study, corn oil-dosed mice weighed significantly more than their pre-dose weight at all time points. Conversely, ANIT-dosed mice lost weight during the course of the experiment at all time points (Fig 3.13A). The weight of ANIT-treated livers at 24 h was significantly reduced compared to vehicle controls, although this effect resolved over the 48 h and 72 h time points (Fig 3.13B). ANIT-treated stomachs were significantly enlarged relative to vehicle controls at 24 h and 48 h post-dose and remained enlarged at 72 h post-dose. The biggest difference in stomach weight between corn oil-dosed and ANIT-dosed mice was observed at 24 h (Fig 3.13C). Similar to the liver, this effect resolved over time.

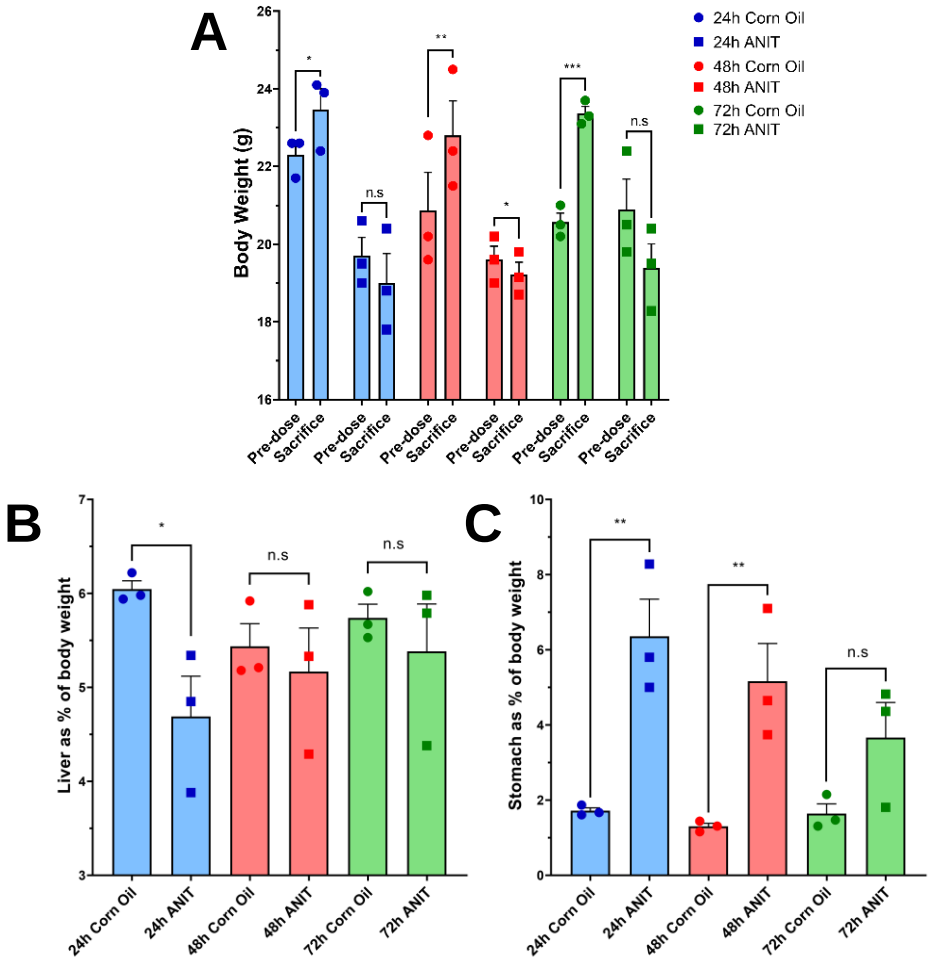

Figure 3.13- A time course of ANIT causes significant changes in liver and stomach weight in fasted C57BL/6J mice

Differences in the (A) total body, (B) liver and (C) stomach weights of C57BL/6J mice dosed with corn oil or ANIT (75 mg/kg). Individual liver and stomach weights were calculated as a percentage of post-mortem body weight. Bars represent the mean value ± SEM. n.s= non-significant, * = p<0.05, ** = p<0.01 and *** = p<0.001.

3.3.8 ANIT causes moderate liver injury in fasted Sprague Dawley rats by histological assessment

The previous experiments within this chapter involving ANIT have demonstrated a degree of stomach perturbation associated with varying degrees of reproducible liver injury in mice. Sensitivities in the stomach and liver to ANIT appeared to vary with the strain of mouse. ANIT is the classic hepatobiliary toxin used in pre-clinical studies, though it is more commonly used in rats than mice. In order to assess both the hepatic

and gastric effects of ANIT between pre-clinical species, Sprague Dawley rats were dosed with corn oil (n=6) or 50 mg/kg ANIT (n=6) and culled 30 h post-dose. Throughout the study, ANIT appeared to be well tolerated by the rats.

H&E liver staining revealed no histological changes to the perivenous area of ANIT-dosed rats (Fig 3.14A). In the periportal areas, infiltrating immune cells with moderate coagulative necrosis were observed (Fig 3.14C). The degree and features of the injury were noted to be similar to the lesions detected in the ANIT-treated C57BL/6J mouse (Fig 3.11).

A

Sprague Dawley, Male, 6-8 weeks old, Fasted, ANIT 75 mg/kg, 10mL/kg, o.g administration, 30h Timepoint

Dose (mg/kg)	Perivenous Effects	Incidence	Periportal Effects	Incidence
Corn Oil	None	High	None	High
			Inflamatory infiltration (mild)	Low
ANIT (50)	None	High	None	Low
			Inflamatory infiltration (moderate), Coagulative necrosis (mild), possible hyperplasia	Moderate

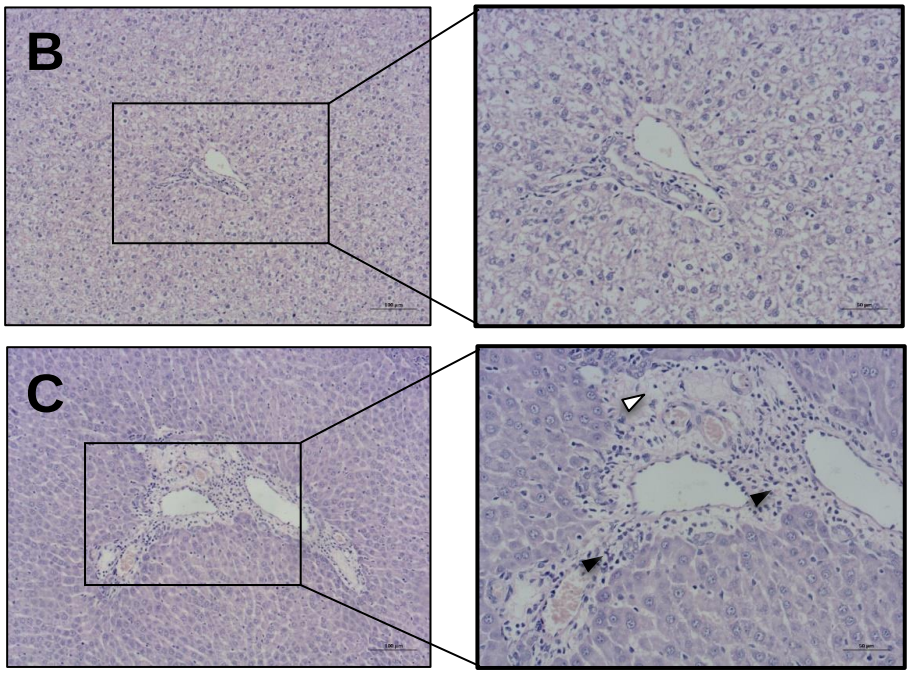

Figure 3.14- ANIT causes minor liver injury in fasted Sprague Dawley rats by histological assessment

(A) Histopathological assessment and representative images of H&E stained liver sections from fasted Sprague Dawley rats dosed with (B) corn oil or (C) ANIT (50 mg/kg) 30 h post-dose. White arrows indicate coagulative necrosis, black arrows indicate infiltrating immune cells. Magnification x10 and x20, scale bar 100 µm, and 50 µm.

Serum biomarker analysis revealed a significant rise in ALT in ANIT-treated rats compared to the corn oil controls (Fig 3.15A). The levels of ALP were also significantly higher in ANIT-treated rats compared to corn oil controls, although these values were more variable than the ALT measurements (Fig 3.15B).

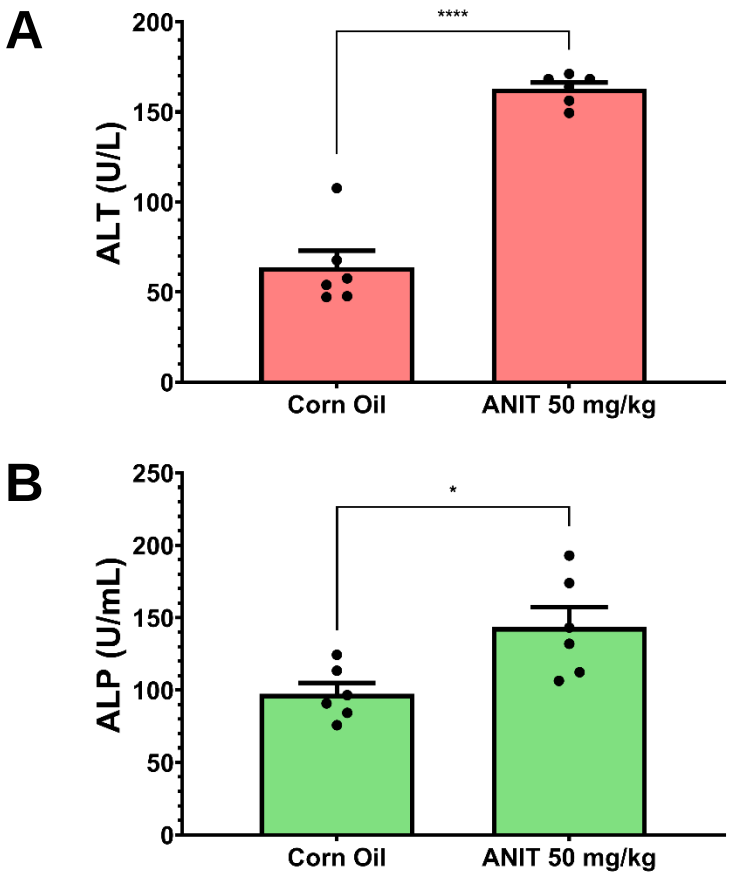

Figure 3.15- ANIT causes minor liver injury in fasted Sprague Dawley rats by serum biomarker assessment

Liver injury in fasted Sprague Dawley rats dosed with corn oil or ANIT (50 mg/kg) was assessed by serum (A) ALT and (B) ALP. n=3 per group, bars represent the mean value ± SEM. * = p<0.05 and **** = p<0.0001.

3.3.9 ANIT causes significant changes in liver and stomach weight in fasted Sprague Dawley rats

Upon post-mortem examination, the stomachs of ANIT-treated rats were enlarged relative to the vehicle controls, therefore measurements of total body, liver and stomach weight were recorded.

Upon sacrifice, corn oil-dosed rats weighed significantly more than their pre-dose weight. However, ANIT-dosed rats maintained a similar weight throughout the study (Fig 3.16A). The weight of the liver was also significantly lower in ANIT treated rats compared to vehicle control (Fig 3.16B), as was seen in the previous mouse studies. The stomach weights of ANIT-dosed rats were significantly higher than corn oil-treated rats (Fig 3.16C).

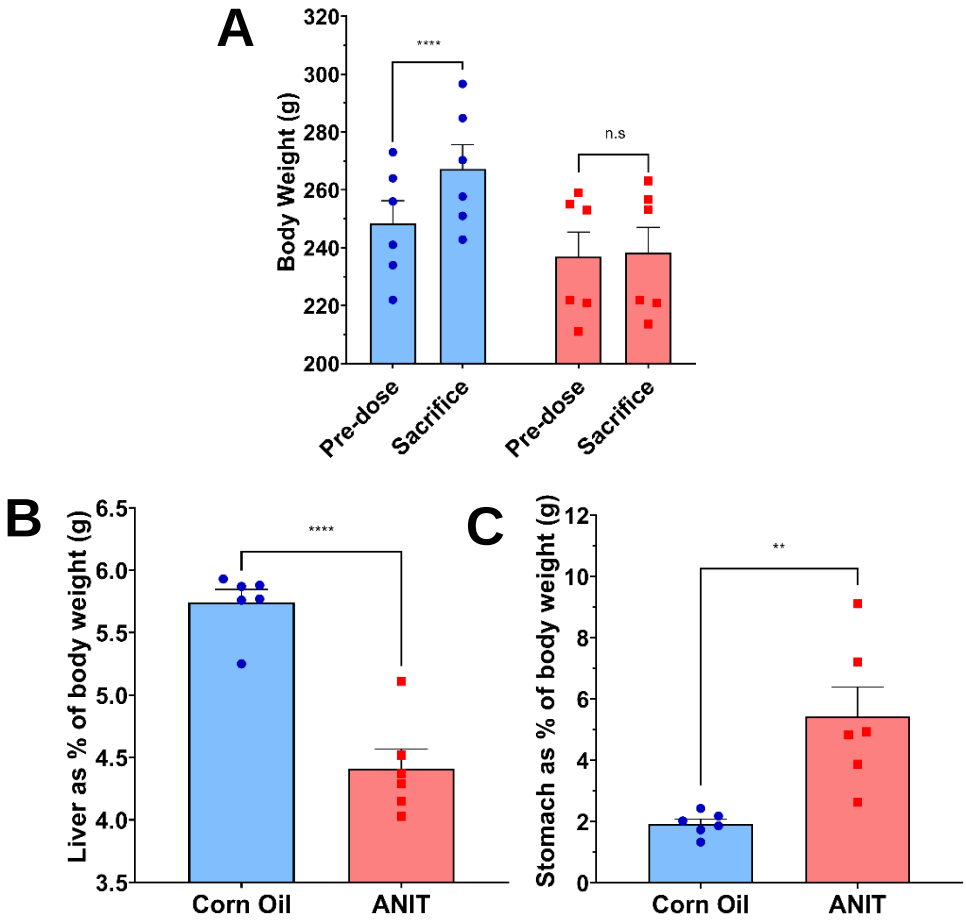

Figure 3.16- ANIT causes significant changes in liver and stomach weight in fasted Sprague Dawley rats

Differences in the (A) total body, (B) liver and (C) stomach weights of Sprague Dawley rats dosed with corn oil or ANIT (50 mg/kg). Individual liver and stomach weights were calculated as a percentage of post-mortem body weight. Bars represent the mean value ± SEM. n.s= non-significant, ** = p<0.01 and **** = p<0.0001.

As ANIT-associated stomach enlargement did not appear to be species dependant, stomachs underwent histological assessment (Fig 3.17A). Control stomachs were unremarkable in both glandular and non-glandular areas (Fig 3.17B). In the glandular region of ANIT-treated rats, a slight flattening of the epithelium was noted (Fig 3.17C). In the non-glandular area, a mild extravasation of neutrophils into the tissue was also apparent (Fig 3.17D). The increase in size difference between three representative control and ANIT-dosed stomachs is demonstrated in Fig 3.17E.

A

Sprague Dawley, Male, 6-8 weeks old, Fasted, ANIT 75 mg/kg, 10mL/kg, o.g administration, 30h Timepoint

Dose (mg/kg)	Stomach Effects	Incidence
Corn Oil	None	High
ANIT (50)	None	Low
	Potential errosion, mild-moderate neutrophil infiltration into lamina propria, some epithelium flattening	Moderate

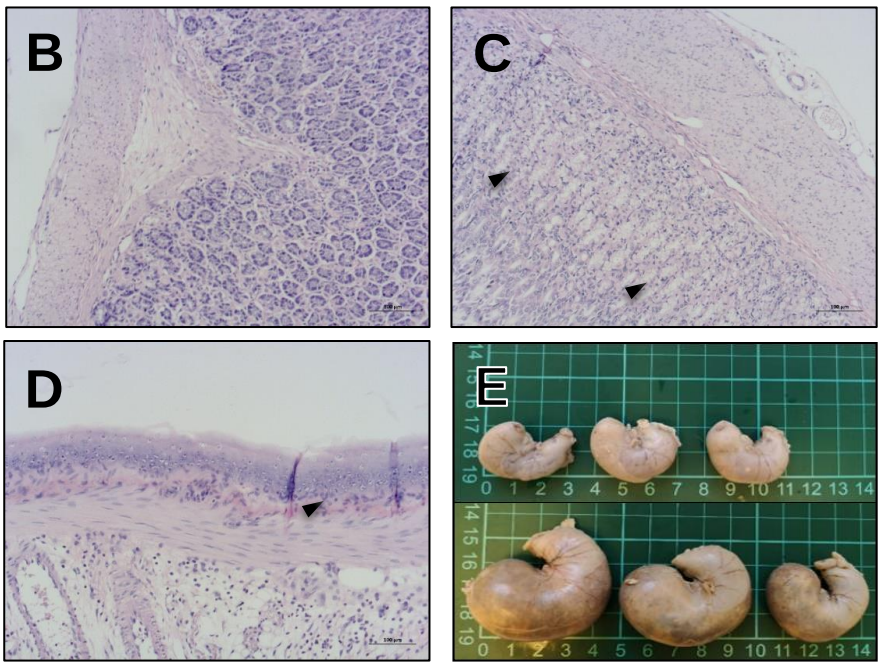

Figure 3.17- ANIT causes minor stomach toxicity in fasted Sprague Dawley rats by histological assessment

(A) Histopathological assessment and representative images of H&E stained stomach sections from fasted Sprague Dawley rats dosed with corn oil or ANIT (50 mg/kg) 30 h post-dose. (B) corn oil treated stomach, (C) ANIT treated, glandular stomach, black arrows indicate flattened epithelium, (D) ANIT treated, non-glandular stomach, black arrow indicates neutrophil extravasation. Magnification x10, scale bar 100 µm. (E) Image of corn oil and ANIT treated Sprague Dawley stomachs.

3.3.10 Murine serum preparation for miRNA analysis

Although the degree of biliary injury varied greatly across the different mouse studies, it was still important to assess if any cholangiocyte enriched or unique miRNAs could be detected as circulating biomarkers. Therefore, total RNA was isolated from serum of hepatotoxin-dosed and time-matched controls (n=3 per treatment and time point) from non-fasted ANIT-treated CD-1 mice at 24 h post-dose, fasted ANIT-treated CD-1 mice at 24 h and 72 h post-dose, fasted CD-1 mice dosed with 200 mg/kg DAPM and fasted ANIT-treated C57BL/6J mice at 24 h, 48 h and 72 h post-dose. These samples were chosen based upon identification of histopathological perturbation of the bile ducts and/or increases in circulating ALT and ALP.

The concentration of RNA in serum is typically very low. Therefore, any technical variations in the isolation and reverse transcription of RNA induces discrepancies in the PCR reaction, leading to inaccurate interpretation of the data. In order to identify any potential technical inconsistencies, all serum samples were spiked with exogenous cel-lin-4 miRNA prior to RNA extraction and reverse transcription. The raw CT values of cel-lin-4 in each experimental group were similar (Fig 3.18), with an intra-group coefficient of variation of <5 %, shown in Appendix 3.1. This suggests any differences in miRNA expression would be due to biological variation and not technical error.

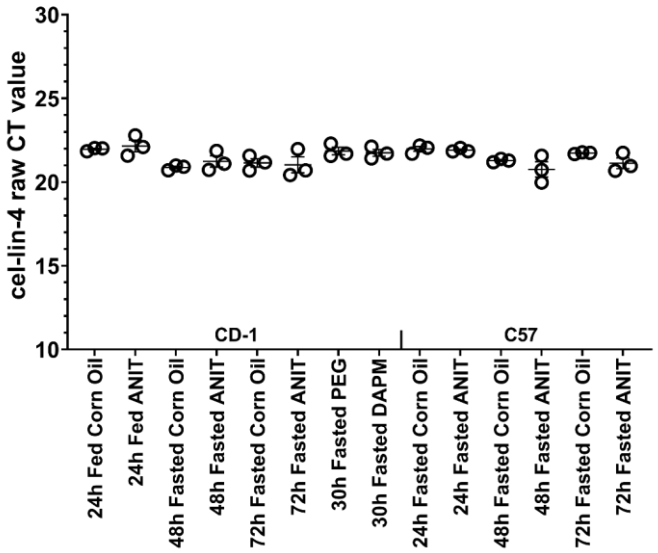

Figure 3.18- RNA extraction and reverse transcription efficiency is even across all murine serum samples

In order to ensure any variation in serum miRNAs were not a product of technical discrepancies, the CT values of cel-lin-4, an exogenous spike-in, were assessed in 42 murine serum samples. Bars represent the mean value ± SEM, n=3 per group.

The serum from multiple time points was analysed for the presence of cholangiocyte enriched (miR-200a, -200b and -429) or unique (miR-141 and -200c) miRNAs, identified in the previous chapter. miR-122 was included as a control and reference point for liver injury. All miRNAs were normalised to let-7d, an endogenous miRNA, previously used in our group as a normaliser for serum derived samples [237,238].

3.3.11 Serum miRNA alterations in non-fasted CD-1 mice dosed with ANIT

Immediate DILI was not detected by histopathology in non-fasted ANIT-treated CD-1 mice 24 h post-dose, along with no significant change in ALT and ALP (Fig 3.1-3.5).

However, by qPCR miRNA analysis, miR-141, -200b and -200c were significantly elevated compared to time-matched vehicle controls. miR-200a and -429 were also increased in the ANIT-treated samples. The levels of miR-122 remained unchanged (Fig 3.19).

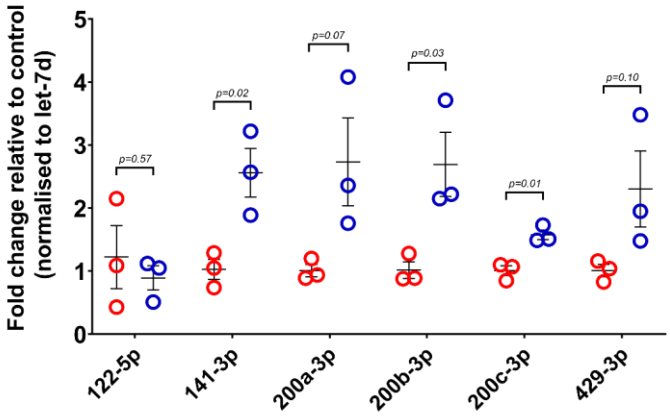

Figure 3.19- Serum miRNA alterations in non-fasted CD-1 mice dosed with ANIT at 24h

The fold change of 6 hepatic miRNAs of interest detected in the serum of non-fasted CD-1 mice following a single dose of o corn oil or o ANIT (75 mg/kg) 24 h post-dose is shown. Bars represent the mean value ± SEM, n=3 per group.

3.3.12 Serum miRNA alterations in fasted CD-1 mice dosed with ANIT

DILI observed in fasted ANIT-treated CD-1 mice was highly variable by histopathology and serum biomarker analysis (Fig 3.3-3.5). Indeed, this was also the group with the highest degree of stomach toxicity (Fig 3.6-3.7). There were minor, yet significant, increases in ALT and ALP at 24 h post-dose. The levels of ALT in ANIT-dosed mice remained elevated at 72h post-dose, indicating prolonged hepatocellular injury.

The variability of this study was also mirrored in the changes of circulating miRNAs. In ANIT-treated mice at 24 h post-dose, 1-2 mice per group showed an increase in the detection of miR-141, -200a, -200c and -429, relative to vehicle control. miR-200b showed a consistently small, yet significant, increase relative to vehicle control. The levels of miR-122 did not change at this time point (Fig 3.20A). By 72 h post-dose, no difference was seen in the cholangiocyte miRNAs of interest between vehicle control and ANIT-dosed samples. However, miR-122 was elevated in 2/3 samples, although this signal was highly variable (Fig 3.20B)

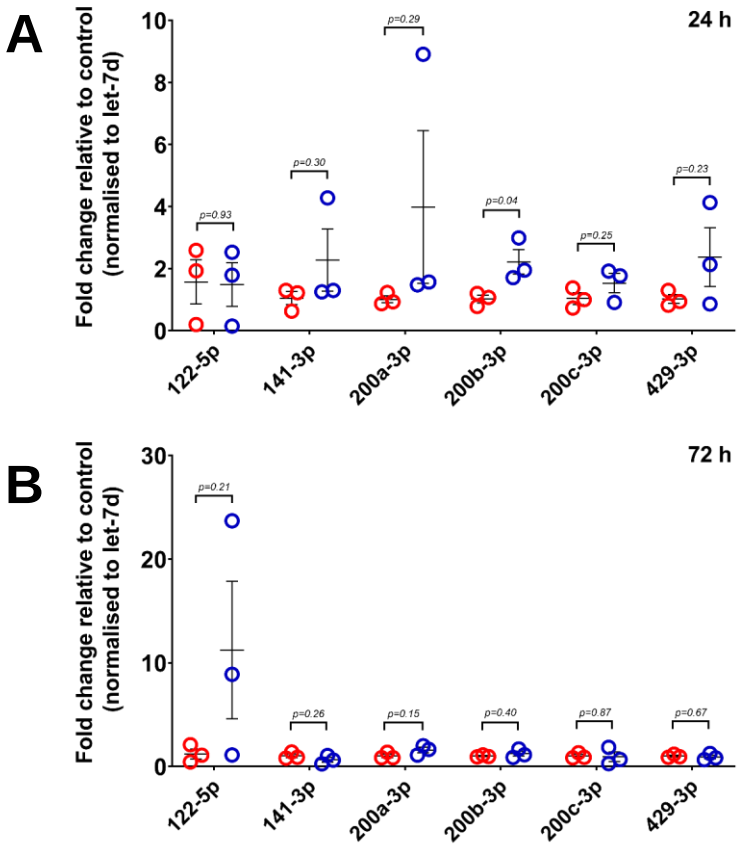

Figure 3.20- Serum miRNA alterations in fasted CD-1 mice dosed with ANIT

The fold change of 6 hepatic miRNAs of interest detected in the serum of non-fasted CD-1 mice following a single dose of o corn oil or o ANIT (75 mg/kg) (A) 24 h and (B) 72 h post-dose are shown. Bars represent the mean value ± SEM, n=3 per group.

3.3.13 Serum miRNA alterations in fasted CD-1 mice dosed with DAPM

200 mg/kg DAPM-dosed CD-1 mice did not experience significantly altered stomach weights (Fig 3.10B). A degree of mixed liver injury was identified by histopathological analysis and ALT and ALP serum elevations (Fig 3.8-3.9).

In the DAPM-dosed serum miRNA signature, there was no increase in unique cholangiocyte miRNAs (miR-141 and -200c), though cholangiocyte enriched miRNAs (miR-200a, -200b and -429) were increased relative to vehicle control, but not to a significant extent. The levels of miR-122 also saw a large, variable increase (Fig 3.21).

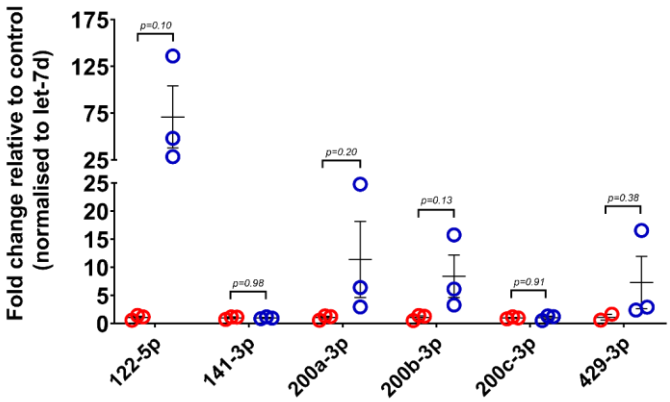

Figure 3.21- Serum miRNA alterations in fasted CD-1 mice dosed with DAPM

The fold change of 6 hepatic miRNAs of interest detected in the serum of non-fasted CD-1 mice following a single dose of o PEG or o DAPM (200 mg/kg) 30h post-dose are shown. Bars represent the mean value ± SEM.

3.3.14 Serum miRNA alterations in fasted C57BL/6J mice dosed with ANIT

ANIT-treated C57BL/6J mice exhibited reliable liver toxicity, albeit with apparent off-target stomach toxicity. Histopathological scoring indicated worsening periportal necrosis over time, with associated immune infiltration (Fig 3.11). This damage was mirrored in serum biomarker detection, whereby significant elevations in ALT were observed at all time points and in ALP at 24 h and 48 h post-dose (Fig 3.12)

The circulating miRNA signature of ANIT-treated mice at 24 h showed non-significant rises in all cholangiocyte miRNAs, except miR-200c. The levels of miR-122 were significantly elevated >10-fold compared to vehicle control (Fig 3.22A). At 48 h post-dose, a small but significant increase in the circulating levels of miR-200b was detected. A slight increase in miR-200c was also seen. Two mice showed a moderate increase in miR-141, -200a and -429 relative to vehicle control and one mouse showed a marked increase in the circulating levels of each miRNA. Levels of miR-122 were raised nearly 100-fold higher than vehicle control (Fig 3.22B). By 72 h, the levels of all cholangiocyte miRNAs of interest were elevated relative to vehicle controls, with the exception of miR-200c, whereby only one sample elicited a larger

response. Two mice showed a >20-fold increase in the circulating levels of miR-141, -200a and -429 relative to control. miR-122 was detected at approximately 160-fold higher in ANIT samples compared to vehicle control (Fig 3.22C). There was high intra-group variability in all assayed miRNAs.

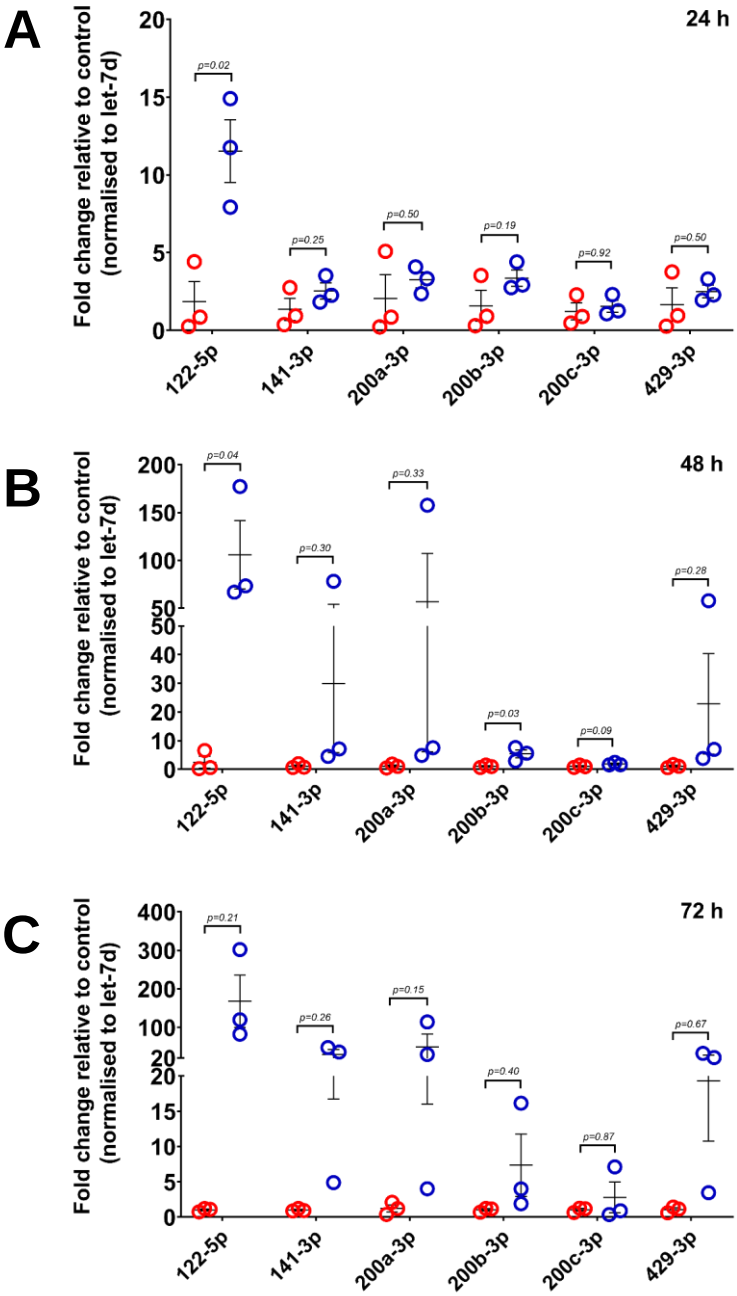

Figure 3.22- Serum miRNA alterations in fasted C57BL/6J mice dosed with ANIT

The fold change of 6 hepatic miRNAs of interest detected in the serum of non-fasted C57BL/6J mice following a single dose of o corn oil or o ANIT (75 mg/kg) (A) 24 h, (B) 48 h and (C) 72 h post-dose are shown. Bars represent the mean value ± SEM, n=3 per group.

3.3.15 Correlation of hepatic serum miRNAs with ALT and ALP

In order to assess if the miRNAs of interest correlated with hepatocellular (defined by ALT) or cholestatic (defined by ALP) injury, Log2 ALT and ALP concentrations were plotted against the ΔCT PCR value for each miRNA. Of all miRNAs, miR-122 correlated highest to Log2 ALT concentration (R^2=0.32). miR-200a, -200b and -429 are enriched in cholangiocytes, but their detection in serum may still increase during hepatocellular injury. These miRNAs poorly correlated with ALT (R^2=0.09-0.18). Finally, miR-141 and -200c, which are unique to cholangiocytes, did not correlate to ALT (R^2=0.0003-0.03) (Fig 3.23).

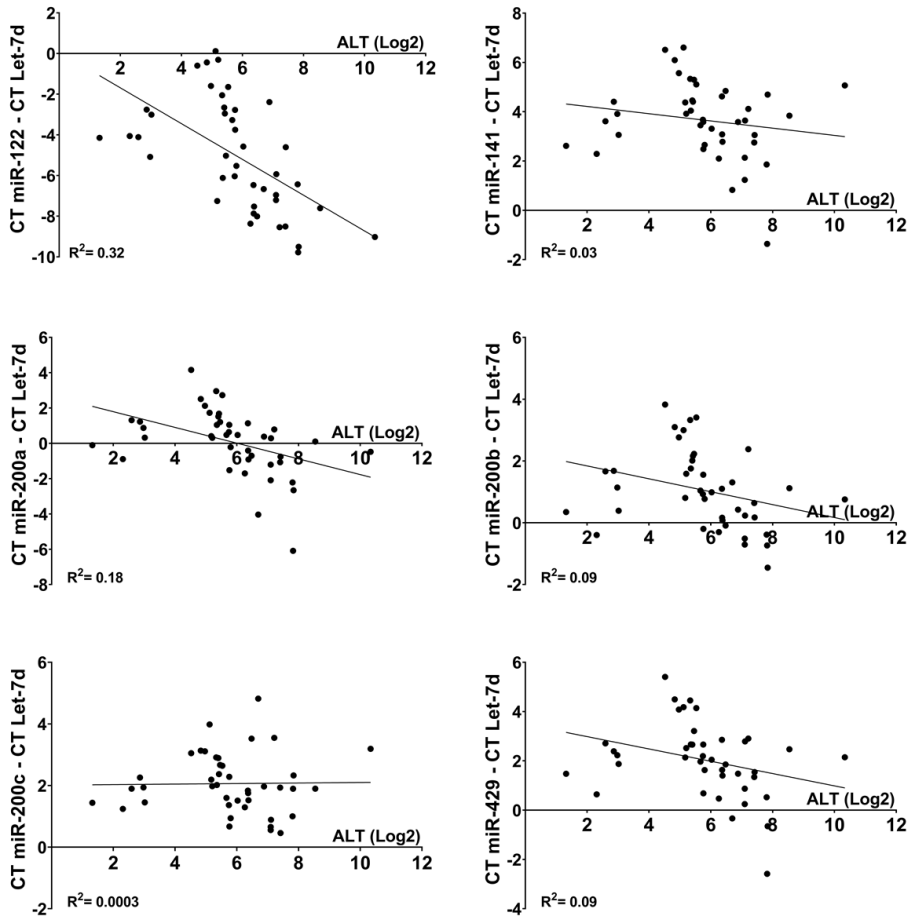

Figure 3.23- Correlation of hepatic serum miRNAs of interest with ALT

The levels of circulating hepatic miRNAs of interest relative to let-7d and Log2 transformed ALT values from 42 murine serum samples were correlated and analysed by Pearson correlation coefficient.

No single miRNA correlated well to ALP; miR-122 correlated strongest to ALP with an R^2=0.09. There was no discernible difference in the correlation of either cholangiocyte enriched or unique miRNA to ALP (R^2=0.01-0.07) (Fig 3.24).

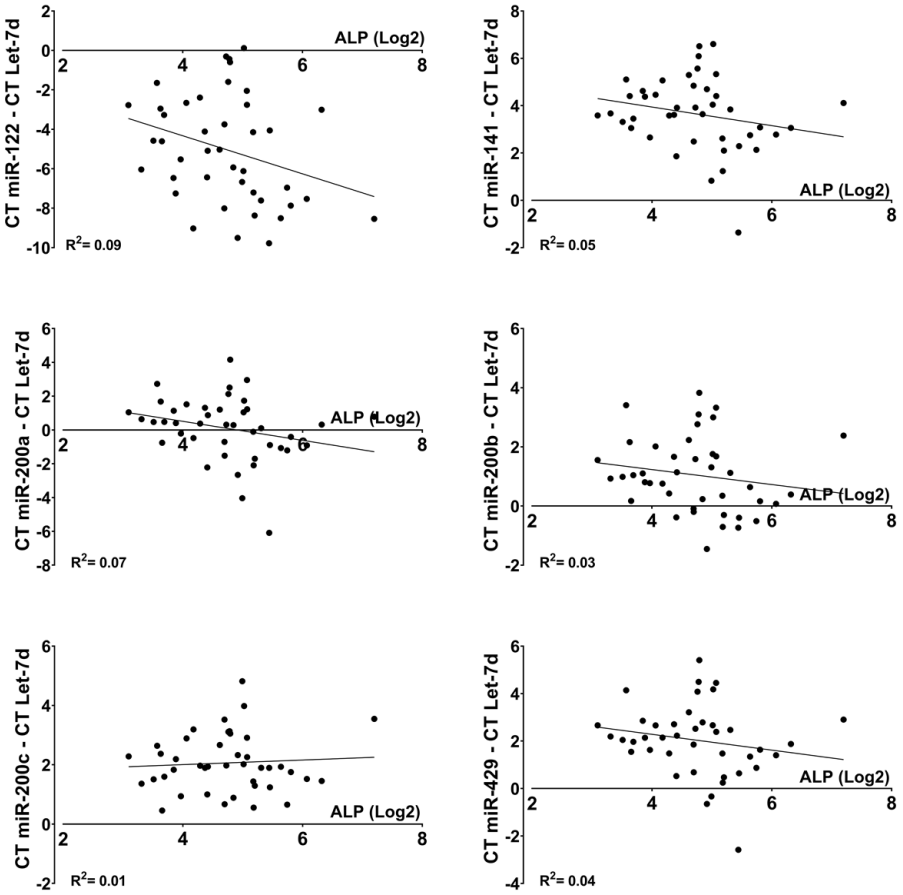

Figure 3.24- Correlation of hepatic serum miRNAs of interest with ALP

The levels of circulating hepatic miRNAs of interest relative to let-7d and Log2 transformed ALP values from 42 murine serum samples were correlated and analysed by Pearson correlation coefficient.

Due to the multifaceted nature of this work, the main toxicological findings are summarised in Table 3.2

Liver Injury	Histopathology	ALT	ALP	miRNA
CD-1 ANIT Fed	-	-	-	+
CD-1 ANIT Fasted	+	+	-	-/+
CD-1 DAPM Fasted	++	+	-/+	+
C57BL/6J Fasted	++	+++	+	++
Sprague Dawley Fasted	++	++	+	N/A

Stomach Injury	
CD-1 ANIT Fasted	+++
C57BL/6J Fasted	N/A
Sprague Dawley Fasted	++

Table 3.2- Summation of liver and stomach injury in ANIT and DAPM-dosed rodent models

Injury induced in each study was assessed by histology, traditional serum biomarkers and circulating levels of the miR-200 family. The degree of injury relative to control is indicated as none (-), mild (+), moderate (++) or high (+++).

3.4 Discussion-

The biomarkers for detecting abnormal liver function revolve around a core of serum ALT/AST and ALP measurements, whereby ALP is the current gold standard for detecting cholestatic injury. However, miRNAs enriched or unique to cholangiocytes may offer improved mechanistic insight and clinical utility over ALP in the detection and potentially, prediction of DILI. Throughout this chapter, there has been an attempt to induce cholangiocyte injury with different pre-clinical models using a single acute dose of different hepatobiliary toxins, with the aim of detecting circulating miRNAs indicative of cholangiocyte injury.

The propensity of ANIT to cause reproducible cholangiocyte liver injury in this chapter was highly variable. This was especially notable in CD-1 mice by H&E liver staining, where only a small number of mice displayed overt liver injury (Fig 3.1-3.5). Whilst this is the first study of its kind to examine hepatobiliary toxicity in CD-1 mice, ANIT has been previously utilised in C57BL/6J mice and more commonly, in rat.

The degree of liver injury presented in this chapter was shown to be relatively minor, yet highly inconsistent, by traditional biomarkers. However, this variability is also reflected in the literature, in studies with similar histopathological findings. In C57BL/6J mice dosed with ANIT by *o.g* and sacrificed 48 h post-dose, ALT values range from ~500-2000 U/L and ALP is detected at >2-4 the level of control [229,234,239]. A study of 100 mg/kg DAPM in ICR mice, a genetically similar mouse to CD-1, showed a significant increase in ALT at 24 h post-dose, though circulating levels of ALP were reduced in the dosed group, indicating only hepatocellular injury [232].

In rats, Church *et al.* showed Sprague Dawley rats dosed with 50 mg/kg ANIT displayed circulating ALT values at approximately 200 U/L, with a minor increase in ALP at 24 h post-dose, which is similar to the values shown in this work (Fig 3.15) [154]. However, Sprague Dawley rats subjected to the same conditions showed no

significant differences in ALT or ALP 24 h post-dose [240] and in another study, ALT and ALP was not significantly different until 48 h and 72 h post-dose, respectively [241]. Finally, Sprague Dawley rats dosed with 100 mg/kg ANIT and sacrificed 24 h post-dose showed alterations in miR-122, ALT, AST, GLDH and bilirubin, but no change in ALP or GGT [242].

Throughout this chapter, there were consistent elevations in the weights of stomachs in all ANIT-dosed animals, independent of mouse strain or pre-clinical species. In C57BL/6J, it was demonstrated that this enlargement was persistent up to 72 h post-dose. This off-target effect of ANIT is not reported in the literature.

In Sprague Dawley rats 30 h post-dose, C57BL/6J mice 24 h post-dose, and CD-1 mice 30 h post-dose, the average weight of the stomach made up 5.43 %, 6.36 % and 8.86 % of total body weight respectively (Fig 3.6C, Fig 3.13C, Fig 3.16C). Incidentally, CD-1 mice appeared to exhibit the most inconsistent response to ANIT, both histologically and by serum biomarker analysis. There may be a causal link between reduced gastric motility and the degree of hepatobiliary injury in animals dosed *o.g* with ANIT. A similar study of Sprague Dawley rats dosed with 50 mg/kg ANIT showed decreased body weight over the course of the study compared to corn oil controls. In agreement with this study, the average stomach contents of corn oil-dosed rats weighed 6.7 g opposed to 15.9 g in ANIT-treated rats 24 h post-dose. The authors noted that ANIT may result in delayed gastric emptying, but this was not further investigated [241].

The work presented here is the first study to date to examine the stomachs of pre-clinical models dosed with ANIT by o.g. ANIT appeared to damage to both the glandular and non-glandular areas of the stomach by histology (Fig 3.7, Fig 3.17). This effect appeared more severe in the CD-1 mouse than the Sprague Dawley rat. Histological scoring of C57BL/6J livers should also be performed to assess strain differences in the sensitivity of different mouse strains to direct toxicity of ANIT, which

may affect the outcome of future toxicity studies [243]. The reduction in liver weight observed in all ANIT-dosed animals is likely caused by a reduced gastric motility stemming from stomach toxicity, opposed to liver toxicity itself [244].

Work in the previous chapter identified miR-141, -200a, -200b, -200c and -429 as miRNAs enriched or unique to cholangiocytes. These five highly conserved members of the miR-200 family have been implicated in various hepatic pathophysiological processes, but their role as circulating biomarkers of biliary injury is not yet defined [245,246]. Although the miRNA signatures following hepatobiliary toxicity were generally increased relative to vehicle controls, though there was a high degree of variability in this study.

The miRNA elevated to the highest degree throughout this study was miR-122. Previous studies in rats dosed with ANIT have demonstrated peak miR-122 injury 48 h post-dose, at nearly 200-fold increase versus control [154]. In the C57BL/6J experiment, a smaller but more prolonged detection of miR-122 was noted, with circulating levels being detected at >100- and >150-fold higher relative to controls at 48 h and 72 h post-dose, respectively (Fig 3.22). The fold change of miR-122 at the 24 h time point was higher than that of ALT relative to control, indicating miR-122 is released from the liver earlier, or has a larger dynamic range than ALT. Both options have been previously suggested for miRNAs [138,139]. Unsurprisingly, miR-122 correlated strongest with ALT concentration (Fig 3.23), in line with previous work [247]. It was also the miRNA with strongest correlation to ALP (Fig 3.24), though this may be due to the variability seen in both liver injury and ALP measurements.

The detection of cholangiocyte enriched miRNAs (miR-200a -200b and -429) in the serum may be due to pure cholangiocyte injury, pure hepatocyte injury or a combination of the two. For example, only elevations of miR-122 and cholangiocyte enriched miRNAs were observed in DAPM toxicity 30 h post-dose with no difference in cholangiocyte unique miRNAs. This indicates, at this time point, a purely

hepatocellular injury. Indeed, serum expression of miR-200a has been shown to be upregulated in response to both perivenous and periportal hepatocellular DILI, caused by APAP and methapyrilene, respectively [153]. Moreover, miR-200a and -200b have been shown to increase in the liver following chronic (4-8 week) dosing of CCL_4, a perivenous hepatocyte toxin, though the presence of each miRNA in the circulation was not evaluated [248]. Nevertheless, these studies highlight the need to excise caution when evaluating cholangiocyte-enriched miRNAs detected in the serum. Due to the abundance of hepatocytes in the liver, a small degree of hepatocyte-specific injury could cause the release of low-expression hepatocyte miRNAs that could be falsely identified as highly abundant cholangiocyte-enriched miRNA.

However, Church *et al.* demonstrated in ANIT-dosed rats, peak miR-200a -200b and -429 serum expression was observed at 24 h, which correlated with peak cholangiocyte injury; whereas peak miR-122 was detected at 48h, which correlated with peak hepatocyte injury [154]. This may indicate the release of these specific miRNAs from cholangiocytes, not hepatocytes. Finally, in the initial non-fasted CD-1 study, the levels of miR-122 did not change relative to control, indicating a lack of hepatocellular injury (Fig 3.19). However, all cholangiocyte miRNAs of interest were elevated, indicating that cholangiocytes may have actually been injured and releasing miRNAs.

This same effect was observed with unique cholangiocyte miRNAs (miR-141 and -200c) in the non-fasted CD-1 model, whereby elevations of these miRNAs further support the idea of cholangiocyte injury. Circulating serum levels of miR-141 have been shown to correlate with levels of GGT [249] and elevations in miR-200c have been detected before levels of miR-122 in ANIT-dosed rats, indicating an initial non-hepatocellular injury [154]. Furthermore, miR-200c was shown to be uniquely elevated in rats dosed with ANIT or DAPM to induce cholestatic injury and it was not detected in the serum of hepatocellular and steatosis injury models [250]. Conversely, Yamaura

et al. demonstrated that miR-200c was uniquely detected in response to methapyrilene toxicity, but not APAP, ANIT or BDL in rats, highlighting further inconsistencies in miRNA signatures of hepatobiliary injury [153].

However, the interpretation of the presence of these circulating miRNAs in this study is limited. The work in the previous chapter identified enriched or unique cholangiocyte miRNAs, yet it also revealed that none of these were liver specific. Although ANIT does cause hepatobiliary toxicity in certain pre-clinical models, the co-current stomach toxicity, highlighted in this work for the first time, may cause the release of gastric derived miR-141, -200a, -200b, -200c or -429.

3.4.1 Conclusions & future work

In this chapter, it has been demonstrated that the use of two hepatobiliary toxins, ANIT and DAPM, produces a highly variable degree of liver injury in rodent pre-clinical models. Hepatobiliary toxicity associated with ANIT was inconsistent in the CD-1 mouse, but more reliable in C57BL/6J mice and Sprague Dawley rat. The amount of DILI seen in the animals was generally low by traditional serum biomarkers. With ANIT-dosed animals, significant enlargement and toxicity of the stomach was observed, which has not been previously reported. In DAPM and ANIT-treated animals, miR-122 was increased in response to liver injury. Five cholangiocyte-associated miRNAs were also elevated with a large dynamic range, although it is unclear if they derive from the liver or stomach. Whilst previous miRNA studies have utilised the rat as a model of hepatobiliary injury [154], this work is the first miRNA study to utilise the mice challenged by ANIT and to demonstrate the associated gastric toxicity. Furthermore, the novel work presented in this chapter assesses miRNA signatures that can be used to identify cholangiocyte perturbations within a mixed or cholestatic DILI, which will aid further mechanistic understanding of these forms of injury.

Future work should aim to consolidate a dosing regimen in an appropriate pre-clinical model that gives reliable hepatobiliary injury, whilst minimising or eliminating gastric toxicity. This could be achieved by altering the administration route or the toxic compound itself. ANIT has been shown to cause hepatobiliary toxicity when administered by *i.p* [251], though it is not clear if direct abdominal toxicity would occur.

In light of the variable DILI and gastric toxicity associated with ANIT, further investigations into the relationship between toxicity and pharmacokinetic profiles of ANIT should be considered. In fasted animals, a gastric toxicity that has not been previously reported was observed. It is possible that ANIT shows a high degree of promiscuity and bound to hydrophobic gastric targets, due to the lipophilic nature of ANIT, which potentially caused localised toxicity [252]. The stomach toxicity could have attenuated gastric motility, which would have resulted in lower absorption into the GI tract, and ultimately the liver. This may explain some of the variation observed by serum biomarker measurements.

Conversely, in the non-fasted CD-1 model, the stomachs and livers appeared unremarkable following administration of ANIT. Free access to food would increase splanchnic blood flow, increasing absorption from the GI tract. Food may also have been cytoprotective to both the liver and the stomach, reducing the toxicity in both organs. Differential toxicities between non-fasted and fasted rats following acute oral dosing of 9 different chemicals suspended in corn oil demonstrated a marginally lower LD_{50} in fasted animals in 7 of the chemicals [253]. Therefore, characterising the concentration of ANIT in plasma, in addition to ANIT bound within the liver and stomach, would aid further understanding to the toxicities observed in this chapter.

Repeated dosing of compounds with a known hepatobiliary liability held by the pharmaceutical industry have also shown to be damaging to the cholangiocytes, as recently shown by Church *et al.* in collaboration with Bayer Pharma AG [154]. Other compounds, such as a DDC diet could be used as a more chronic method of

cholangiocyte toxicity [254] . Many of these are understudied in the mouse and would require further work and validation. However, human UpCyte cells dosed with the cholestatic compounds chlorpromazine, cyclosporin A, and ANIT showed no common miRNA signature between them, which highlights the variation and different mechanisms at play in detecting hepatobiliary injury with miRNAs [255].

In order to comprehensively understand the release of cholangiocyte enriched and unique miRNAs in response to DILI, a new study, with sufficient time points and time-matched controls, should be performed. This study should consist of two dosed groups of animals, one group with biliary DILI and one with hepatocellular DILI. A custom miRNA array accounting for the 50 unique and 13 shared miRNAs identified in the previous chapter should then be performed on the isolated serum of these animals. Further to this, *in situ* hybridisation of the liver for select miRNAs of interest could correlate the loss of these miRNAs from biliary structures to their appearance in the serum. The translational nature of these miRNAs could then be assessed in other pre-clinical models and human cholestatic clinical DILI samples.

3.4.2 Limitations

A potential caveat of this study is the sole use of ALP as a marker of cholestatic injury. ALP was originally chosen due to its supposed preferential rise over GGT in drug-induced cholestasis [256]. However, the study may have benefitted from supplementary markers, such as GGT, serum bile acids and bilirubin, which have been used previously alongside ALP in toxicology testing and appear to be more sensitive [229,231].

The values of ALP in control samples between experiments appeared to vary which may limit interpretation. As serum samples were collected, stored and assessed over a period of approximately 14 months, there may be significant alterations in the enzyme caused by technical variation. An elevation of ALP at the 0 h time point compared to corn oil controls was also detected. This increase in circulating ALP was

also observed by Church *et al*, suggesting fasting may alter the interpretation of its serum concentration [154].

Finally, due to the inconsistent nature of the biliary injury seen in the initial ANIT-dosed CD-1 studies, the follow-up experiments involving DAPM, C57BL/6J mice and Sprague Dawley rats were small-scale studies, limiting statistical power. Interpretation of the data presented in these studies must therefore be taken with caution, pending future experiments.

Chapter Four:

Proteomic profiling of murine biliary-derived hepatic organoids

Contents

4.1 Introduction

DILI is characterised by significant high financial costs to the pharmaceutical industry. Therefore, a predictive and proactive approach in determining DILI as a potential outcome during drug development is warranted. While necessary, current *in vitro* models of hepatotoxicity are insufficiently predictive of the mechanisms and severity of DILI, for both pre-clinical models and humans [257].

Primary hepatocytes have often been described as the gold standard cell model for hepatotoxicity testing. However, their availability, stability during long-term culture and high inter-individual variation limit their utility. Furthermore, their inability to proliferate make them an expensive single-use option. Therefore, the use of proliferative cell lines is commonplace. A portfolio of cell lines of varying complexity, such as HepG2, HepaRG and Upcyte cells, cultured in 2D or 3D, signify a varied representation of the *in vivo* phenotype. However, to date there is no single cell culture model that sufficiently satisfies the wide-reaching requisites of DILI prediction [258–260].

The liver is responsible for a number of key physiological processes in the body, which is reflected in its abundant and diverse proteome. Nevertheless, current *in vitro* models poorly represent the *in vivo* organ phenotype. For example, a common criticism of the existing *in vitro* models is the low-level expression or gradual depletion of key drug metabolising enzymes and transporters (DMET) proteins, which is essential when evaluating potential hepatotoxicity of compounds [193,261]. Furthermore, key cellular defence proteins and pathways involved in the response to a toxic insult, such as the Nrf2-Keap1 signalling cascade, may also be dysregulated. This may be an inherent attribute due to the source of the model (e.g. cancer-derived cell lines) or as an adapted response over time to cell culture conditions [262,263].

Poorly predictive *in vitro models* ultimately necessitate the use of multiple, expensive and ethically challenging pre-clinical models in order to calculate hepatotoxicity, which in themselves are not absolutely predictive [158]. Therefore, there is an unmet need for an *in vitro* hepatic model that shows physiological improvement over the currently used systems.

Organoids are a recent innovation in *in vitro* modelling. They are described as a 3D cell model consisting of self-organising, organ-specific cell types that mimics the corresponding *in vivo* tissue [174]. They are typically derived from pluripotent or resident adult stem cells within a primary tissue. In liver, these are thought to be the liver progenitor or oval cells located within biliary ductal structures [41]. Organoid development is typically driven through specific cell culture conditions, such as extracellular matrix formation and growth factor-driven differentiation. To date, organoids generated from multiple organs such as brain [264], kidneys [265], lungs [266], pancreas [267], and gastrointestinal tract [268] have been reported.

Organoids have garnered interest as an attractive physiological model due to their ability to recapitulate the phenotype of their derived donor tissue in both rodents and humans. For example, α1-antitrypsin deficiency and Alagille syndrome have both been modelled using patient-derived hepatic organoids [179] and organoids derived from pancreatic cancer formed carcinomas when orthotopically transplanted into mice [269].

To date, the primary reported use of organoids has been to model physiological disease states [270]. However, the use of hepatic organoids as a model of DILI remains to be explored. It has been demonstrated that biliary-derived organoids are capable of CYP450 3A4 mediated detoxification of midazolam, although the metabolism of additional drugs by different CYP450 families remains to be elucidated. As hepatic organoids are reported to maintain genetic stability throughout long-term culture and

produce a mature hepatocyte-like phenotype when fully differentiated, they may offer an improvement over currently available hepatotoxicity models [179].

Whilst organoids could be considered nascent a model of DILI, they are yet to be fully characterised to a comparable standard of pre-existing models. The assessment of the suitability of organoids as a model for hepatotoxicity is dependent on the DMET and Nrf2 protein expression when compared to liver. A global proteomic profiling of hepatic organoids and the livers from which they were derived from would allow a direct comparison of their relative phenotypes.

4.1.1 Aims and hypothesis

The aims of this chapter were to:

- Isolate and culture ductal structures from the liver into undifferentiated organoids.
- Differentiate organoids to a mature hepatic phenotype using targeted cell culture conditions.
- Compare the proteome of undifferentiated and differentiated organoids and donor matched liver tissue by mass spectrometry to assess phenotypic differences.

The main hypothesis within this chapter was that organoids derived from ductal structures in the liver could be differentiated to generate a phenotype comparable to liver tissue. From a toxicological perspective, differentiation would induce key CYP450, phase II and transporter proteins, which would validate organoids as an *in vitro* model for hepatotoxicity.

4.2 Materials and Methods

Unless otherwise stated, all organoid reagents were purchased from STEMCELL technologies (Grenoble, France) and general reagents were purchased from Sigma Aldrich (Poole, UK).

4.2.1 Experimental animals

The protocols described were undertaken in accordance with the criteria outlined in a project licence granted under the Animals Scientific Procedures Act 1986 and approved by the University of Liverpool Animals Ethics Committee. 5-7-week-old male CD-1 mice were purchased from Charles River laboratories (Cambridge, UK) and had a 7-day acclimatisation period prior to experimentation. Animals were maintained in a 12 h light/dark cycle with free access to food and water.

4.2.2 Isolation of murine hepatic duct fragments

A male CD-1 mouse was sacrificed by schedule 1 cervical dislocation. The liver was removed, dissected into 3-5 mm pieces, suspended in ice-cold DMEM/F12 and allowed to rest for approximately 2 min.

The supernatant was discarded and replaced with digestion solution (DMEM/F12 supplemented with 15 mM HEPES, collagenase IV (1 mg/mL), dispase (1 U/mL)) and the suspension was incubated at 37 °C for 20 min in a water bath. The liver tissue was vigorously pipetted to break up the material and the mixture was allowed to settle. The supernatant was then removed and discarded, and fresh digestion solution was added. The suspension was returned to the water bath for 20 min and the supernatant was removed and retained on ice. This process was repeated a further four times. The pooled digestion mixture was passed through a 70 µm filter and the cell suspension retained. This was subsequently passed through a reversible 37 µm strainer and the cell suspension discarded.

The filter was inverted, and ductal fragments captured on the strainer were eluted into ice-cold DMEM/F12 media. The mixture was divided between 4 ice-cold tubes, which were centrifuged at 300 x *g* at 4 °C for 5 min. The supernatant was discarded, leaving pellets of ductal fragments.

4.2.3 Culturing and cryopreservation of hepatic organoids

200 µL of growth factor reduced Matrigel (356231, Corning, MA, USA) was added to the pelleted ductal fragments and gently resuspended by pipette. 40 µL of the mixture was pipetted into the middle of well of a pre-warmed 24-well plate. The plate was incubated at 37 °C for 15 min to allow the Matrigel suspension to solidify into a dome. 700 µL of HepatiCult media was added per well and the organoids were incubated at 37 °C in a humidified atmosphere of 5 % CO_2. Organoids were monitored daily, with media changes every 2-3 days.

Organoids were passaged when their lumens started to turn black, indicating the organoids had started to collapse. The HepatiCult media was discarded and the organoids were broken apart by pipetting ice-cold DMEM/F12 onto the Matrigel dome. The suspensions were then collected and vortexed at a medium speed for 5 seconds (s) in order to break the organoids into 30-100 µm fragments. The fragments were then pelleted at 300 x *g* at 4 °C for 5 min and plated as described above at a 1:4 sub-culture.

To cryopreserve the organoids, pellets of organoid fragments from four domes were resuspended in 2 mL CryoStor CS10. They were then transferred to a controlled-rate cell freezing container at -80 °C and then retained liquid nitrogen for long term storage.

4.2.4 Differentiation of hepatic organoids

At the start of differentiation, organoids were passaged and grown in HepatiCult media to promote outgrowth from fragments into organoids for 3 days. The media

was changed to differentiation media (Advanced DMEM/F12 supplemented with 1% penicillin/streptomycin, 1% GlutaMAX, 10 mM HEPES, 1:50 B27 supplement with vitamin A, 1 mM N-acetylcysteine, 10 µM DAPT, 10 nM recombinant human [Leu15]-gastrin I, 50 ng/mL recombinant mouse EGF (Peprotech, US), 100 ng/mL recombinant human FGF10 (Peprotech) and 50 nM A83-01 (Tocris Bioscience, Bristol, UK)) as defined by Broutier *et al.* [180] for 9 days.

To promote complete differentiation, the media was supplemented with 3 µM dexamethasone for 3 days. The media was changed daily throughout the differentiation protocol.

4.2.5 Immunofluorescence analysis of hepatic markers

All steps were performed at RT unless otherwise stated. All steps apart from permeabilisation were performed on an orbital shaker at 30 RPM at 4 °C.

Media was removed from the organoids and the Matrigel domes were gently washed with PBS. Organoids were then fixed with 2 % PFA for 20 min and subsequently washed three times with PBS with 0.1 M glycine. The organoids were permeabilised with PBS with 0.5 % Triton-X for 10 min and washed three times with IF wash buffer (PBS with 0.25 % Triton-X and 0.05 % Tween-20) for 10 min.

Organoids were then incubated for 1 h in blocking buffer (IF wash buffer with 10% casein blocking solution). The blocking solution was removed and replaced with the primary antibodies diluted in blocking solution overnight at 4 °C. The following antibodies were used: CK19 (ab52625, Abcam (Cambridge, UK,), 1:200), AFP (ab213328, Abcam, 1:100), ALB (ab207327, Abcam, 1:500) and CYP2E1 (ab28146, Abcam, 1:1,000).

The antibody solution was removed and washed three times with IF wash buffer for 10 min and the organoids were incubated with Alexa Fluor 488 (ab150077, Abcam, 1:500) and phalloidin 594 (ab176757, Abcam, 1:500) in blocking buffer for 1 h. The

organoids were then washed twice with IF wash buffer for 10 min and then incubated with PBS with Hoescht (1:10,000) for 10 min. Organoids were then washed three times with PBS. 100 µL of PBS was added to the well to prevent domes from drying and organoids were imaged on an Axio observer Z1 microscope (Zeiss, Germany).

4.2.6 Isobaric tagging for relative and absolute quantitation (iTRAQ) and LC-MS/MS analysis

The preparation and running of the iTRAQ samples were performed in collaboration with Dr Roz Jenkins at the Centre of Drug Safety Science, University of Liverpool.

Organoids were broken from their Matrigel domes and pelleted at 300 x *g* at 4 °C for 5 min. Organoid fragments were then washed three times in ice-cold PBS and pelleted at 300 x g at 4 °C for 5 min. The pellets were then stored at -80 °C for subsequent analysis.

Undifferentiated organoids, fully differentiated organoids and donor-matched liver tissue (n=4 per group) were prepared for iTRAQ analysis. Liver samples were homogenised with a Mixer Mill 220 ball homogeniser (Retsch, Haan, Germany) and all samples were mixed with dissolution buffer (0.5 M triethylammonium bicarbonate, 0.1 % SDS, pH 8.5) and processed with a sonicator (3 x 10 s, 5 µm amplitude). The samples were centrifuged at 14,000 x *g* at 4 °C for 15 min, then frozen at -80 °C with a small sample retained for the determination of protein concentration. Protein concentration was determined by BCA assay and the samples were diluted in dissolution buffer to a concentration of 5 mg/mL. To confirm that the concentration was equal across all samples, protein aliquots were separated by SDS-PAGE and the gels were stained with Coomassie Blue according to the manufacturer's instructions.

100 µg of protein from each sample was denatured, reduced, cysteine blocked, digested and labelled by iTRAQ Reagents Multiplex Kit (Applied Biosystems, UK)

according to manufacturer's protocol. Briefly, samples were denatured with 0.1 % SDS and reduced by incubating with 5 mM tris-(2-carboxyethyl)phosphine solution at 60 °C for 1 h. Cysteine groups were then blocked by incubating samples at RT for 10 min with 10 mM methyl methanethiosulfonate (MMTS). Proteins were subsequently digested by incubation with trypsin (10 µg per sample) at 37 °C overnight and each sample was then labelled with a randomly assigned ITRAQ isobaric tag (113-121) for 2 separate ITRAQ runs as follows:

	113	**114**	**115**	**116**	**117**	**118**	**119**	**121**
iTRAQ Run 1	Undiff 4	Liver 3	Liver 4	Diff 2	Undiff 2	Diff 4	Pool 1	Pool 2
iTRAQ Run 2	Undiff 1	Liver 1	Diff 1	Undiff 3	Liver 2	Diff 3	Pool 3	Pool 4

Unbound reagent and trypsin were removed by cation exchange chromatography and fractions were desalted using a macroporous C18 column (Agilent, UK) and dried by centrifugation under vacuum (SpeedVac, Eppendorf, Germany). Samples were analysed by LC-MS/MS on a Triple TOF 6600 mass spectrometer (Sciex, UK), delivered into the instrument by automated in-line liquid chromatography using an Eksigent nanoLC 415 System. Spectra were acquired in positive ion mode with up to 25 MS/MS spectra acquired per 2.5 s cycle throughout the course of the 90 min LC gradient.

4.2.7 iTRAQ protein identification and statistical analyses

Protein identification and relative quantification were performed using ProteinPilot 5 (Sciex) with the latest version of the SwissProt database (July 2018), with trypsin as the digestion agent, MMTS as a modifier of cysteine residues and biological modifications allowed. The data were also searched against the decoy reversed database in order to establish the cut-off point for false positives (FDR). Proteins

identified with more than 95 % confidence and within a global FDR of 1% were included in the statistical analysis.

Ratios for each iTRAQ label were obtained, using the common pools as the denominator (iTRAQ label 119 and 121). Data from the two iTRAQ runs were merged using RStudio V.1.0.143. Ratios were converted to their natural log and data analysis was performed using Partek Genomic Suite software V.7.18.0518, (Partek, MO, US). A batch correction algorithm was applied to the data in order to account for technical bias between iTRAQ runs. Hierarchical clustering and PCA were then performed on the batch corrected data. Proteins that were differentially expressed between the sample types were revealed using a 2-way ANOVA on the non-corrected data, taking both sample type and iTRAQ run 1 or 2 into consideration.

4.2.8 KEGG pathway analysis of significantly different proteins

Kyoto Encyclopedia of Genes and Genomes (KEGG) analysis was performed on proteins with significant differing abundance ($p<0.05$) identified by 2-way ANOVA, using Database for Annotation, Visualization and Integrated Discovery (DAVID) V.6.8 software [271,272] in order to functionally annotate differentially enriched pathways. The analysis was performed with default settings (minimum count threshold= 2, EASE threshold= 0.1) and the most significant 25 up and down regulated pathways were recorded, alongside the number of proteins contributing to the pathway and the EASE score (*p* value).

4.2.9 Immunoblotting of protein lysates

Validation of protein expression in iTRAQ samples (n=2 per group) was performed as described in section 2.2.5 with the following changes: Resolved proteins were transferred using a Trans-Blot turbo transfer system (Bio-Rad, UK). Membranes were then probed with anti-ALT 1 (ab202083, Abcam, 1:2,000 in 2.5 % milk), anti-CYP450 3A4 (ab3572, Abcam, 1:2,000 in 2.5 % milk), anti-GSTA 1 (ab135709, Abcam, 1:250

in 2.5 % milk), anti-peroxiredoxin 1 (ab15571, Abcam, 1:1,000 in 2.5 % milk) and anti-GAPDH (G9545, Sigma, 1:5,000 in 2.5 % milk). Proteins were visualised with a Chemidoc imaging system and band density was calculated with Image Lab software V.6.0.1 (Bio-Rad). Densitometry analysis was performed by normalising protein expression to GAPDH and quantifying each sample relative to the pool sample.

4.3 Results

4.3.1 Freshly isolated ductal fragments and cryopreserved organoid fragments form undifferentiated organoids in culture

In order to generate hepatic organoids for proteomic profiling, whole murine livers were digested and the ductal fragments isolated. As the isolation technique only uses cell strainers to capture the ductal fragments, a mixed population of cell digest was obtained and seeded into Matrigel domes. Early organoid formation was observed at 24-72 h post-seeding and fully-grown organoids were achieved at 120 h post-seeding (Fig 4.1).

Successful cryopreservation and resurrection of organoids is essential for their feasibility and utility as a reproducible *in vitro* model. Undifferentiated organoids were fragmented, stored in liquid nitrogen for six months and were successfully revived in culture. Organoid growth profiles from cryopreserved fragments were similar to that of freshly isolated ductal fragments (Fig 4.1).

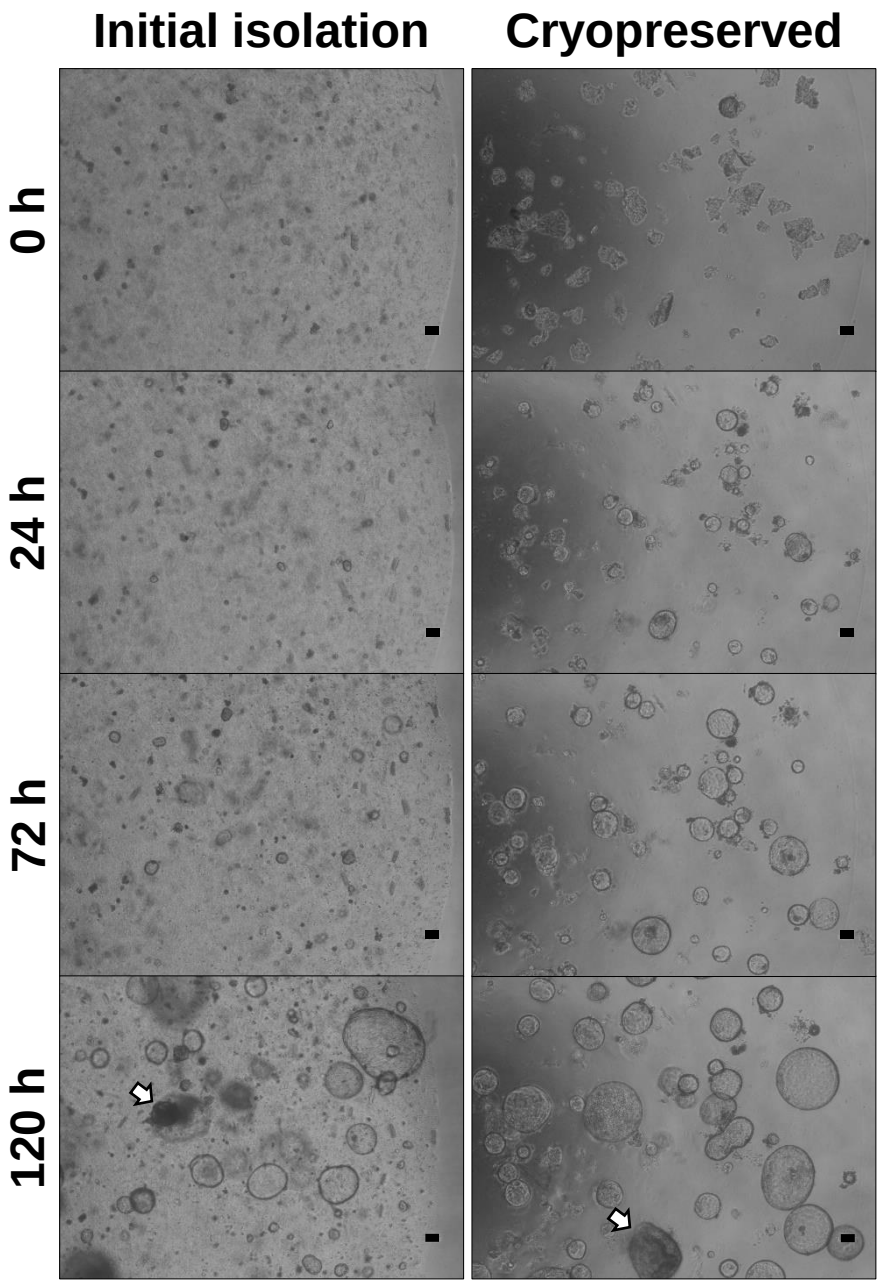

Figure 4.1- Growth profile of undifferentiated hepatic organoid formation.

Freshly isolated ductal fragments from CD-1 mice and organoid fragments that were cryopreserved for 6 months were seeded and cultured in HepatiCult media. The growth profile of undifferentiated organoids was assessed over a 120-hour period. White arrow shows collapsed organoids. Scale bar 100 µm.

4.3.2 Differentiated organoids express hepatic markers of varying maturity

In order to accurately mimic the phenotype of an *in vivo* liver, hepatic organoids should be able to demonstrate essential physiological attributes, such as albumin production and CYP450 expression.

As organoids originate from ductal fragments, they require differentiation to exhibit a mature hepatocyte phenotype. This is achieved using a combination of small molecules and growth factors over a period of 12 days (Fig 4.2A)**.** Undifferentiated organoids were maintained and outgrown in HepatiCult media (Fig 4.2B). Differentiation media contains small molecules such as A83-01 and DAPT, which promote differentiation and inhibit or interfere with Notch signalling, an essential pathway in biliary development [273]. Organoids were cultured in differentiation media for 9 days, and a further 3 days in differentiation media supplemented with dexamethasone, a known CYP P450 inducer [274] (Fig 4.2C).

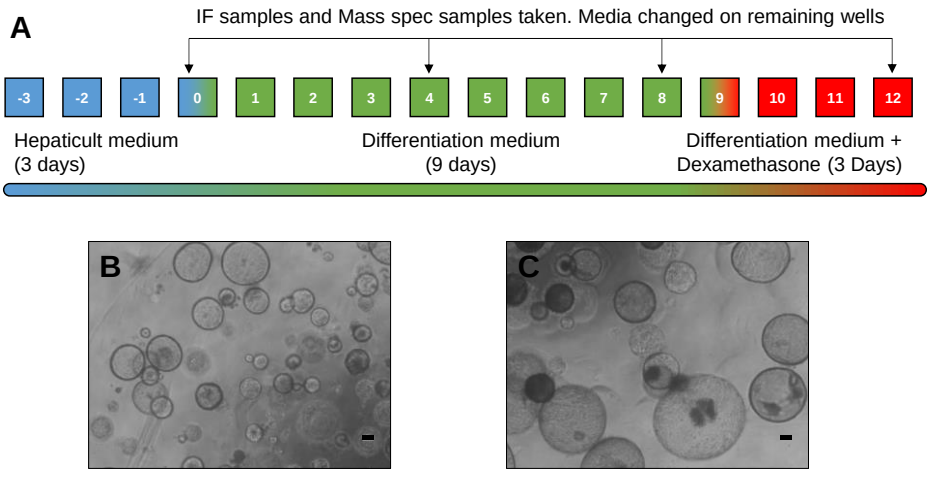

Figure 4.2- Hepatic organoids are differentiated over 15 days with defined culture media.

(A) Differentiation and sample analysis timeline for hepatic organoids. Differentiation media inhibits Notch signalling, which changed organoids from a biliary phenotype to a mature hepatic phenotype. (B) Small, undifferentiated organoids are maintained in HepatiCult media, prior to differentiation. (C) Fully differentiated organoids are much larger, and express mature hepatic markers. Scale bar 100 µm.

In order to assess the extent and suitability of the differentiation from a biliary phenotype to a mature hepatocyte phenotype, a series of IF images were taken of undifferentiated, partially differentiated and fully differentiated organoids. Organoids were stained for actin, CYP450 2E1, the biliary marker CK19, the immature hepatocyte marker alpha-fetoprotein (AFP) and the mature hepatocyte marker albumin.

Undifferentiated organoids had a relatively small diameter of approximately 80-250 µm and strongly expressed both CK19 and CYP450 2E1. There was no observed expression of either immature or mature hepatocyte markers (Fig 4.3A).

After four days of differentiation, there was a low-level expression of AFP indicating a shift toward an early hepatocyte phenotype. The expression of CK19 and albumin did not appear to change compared to undifferentiated organoids, although CYP450 2E1 appeared slightly lower (Fig 4.3B).

At day eight of differentiation, before the inclusion of dexamethasone, the levels of CK19 appear to remain unchanged compared to previous time points. There was continued low level expression of AFP and pockets of suspected albumin deposition were detected, indicating the development of a mature hepatocyte phenotype in a few select organoids. There was minimal expression of CYP450 2E1 at this stage (Fig 4.3C).

At day twelve of the differentiation protocol, organoids were significantly larger, with an approximate diameter of 300-500 µm. Organoids maintained the expression of CK19. However, expression of immature and mature hepatocyte markers was highest at this stage of the organoid culture, although this was not uniform across all organoids. Notably, after the inclusion of dexamethasone, there appeared to be a slight re-emergence of CYP 2E1 expression (Fig 4.3D).

Actin staining was utilised as a measure of examining organoid and individual cell size over time, as cholangiocytes and hepatocytes are morphologically very different. Throughout the differentiation process, it appeared that the size of the cells remained unchanged.

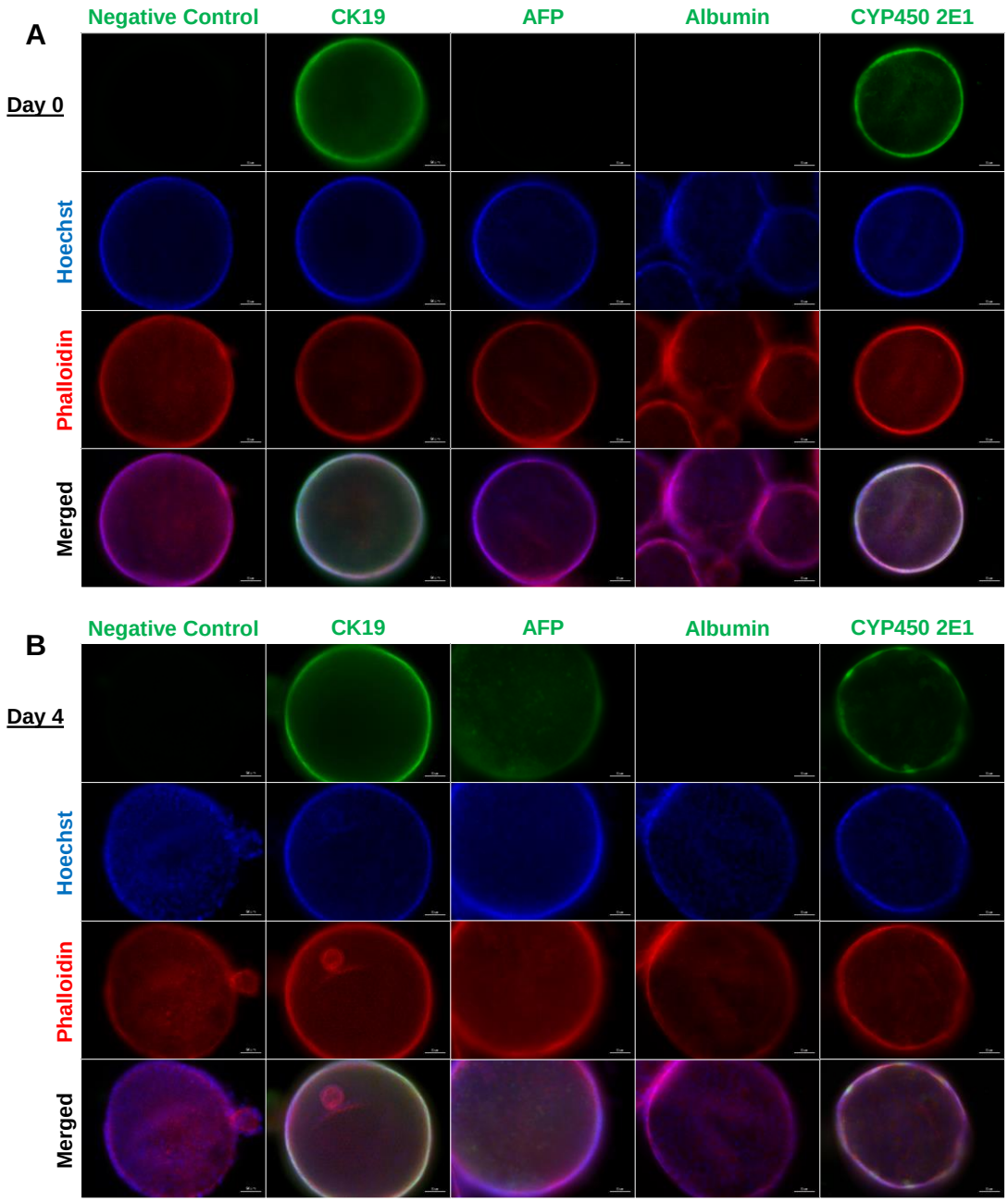

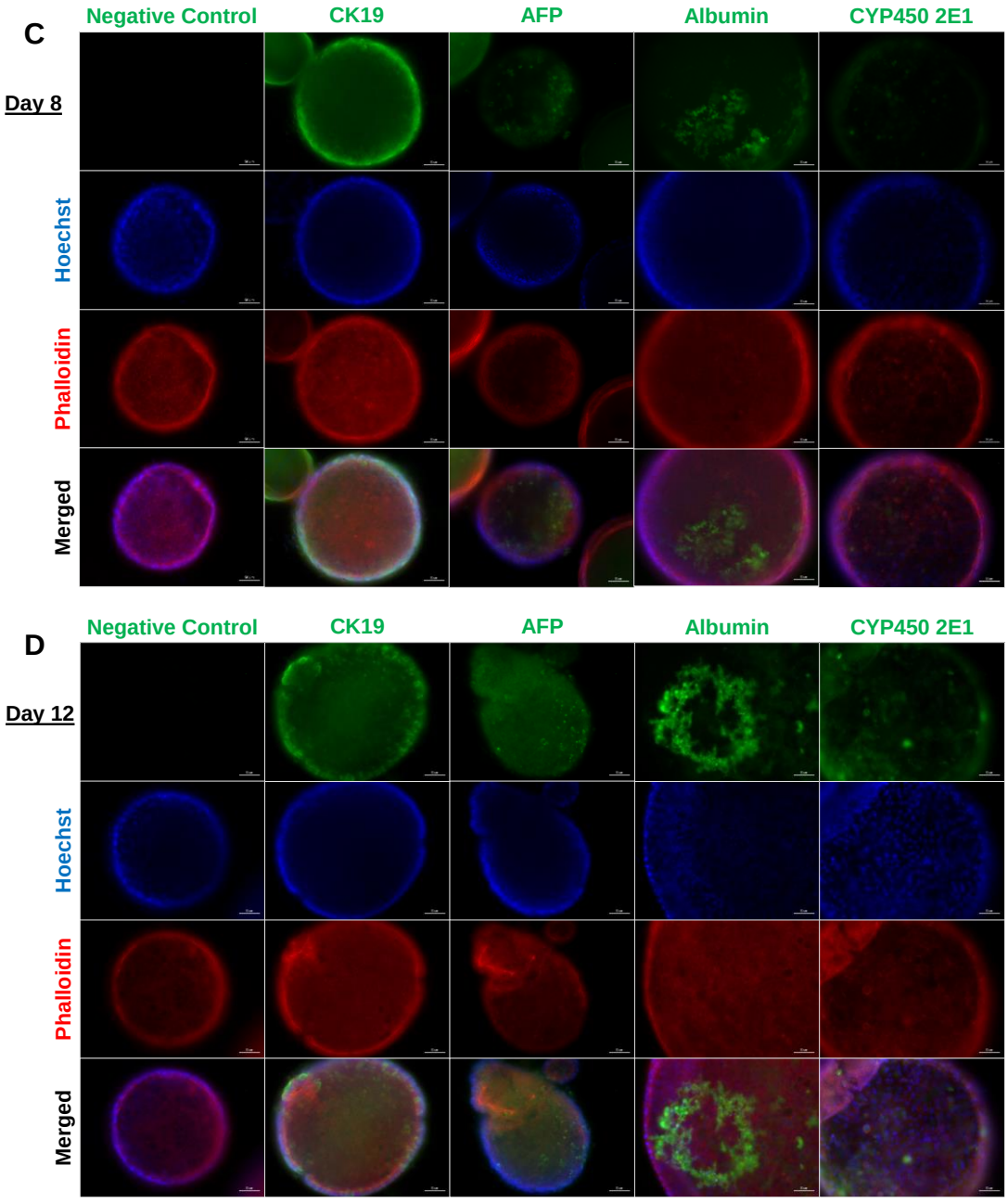

Figure 4.3- Organoids express hepatic markers of varying maturity throughout their differentiation

Organoids were stained for hepatic markers at (A) day 0, (B) day 4, (C) day 8 and (D) day 12 of differentiation. Cells were stained for the biliary marker CK19, the immature hepatocyte marker alpha-fetoprotein (AFP), the mature hepatocyte marker albumin and CYP2E1 (all green). Organoids were counterstained for actin (red) and Hoechst (blue). A negative control with no primary antibody was used for comparison. Scale bar 50 µm.

4.3.3 Preparation and initial analysis of mass spectrometry

In order to evaluate differential protein expression in liver and undifferentiated and differentiated organoids, samples were lysed and prepared for iTRAQ. Due to the quantitative nature of iTRAQ, it was necessary to confirm equal protein concentration by SDS-PAGE protein separation and Coomassie Blue staining (Fig 4.4). Samples were then labelled by iTRAQ reagent and relative global protein abundance was analysed by LC-MS/MS.

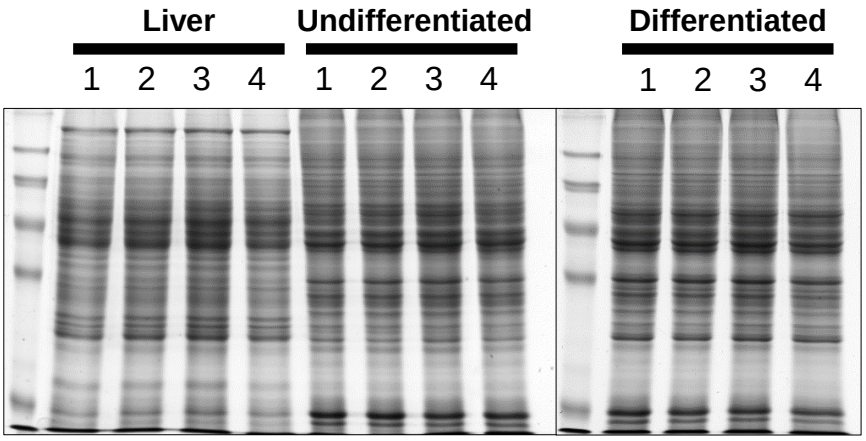

Figure 4.4- Coomassie Blue staining shows equal protein concentrations in all samples

Liver, undifferentiated and fully differentiated organoid (n=4) protein samples were diluted to 5 mg/mL in preparation of iTRAQ analysis. Equal protein concentration across all samples was confirmed by Coomassie Blue staining.

The mass spectrometry data identified 4,405 proteins consistently expressed in all samples, which allowed statistical comparison of each protein in each sample. PCA analysis of the proteome datasets revealed distinct clustering populations of liver, differentiated and undifferentiated organoid samples. The clustering of the undifferentiated and differentiated organoids on the PCA1 axis indicated they both exhibited a similar protein expression profile when compared to liver samples (Fig 4.5). This was confirmed by hierarchical clustering, which demonstrated similar expression profiles and tight clustering of organoid samples when compared to liver tissue (Fig 4.6).

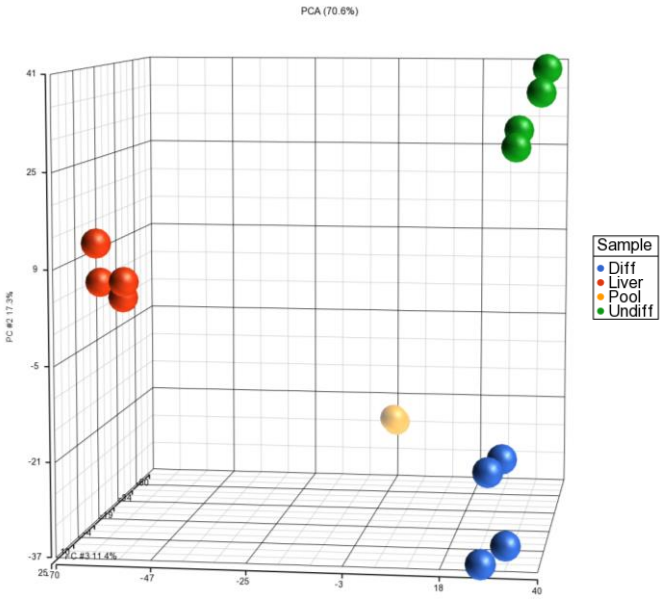

Figure 4.5- PCA analysis reveals distinct clustering of iTRAQ samples

Liver, undifferentiated and differentiated samples cluster apart from each other following principle component analysis (PCA) of merge, batch corrected iTRAQ data.

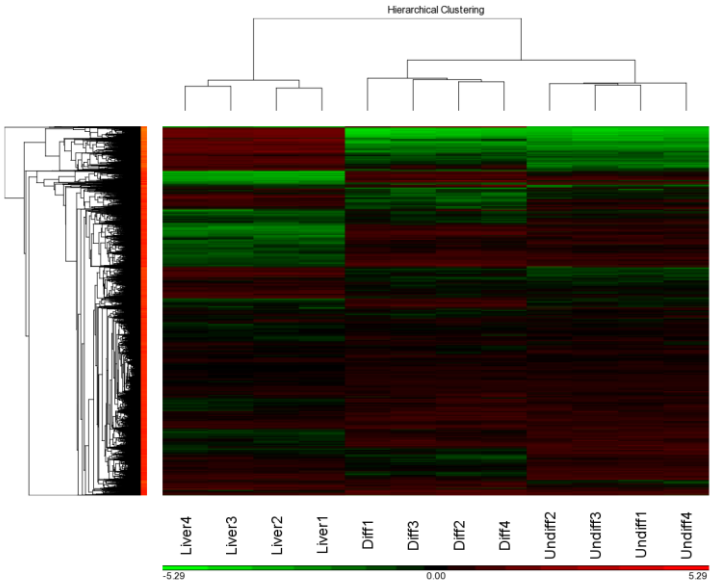

Figure 4.6- Characterisation of protein expression in liver and organoid samples

An expression heatmap of all detected proteins by iTRAQ reveals tighter clustering of differentiated and undifferentiated organoid samples than to liver.

4.3.4 Global protein expression in liver, undifferentiated organoids and differentiated organoids

In order to visualise the significance and magnitude of change in protein expression between livers, undifferentiated and differentiated organoids, volcano plots were generated of the p-values (-log10 p-value) and log2 fold change for each protein.

Proteins were considered significantly differentially expressed if $p<0.05$. To examine the range of significance, proteins were further stratified into $p>0.05$, $0.05>p>0.01$, $0.01>p>0.001$ and $p<0.001$. The number of individual protein species at each level of significance is indicated in Fig 4.7A.

A

	Diff./Liver		Undiff./Liver		Diff./Undiff.	
	Upreg.	Downreg.	Upreg.	Downreg.	Upreg.	Downreg.
$p > 0.05$	827	853	940	803	1269	1396
$0.05> p >0.01$	293	282	319	240	277	331
$0.01> p >0.001$	288	310	321	218	259	267
$p <0.001$	700	846	800	758	241	351
No Change	6		6		14	

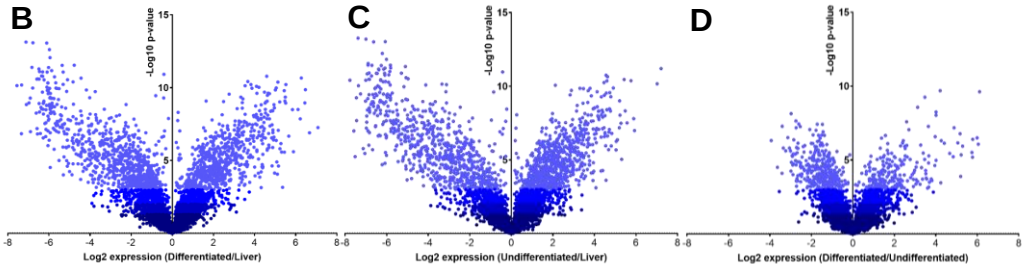

Figure 4.7- Global differential protein expression between organoids and livers varies by significance

(A) Stratification of the number of proteins found differentially expressed between samples, ranked by their statistical significance. Volcano plots of (B) differentiated organoids/liver, (C) undifferentiated organoids/liver and (D) differentiated organoids/undifferentiated organoids indicating statistical significance (-log10 *p*-value) versus log2 fold change. Statistical significance is defined as ●= $p>0.05$, ●= $0.05>p>0.01$, ●= $0.01>p>0.001$ and ●= $p<0.001$

The volcano plots comparing both differentiated (Fig 4.7B) and undifferentiated (Fig 4.7C) organoids to liver, both demonstrated a similar distribution of points, with large expression changes at a high degree of significance. Of the total 4,405 proteins detected, 2,725 (61.8 %) and 2,662 (60.4 %) were significantly (p<0.05) altered in differentiated and undifferentiated organoids respectively.

Conversely, when differentiated and undifferentiated organoids were compared, the relative change of protein expression and level of significance was small (Fig 4.7D). A total of 1740 (39.5 %) proteins were significantly (p>0.05) altered, further indicating both sets of organoid samples were more similar to each other than their original liver tissue.

4.3.5 DMET and Nrf2 proteins in the context of global protein expression

In order to assess the parameters of organoids with respect to their potential ability for drug metabolism and detoxification, alterations in the expression and significance of DMET and Nrf2-target proteins were highlighted in the context of their global protein expression.

The DMET proteins of interest included 30 cytochrome P450 enzymes (Fig 4.8A), 32 Phase II enzymes (Fig 4.8B) and 45 transporter (Fig 4.8C) proteins; 14 Nrf2-target (Fig 4.8D) and 14 hepatic biomarker (Fig 4.8E) proteins of interest were also included. The full individual p-values and changes in expression of these proteins are listed in Appendix 4.1. The expression of CYP450 (Fig 4.8A) and Phase II (Fig 4.8B) enzymes in both undifferentiated and differentiated organoids were generally downregulated when compared to liver tissue. However, upon differentiation, there was an upregulation of these key DMET enzymes. There was a similar trend observed with transporter proteins, although their downregulation and subsequent upregulation upon differentiation was not as pronounced (Fig 4.8C). Alterations in the level of Nrf2

and auxiliary hepatic proteins after differentiation were relatively modest compared with the differences observed in DMET proteins. However, there was still a trend for these proteins to be downregulated in organoids compared to liver (Fig 4.8D).

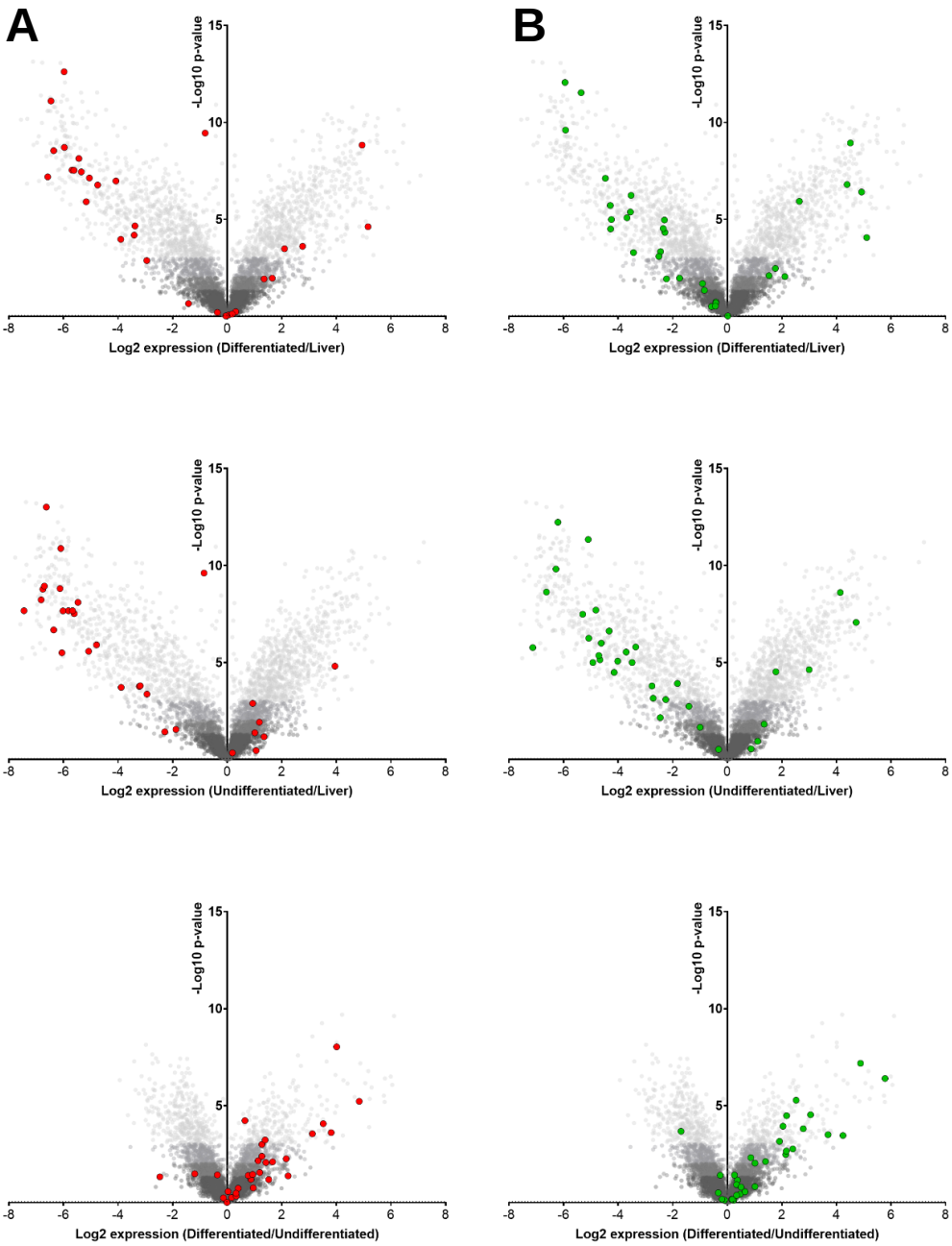

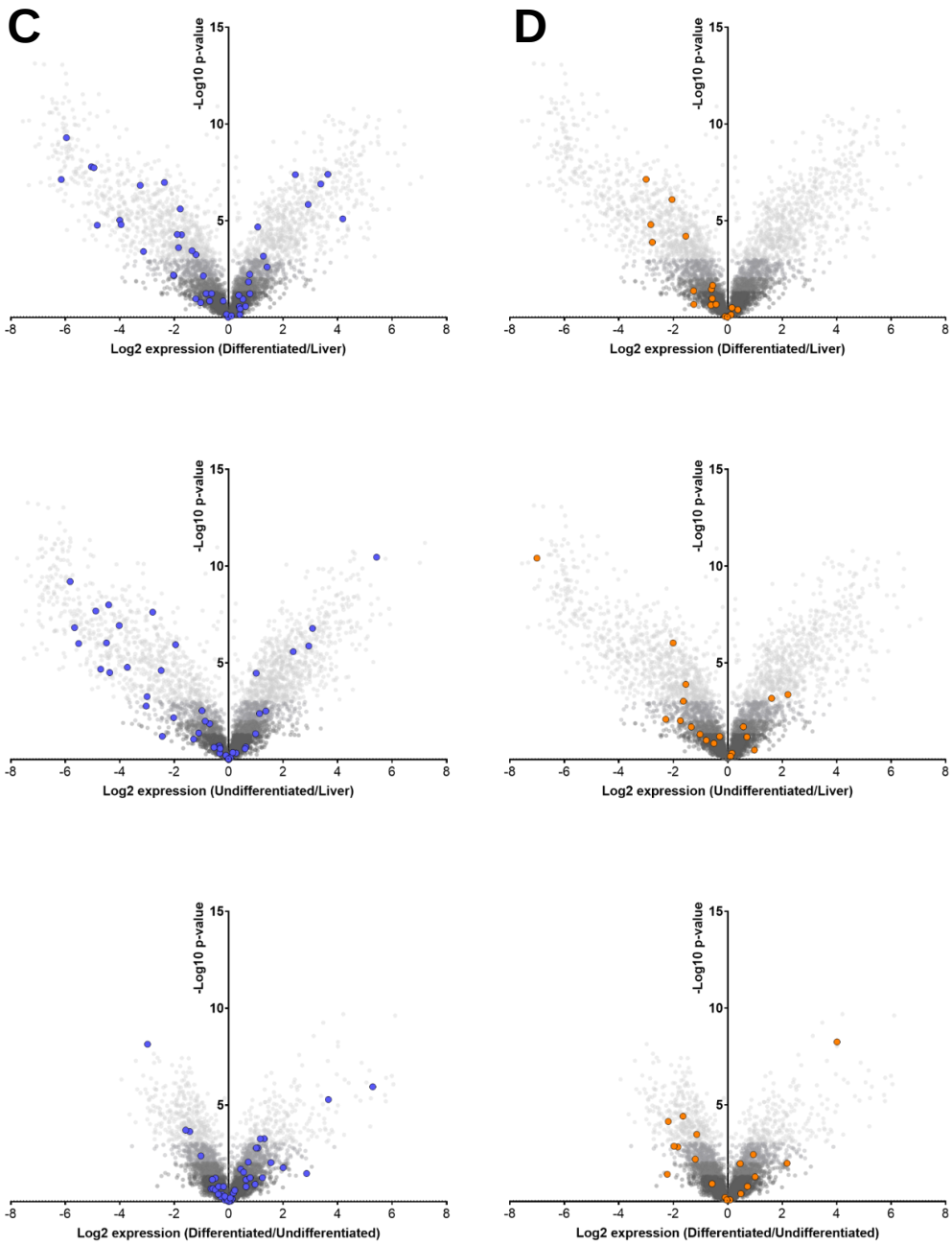

Figure 4.8- Comparison of DMET and Nrf2 target proteins in the context of global protein expression

The expression of (A) ● CYP450, (B) ● Phase II, (C) ● transporters and (D) ● Nrf2 proteins were highlighted on volcano plots of global protein expression comparing the differentiated organoids, undifferentiated organoids and livers. The volcano plots indicate statistical significance (-log10 *p*-value) versus log2 fold change.

4.3.6 Expression of key hepatic proteins in liver, undifferentiated organoids and differentiated organoids

Due to the implicit roles of metabolic turnover, conjugation and elimination of xenobiotics and chemicals by the liver, a focussed examination of individual proteins responsible for these processes was therefore warranted.

It should be noted that CYP450 isoform and nomenclature differences exist between species. The human homologs of the murine CYP450s detected in this work are highlighted in Appendix 4.2 [157].

Fig 4.9A shows the log2 change in expression of 30 CYP450 enzymes between liver, differentiated and undifferentiated organoids. Levels of CYP450 in organoids were consistently lower than in liver, except for CYP450 2C55, 2J6, 2S1, 2U1 and 4B1. Upon differentiation, there was a significant increase in expression of multiple CYP450s; notable examples include CYP450 1A2, 2A5, 2D10, 2D26, 3A11 and 3A13. CYP450 3A13 was particularly sensitive to differentiation and was the only CYP450 whose abundance was significantly lower in undifferentiated/liver that was also significantly higher in differentiated/liver. There was no substantial change in the expression of CYP450 2E1, however, it was previously demonstrated that 2E1 was expressed both pre- (Fig 4.3A) and post- (Fig 4.3D) differentiation.

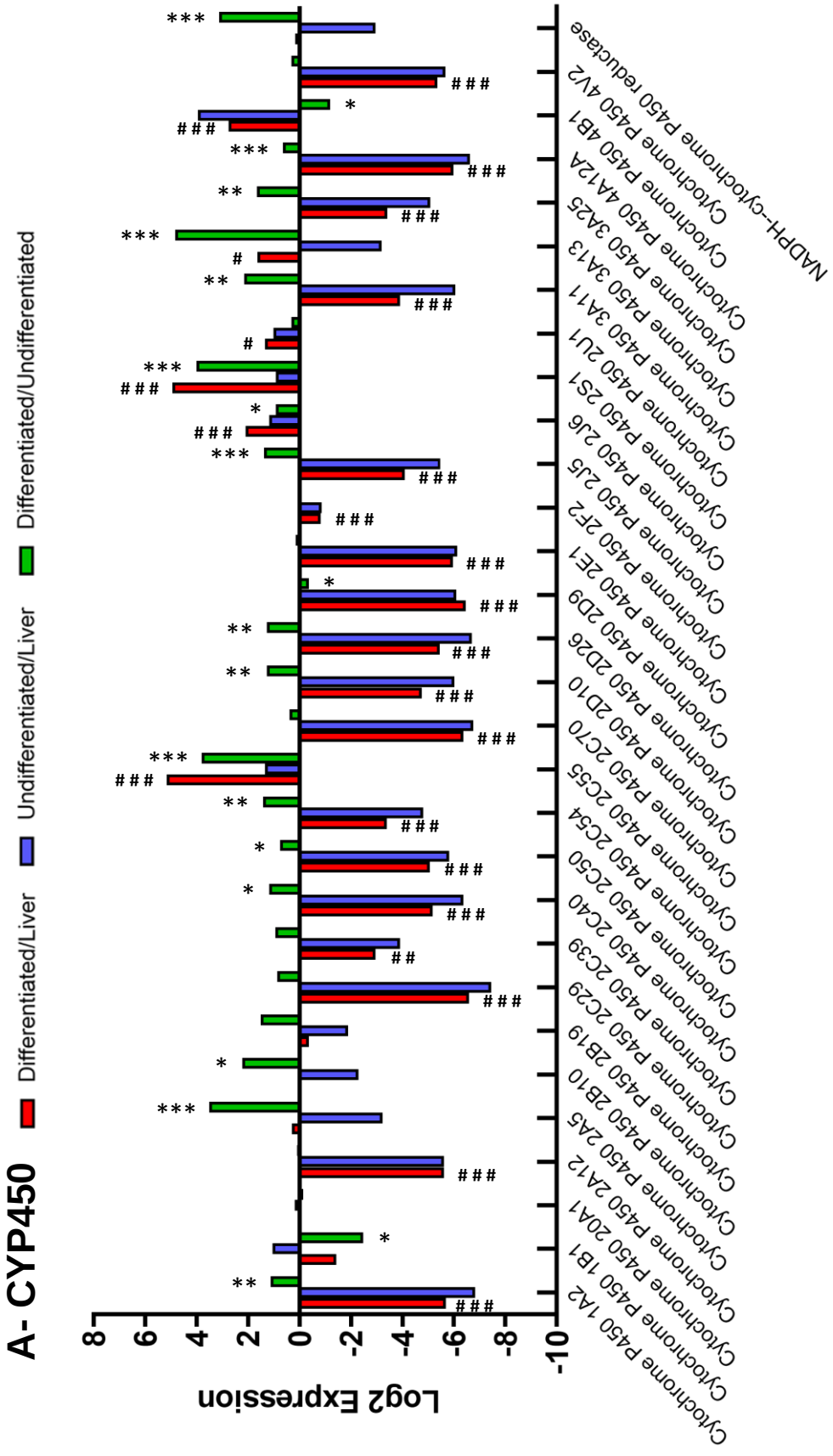
A- CYP450
Differentiated/Liver
Undifferentiated/Liver
Differentiated/Undifferentiated
Log2 Expression
8
6
4
2
0
-2
-4
-6
-8
-10
Cytochrome P450 1A2
Cytochrome P450 1B1
Cytochrome P450 20A1
Cytochrome P450 24A12
Cytochrome P450 2A5
Cytochrome P450 2B10
Cytochrome P450 2B19
Cytochrome P450 2C29
Cytochrome P450 2C39
Cytochrome P450 2C40
Cytochrome P450 2C50
Cytochrome P450 2C54
Cytochrome P450 2C55
Cytochrome P450 2C70
Cytochrome P450 2D10
Cytochrome P450 2D26
Cytochrome P450 2D9
Cytochrome P450 2E1
Cytochrome P450 2F2
Cytochrome P450 2J5
Cytochrome P450 2J6
Cytochrome P450 2S1
Cytochrome P450 2U1
Cytochrome P450 3A11
Cytochrome P450 3A13
Cytochrome P450 3A25
Cytochrome P450 4A12A
Cytochrome P450 4B1
Cytochrome P450 4V2
NADPH--cytochrome P450 reductase

The expression of phase II enzymes was largely lost in organoids when compared to liver, except various subclasses of the glutathione S-transferase (GST) family and sulfotransferase family. Differentiation of organoids broadly reversed this trend and the majority of phase II enzymes were significantly increased. However, the N-acetyltransferase and UGT family was largely unchanged, except for UDP-glucuronosyltransferase 2A3 (Fig 4.9B).

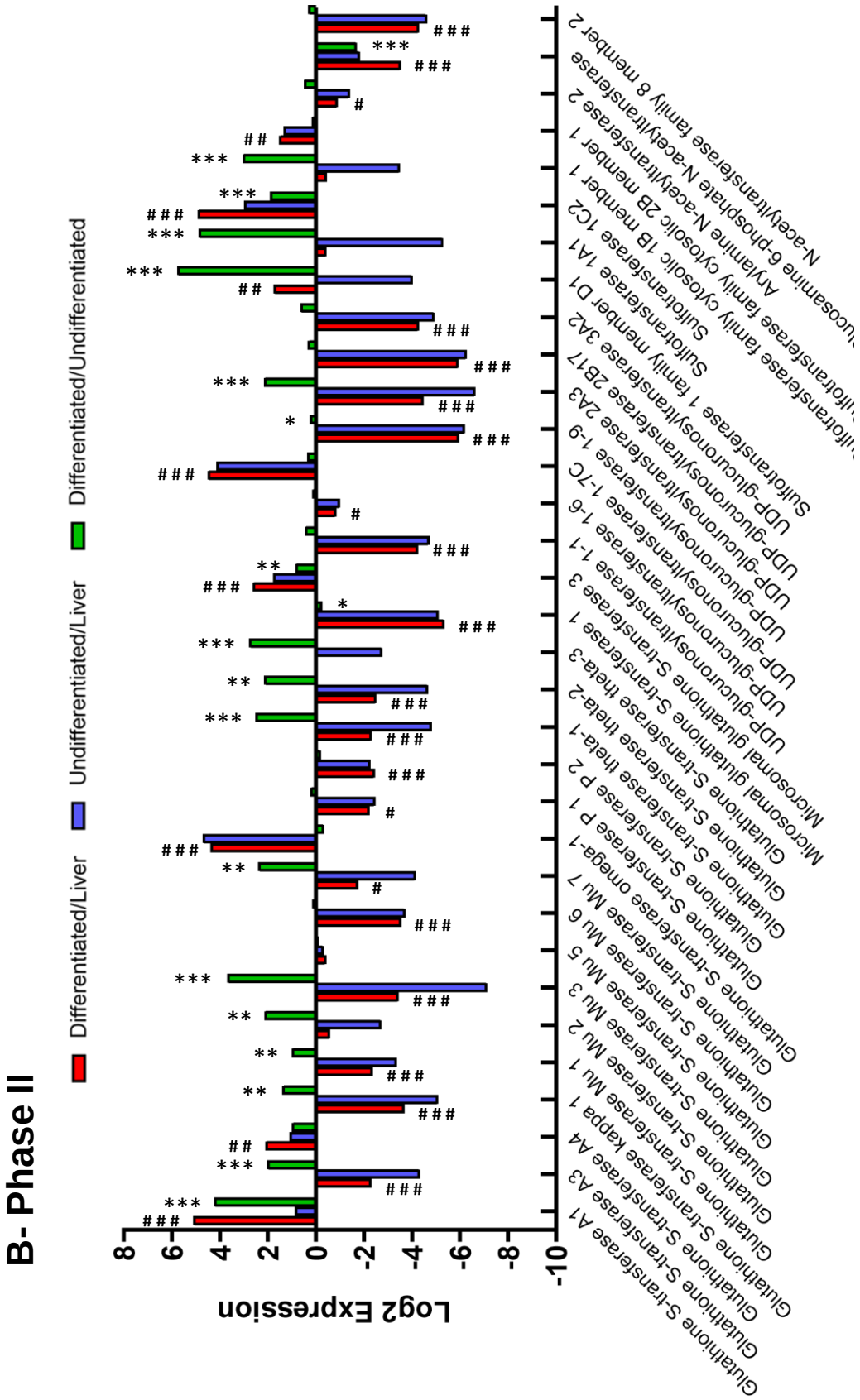
B- Phase II
Differentiated/Liver
Undifferentiated/Liver
Differentiated/Undifferentiated
Log2 Expression
8
6
4
2
0
-2
-4
-6
-8
-10
Glutathione S-transferase A1
Glutathione S-transferase A3
Glutathione S-transferase A4
Glutathione S-transferase kappa 1
Glutathione S-transferase Mu 1
Glutathione S-transferase Mu 2
Glutathione S-transferase Mu 3
Glutathione S-transferase Mu 5
Glutathione S-transferase Mu 6
Glutathione S-transferase Mu 7
Glutathione S-transferase omega-1
Glutathione S-transferase P 1
Glutathione S-transferase P 2
Glutathione S-transferase theta-1
Glutathione S-transferase theta-2
Glutathione S-transferase theta-3
Microsomal glutathione S-transferase 1
Microsomal glutathione S-transferase 3
UDP-glucuronosyltransferase 1-1
UDP-glucuronosyltransferase 1-6
UDP-glucuronosyltransferase 1-7C
UDP-glucuronosyltransferase 1-9
UDP-glucuronosyltransferase 2A3
UDP-glucuronosyltransferase 2B17
Sulfotransferase 1 family member A2
Sulfotransferase 1 family member D1
Sulfotransferase 1A1
Sulfotransferase 1C2
Aryl/amine cytosolic 1B member 1
Aryl/amine cytosolic 2B member 1
N-acetyltransferase 2
6-phosphate N-acetyltransferase
N-acetyltransferase family 8 member 2

Transporters were generally downregulated in organoids compared to livers, though not to the extent of CYP450 and phase II proteins. There was no significant change in solute carrier family 22 member 1 (OCT1), multidrug resistance-associated protein 1 and 7 (MRP1/7) expression in differentiated organoids compared to both liver and undifferentiated organoids. Conversely, solute carrier organic anion transporter 2A1 (OATP-2A1), Multidrug resistance protein 1A (MDR1A) and Canalicular multispecific organic anion transporter 2 (MRP3) were all significantly upregulated in differentiated organoids compared to both liver and undifferentiated organoids.

The majority of hepatic influx and efflux proteins were significantly underexpressed in differentiated organoids relative to liver, including OATP-A1 and -1B2, ATP-binding cassette sub-family G member 2 (BCRP), and the bile salt export pump (BSEP). Differentiation did not significantly affect the expression of these proteins compared to undifferentiated organoids. MRP6, canalicular multispecific organic anion transporter 1 (MRP2) and the sodium/bile acid cotransporter were all downregulated in differentiated organoids compared to liver, although differentiation did significantly increase their expression. (Fig 4.9C).

C- Transporters (1/2)

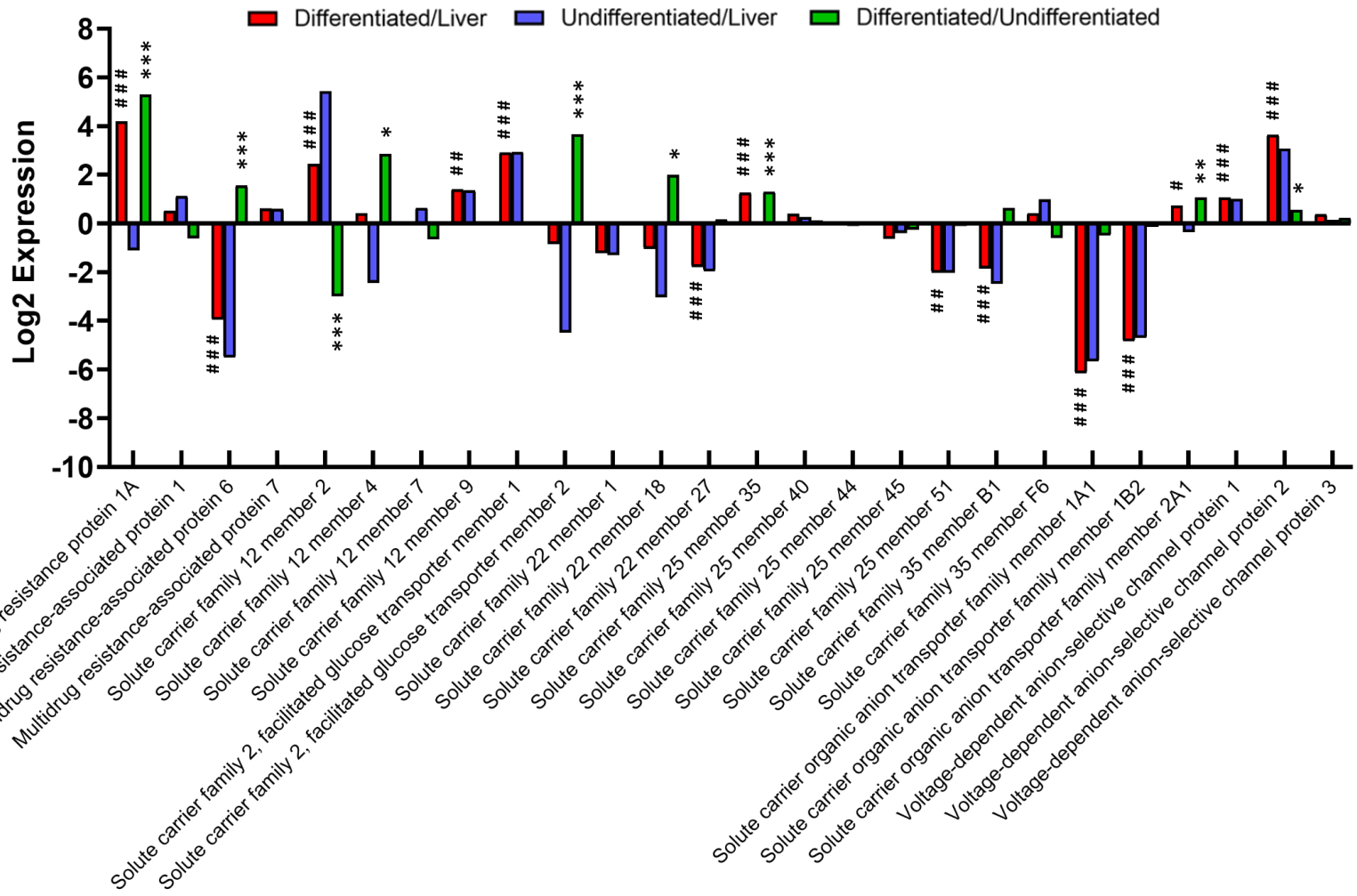

Multidrug resistance protein 1A (MDR1A), Multidrug resistance-associated protein 1/6/7 (MRP1/6/7), Solute carrier family 22 member 1 (Organic cation transporter 1, OCT1), Solute carrier organic anion transporter family member 1A1 (Organic anion-transporting polypeptide 1, OATP-1)

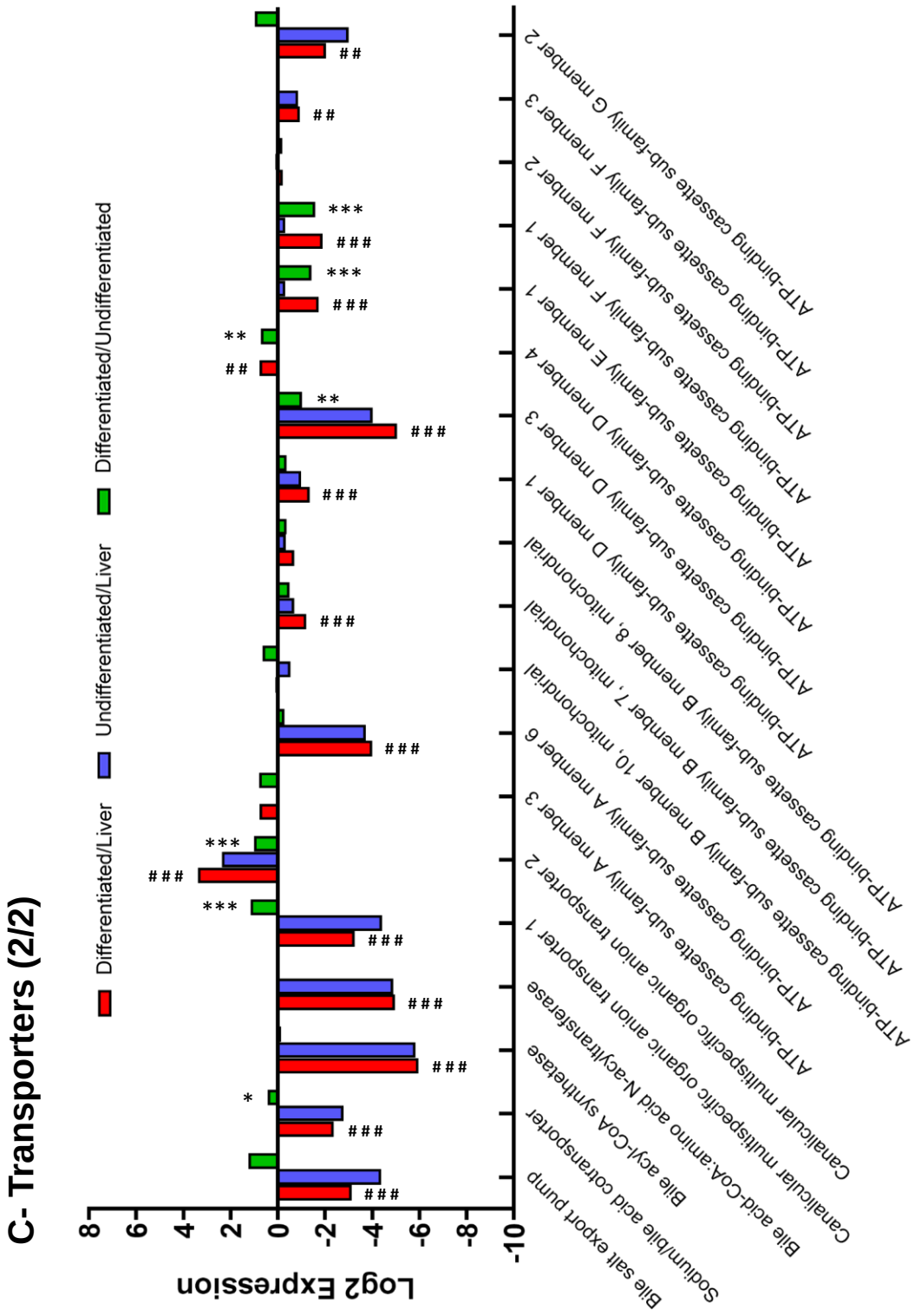

Bile salt export pump (BSEP), Canalicular multispecific organic anion transporter 1/2 (MRP2/3), ATP-binding cassette sub-family G member 2 (Breast Cancer Resistance Protein, BCRP)

The changes in abundance of key Nrf2 related proteins [275] of interest were also analysed. The relative levels of KEAP1, the repressor protein of Nrf2, and HO-1 and NQO1, two commonly used reporters of Nrf2 activation, were similar between differentiated organoids and liver. However, there was some minor up- and down-regulation of GSH- and thioredoxin (TXN)-based Nrf2 antioxidant proteins. The largest observed effect of differentiation was in glutathione peroxidase 1. Protein abundance was diminished in undifferentiated organoids compared to the liver, although this effect was significantly reduced post-differentiation. (Fig 4.9D).

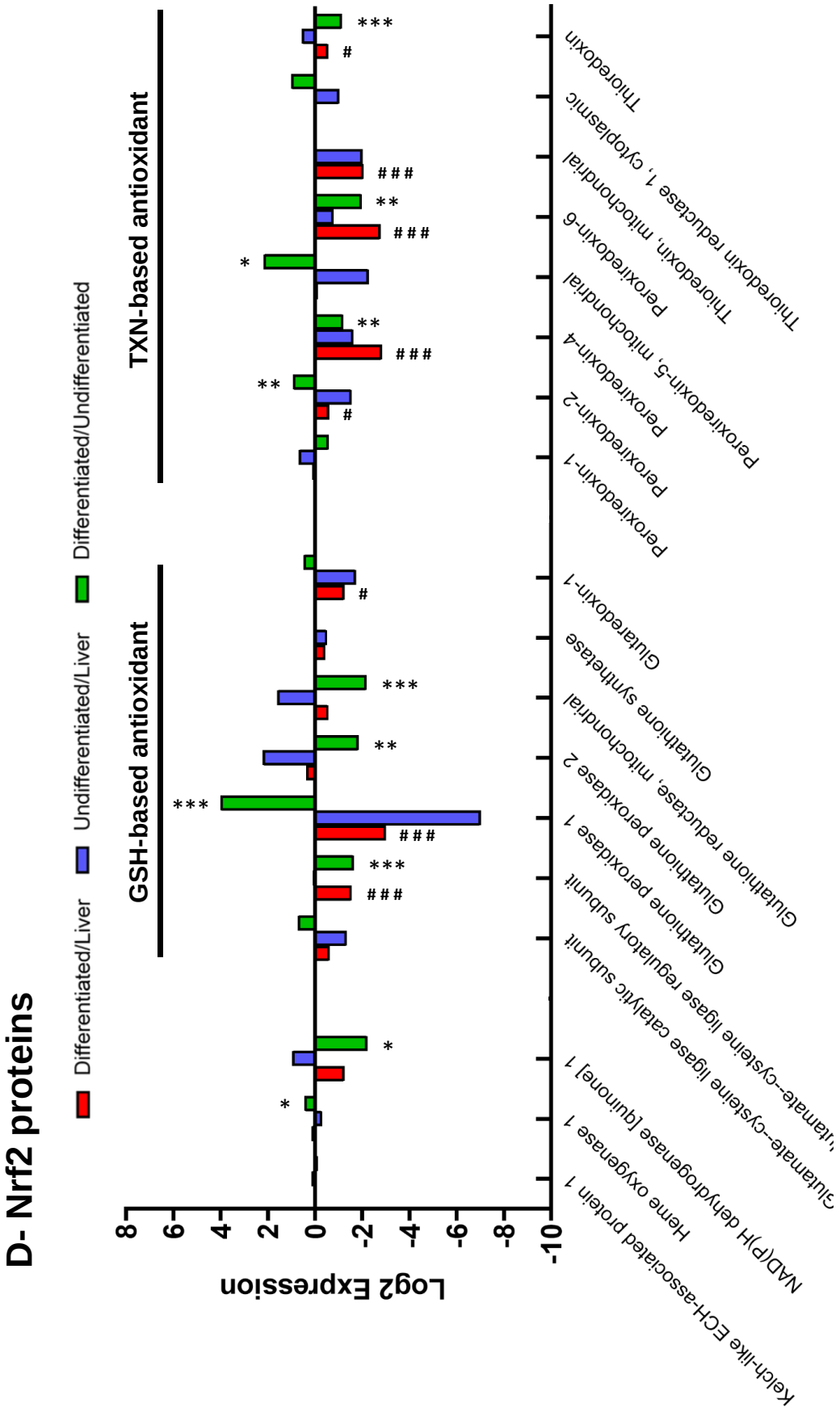
D- Nrf2 proteins
Differentiated/Liver
Undifferentiated/Liver
Differentiated/Undifferentiated
GSH-based antioxidant
TXN-based antioxidant
Log2 Expression
8
6
4
2
0
-2
-4
-6
-8
-10
Kelch-like ECH-associated protein 1
Heme oxygenase 1
NAD(P)H dehydrogenase [quinone] 1
Glutamate--cysteine ligase catalytic subunit
Glutamate--cysteine ligase regulatory subunit
Glutathione peroxidase 1
Glutathione peroxidase 2
Glutathione reductase, mitochondrial
Glutathione synthetase
Glutaredoxin-1
Peroxiredoxin-1
Peroxiredoxin-2
Peroxiredoxin-4
Peroxiredoxin-5, mitochondrial
Peroxiredoxin-6
Thioredoxin, mitochondrial
Thioredoxin reductase 1, cytoplasmic
Thioredoxin

In order to be considered as a predictive model of liver injury, the expression of currently used and recently identified putative protein biomarkers of DILI [276] were also investigated. Differentiation of organoids increased the expression of ALT, AST and GLDH compared to undifferentiated organoids, whereas HMGB1 and CK 18 were unaffected. Of the candidate novel biomarkers, differentiation significantly increased the expression of the phase II enzymes, GSTA1 and GSTA3 (shown in Fig 4.9B), sorbitol dehydrogenase and arginase 2 (Fig 4.9E).

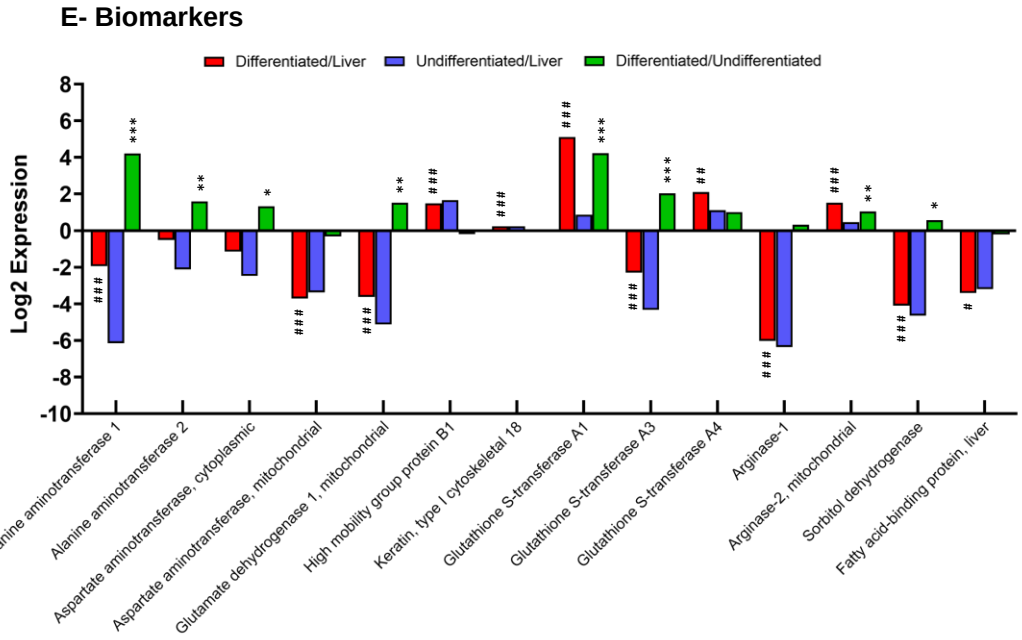

Figure 4.9- Comparison of log2 fold changes of individual key hepatic proteins in undifferentiated organoids, differentiated organoids and liver.

The log2 change in expression of (A) 30 CYP450 enzymes, (B) 30 Phase II, (C) 45 transporter, (D) 25 Nrf2 and auxiliary and (E) 14 biomarker proteins was calculated following iTRAQ analysis. A hash (#) or asterisks (*) indicates significant differential expression of proteins in differentiated organoids/liver or differentiated/undifferentiated organoids respectively. * = 0.05>*p*>0.01, ** = 0.01>*p*>0.001 and *** = *p*<0.001.

4.3.7 KEGG analysis reveals distinctly altered biological pathways in differentiated organoids

Mass spectrometry analysis of differentiated organoids revealed 2,719 and 1,726 significant (p<0.05) differentially expressed proteins when compared to both liver and undifferentiated organoids respectively. These changes in abundance were observed both globally (Fig 4.7) and in DMET and Nrf2 associated proteins (Fig 4.8-13). In order to understand the implications of these changes in expression, KEGG pathway analysis was used to contextualise significantly up and down-regulated proteins within biological pathways. The 25 most significant pathways for each condition were recorded.

Upregulated proteins found in differentiated organoids were associated with pathways of cellular morphology and cell-cell interactions. Glycolysis/gluconeogenesis and metabolic pathways were also significantly upregulated. Conversely, multiple metabolic processes, including fatty acid degradation and metabolism were downregulated in differentiated organoids compared to liver. With respect to a hepatic phenotype, there was a loss of drug metabolising pathways. In line with the upregulation of the glycolysis pathway, a loss of ATP producing pathways, such as the TCA cycle and oxidative phosphorylation was observed (Fig 4.10)

Differentiated/Liver upregulated pathways

Term	Count	*p* Value
Spliceosome	59	1.53E-27
Regulation of actin cytoskeleton	55	2.10E-13
Bacterial invasion of epithelial cells	31	5.24E-13
Salmonella infection	27	7.66E-10
Focal adhesion	47	1.58E-09
Fc gamma R-mediated phagocytosis	26	2.24E-08
Endocytosis	50	1.52E-07
Biosynthesis of antibiotics	43	3.46E-07
Adherens junction	22	4.40E-07
Tight junction	24	1.66E-06
Glycolysis / Gluconeogenesis	20	1.94E-06
Amino sugar and nucleotide sugar metabolism	17	2.00E-06
Fructose and mannose metabolism	14	2.45E-06
Biosynthesis of amino acids	21	4.85E-06
Sphingolipid signaling pathway	28	6.00E-06
Amoebiasis	27	6.01E-06
Galactose metabolism	13	7.64E-06
Proteoglycans in cancer	38	1.06E-05
Carbon metabolism	26	1.60E-05
Central carbon metabolism in cancer	18	2.18E-05
Pentose phosphate pathway	12	2.36E-05
ECM-receptor interaction	21	5.03E-05
Synaptic vesicle cycle	17	5.56E-05
Leukocyte transendothelial migration	25	6.37E-05
Lysosome	25	1.11E-04

Differentiated/Liver downregulated pathways

Term	Count	*p* Value
Metabolic pathways	377	7.68E-86
Ribosome	81	5.19E-38
Oxidative phosphorylation	75	8.39E-34
Parkinson's disease	75	3.50E-31
Biosynthesis of antibiotics	88	1.87E-28
Valine, leucine and isoleucine degradation	40	7.19E-25
Alzheimer's disease	74	1.86E-24
Peroxisome	46	2.19E-21
Carbon metabolism	53	1.13E-19
Huntington's disease	71	4.95E-19
Proteasome	31	3.27E-18
Non-alcoholic fatty liver disease (NAFLD)	60	1.17E-17
Fatty acid metabolism	30	6.22E-15
Fatty acid degradation	29	1.56E-14
Glyoxylate and dicarboxylate metabolism	22	3.19E-14
Propanoate metabolism	21	6.53E-14
Tryptophan metabolism	27	3.92E-13
Glycine, serine and threonine metabolism	22	2.77E-10
Butanoate metabolism	18	2.99E-10
Chemical carcinogenesis	34	9.27E-10
Protein processing in endoplasmic reticulum	49	1.27E-09
Pyruvate metabolism	21	1.28E-09
Citrate cycle (TCA cycle)	18	1.13E-08
Metabolism of xenobiotics by cytochrome P450	26	1.40E-08
Drug metabolism - cytochrome P450	26	2.91E-08

Cytoskeleton Interaction | Bio-energetics | Metabolic processes | Hepatic processes

Figure 4.10- The top 25 up- and down-regulated biological pathways in differentiated organoids compared to liver.

KEGG pathway analysis was performed on significantly (p<0.05) up- and down-regulated proteins in differentiated organoids compared to liver. The 25 most significant pathways were recorded, alongside the total number of proteins contributing to each pathway.

A comparison of biological pathways between differentiated organoids and undifferentiated organoids revealed an upregulation of pathways that were typically downregulated when differentiated organoids were compared to liver. For example, the metabolism of xenobiotics by CYP450 pathway was downregulated in differentiated organoids/liver ($p=1.40x10^{-8}$) but upregulated in differentiated/undifferentiated organoids ($p=1.67x10^{-8}$) There was an upregulation of multiple metabolic process, including fatty acid, glutathione and retinol metabolism. Pathways that were downregulated between differentiated and undifferentiated organoids represented RNA translation and protein synthesis. Downregulation of carbon and fatty acid metabolism pathways were also observed. However, the protein count contributing to each pathway was relatively low compared to the other pathway analyses. This is reflected in the fact that only 21 pathways were significantly altered (Fig 4.11).

Differentiated/Undifferentiated upregulated pathways

Term	Count	*p* Value
Metabolic pathways	219	7.38E-59
Parkinson's disease	48	1.14E-22
Alzheimer's disease	52	1.60E-22
Oxidative phosphorylation	46	2.91E-22
Valine, leucine and isoleucine degradation	30	8.86E-22
Huntington's disease	51	2.34E-19
Biosynthesis of antibiotics	50	4.27E-17
Non-alcoholic fatty liver disease (NAFLD)	42	1.31E-16
Chemical carcinogenesis	27	9.12E-12
Fatty acid degradation	20	1.21E-11
Carbon metabolism	29	8.96E-11
Tryptophan metabolism	17	4.90E-09
Metabolism of xenobiotics by cytochrome P450	19	1.67E-08
beta-Alanine metabolism	13	1.85E-07
Glutathione metabolism	16	4.13E-07
Amino sugar and nucleotide sugar metabolism	15	5.39E-07
Propanoate metabolism	11	1.65E-06
Glyoxylate and dicarboxylate metabolism	11	3.51E-06
Retinol metabolism	19	3.51E-06
Drug metabolism - cytochrome P450	16	5.08E-06
Fatty acid metabolism	14	5.63E-06
Fructose and mannose metabolism	11	1.75E-05
Histidine metabolism	9	3.19E-05
Pyruvate metabolism	11	6.50E-05
Arginine biosynthesis	8	6.64E-05

Differentiated/Undifferentiated downregulated pathways

Term	Count	*p* Value
Ribosome	87	4.12E-63
Proteasome	33	1.43E-27
Spliceosome	38	1.13E-13
RNA transport	41	4.27E-12
Ribosome biogenesis in eukaryotes	25	1.09E-09
Protein processing in endoplasmic reticulum	35	1.21E-08
Aminoacyl-tRNA biosynthesis	20	6.58E-08
Biosynthesis of antibiotics	38	2.10E-07
One carbon pool by folate	8	1.91E-04
Carbon metabolism	20	4.06E-04
Epstein-Barr virus infection	22	4.68E-04
RNA degradation	16	4.92E-04
DNA replication	10	5.18E-04
Protein export	9	6.35E-04
Fatty acid metabolism	12	6.56E-04
Biosynthesis of amino acids	14	2.17E-03
Pentose phosphate pathway	8	3.94E-03
Terpenoid backbone biosynthesis	6	1.94E-02
Peroxisome	12	2.94E-02
Fatty acid elongation	6	3.20E-02
Biosynthesis of unsaturated fatty acids	6	3.71E-02
Antigen processing and presentation	11	*5.95E-02*
Proximal tubule bicarbonate reclamation	5	*6.37E-02*
Purine metabolism	19	*7.62E-02*
Metabolic pathways	102	*8.16E-02*

Cytoskeleton Interaction | Bio-energetics | Metabolic processes | Hepatic processes

Figure 4.11- The top 25 up- and down-regulated biological pathways in differentiated organoids compared to undifferentiated organoids.

KEGG pathway analysis was performed on significantly (p<0.05) up- and down-regulated proteins in differentiated organoids compared to undifferentiated organoids. The 25 most significant pathways were recorded, alongside the total number of proteins contributing to each pathway.

4.3.8 Validation of mass spectrometry by immunoblotting

In order to validate the differential expression of proteins by iTRAQ, the expression of a CYP450 (3A11), phase II (GSTA1), DILI biomarker (ALT1) and Nrf2 associated protein (PRDX1) were further analysed by immunoblotting (n=2 per group). Samples from day four and day eight of differentiation were also included to show the change of protein induction over time.

The result of the immunoblot (Fig 4.12A) was compared to the iTRAQ abundance data (Fig 4.12B) for these markers. The trend in protein expression appeared to reflect the iTRAQ data. Densitometry analysis was performed to quantitatively assess change in protein expression. Band intensities calculated relative to GAPDH revealed an increase in CYP450 3A11, GSTA1 and ALT1 over time. The levels of PRDX1 remained constant throughout the differentiation (Fig 4.12C). Overall, changes in

protein expression determined by immunoblotting was shown to be an accurate reflection of the data obtained from the iTRAQ.

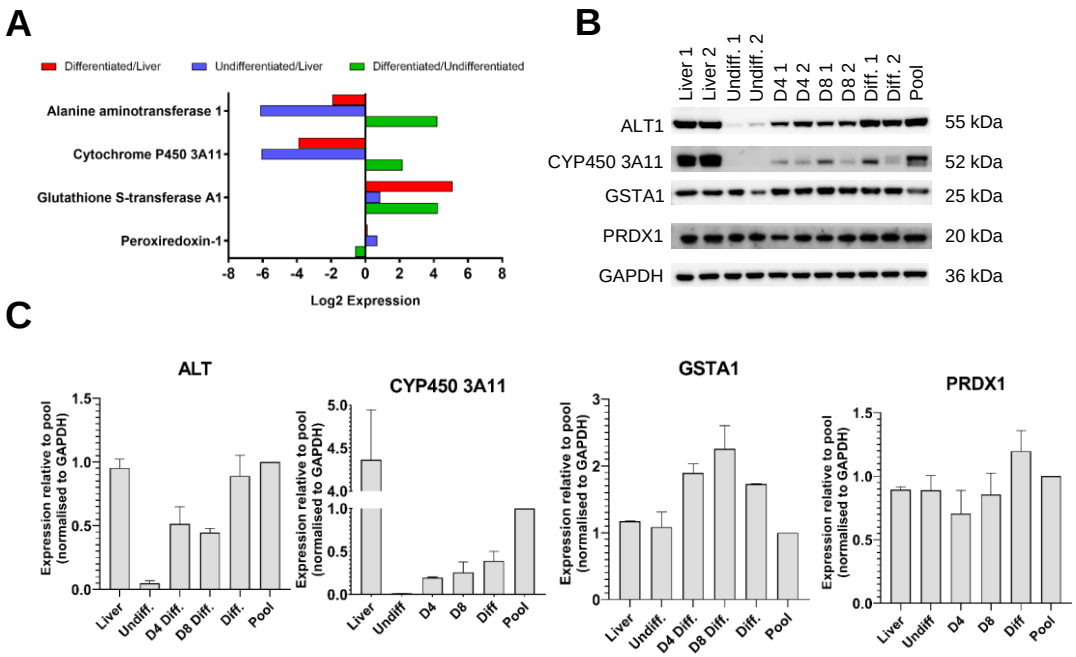

Figure 4.12- Similar protein expression is detected by both iTRAQ and immunoblotting.

(A) Log2 change in expression of DMET and Nrf2 proteins detected by iTRAQ. (B) Immunoblot of DMET and Nrf2 proteins in liver and organoids at various stages of differentiation (n=2). (C) Densitometry analysis of DMET and Nrf2 proteins relative to GAPDH revealed a similar protein expression as observed in the iTRAQ experiment.

4.4 Discussion

The value of any cultured cell as a disease model is the ability to robustly reflect the *in vivo* phenotype. Whilst primary hepatocytes are the current gold standard for modelling the liver, their availability, reproducibility and DMET stability in culture negatively affect their wide-spread use. Hepatic organoids are a novel, but poorly characterised, *in vitro* system that may meet the current need for a more physiologically relevant, proliferative, liver-derived cell model. In this study, the global proteome of undifferentiated and differentiated murine organoids and donor derived liver tissue were compared in order to better characterise this nascent hepatic model.

The *in vitro* proliferation of hepatocytes is typically not possible under standard culture conditions and therefore requires extensive measures such as viral transfection [277] or culture with TNFα [278]. Conversely, it was observed that hepatic organoids from a single donor could be expanded and passaged multiple times in basal expansion media. The proliferative and differential potential of murine HPC over hepatocytes has been previously demonstrated [279]. Long term cryopreservation and resurrection of organoids was also possible (Fig 4.1), which would be beneficial for retaining high value samples and potentially lowering the number of single-use animals for research [280]. However, potentiation morphological and functional differences in freshly isolated and cryopreserved organoids would need to be evaluated [281].

As organoids are biliary-derived, a defined differentiation protocol of Notch signalling inhibition and dexamethasone produces a mature hepatocyte phenotype [180]. At the final stage of differentiation, organoids expressed low levels of AFP, select organoids expressed albumin; however, organoids remained $CK19^{+}$ (Fig 4.3A-D). This suggests that differentiation of organoids does not induce a complete transdifferentiation from a biliary to hepatocyte phenotype, only a gain of hepatocyte function. Li *et al*. has also demonstrated that human HPC cultured in hepatocyte medium were

CK19^{+}/AFP^{+}/Albumin^{+} [282]. Fully differentiated human organoids have also been shown to be EpCAM^{+}/HNF4α^{+}/Albumin^{+} [180] and CK19^{+}/Albumin^{+}/CYP450 3A4^{+} [179].

This shift toward a hepatocyte-like cell was confirmed by KEGG pathway analysis, with the upregulation of multiple metabolic and CYP450 pathways in differentiated organoids compared to undifferentiated organoids (Fig 4.11). Further evidence for a small-scale phenotypic change is reflected by the tight clustering of undifferentiated and differentiated organoids compared to liver tissue by hierarchal and PCA analysis (Fig 4.5, Fig 4.6). The same tight clustering of organoids relative to donor-matched liver tissue has also been observed on a gene level by whole-genome transcriptomic analysis of essential liver function markers [179].

The expression of DMET proteins in hepatic organoids remain to be comprehensively defined. Within our dataset, the differentiation protocol partially restored the expression of the majority of CYP450 enzymes, though not to the level as observed in the liver. The murine equivalent families of CYP450 3A4, 2D6, 2C19, 1A2 and 2B6, which oxidatively metabolise the most commonly prescribed drugs [283], were all significantly upregulated in differentiated organoids compared to undifferentiated organoids (Fig 4.9A).

Previous work has shown that differentiated human organoids demonstrated CYP450 3A4 activity and were capable of metabolising midazolam, a commonly used probe of CYP450 3A4 activity [284,285]. In agreement with previous studies, the expression of CYP450 3A proteins in our data increased in differentiated organoids following culture with dexamethasone [286,287]. The metabolism of midazolam is not strictly unique to CYP450 3A4, it is also turned over by CYP450 3A3 and 3A5 [288]. Interestingly, the level of CYP450 3A13 (equivalent to human CYP3A5) was the only CYP450 enzyme significantly higher in differentiated organoids compared to both liver and undifferentiated organoids and may be primarily responsible for the midazolam metabolism seen in the original study.

Finally, differentiation induced high expression of CYP450 2C55 and 2S1 (Fig 4.9A). While relatively little is known about these CYP450 enzymes, Waterschoot *et al.* observed a >30-fold increase in gene expression of CYP450 2C55 in a CYP450 3A^{-}/$^{-}$ mouse model, which was capable of midazolam metabolism [289]. CYP450 2S1 has been shown to be mainly expressed in extrahepatic tissue within epithelial cells and to metabolise retinoic acid, a key driver of differentiation [290]. The increase of these two CYP450 proteins in fully differentiated organoids warrants further investigation.

At the time of writing, this is the first study to profile phase II and hepatic transporters in biliary derived hepatic organoids. Differentiation upregulated the expression of the GST and sulfotransferase family, with many proteins expressed at near-identical (GST-M2, sulfotransferase 1A1) or higher (GST-A1, sulfotransferase 1C2) levels of expression to the liver (Fig 4.9B). Although hepatic transporters generally had lower expression in organoids compared to liver, the magnitude of difference was relatively small compared to CYP450 and phase II proteins. There are a number of essential hepatobiliary influx and efflux transporters expressed in differentiated organoids, such as MDR1A, MRP1/2/3/6/7, OCT1, OATP-1, BSEP, BCRP and the sodium/bile acid cotransporter (Fig 4.9C). Critically, many of these proteins are lacking in currently used hepatic models, such as HepG2 [291,292].

In particular, parallels can be drawn between organoids and HepaRG cells as they are both derived from a progenitor cell that requires differentiation to a hepatobiliary phenotype, with useful CYP450 3A expression [293]. Unlike HepaRG, organoids are not cancer derived, thus may have more favourable Nrf2 and bioenergetic profile for toxicity testing. The levels of free radical production and Nrf2 activation in HepaRG varies throughout differentiation, which may harm mechanistic understanding of drug-induced cellular defence activation [294]. Within this dataset, no significant change in the levels of KEAP1, HO-1 or NQO1 between liver and organoids was detected, indicating a stable Nrf2 system throughout culture (Fig 4.9D). Furthermore,

differentiated organoids expressed the most commonly used current gold standard DILI biomarkers to a similar level as the liver, which would aid in their use as a translational tool for evaluating hepatotoxicity (Fig 4.9E).

4.4.1 Conclusions and future work

In this chapter, it has been shown that biliary-derived organoids are a proliferative cell system, capable of long-term culture and cryopreservation. Through a combination of 3D culture, growth factors and small molecules, organoids can be differentiated to a hepatocyte-like phenotype. The final organoid proteomic profile contains multiple DMET proteins necessary for liver function and drug metabolism. However, the final phenotype is distinct from liver tissue; organoids retain a biliary phenotype and the majority of DMET enzymes are generally lower than donor-derived liver tissue. However, this does not mean to say that their expression is not useful for ADMET studies, relative to pre-existing models.

Organoids may offer utility compared to other advanced hepatic models such as HepaRG, spheroid and iPSC models. Unlike HepaRG cells, organoids form from a non-cancerous, patient-specific donor cell and reach differentiation in a shorter timeframe. While spheroids can be formed from patient specific hepatocytes, their lack of availability, proliferation and de-differentiation in culture limits their use in routine drug testing. Finally, though iPSC cells are non-cancerous and patient specific, a lack of standardised differentiation protocol and ability to form 3D structures restricts their utility.

However, for *in vitro* toxicological studies, there is concern surrounding the accuracy and normalising of seeding organoid fragments compared to an exact cell count seen in the other hepatic models. Further investigation to determine which model is fit for a specific purpose is therefore required.

We have shown that differentiated organoids express high levels of certain essential metabolising and transport proteins, such as CYP450 3A, GSTA and MDR1A. Therefore, organoids may be the most appropriate model for assessing drug classes that are processed through these pathways, such as such as alkylating chemotherapy agents [295]. Furthermore, the expression of multiple hepatobiliary transporters may enable mechanistic insight into biliary efflux of metabolised compounds and inform of potential cholestatic perturbations, which are typically difficult to model *in vitro* [296].

Since the publication of biliary-derived organoids, a recent development has achieved organoid outgrowth from albumin^{+}/Axin2^{+} hepatocytes. Compared to biliary-derived organoids, gene expression of cholangiocyte/HPC markers (CK19, SOX9) was significantly lower and hepatic markers (albumin, HNF4α and CYP450 1A2 and 3A11), were comparable to primary hepatocytes, which may offer a more physiologically relevant hepatocyte model [59]. As the field of hepatic organoids is relatively novel, organoid isolation and differentiation protocols will require further experimentation, optimisation and characterisation.

Future work for biliary derived organoids should aim to compare the phenotype of differentiated murine organoids to both *in vivo* mouse studies and human derived organoids. Assessing the differences and similarities between *in vitro* dosing of organoids and *in vivo* toxicological studies would aid the understanding of how human derived organoids could predict clinically observed toxicity. Ultimately, this could identify translational differences which may help predict complexities when moving from pre-clinical models to phase I trials. Furthermore, organoids should be challenged with curated hepatotoxic test and training compounds in order to evaluate their response to toxicity, with both standardised cytotoxic and mechanistic end points. This response should then be contextualised relative to existing 2D and 3D *in vitro* models in order to assess their utility as a predictive and sensitive model of DILI.

Finally, while organoids appear to mimic the hepatobiliary aspect of the liver, other NPC are not reflected in the current system. Patient-derived cancer organoid models have started to incorporate immune cells to better reflect the *in vivo* phenotype of the tumour microenvironment [297]. While initial studies have co-cultured HPC with fibroblasts to alter differentiation, the effects of culturing with other key NPC, such as LSEC, remain to be evaluated [298].

4.4.2 Limitations

A caveat of this work was the use of DMET, Nrf2 and biomarker proteins used to evaluate the similarities between organoids and liver, which represented <3 % of all proteins detected by iTRAQ. Whilst care was taken to contextualise these DMET proteins in line with previous publications [275,299], some proteins were omitted for ease of analysis, such as phase I CYP450-independent metabolising enzymes and non-GSH and TXN-based Nrf2 defence mechanisms. Furthermore, the assessment of how suitable organoids are at reflecting the *in vivo* phenotype was made solely upon DMET activity, whereby other key physiological metrics, such as zonated hepatic proteins, may still be relevant to fully profiling hepatic organoids.

Finally, large proteomic differences were observed between both undifferentiated and differentiated organoids compared to liver. For example, Fig 4.10 shows an upregulation of cytoskeleton, glycolytic and cell-cell interaction pathways and a down regulation of oxidative phosphorylation pathways in differentiated organoids compared to liver. This is indicative of the proteome adapting from an *in vivo* environment to an *in vitro* environment, whereby cells are proliferating in glucose-rich media [300]. A comparison against donor-derived hepatocytes may also have been useful to contextualise biliary-derived organoids against the current gold standard model. However, due to the size of the liver and nature of both the organoid and hepatocyte isolation procedures, this was not feasible in mouse, but would be in human samples.

Chapter Five:
Concluding discussion

Contents

5.1 Introduction

DILI is a major cause of patient morbidity and mortality and impedes the development of novel drug therapies. In order to address these issues, a better understanding in the prediction and detection of hepatic toxicological outcomes is needed. There is a well-established requirement for both novel *in vitro* systems and biomarkers for DILI. Whilst the majority of hepatotoxicity research has historically focused on the hepatocytes, cholangiocytes are both possible targets of DILI and potential tools in predicting toxicity.

Improved prediction of DILI would primarily depend upon a robust *in vitro* model that accurately reflects the *in vivo* hepatic physiology. However, current routine assessment in *in vitro* modelling of DILI is still largely reliant upon proliferative cancer-derived cells, which typically have low DMET activity and an altered Nrf2 cell defence signalling pathway [301]. Biliary-derived hepatic organoids have recently been described as a more physiologically relevant *in vitro* system, though they remain to be characterised to the same level of pre-existing models.

The enhanced detection of DILI would require specific, sensitive and mechanistically informative biomarkers. Elevations in the current gold standard biomarkers are purely diagnostic and can be caused by diseases unrelated to the liver or liver injury in the absence of DILI [276]. miRNAs have previously been shown to be an attractive circulating biomarker of hepatocellular liver injury, accounting for many of the shortcomings of the current serum biomarkers [124]. However, the identification of cholangiocyte-enriched miRNAs and their detection following DILI remains to be elucidated.

5.2 Summary of the work in this thesis

This thesis set out to elucidate how cholangiocytes can be utilised as potential tools of improving the detection and prediction of DILI. Specifically, studies within this thesis

were designed to characterise global miRNA expression in murine cholangiocytes, in order to identify and detect novel circulating biomarkers in serum following cholangiocyte-specific toxicity *in vivo*. Moreover, this thesis aimed to characterise the proteome of biliary-derived organoids to assess their phenotype relative to donor-derived liver tissue.

In Chapter 2, a novel discovery of 63 statistically significant miRNAs that were either enriched or uniquely expressed in a pure population of freshly isolated murine cholangiocytes were identified as putative circulating biomarkers. Importantly, these miRNAs were all translational to human, though ultimately not shown to be liver specific. These putative miRNAs may be useful as part of a panel of biomarkers in the diagnosis and understanding of mechanistic cholangiocyte DILI, either clinically, or in a controlled point-of-care environment, such as clinical trials

In Chapter 3, a panel of five cholangiocyte-derived miRNAs from the miR-200 family were investigated in the response to cholangiocyte toxicity. Liver injury was not shown to be cholangiocyte specific and in ANIT-treated animals, overt stomach toxicity was observed, which has not been previously reported. While some members of the miR-200 family were detected in the serum of dosed animals, this chapter highlighted the difficulties in modelling both cholangiocyte and cholestatic liver injury, which has valuable implications for the design and interpretation of future toxicological and biomarker discovery studies

In Chapter 4, the proteome of biliary-derived organoids and donor-derived liver was assessed to better characterise this nascent in *vitro* model. Differentiated organoids expressed higher levels of key DMET proteins compared to undifferentiated organoids. Although the final differentiated organoid phenotype was distinct from donor-derived liver tissue, the in-depth proteomic characterisation of biliary-derived organoids will aid researchers in the selection of the most appropriate *in vitro* tool for the future.

Overall, the majority of the aims outlined at the beginning of this thesis were successfully achieved.

5.3 General limitations of experimental studies

5.3.1 Limitations of animal studies

The data presented within this thesis must be interpreted within the context and limitations of the experimental design. A selection criterion for the candidate murine miRNAs identified in Chapter 2 was that an equivalent human miRNA also existed, to ensure any findings were translational to the clinic. However, in Chapter 3, cholangiocyte injury was modelled predominantly in fasted mice and rats, with an acute dose of a non-clinically relevant compound. Whilst the compounds used in this work may cause the same cholestatic adverse outcomes associated with clinically relevant xenobiotics, the mechanisms of injury and miRNA release may be altered. Therefore, the translational relevancy of fasting and single acute dosing must be considered [302]. Although VBDS is the most severe clinical manifestation of cholangiocyte toxicity, clinical case studies show this injury is caused by a prolonged daily exposure to a drug [303–306]. A large disparity in how cholangiocyte injury and cholestasis is modelled *in vitro* and *in vivo* compared to patient injury remains [255].

5.3.2 Limitations of miRNAs

The limitations of miRNAs as biomarkers are both technical and biological in nature. The use of circulating miRNAs as biomarkers has been limited due to a lack of standardised and universally accepted normalisation methodology. Over the last decade, published literature has presented miRNA data normalised to snoRNAs [307], endogenous miRNAs [308], exogenous miRNAs [309], standard curve [310], a combination of miRNAs [311] or no normalisation at all [312]. Indeed, this thesis also presents miRNA qPCR data with dissimilar normalisers, which followed the best agreed method at the

time of experimentation. Ultimately, this represents a major issue for the reproducibility, understanding and translation of miRNA studies [313].

An incomplete understanding surrounding the biological release of miRNAs is another contributing factor to the high variability and large dynamic range seen with circulating miRNA signatures. Unlike traditional biomarkers, miRNAs are not only passively released into the serum following cell death. For example, in the absence of overt toxicity, miR-122-containing exosomes may be actively released from the liver, which is thought to contribute to the high variation of circulating miRNA values [314]. Due to this miRNA variation, the Predictive Safety Testing Consortium (PSTC) has recently started perusing GLDH as a novel DILI biomarker over miR-122 [276].

5.4 Future perspectives

The work in this thesis identified 63 cholangiocyte enriched or unique murine miRNAs as candidate circulating biomarkers for the first time. However, difficulties in inducing sufficient and reproducible cholangiocyte damage were encountered *in vivo* due to a lack of clinically relevant compounds and potential strain and species differences in response to toxicity. Consequently, new experimentation is needed to ratify these putatively discovered miRNA biomarkers in confirmed instances of cholangiocyte injury.

In order to confirm reproducible cholangiocyte toxicity *in vivo*, a larger experiment consisting of different pre-clinical models dosed with different hepatobiliary toxins at multiple time points could be performed. The serum from all these animals could then be probed for the 63 miRNAs of interest, or a common miRNA signature in response to biliary injury. However, the degree of injury and miRNAs released may still be translationally irrelevant.

It may therefore be worthwhile to assess translational relevancy by examining if the 63 miRNAs of interest are present in rat and human cholangiocytes, by both *in situ*

hybridisation and cell isolation procedures. From a mechanistic perspective of identifying cholangiocyte injury, if *in vivo* studies necessitate utilising non-clinically relevant compounds, which ultimately poorly translate to clinically observed cholangiocyte DILI, it may therefore be justified to directly analyse human DILI serum samples for any miRNAs identified to be present in murine, rat and human cholangiocytes. Importantly, future circulating miRNA biomarkers should always be used in a panel alongside established hepatic biomarkers as currently no single biomarker is truly informative of the degree or type of DILI.

Work in this thesis has helped to characterise biliary-derived organoids by their proteome, though they are still in their infancy as an *in vitro* model. While the proteomic screening yielded promising DMET expression, more work is required to fully characterise their phenotype and qualify them as a cohesive model of DILI to the same degree as pre-existing advanced hepatic *in vitro* models. Currently, other 'omics approaches and high-throughput testing of known hepatotoxic compounds remains to be performed. This thesis demonstrates differentiated organoids retain a biliary phenotype, which may implicate them in the future as a 3D, patient specific *in vitro* model of hepatobiliary DILI, which does not exist in current drug-development.

5.5 Summation of key findings

In summary, the key findings presented in this thesis are:

- A population of miRNAs exist that are enriched or unique to cholangiocytes compared to the liver parenchyma, which may serve as potential circulating biomarkers of cholangiocyte DILI.
- Cholangiocyte injury *in vivo* is highly variable depending on the strain, species and toxin used, determined by histopathology and both traditional and miRNA circulating biomarkers.
- ANIT, a classic hepatobiliary toxicant, causes previously unidentified stomach toxicity when administered by oral gavage.
- Biliary-derived organoids can be differentiated to a more hepatic proteomic phenotype with increased DMET expression under targeted cell culture conditions.

Appendix

	BEC expression	Hep Expression	Unlogged FC	t-test FDR	SAMR FDR (%)
Unique BEC miRNAs (n=69)					
miR-M87-1	3.57	-1.00	23.82	0.01	0.00
miR-1249-3p	1.81	-1.00	7.02	0.01	0.00
miR-125a-3p	2.61	-1.00	12.17	0.01	0.00
miR-125a-5p	5.14	-1.00	70.43	0.01	0.00
miR-128-3p	1.65	-1.00	6.29	0.01	0.00
miR-132-3p	2.37	-1.00	10.36	0.02	0.00
miR-141-3p	5.77	-1.00	109.14	0.01	0.00
miR-142a-3p	4.88	-1.00	58.89	0.01	0.00
miR-142a-5p	3.38	-1.00	20.80	0.01	0.00
miR-143-3p	3.88	-1.00	29.53	0.01	0.00
miR-146a-5p	5.36	-1.00	82.37	0.01	0.00
miR-155-5p	2.19	-1.00	9.15	0.01	0.00
miR-181a-5p	2.16	-1.00	8.93	0.01	0.00
miR-183-5p	3.66	-1.00	25.30	0.01	0.00
miR-1896	3.38	-1.00	20.85	0.01	0.00
miR-18a-5p	1.88	-1.00	7.36	0.01	0.00
miR-1901	1.93	-1.00	7.61	0.01	0.00
miR-1967	2.92	-1.00	15.17	0.02	0.00
miR-199b-5p	3.54	-1.00	23.33	0.01	0.00
miR-200c-3p	6.08	-1.00	135.21	0.01	0.00
miR-214-3p	4.35	-1.00	40.81	0.01	0.00
miR-24-1-5p	1.91	-1.00	7.54	0.01	0.00
miR-28c	1.60	-1.00	6.05	0.01	0.00
miR-301a-3p	4.10	-1.00	34.27	0.01	0.00
miR-3067-3p	2.29	-1.00	9.81	0.01	0.00
miR-30b-3p	1.30	-1.00	4.93	0.01	0.00
miR-3113-5p	2.33	-1.00	10.09	0.01	0.00
miR-324-5p	3.03	-1.00	16.34	0.01	0.00
miR-326-3p	1.74	-1.00	6.67	0.01	0.00
miR-335-5p	2.20	-1.00	9.21	0.02	0.00
miR-338-3p	3.92	-1.00	30.26	0.01	0.00
miR-340-5p	2.83	-1.00	14.24	0.01	0.00
miR-374c-5p	1.52	-1.00	5.72	0.01	0.00
miR-5121	6.79	-1.00	221.12	0.01	0.00
miR-532-5p	2.92	-1.00	15.14	0.01	0.00
miR-542-5p	1.29	-1.00	4.88	0.01	0.00
miR-551b-3p	2.24	-1.00	9.45	0.01	0.00
miR-669n	2.68	-1.00	12.81	0.02	0.00
miR-674-3p	2.24	-1.00	9.47	0.01	0.00
miR-872-5p	1.95	-1.00	7.72	0.01	0.00
miR-877-5p	2.56	-1.00	11.81	0.01	0.00
miR-99b-5p	4.56	-1.00	47.08	0.01	0.00
miR-126a-5p	1.98	-1.00	7.87	0.01	0.00
miR-511-3p	6.31	-1.00	158.26	0.01	0.00
miR-210-3p	2.80	-1.00	13.94	0.01	0.02
miR-199a-5p	3.77	-1.00	27.37	0.01	0.06
miR-96-5p	4.41	-1.00	42.37	0.01	0.06
miR-181c-5p	4.25	-1.00	38.11	0.01	0.07
miR-503-5p	1.93	-1.00	7.64	0.01	0.08
miR-5130	3.24	-1.00	18.88	0.01	0.08
miR-193b-3p	3.70	-1.00	26.08	0.01	0.08
miR-340-3p	1.60	-1.00	6.05	0.01	0.09
miR-342-3p	6.68	-1.00	205.09	0.01	0.09
miR-29c-5p	1.82	-1.00	7.07	0.01	0.09
miR-1306-3p	2.82	-1.00	14.14	0.01	0.09
miR-154-5p	2.59	-1.00	12.06	0.02	1.01
miR-300-3p	2.25	-1.00	9.51	0.03	1.90
miR-129-1-3p	1.42	-1.00	5.35	0.02	2.00
miR-127-3p	2.08	-1.00	8.44	0.03	2.86
miR-182-5p	1.59	-1.00	6.02	0.03	3.92
miR-299b-5p	1.42	-1.00	5.36	0.03	4.37
miR-3075-5p	1.86	-1.00	7.26	0.03	5.33
miR-379-5p	1.98	-1.00	7.92	0.04	8.00
miR-195a-3p	1.27	-1.00	4.83	0.04	9.11
miR-375-3p	2.25	-1.00	9.55	0.06	16.54
miR-200b-5p	1.00	-1.00	3.99	0.07	22.05
miR-200a-5p	0.78	-1.00	3.42	0.10	26.31
miR-466f-3p	0.76	-1.00	3.39	0.12	29.64
miR-450a-2-3p	0.84	-1.00	3.58	0.13	30.30
BEC enriched miRs (n=52)					
miR-126a-3p	11.68	8.08	12.06	0.01	0.00
miR-200a-3p	8.02	4.34	12.89	0.01	0.00
miR-200b-3p	8.36	5.39	7.81	0.02	0.00
miR-27a-3p	7.98	5.02	7.82	0.02	0.00
miR-3960	9.74	8.67	2.09	0.01	0.00
miR-429-3p	7.59	4.69	7.50	0.01	0.00
miR-497a-5p	7.44	3.94	11.30	0.01	0.00
miR-195a-5p	7.98	4.08	15.02	0.01	0.09
miR-24-3p	9.30	7.16	4.42	0.02	1.15
miR-23a-3p	8.48	5.54	7.67	0.02	1.58
let-7e-5p	7.77	4.65	8.67	0.02	1.78
miR-199a-3p	6.80	3.85	7.73	0.03	3.90
let-7i-5p	8.94	7.69	2.36	0.02	4.00
miR-223-3p	7.86	3.75	17.31	0.03	5.75
miR-652-3p	6.00	4.05	3.88	0.03	6.22
miR-26a-5p	8.96	8.15	1.75	0.02	8.06
miR-10a-5p	6.90	4.23	6.36	0.04	8.97
miR-23b-3p	8.12	7.28	1.80	0.02	9.68
let-7b-5p	10.77	9.86	1.87	0.03	14.38
miR-331-3p	5.10	3.87	2.34	0.05	16.38
miR-151-5p	7.29	6.39	1.87	0.04	16.49
miR-466i-5p	8.22	7.07	2.21	0.05	17.13
let-7c-5p	10.50	9.48	2.03	0.05	18.02
miR-322-5p	6.67	3.87	6.95	0.06	18.12
miR-5126	10.83	9.30	2.88	0.06	20.15
miR-721	5.96	3.80	4.47	0.07	20.35
miR-574-5p	5.85	4.68	2.25	0.06	21.51
miR-3473b	10.55	8.61	3.85	0.07	21.53
miR-125b-5p	7.50	6.72	1.72	0.07	25.62
miR-16-5p	8.09	7.65	1.36	0.07	30.31
miR-15a-5p	8.65	8.09	1.48	0.10	31.32
miR-1224-5p	10.49	9.79	1.63	0.12	32.37

	BEC expression	Hep Expression	Unlogged FC	t-test FDR	SAMR FDR (%)
miR-15b-5p	7.10	6.69	1.32	0.12	34.96
miR-30d-5p	6.44	6.24	1.15	0.05	35.48
miR-29a-3p	10.41	9.94	1.39	0.16	36.51
let-7d-5p	9.24	8.85	1.31	0.16	37.51
miR-350-3p	4.52	3.97	1.47	0.21	38.44
miR-709	9.53	8.85	1.60	0.24	38.79
miR-3470a	7.02	5.98	2.06	0.25	39.17
miR-3473a	5.08	4.49	1.50	0.26	40.38
miR-140-3p	4.60	4.33	1.21	0.33	43.39
miR-211-3p	8.31	7.86	1.37	0.46	44.74
miR-99a-5p	7.12	7.04	1.06	0.43	46.21
miR-3102-5p	7.20	7.12	1.05	0.47	46.62
miR-221-3p	3.78	3.67	1.08	0.59	46.78
miR-494-3p	8.51	8.31	1.15	0.72	47.34
miR-30a-5p	8.99	8.96	1.02	0.25	47.38
miR-680	4.59	4.48	1.08	0.81	47.97
miR-130a-3p	8.57	8.54	1.02	0.77	48.15
miR-29b-3p	8.29	8.26	1.03	0.87	48.41
miR-152-3p	5.38	5.36	1.01	0.96	48.83
miR-103-3p	7.25	7.25	1.00	0.99	48.95
Hep Enriched miRNAs (n=82)					
miR-148a-3p	6.03	8.77	0.15	0.01	0.00
miR-193a-3p	3.83	7.95	0.06	0.02	0.00
miR-21a-3p	1.36	3.39	0.24	0.01	0.00
miR-30a-3p	4.71	5.91	0.44	0.01	0.00
miR-320-3p	2.48	4.94	0.18	0.01	0.00
miR-345-5p	3.47	5.42	0.26	0.01	0.00
miR-365-3p	3.55	6.58	0.12	0.01	0.00
miR-697	2.79	5.70	0.13	0.01	0.00
miR-712-5p	2.37	4.44	0.24	0.01	0.00
miR-30e-3p	2.39	4.11	0.30	0.01	0.35
miR-30e-5p	5.99	7.22	0.43	0.01	0.55
miR-194-5p	5.98	8.62	0.16	0.02	0.65
miR-5100	9.84	10.97	0.45	0.01	1.42
miR-19a-3p	3.91	5.46	0.34	0.01	2.95
miR-212-3p	4.69	7.49	0.14	0.02	3.02
miR-3968	7.27	10.26	0.13	0.02	3.83
miR-185-5p	2.98	5.08	0.23	0.02	5.11
miR-202-3p	5.26	7.80	0.17	0.02	5.69
miR-107-3p	7.03	8.20	0.44	0.01	7.10
miR-1897-3p	2.36	5.44	0.12	0.02	7.70
miR-m88-1-3p	4.65	5.92	0.42	0.02	7.78
miR-92a-3p	6.54	7.83	0.41	0.02	7.83
miR-192-5p	8.21	10.65	0.18	0.02	8.96
miR-93-5p	4.17	5.26	0.47	0.01	9.16
miR-31-5p	3.89	5.98	0.23	0.02	9.32
miR-455-3p	1.99	4.16	0.22	0.02	9.55
miR-22-3p	8.46	10.51	0.24	0.02	9.64
miR-378a-3p	3.67	6.44	0.15	0.02	11.34
miR-30c-2-3p	2.66	4.45	0.29	0.02	11.62
miR-30c-5p	6.74	7.49	0.59	0.01	12.65

	BEC expression	Hep Expression	Unlogged FC	t-test FDR	SAMR FDR (%)
miR-M23-1-5p	4.52	7.68	0.11	0.03	12.84
miR-219a-5p	2.39	4.06	0.31	0.02	13.95
miR-1949	3.47	4.02	0.68	0.01	16.94
miR-378b	3.92	6.80	0.14	0.03	20.34
miR-1839-3p	3.04	4.48	0.37	0.03	20.88
miR-1906	3.35	4.57	0.43	0.03	21.08
miR-188-5p	5.38	6.15	0.58	0.02	25.53
miR-3098-5p	4.04	5.37	0.40	0.03	25.56
miR-139-3p	2.26	3.88	0.33	0.03	26.03
miR-20a-5p	6.38	7.39	0.50	0.03	27.15
miR-19b-3p	7.55	8.37	0.56	0.03	28.73
miR-101c	4.45	5.99	0.34	0.04	29.12
miR-361-5p	4.80	5.65	0.55	0.03	31.21
miR-98-5p	4.28	5.18	0.54	0.03	31.28
miR-2137	5.49	6.86	0.39	0.05	33.57
miR-122-5p	11.54	13.69	0.23	0.06	34.68
miR-677-3p	2.05	4.27	0.22	0.06	35.11
miR-101a-3p	5.62	6.81	0.44	0.05	35.52
miR-1904	5.86	7.11	0.42	0.05	36.07
miR-652-5p	5.57	6.33	0.59	0.04	36.81
miR-34a-5p	5.84	6.18	0.79	0.02	38.81
miR-1982-5p	4.60	5.61	0.50	0.06	39.83
miR-423-5p	3.79	4.29	0.71	0.04	40.80
miR-3081-5p	3.63	4.85	0.43	0.07	42.17
miR-29c-3p	8.60	9.15	0.68	0.05	42.86
miR-7a-5p	3.10	4.82	0.30	0.11	44.84
miR-28a-5p	3.68	4.07	0.77	0.06	46.29
miR-690	6.39	7.17	0.58	0.12	47.65
miR-1839-5p	2.55	3.51	0.51	0.15	48.42
miR-20b-5p	4.16	5.08	0.53	0.15	48.63
miR-26b-5p	7.69	8.11	0.75	0.12	49.03
miR-362-3p	3.64	3.65	1.00	0.99	49.05
miR-5107-5p	4.93	4.94	0.99	0.99	49.06
let-7a-5p	10.32	10.34	0.99	0.94	49.23
miR-3072-5p	5.66	5.70	0.97	0.88	49.51
miR-466h-3p	3.75	3.88	0.91	0.85	49.71
miR-106b-5p	6.03	6.09	0.96	0.71	49.99
let-7f-5p	10.12	10.19	0.95	0.66	50.18
miR-25-3p	5.51	5.83	0.80	0.16	50.23
miR-2861	6.45	6.60	0.90	0.63	50.39
miR-3095-3p	5.13	5.54	0.75	0.60	50.60
miR-1897-5p	5.64	5.81	0.89	0.54	50.62
miR-140-5p	4.82	5.03	0.86	0.53	50.70
miR-425-5p	3.66	4.00	0.79	0.24	50.76
miR-21a-5p	10.87	11.29	0.75	0.25	50.76
miR-30b-5p	5.48	5.65	0.89	0.45	50.80
let-7g-5p	9.52	9.73	0.86	0.45	50.86
miR-1895	6.13	6.29	0.90	0.39	50.89
miR-27b-3p	5.79	6.04	0.84	0.27	50.98
miR-467f	3.81	4.38	0.67	0.42	50.99
miR-3963	12.04	12.39	0.78	0.31	50.99
miR-671-5p	4.82	5.62	0.58	0.36	51.00

Appendix 2.1 Statistical analysis of miRNAs found in all biological samples.

All unique and shared miRNAs detected on the array were analysed by both SAM analysis and t-test in order to identify differentially expressed miRNAs. SAM analysis was used for differential expression analysis as it was more stringent than t-test. The threshold for significance was 5 % False detection rate (FDR) and 0.05 adjusted p-value FDR for SAM and t-test analysis respectively. Non- significant values are highlighted in red.

A

miRNA	Mouse	Human	Notes
miR-342-3p	UCUCACACAGAAAUCGCACCCGU	UCUCACACAGAAAUCGCACCCGU	
miR-511-3p	AAUGUGUAGCAAAAGACAGGAU	AAUGUGUAGCAAAAGACAGA	
miR-200c-3p	UAAUACUGCCGGGUAAUGAUGGA	UAAUACUGCCGGGUAAUGAUGGA	
miR-141-3p	UAACACUGUCUGGUAAAGAUGG	UAACACUGUCUGGUAAAGAUGG	
miR-146a-5p	UGAGAACUGAAUUCCAUGGGUU	UGAGAACUGAAUUCCAUGGGUU	
miR-125a-5p	UCCCUGAGACCCUUUAACCUGUGA	UCCCUGAGACCCUUUAACCUGUGA	
miR-142a-3p	UGUAGUGUUUCCUACUUUAUGGA	UGUAGUGUUUCCUACUUUAUGGA	Exists as hsa-miR-142-3p
miR-99b-5p	CACCCGUAGAACCGACCUUGCG	CACCCGUAGAACCGACCUUGCG	
miR-96-5p	UUUGGCACUAGCACAUUUUUGCU	UUUGGCACUAGCACAUUUUUGCU	
miR-214-3p	ACAGCAGGCACAGACAGGCAGU	ACAGCAGGCACAGACAGGCAGU	
miR-181c-5p	AACAUUCAACCUGUCGGUGAGU	AACAUUCAACCUGUCGGUGAGU	
miR-301a-3p	CAGUGCAAUAGUAUUGUCAAAGC	CAGUGCAAUAGUAUUGUCAAAGC	
miR-338-3p	UCCAGCAUCAGUGAUUUUGUUG	UCCAGCAUCAGUGAUUUUGUUG	
miR-143-3p	UGAGAUGAAGCACUGUAGCUC	UGAGAUGAAGCACUGUAGCUC	
miR-199a-5p	CCCAGUGUUCAGACUACCUGUUC	CCCAGUGUUCAGACUACCUGUUC	
miR-193b-3p	AACUGGCCCACAAAGUCCCGCU	AACUGGCCCUCAAAGUCCCGCU	
miR-183-5p	UAUGGCACUGGUAGAAUUCACU	UAUGGCACUGGUAGAAUUCACU	
miR-199b-5p	CCCAGUGUUUAGACUACCUGUUC	CCCAGUGUUUAGACUAUCUGUUC	
miR-142a-5p	CAUAAAGUAGAAAGCACUACU	CAUAAAGUAGAAAGCACUACU	Exists as hsa-miR-142-5p
miR-324-5p	CGCAUCCCCUAGGGCAUUGGUGU	CGCAUCCCCUAGGGCAUUGGUG	
miR-532-5p	CAUGCCUUGAGUGUAGGACCGU	CAUGCCUUGAGUGUAGGACCGU	
miR-340-5p	UUAUAAAGCAAUGAGACUGAUU	UUAUAAAGCAAUGAGACUGAUU	
miR-1306-3p	ACGUUGGCUCUGGUGGUGAUG	ACGUUGGCUCUGGUGGUG	
miR-210-3p	CUGUGCGUGUGACAGCGGCUGA	CUGUGCGUGUGACAGCGGCUGA	
miR-125a-3p	ACAGGUGAGGUUCUUGGGAGCC	ACAGGUGAGGUUCUUGGGAGCC	
miR-154-5p	UAGGUUAUCCGUGUUGCCUUCG	UAGGUUAUCCGUGUUGCCUUCG	
miR-877-5p	GUAGAGGAGAUGGCGCAGGG	GUAGAGGAGAUGGCGCAGGG	
miR-132-3p	UAACAGUCUACAGCCAUGGUCG	UAACAGUCUACAGCCAUGGUCG	
miR-300-3p	UAUGCAAGGGCAAGCUCUCUUC	UAUACAAGGGCAGACUCUCUCU	Exists as hsa-miR-300
miR-551b-3p	GCGACCCAUACUUGGUUUCAG	GCGACCCAUACUUGGUUUCAG	
miR-335-5p	UCAAGAGCAAUAACGAAAAAUGU	UCAAGAGCAAUAACGAAAAAUGU	
miR-155-5p	UUAAUGCUAAUUGUGAUAGGGGU	UUAAUGCUAAUCGUGAUAGGGGUU	
miR-181a-5p	AACAUUCAACGCUGUCGGUGAGU	AACAUUCAACGCUGUCGGUGAGU	
miR-127-3p	UCGGAUCCGUCUGAGCUUGGCU	UCGGAUCCGUCUGAGCUUGGCU	
miR-126a-5p	CAUUAUUACUUUUGGUACGCG	CAUUAUUACUUUUGGUACGCG	Exists as hsa-miR-126-5p
miR-503-5p	UAGCAGCGGGAACAGUACUGCAG	UAGCAGCGGGAACAGUUCUGCAG	
miR-24-1-5p	GUGCCUACUGAGCUGAUAUCAGU	UGCCUACUGAGCUGAUAUCAGU	
miR-18a-5p	UAAGGUGCAUCUAGUGCAGAUAG	UAAGGUGCAUCUAGUGCAGAUAG	
miR-29c-5p	UGACCGAUUUCUCCUGGUGUUC	UGACCGAUUUCUCCUGGUGUUC	
miR-1249-3p	ACGCCCUUCCCCCCCCUUCUUCA	ACGCCCUUCCCCCCCCUUCUUCA	
miR-326-3p	CCUCUGGGCCCUUCCUCCAGU	CCUCUGGGCCCUUCCUCCAG	Exists as hsa-miR-326
miR-128-3p	UCACAGUGAACCGGUCUCUUU	UCACAGUGAACCGGUCUCUUU	
miR-340-3p	UCCGUCUCAGUUACUUUAUAGC	UCCGUCUCAGUUACUUUAUAGC	
miR-28c	AGGAGCUCACAGUCUAUUGA	AAGGAGCUCACAGUCUAUUGAG	Exists as hsa-miR-28-5p
miR-182-5p	UUUGGCAAUGGUAGAACUCACACCG	UUUGGCAAUGGUAGAACUCACACU	
miR-374c-5p	AUAAUACAACCUGCUAAGUG	AUAAUACAACCUGCUAAGUGCU	
miR-299b-5p	GGUUUACCGUCCCACAUACAU	UGGUUUACCGUCCCACAUACAU	Exists as hsa-miR-299-5p
miR-129-1-3p	AAGCCCUUACCCCAAAAAGUAU	AAGCCCUUACCCCAAAAAGUAU	
miR-30b-3p	CUGGGAUGUGGAUGUUUACGUC	CUGGGAGGUGGAUGUUUACUUC	
miR-542-5p	CUCGGGGAUCAUCAUGUCACGA	UCGGGGAUCAUCAUGUCACGAGA	
miR-5121	AGCUUGUGAUGAGACAUCUCC	N/A	
miR-M87-1	AGGCAGCCGUCGGCAGCGGCAGC	N/A	
miR-1896	CUCUCUGAUGGUGGGUGAGGAG	N/A	
miR-5130	CUGGAGCGCGCGGGCGAGGCAGGC	N/A	
miR-1967	UGAGGAUCCUGGGGAGAAGAUGC	N/A	
miR-669n	AUUUGUGUGUGGAUGUGUGU	N/A	
miR-3113-5p	GUCCUGGCCCUGGUCCGGGUCC	N/A	
miR-3067-3p	CCAAGCGGCUGCCCUGGGAGAGG	N/A	
miR-674-3p	CACAGCUCCCAUCUCAGAACAA	N/A	
miR-872-5p	AAGGUUACUUGUUAGUUCAGG	N/A	
miR-1901	CCGCUCGUACUCCCGGGGGUCC	N/A	

B

miRNA	Mouse Sequence	Human Sequence	Notes
miR-195a-5p	UAGCAGCACAGAAAUAUUGGC	UAGCAGCACAGAAAUAUUGGC	Exists as hsa-miR-195-5p
miR-200a-3p	UAACACUGUCUGGUAACGAUGU	UAACACUGUCUGGUAACGAUGU	
miR-126a-3p	UCGUACCGUGAGUAAUAAUGCG	UCGUACCGUGAGUAAUAAUGCG	Exists as hsa-miR-126-3p
miR-497a-5p	CAGCAGCACACUGUGGUUUGU***A***	CAGCAGCACACUGUGGUUUGU	Exists as hsa-miR-497-5p
let-7e-5p	UGAGGUAGGAGGUUGUAUAGUU	UGAGGUAGGAGGUUGUAUAGUU	
miR-27a-3p	UUCACAGUGGCUAAGUUCCGC	UUCACAGUGGCUAAGUUCCGC	
miR-200b-3p	UAAUACUGCCUGGUAAUGAUGA	UAAUACUGCCUGGUAAUGAUGA	
miR-199a-3p	ACAGUAGUCUGCACAUUGGUUA	ACAGUAGUCUGCACAUUGGUUA	
miR-23a-3p	AUCACAUUGCCAGGGAUUUCC	AUCACAUUGCCAGGGAUUUCC	
miR-429-3p	UAAUACUGUCUGGUAAUGCCGU	UAAUACUGUCUGGUAA***AA***CCGU	
miR-24-3p	UGGCUCAGUUCAGCAGGAACAG	UGGCUCAGUUCAGCAGGAACAG	
let-7i-5p	UGAGGUAGUAGUUUGUGCUGUU	UGAGGUAGUAGUUUGUGCUGUU	
miR-3960	GGCGGCGGCGGAGGCGGGGG	GGCGGCGGCGGAGGCGGGGG	

Appendix 2.2 Removal of murine miRNAs with no human equivalent as candidate biomarkers

As candidate miRNAs should be translational, shared (A) and unique (B) miRNAs of interest were examined on miRBase V.22 for their human equivalent. Those with no human equivalent were removed from downstream analysis. Differences between murine and human isoforms were noted in bolded red for additional bases and italicised red for base substitutions.

A

miRNA name	Liver	Cerebellum	Spleen	Stomach	Kidney	Oesophagus	Small Intestine	Cerebellum	Lung	Ovary	Uterus	Heart	Colon	Pancreas	Total Reads	% liver expression
miR-122	2,775,249	437	354	324	3,727	382	72	137	109	3	106	384	116	6	2,781,406	99.78
miR-126a-3p	49,642	29,208	42,538	56,900	116,944	77,102	41,314	386	165,599	222	8,299	30,863	244	153	619,414	8.01
miR-24-3p	21,780	19,637	14,061	18,588	77,527	16,143	17,157	2,798	56,551	846	17,690	16,826	583	949	281,136	7.75
let-7i-5p	5,615	47,123	21,504	6,234	18,720	4,822	7,337	4,425	18,682	1,767	4,478	7,688	1,118	1,220	150,733	3.73
miR-27a-3p	484	714	945	1,863	3,480	1,006	1,373	8	3,921	52	1,620	1,100	88	46	16,700	2.90
let-7e-5p	2,733	56,544	5,289	2,210	11,943	3,565	3,614	1,718	6,254	2,039	2,318	1,669	239	710	100,845	2.71
miR-195a-5p	412	2,159	3,829	3,399	4,014	5,448	3,631	259	4,428	157	1,497	690	754	72	30,749	1.34
miR-497a-5p	26	212	212	183	346	216	168	146	457	2	108	90	4	0	2,170	1.20
miR-199a-3p	344	93	2,003	5,604	2,584	7,204	3,094	6	5,703	162	1,915	771	516	18	30,017	1.15
miR-23a-3p	178	1,969	1,486	4,437	2,589	5,192	1,522	59	7,364	26	1,763	1,548	145	26	28,304	0.63
miR-429-3p	120	75	26	3,746	13,155	1,953	5,788	2	1,109	2	4,001	12	2	6	29,997	0.40
miR-200a-3p	140	64	35	6,838	17,892	3,026	10,920	6	1,718	4	9,928	35	10	40	50,656	0.28
miR-200b-3p	208	108	66	9,295	21,600	4,465	23,808	11	2,834	1	21,915	109	25	122	84,567	0.25

B

miRNA name	Liver	Cerebellum	Spleen	Stomach	Kidney	Oesophagus	Small Intestine	Cerebellum	Lung	Ovary	Uterus	Heart	Colon	Pancreas	Total Reads	% liver expression
miR-122	2,775,249	437	354	324	3,727	382	72	137	109	3	106	384	116	6	2,781,406	99.78
miR-340-3p	29	29	30	32	17	27	18	1	20	0	8	3	1	0	215	13.49
miR-193b-3p	19	10	1	72	92	11	7	0	22	0	15	1	1	0	251	7.57
miR-146a-5p	7,490	6,904	34,413	2,151	18,276	884	4,549	483	22,954	119	3,591	3,863	111	26	105,814	7.08
miR-340-5p	730	2,099	1,291	575	2,866	414	777	174	422	68	671	266	137	37	10,527	6.93
miR-126a-5p	5,051	3,665	5,672	6,988	14,388	6,764	4,618	207	19,971	44	2,087	9,029	62	42	78,588	6.43
miR-335-5p	174	1,374	136	186	280	407	125	12	331	2	102	109	3	5	3,246	5.36
miR-511-3p	16	0	98	79	14	42	22	0	31	1	12	9	0	0	324	4.94
miR-96-5p	44	4	4	158	170	57	335	9	187	0	173	0	0	19	1,160	3.79
miR-182-5p	2,820	319	448	9,228	8,976	4,326	16,702	399	10,435	50	19,953	157	52	1,007	74,872	3.77
miR-99b-5p	2,209	3,939	1,781	4,692	13,921	7,257	3,181	6,524	20,580	256	5,294	3,692	77	46	73,449	3.01
miR-125a-3p	24	197	31	58	171	57	27	152	79	3	31	22	5	0	857	2.80
miR-125a-5p	919	5,595	1,037	2,308	4,852	3,494	1,633	7,400	3,513	83	1,781	716	170	6	33,507	2.74
miR-29c-5p	185	2,506	146	421	2,048	308	274	89	418	3	204	255	2	41	6,900	2.68
miR-532-5p	154	1,084	751	440	1,025	611	326	295	579	2	398	185	2	2	5,854	2.63
miR-24-1-5p	5	32	5	25	34	36	15	4	20	0	11	12	2	0	201	2.49
miR-542-5p	8	16	31	25	40	26	6	2	204	2	14	13	1	0	388	2.06
miR-199a-5p	118	75	1,131	1,924	482	577	445	5	744	8	401	270	48	1	6,229	1.89
miR-503-5p	11	28	32	20	187	61	28	1	98	48	40	37	3	0	594	1.85
miR-1249-3p	1	25	2	1	4	3	2	15	2	0	3	0	1	0	59	1.69
miR-210-3p	11	34	17	103	73	268	9	8	27	1	96	27	1	0	675	1.63
miR-30b-3p	1	2	8	2	18	6	0	2	11	0	2	10	0	0	62	1.61
miR-142a-3p	1,048	363	51,657	1,165	2,461	1,786	7,382	9	3,636	5	1,449	249	36	9	71,255	1.47
miR-183-5p	813	79	263	4,652	4,468	16,499	11,515	158	6,348	15	13,674	81	15	166	58,746	1.38
miR-18a-5p	14	33	151	76	117	119	380	0	52	0	89	14	3	1	1,049	1.33

B

miRNA name	Liver	Cerebellum	Spleen	Stomach	Kidney	Oesophagus	Small Intestine	Cerebellum	Lung	Ovary	Uterus	Heart	Colon	Pancreas	Total Reads	% liver expression
miR-301a-3p	23	481	164	196	327	74	162	44	139	0	91	36	0	0	1,737	1.32
miR-155-5p	26	13	1,175	49	276	71	83	1	91	0	40	149	1	1	1,976	1.32
miR-338-3p	59	2,918	70	128	121	450	56	595	162	0	58	32	0	0	4,649	1.27
miR-214-3p	18	1	86	200	130	373	246	0	147	31	216	51	33	2	1,534	1.17
miR-199b-5p	175	46	1,020	2,843	1,314	3,639	1,569	3	2,882	82	968	386	259	9	15,195	1.15
miR-143-3p	389,618	336,069	2,513,975	5,925,272	2,728,618	1,202,349	5,006,864	51,457	3,629,552	1,974,868	4,944,122	1,485,372	6,586,033	24,978	36,799,147	1.06
miR-181c-5p	31	881	255	166	450	271	237	332	321	1	196	172	0	0	3,313	0.94
miR-877-5p	7	350	46	12	152	98	68	33	55	2	30	11	1	1	866	0.81
miR-342-3p	101	6,359	4,313	642	160	233	228	145	497	30	305	197	42	7	13,259	0.76
miR-324-5p	6	481	29	36	60	40	55	54	117	0	25	9	1	0	913	0.66
miR-181a-5p	258	7,131	3,999	2,666	9,740	4,062	3,337	3,454	4,446	111	2,604	1,202	150	20	43,180	0.60
miR-142a-5p	115	367	10,490	409	559	894	2,138	3	3,723	64	536	224	120	59	19,701	0.58
miR-132-3p	21	3,574	30	143	68	52	102	138	26	3	131	21	0	0	4,309	0.49
miR-326-3p	25	4,011	155	280	154	14	57	282	682	1	105	28	1	0	5,795	0.43
miR-300-3p	6	2,226	8	129	7	258	49	787	20	0	119	12	0	1	3,622	0.17
miR-127-3p	194	65,047	262	7,201	267	6,495	2,099	56,106	1,014	25	3,071	779	34	53	142,647	0.14
miR-128-3p	40	33,818	158	229	148	521	193	1,439	153	0	83	98	3	1	36,884	0.11
miR-141-3p	47	83	240	8,465	7,230	2,771	17,284	3	2,366	11	5,165	30	24	117	43,836	0.11
miR-200c-3p	185	169	435	21,942	16,650	19,991	70,528	23	12,248	32	42,592	290	67	439	185,591	0.10
miR-1306-3p	0	4	0	0	1	0	1	1	0	0	0	0	0	0	7	0.00
miR-154-5p	0	199	1	18	0	23	5	4	1	0	2	1	0	0	254	0.00
miR-551b-3p	0	154	1	0	3	0	0	0	0	0	1	0	0	0	159	0.00
miR-374c-5p	0	0	0	2	3	1	1	0	0	0	1	0	0	0	8	0.00
miR-129-1-3p	0	91	1	7	1	1	1	50	0	0	0	1	0	0	153	0.00

Appendix 2.3 Candidate miRNAs do not exhibit liver specific tissue expression.

The expression of the 13 shared (A) and 50 unique (B) miRNAs of interest were cross referenced in a gene expression tissue library (GEO accession: GSE67885) to examine liver specificity. The miRNAs are listed in descending order of percentage liver abundance, alongside the raw number of sequence reads for each miRNA in the 14 tissues. miR-122 was included as an example of a liver specific miRNA.

	24h non-fasted CD-1 Corn Oil	24h non-fasted CD-1 ANIT	24h fasted CD-1 Corn Oil	24h fasted CD-1 ANIT	72h fasted CD-1 Corn Oil	72h fasted CD-1 ANIT	30h fasted CD-1 PEG	30h fasted CD-1 DAPM	24h fasted C57BL/6J Corn Oil	24h fasted C57BL/6J ANIT	48h fasted C57BL/6J Corn Oil	48h fasted C57BL/6J ANIT	72h fasted C57BL/6J Corn Oil	72h fasted C57BL/6J ANIT
Number of values	3	3	3	3	3	3	3	3	3	3	3	3	3	3
Minimum	21.84	21.58	20.7	20.73	20.69	20.42	21.57	21.41	21.7	21.83	21.19	19.97	21.68	20.67
Maximum	22.03	22.79	20.99	21.86	21.57	21.97	22.3	22.12	22.18	22.04	21.38	21.57	21.77	21.74
Range	0.183	1.213	0.285	1.137	0.882	1.551	0.73	0.707	0.48	0.203	0.19	1.597	0.096	1.069
Mean	21.96	22.15	20.87	21.23	21.15	21.03	21.85	21.74	21.98	21.9	21.28	20.75	21.73	21.12
Std. Deviation	0.1029	0.6087	0.1479	0.5799	0.4416	0.8276	0.3894	0.3553	0.2489	0.1161	0.09509	0.799	0.04924	0.5536
Std. Error of Mean	0.0594	0.3514	0.08538	0.3348	0.2549	0.4778	0.2248	0.2052	0.1437	0.06701	0.0549	0.4613	0.02843	0.3196
Coefficient of variation	0.4685%	2.748%	0.7087%	2.732%	2.088%	3.935%	1.782%	1.634%	1.132%	0.5299%	0.4468%	3.850%	0.2266%	2.621%

Appendix 3.1- Statistical analysis of cel-lin-4 CT values in serum miRNA qPCR

In order to assess potential technical variation in miRNA extracted from hepatobiliary toxin-dosed mice, the levels and variation in the exogenous miRNA, cel-lin-4, were assessed. Coefficient of variation for all samples was <5 %.

CYP450 Protein	Accession	p-value(Diff vs. Liver)	-log10 p-value Diff/Liver	Ratio(Diff vs. Liver)	Log2 Diff/Liver	p-value(Undiff vs. Liver)	-log10 p-value Undiff/Liver	Ratio(Undiff vs. Liver)	Log2 Undiff/Liver	p-value(Undiff vs. Diff)	-log10 p-value Undiff/Diff	Ratio(Undiff vs. Diff)	Log2 Undiff/Diff
Cytochrome P450 1B1	Q64429	0.22	**0.66**	0.37	**-1.42**	0.35	**0.46**	2.08	**1.06**	0.05	**1.33**	5.56	**2.47**
Cytochrome P450 20A1	Q8BKE6	0.85	**0.07**	1.04	**0.05**	0.46	**0.34**	1.14	**0.19**	0.58	**0.24**	1.10	**0.14**
Cytochrome P450 2A12	P56593	0.00	**7.53**	0.02	**-5.62**	0.00	**7.52**	0.02	**-5.61**	0.98	**0.01**	1.00	**0.01**
Cytochrome P450 2A5	P20852	0.57	**0.24**	1.24	**0.31**	0.00	**3.77**	0.11	**-3.22**	0.00	**4.07**	0.09	**-3.52**
Cytochrome P450 2B10	P12791	0.96	**0.02**	0.96	**-0.05**	0.04	**1.43**	0.21	**-2.29**	0.04	**1.38**	0.21	**-2.23**
Cytochrome P450 2B19	O55071	0.63	**0.20**	0.78	**-0.36**	0.03	**1.55**	0.27	**-1.88**	0.06	**1.19**	0.35	**-1.52**
Cytochrome P450 2C29	Q64458	0.00	**7.19**	0.01	**-6.58**	0.00	**7.67**	0.01	**-7.45**	0.06	**1.20**	0.55	**-0.87**
Cytochrome P450 2C39	P56656	0.00	**2.88**	0.13	**-2.95**	0.00	**3.72**	0.07	**-3.89**	0.17	**0.76**	0.52	**-0.95**
Cytochrome P450 2C40	P56657	0.00	**5.91**	0.03	**-5.17**	0.00	**6.68**	0.01	**-6.36**	0.03	**1.55**	0.44	**-1.19**
Cytochrome P450 2C50	Q91X77	0.00	**7.13**	0.03	**-5.05**	0.00	**7.67**	0.02	**-5.82**	0.04	**1.40**	0.59	**-0.77**
Cytochrome P450 2C54	Q6XVG2	0.00	**4.66**	0.10	**-3.38**	0.00	**5.91**	0.04	**-4.79**	0.01	**2.07**	0.37	**-1.42**
Cytochrome P450 2C55	Q9D816	0.00	**4.62**	35.73	**5.16**	0.07	**1.17**	2.55	**1.35**	0.00	**3.61**	0.07	**-3.81**
Cytochrome P450 2C70	Q91W64	0.00	**8.54**	0.01	**-6.36**	0.00	**8.78**	0.01	**-6.76**	0.18	**0.74**	0.76	**-0.40**
Cytochrome P450 2D10	P24456	0.00	**6.77**	0.04	**-4.75**	0.00	**7.66**	0.02	**-6.02**	0.00	**2.39**	0.41	**-1.27**
Cytochrome P450 2D26	Q8CIM7	0.00	**8.14**	0.02	**-5.44**	0.00	**8.94**	0.01	**-6.70**	0.00	**3.00**	0.42	**-1.27**
Cytochrome P450 2D9	P11714	0.00	**11.10**	0.01	**-6.46**	0.00	**10.88**	0.01	**-6.10**	0.04	**1.43**	1.28	**0.36**
Cytochrome P450 2E1	Q05421	0.00	**8.71**	0.02	**-5.97**	0.00	**8.81**	0.01	**-6.13**	0.55	**0.26**	0.90	**-0.16**
Cytochrome P450 2F2	P33267	0.00	**9.45**	0.57	**-0.81**	0.00	**9.61**	0.56	**-0.85**	0.27	**0.57**	0.98	**-0.03**
Cytochrome P450 2J5	O54749	0.00	**6.98**	0.06	**-4.08**	0.00	**8.10**	0.02	**-5.47**	0.00	**3.23**	0.38	**-1.39**
Cytochrome P450 2J6	O54750	0.00	**3.49**	4.30	**2.10**	0.01	**1.92**	2.26	**1.18**	0.04	**1.45**	0.53	**-0.93**
Cytochrome P450 2S1	Q9DBX6	0.00	**8.83**	30.62	**4.94**	0.00	**2.89**	1.90	**0.93**	0.00	**8.03**	0.06	**-4.01**
Cytochrome P450 2U1	Q9CX98	0.01	**1.93**	2.54	**1.35**	0.04	**1.38**	2.02	**1.01**	0.46	**0.34**	0.79	**-0.33**
Cytochrome P450 3A11	Q64459	0.00	**3.97**	0.07	**-3.90**	0.00	**5.50**	0.01	**-6.06**	0.01	**2.26**	0.22	**-2.16**
Cytochrome P450 3A13	Q64464	0.01	**1.97**	3.13	**1.65**	0.00	**3.80**	0.11	**-3.19**	0.00	**5.22**	0.03	**-4.84**
Cytochrome P450 3A25	O09158	0.00	**4.19**	0.09	**-3.41**	0.00	**5.58**	0.03	**-5.08**	0.01	**2.10**	0.32	**-1.66**
Cytochrome P450 4A12A	Q91WL5	0.00	**12.61**	0.02	**-5.98**	0.00	**13.01**	0.01	**-6.63**	0.00	**4.23**	0.64	**-0.65**
Cytochrome P450 4B1	Q64462	0.00	**3.61**	6.76	**2.76**	0.00	**4.81**	15.45	**3.95**	0.03	**1.49**	2.29	**1.19**
Cytochrome P450 4V2	Q9DBW0	0.00	**7.45**	0.02	**-5.35**	0.00	**7.67**	0.02	**-5.67**	0.33	**0.48**	0.80	**-0.32**
NADPH--cytochrome P450 reductase	P37040	0.75	**0.12**	1.13	**0.18**	0.00	**3.37**	0.13	**-2.94**	0.00	**3.55**	0.12	**-3.12**

Phase II Protein	Accession	p-value(Diff vs. Liver)	-log10 p-value Diff/Liver	Ratio(Diff vs. Liver)	Log2 Diff/Liver	p-value(Undiff vs. Liver)	-log10 p-value Undiff/Liver	Ratio(Undiff vs. Liver)	Log2 Undiff/Liver	p-value(Undiff vs. Diff)	-log10 p-value Undiff/Diff	Ratio(Undiff vs. Diff)	Log2 Undiff/Diff
Glutathione S-transferase A3	P30115	0.00	**4.33**	0.20	**-2.29**	0.00	**6.62**	0.05	**-4.33**	0.00	**3.94**	0.24	**-2.04**
Glutathione S-transferase A4	P24472	0.01	**2.05**	4.33	**2.11**	0.12	**0.94**	2.15	**1.11**	0.15	**0.83**	0.50	**-1.01**
Glutathione S-transferase kappa 1	Q9DCM2	0.00	**5.08**	0.08	**-3.68**	0.00	**6.25**	0.03	**-5.08**	0.01	**2.12**	0.38	**-1.40**
Glutathione S-transferase Mu 1	P10649	0.00	**4.53**	0.20	**-2.35**	0.00	**5.80**	0.10	**-3.36**	0.01	**2.04**	0.50	**-1.01**
Glutathione S-transferase Mu 2	P15626	0.31	**0.51**	0.67	**-0.58**	0.00	**3.16**	0.15	**-2.72**	0.00	**2.48**	0.23	**-2.14**
Glutathione S-transferase Mu 3	P19639	0.00	**3.29**	0.09	**-3.44**	0.00	**5.77**	0.01	**-7.13**	0.00	**3.50**	0.08	**-3.69**
Glutathione S-transferase Mu 5	P48774	0.18	**0.74**	0.75	**-0.42**	0.30	**0.52**	0.80	**-0.32**	0.74	**0.13**	1.07	**0.10**
Glutathione S-transferase Mu 6	O35660	0.00	**5.38**	0.09	**-3.55**	0.00	**5.54**	0.08	**-3.71**	0.67	**0.17**	0.90	**-0.16**
Glutathione S-transferase Mu 7	Q80W21	0.01	**1.97**	0.30	**-1.75**	0.00	**4.49**	0.06	**-4.15**	0.00	**2.77**	0.19	**-2.40**
Glutathione S-transferase omega-1	O09131	0.00	**6.80**	20.99	**4.39**	0.00	**7.07**	26.30	**4.72**	0.31	**0.51**	1.25	**0.33**
Glutathione S-transferase P 1	P19157	0.01	**1.93**	0.21	**-2.23**	0.01	**2.16**	0.18	**-2.46**	0.75	**0.12**	0.85	**-0.23**
Glutathione S-transferase P 2	P46425	0.00	**3.34**	0.18	**-2.45**	0.00	**3.09**	0.21	**-2.26**	0.68	**0.17**	1.15	**0.20**
Glutathione S-transferase theta-1	Q64471	0.00	**4.97**	0.20	**-2.31**	0.00	**7.70**	0.04	**-4.82**	0.00	**5.28**	0.17	**-2.52**
Glutathione S-transferase theta-2	Q61133	0.00	**3.09**	0.18	**-2.51**	0.00	**5.14**	0.04	**-4.67**	0.00	**2.66**	0.22	**-2.16**
Glutathione S-transferase theta-3	Q99L20	0.96	**0.02**	1.02	**0.02**	0.00	**3.79**	0.15	**-2.76**	0.00	**3.81**	0.15	**-2.78**
Microsomal glutathione S-transferase 1	Q91VS7	0.00	**11.53**	0.02	**-5.36**	0.00	**11.34**	0.03	**-5.10**	0.04	**1.41**	1.20	**0.26**
Microsomal glutathione S-transferase 3	Q9CPU4	0.00	**5.93**	6.25	**2.64**	0.00	**4.52**	3.44	**1.78**	0.00	**2.32**	0.55	**-0.86**
UDP-glucuronosyltransferase 1-1	Q63886	0.00	**4.99**	0.05	**-4.25**	0.00	**5.36**	0.04	**-4.71**	0.36	**0.44**	0.72	**-0.47**
UDP-glucuronosyltransferase 1-6	Q64435	0.05	**1.35**	0.56	**-0.84**	0.02	**1.66**	0.50	**-1.00**	0.67	**0.18**	0.90	**-0.16**
UDP-glucuronosyltransferase 1-7C	Q6ZQM8	0.00	**8.94**	22.80	**4.51**	0.00	**8.61**	17.66	**4.14**	0.07	**1.16**	0.77	**-0.37**
UDP-glucuronosyltransferase 1-9	Q62452	0.00	**12.06**	0.02	**-5.95**	0.00	**12.23**	0.01	**-6.21**	0.04	**1.42**	0.84	**-0.26**
UDP-glucuronosyltransferase 2A3	Q8BWQ1	0.00	**7.12**	0.05	**-4.47**	0.00	**8.63**	0.01	**-6.63**	0.00	**4.48**	0.22	**-2.17**
UDP-glucuronosyltransferase 2B17	P17717	0.00	**9.60**	0.02	**-5.93**	0.00	**9.82**	0.01	**-6.28**	0.12	**0.93**	0.79	**-0.34**
UDP-glucuronosyltransferase 3A2	Q8JZZ0	0.00	**4.51**	0.05	**-4.28**	0.00	**5.00**	0.03	**-4.93**	0.28	**0.56**	0.64	**-0.65**
Sulfotransferase 1 family member D1	Q3UZZ6	0.00	**2.47**	3.39	**1.76**	0.00	**5.07**	0.06	**-4.02**	0.00	**6.40**	0.02	**-5.78**
Sulfotransferase 1A1	P52840	0.20	**0.69**	0.75	**-0.42**	0.00	**7.49**	0.03	**-5.30**	0.00	**7.18**	0.03	**-4.88**
Sulfotransferase 1C2	Q9D939	0.00	**6.41**	30.20	**4.92**	0.00	**4.63**	8.02	**3.00**	0.00	**3.16**	0.27	**-1.91**
Sulfotransferase family cytosolic 1B member 1	Q9QWG7	0.30	**0.53**	0.74	**-0.44**	0.00	**5.00**	0.09	**-3.49**	0.00	**4.53**	0.12	**-3.05**
Sulfotransferase family cytosolic 2B member 1	O35400	0.01	**2.10**	2.89	**1.53**	0.02	**1.82**	2.55	**1.35**	0.69	**0.16**	0.88	**-0.18**
Arylamine N-acetyltransferase 2	P50295	0.02	**1.69**	0.53	**-0.91**	0.00	**2.74**	0.38	**-1.41**	0.16	**0.80**	0.71	**-0.50**
Glucosamine 6-phosphate N-acetyltransferase	Q9JK38	0.00	**6.24**	0.09	**-3.53**	0.00	**3.92**	0.28	**-1.83**	0.00	**3.68**	3.25	**1.70**
N-acetyltransferase family 8 member 2	Q8CHQ9	0.00	**5.72**	0.05	**-4.29**	0.00	**6.00**	0.04	**-4.62**	0.42	**0.38**	0.79	**-0.34**

Transporter Protein	Accession	p-value(Diff vs. Liver)	-log10 p-value Diff/Liver	Ratio(Diff vs. Liver)	Log2 Diff/Liver	p-value(Undiff vs. Liver)	-log10 p-value Undiff/Liver	Ratio(Undiff vs. Liver)	Log2 Undiff/Liver	p-value(Undiff vs. Diff)	-log10 p-value Undiff/Diff	Ratio(Undiff vs. Diff)	Log2 Undiff/Diff
Multidrug resistance-associated protein 1	O35379	0.11	0.95	1.44	0.52	0.00	2.38	2.18	1.13	0.07	1.15	1.52	0.60
Multidrug resistance-associated protein 6	Q9R1S7	0.00	4.80	0.06	-3.95	0.00	6.00	0.02	-5.51	0.01	2.02	0.34	-1.55
Multidrug resistance-associated protein 7	Q8R4P9	0.26	0.58	1.54	0.62	0.28	0.56	1.52	0.60	0.97	0.02	0.98	-0.02
Solute carrier family 12 member 2	P55012	0.00	7.38	5.46	2.45	0.00	10.46	43.15	5.43	0.00	8.14	7.91	2.98
Solute carrier family 12 member 4	Q9JIS8	0.73	0.14	1.33	0.41	0.06	1.21	0.18	-2.44	0.03	1.46	0.14	-2.86
Solute carrier family 12 member 7	Q9WVL3	0.97	0.01	0.99	-0.02	0.23	0.65	1.55	0.63	0.21	0.67	1.57	0.65
Solute carrier family 12 member 9	Q99MR3	0.00	2.61	2.66	1.41	0.00	2.51	2.57	1.36	0.89	0.05	0.97	-0.05
Solute carrier family 2, facilitated glucose transporter member 1	P17809	0.00	5.84	7.57	2.92	0.00	5.87	7.69	2.94	0.93	0.03	1.02	0.02
Solute carrier family 2, facilitated glucose transporter member 2	P14246	0.06	1.24	0.56	-0.83	0.00	6.03	0.04	-4.49	0.00	5.28	0.08	-3.66
Solute carrier family 22 member 1	O08966	0.11	0.97	0.43	-1.21	0.09	1.06	0.41	-1.29	0.90	0.04	0.94	-0.08
Solute carrier family 22 member 18	Q78KK3	0.17	0.77	0.49	-1.03	0.00	2.77	0.12	-3.03	0.02	1.76	0.25	-2.00
Solute carrier family 22 member 27	Q76M72	0.00	5.61	0.29	-1.78	0.00	5.94	0.26	-1.95	0.34	0.46	0.89	-0.17
Solute carrier family 25 member 35	Q5SWT3	0.00	3.17	2.40	1.27	0.88	0.06	0.97	-0.04	0.00	3.26	0.40	-1.31
Solute carrier family 25 member 40	Q8BGP6	0.28	0.56	1.31	0.39	0.45	0.34	1.20	0.27	0.72	0.14	0.92	-0.13
Solute carrier family 25 member 44	Q8BGF9	0.69	0.16	0.95	-0.08	0.60	0.22	0.93	-0.10	0.90	0.04	0.98	-0.02
Solute carrier family 25 member 45	Q8CFJ7	0.06	1.24	0.64	-0.63	0.21	0.68	0.76	-0.39	0.43	0.37	1.18	0.24
Solute carrier family 25 member 51	Q5HZI9	0.01	2.16	0.25	-2.01	0.01	2.17	0.25	-2.02	0.99	0.01	0.99	-0.01
Solute carrier family 35 member B1	P97858	0.00	3.61	0.28	-1.84	0.00	4.61	0.18	-2.48	0.07	1.14	0.64	-0.64
Solute carrier family 35 member F6	Q8VE96	0.36	0.45	1.33	0.42	0.05	1.34	1.99	0.99	0.21	0.68	1.49	0.58
Solute carrier organic anion transporter family member 1A1	Q9QXZ6	0.00	7.13	0.01	-6.15	0.00	6.82	0.02	-5.66	0.24	0.61	1.40	0.49
Solute carrier organic anion transporter family member 1B2	Q9JJL3	0.00	4.77	0.04	-4.83	0.00	4.67	0.04	-4.70	0.82	0.09	1.10	0.14
Solute carrier organic anion transporter family member 2A1	Q9EPT5	0.01	1.84	1.66	0.73	0.19	0.71	0.79	-0.34	0.00	2.78	0.48	-1.07
Voltage-dependent anion-selective channel protein 1	Q60932	0.00	4.68	2.10	1.07	0.00	4.47	2.01	1.01	0.65	0.19	0.96	-0.06
Voltage-dependent anion-selective channel protein 2	Q60930	0.00	7.40	12.45	3.64	0.00	6.78	8.47	3.08	0.03	1.53	0.68	-0.55
Voltage-dependent anion-selective channel protein 3	Q60931	0.07	1.15	1.29	0.37	0.42	0.37	1.11	0.15	0.26	0.59	0.86	-0.22
Bile salt export pump	Q9QY30	0.00	3.41	0.11	-3.13	0.00	4.50	0.05	-4.37	0.06	1.24	0.42	-1.24
Bile acyl-CoA synthetase	Q4LDG0	0.00	9.29	0.02	-5.96	0.00	9.20	0.02	-5.82	0.52	0.28	1.10	0.14
Bile acid-CoA:amino acid N-acyltransferase	Q91X34	0.00	7.74	0.03	-4.95	0.00	7.68	0.03	-4.88	0.81	0.09	1.05	0.07
Canalicular multispecific organic anion transporter 1	Q8VI47	0.00	6.83	0.10	-3.25	0.00	8.00	0.05	-4.41	0.00	3.25	0.45	-1.16
Canalicular multispecific organic anion transporter 2	B2RX12	0.00	6.90	10.42	3.38	0.00	5.58	5.18	2.37	0.00	2.78	0.50	-1.01
ATP-binding cassette sub-family A member 3	Q8R420	0.06	1.23	1.72	0.78	0.99	0.00	1.00	0.00	0.06	1.24	0.58	-0.79
ATP-binding cassette sub-family A member 6	Q8K441	0.00	5.03	0.06	-4.00	0.00	4.77	0.08	-3.72	0.54	0.27	1.22	0.29
ATP-binding cassette sub-family B member 10, mitochondrial	Q9JI39	0.82	0.09	1.07	0.10	0.24	0.63	0.69	-0.54	0.17	0.78	0.64	-0.64
ATP-binding cassette sub-family B member 7, mitochondrial	Q61102	0.00	3.25	0.44	-1.20	0.01	1.86	0.62	-0.70	0.06	1.22	1.41	0.49
ATP-binding cassette sub-family B member 8, mitochondrial	Q9CXJ4	0.14	0.86	0.61	-0.70	0.47	0.33	0.80	-0.33	0.41	0.39	1.30	0.38
ATP-binding cassette sub-family D member 1	P48410	0.00	3.45	0.39	-1.35	0.00	2.53	0.51	-0.98	0.16	0.79	1.29	0.37
ATP-binding cassette sub-family D member 3	P55096	0.00	7.79	0.03	-5.04	0.00	6.93	0.06	-4.02	0.00	2.37	2.03	1.02
ATP-binding cassette sub-family D member 4	O89016	0.01	2.23	1.71	0.77	0.80	0.10	1.04	0.06	0.01	2.05	0.61	-0.72
ATP-binding cassette sub-family E member 1	P61222	0.00	4.28	0.30	-1.73	0.23	0.63	0.81	-0.31	0.00	3.63	2.69	1.43
ATP-binding cassette sub-family F member 1	Q6P542	0.00	4.29	0.27	-1.89	0.27	0.57	0.81	-0.31	0.00	3.70	3.00	1.58
ATP-binding cassette sub-family F member 2	Q99LE6	0.14	0.86	0.87	-0.20	0.92	0.04	0.99	-0.01	0.16	0.78	1.14	0.19
ATP-binding cassette sub-family F member 3	Q8K268	0.01	2.15	0.53	-0.93	0.01	1.99	0.55	-0.86	0.82	0.09	1.04	0.06
ATP-binding cassette sub-family G member 2	Q7TMS5	0.01	2.19	0.24	-2.03	0.00	3.26	0.13	-3.00	0.13	0.90	0.51	-0.97

Nrf2 Protein	Accession	p-value(Diff vs. Liver)	-log10 p-value Diff/Liver	Ratio(Diff vs. Liver)	Log2 Diff/Liver	p-value(Undiff vs. Liver)	-log10 p-value Undiff/Liver	Ratio(Undiff vs. Liver)	Log2 Undiff/Liver	p-value(Undiff vs. Diff)	-log10 p-value Undiff/Diff	Ratio(Undiff vs. Diff)	Log2 Undiff/Diff
Heme oxygenase 1	P14901	0.31	0.51	1.11	0.15	0.06	1.20	0.81	-0.30	0.01	1.96	0.73	-0.46
NAD(P)H dehydrogenase [quinone] 1	Q64669	0.21	0.68	0.42	-1.25	0.32	0.50	1.97	0.98	0.04	1.41	4.67	2.22
Glutamate--cysteine ligase catalytic subunit	P97494	0.23	0.64	0.65	-0.62	0.02	1.69	0.39	-1.34	0.17	0.78	0.61	-0.72
Glutamate--cysteine ligase regulatory subunit	O09172	0.00	4.20	0.34	-1.54	0.66	0.18	1.07	0.10	0.00	4.41	3.13	1.64
Glutathione peroxidase 1	P11352	0.00	7.14	0.13	-3.00	0.00	10.41	0.01	-7.01	0.00	8.25	0.06	-4.01
Glutathione peroxidase 2	Q9JHC0	0.39	0.41	1.29	0.37	0.00	3.36	4.61	2.21	0.00	2.82	3.57	1.84
Glutathione reductase, mitochondrial	P47791	0.10	0.98	0.67	-0.57	0.00	3.17	3.05	1.61	0.00	4.14	4.55	2.19
Glutathione synthetase	P51855	0.21	0.68	0.74	-0.43	0.14	0.84	0.70	-0.51	0.81	0.09	0.95	-0.08
Glutaredoxin-1	Q9QUH0	0.04	1.38	0.42	-1.26	0.01	2.01	0.30	-1.74	0.39	0.41	0.72	-0.48
Peroxiredoxin-1	P35700	0.73	0.14	1.09	0.12	0.07	1.17	1.62	0.70	0.12	0.92	1.49	0.58
Peroxiredoxin-2	Q61171	0.03	1.46	0.66	-0.60	0.00	3.89	0.34	-1.54	0.00	2.43	0.52	-0.94
Peroxiredoxin-4	O08807	0.00	4.80	0.14	-2.83	0.00	3.02	0.32	-1.63	0.01	2.19	2.29	1.20
Peroxiredoxin-5, mitochondrial	P99029	0.88	0.05	0.93	-0.10	0.01	2.09	0.21	-2.28	0.01	1.98	0.22	-2.18
Peroxiredoxin-6	O08709	0.00	3.89	0.15	-2.77	0.10	1.00	0.58	-0.79	0.00	2.86	3.93	1.97
Thioredoxin, mitochondrial	P97493	0.00	6.10	0.24	-2.05	0.00	6.03	0.25	-2.01	0.82	0.09	1.03	0.04
Thioredoxin reductase 1, cytoplasmic	Q9JMH6	0.97	0.02	0.99	-0.02	0.05	1.31	0.49	-1.02	0.05	1.28	0.50	-1.00
Thioredoxin	P10639	0.02	1.66	0.68	-0.56	0.02	1.70	1.49	0.57	0.00	3.47	2.20	1.14

Biomarker Protein	Accession	p-value(Diff vs. Liver)	-log10 p-value Diff/Liver	Ratio(Diff vs. Liver)	Log2 Diff/Liver	p-value(Undiff vs. Liver)	-log10 p-value Undiff/Liver	Ratio(Undiff vs. Liver)	Log2 Undiff/Liver	p-value(Undiff vs. Diff)	-log10 p-value Undiff/Diff	Ratio(Undiff vs. Diff)	Log2 Undiff/Diff
Alanine aminotransferase 1	Q8QZR5	0.00	6.73	0.26	-1.94	0.00	11.16	0.01	-6.15	0.00	9.69	0.05	-4.21
Alanine aminotransferase 2	Q8BGT5	0.19	0.73	0.70	-0.51	0.00	3.64	0.23	-2.11	0.00	2.81	0.33	-1.60
Aspartate aminotransferase, cytoplasmic	P05201	0.06	1.20	0.45	-1.14	0.00	2.88	0.18	-2.47	0.04	1.45	0.40	-1.33
Aspartate aminotransferase, mitochondrial	P05202	0.00	7.93	0.08	-3.70	0.00	7.59	0.10	-3.38	0.13	0.88	1.24	0.32
Glutamate dehydrogenase 1, mitochondrial	P26443	0.00	4.99	0.08	-3.62	0.00	6.26	0.03	-5.13	0.01	2.30	0.35	-1.51
High mobility group protein B1	P63158	0.00	4.52	2.80	1.48	0.00	4.93	3.18	1.67	0.36	0.44	1.14	0.19
Keratin, type I cytoskeletal 18	P05784	0.00	3.40	1.18	0.24	0.00	3.45	1.18	0.24	0.94	0.03	1.00	0.00
Glutathione S-transferase A1	P13745	0.00	4.06	34.44	5.11	0.28	0.55	1.83	0.87	0.00	3.46	0.05	-4.24
Glutathione S-transferase A3	P30115	0.00	4.33	0.20	-2.29	0.00	6.62	0.05	-4.33	0.00	3.94	0.24	-2.04
Glutathione S-transferase A4	P24472	0.01	2.05	4.33	2.11	0.12	0.94	2.15	1.11	0.15	0.83	0.50	-1.01
Arginase-1	Q61176	0.00	9.76	0.02	-6.03	0.00	9.96	0.01	-6.36	0.13	0.90	0.80	-0.33
Arginase-2, mitochondrial	O08691	0.00	3.91	2.88	1.52	0.08	1.10	1.39	0.47	0.00	2.78	0.48	-1.05
Sorbitol dehydrogenase	Q64442	0.00	7.90	0.06	-4.09	0.00	8.40	0.04	-4.65	0.03	1.60	0.67	-0.57
Fatty acid-binding protein, liver	P12710	0.01	1.87	0.09	-3.40	0.02	1.74	0.11	-3.20	0.85	0.07	1.16	0.21

Appendix 4.1- *p*-values and ratios in the abundance of DMET proteins in organoids and liver tissue

The full individual *p*-values and changes in expression of 30 cytochrome P450 enzymes, 32 Phase II enzymes, 45 transporter proteins ,14 Nrf2-target and 14 hepatic biomarker proteins. Data is also shown as –log10 *p-values* and log2 transformed fold-change.

Human	Mouse	Human	Mouse
1A2	1A2	2D6	2D9
1B1	1B1		2D10
20A1	20A1		2D26
2A13	2A12	2E1	2E1
2A7	2A5	2F1	2F2
2B6	2B10	2J2	2J5
	2B19		2J6
2C8	2C29	2S1	2S1
2C19	2C39	2U1	2U1
	2C40	3A4	3A11
	2C50	3A5	3A13
	2C54	3A43	3A25
	2C55	4A22	4A12A
	2C70	4B1	4B1
		4V2	4V2

Appendix 4.2- Table of human and murine CYP450 homologs

CYP450 isoform and nomenclature differences exist between species. The human homologs of the murine CYP450s detected in Chapter 4 are shown above.

Bibliography

1. Krishna, M. Microscopic anatomy of the liver. *Clin. Liver Dis.* **2**, S4–S7 (2013).

2. Eipel, C., Abshagen, K. & Vollmar, B. Regulation of hepatic blood flow: the hepatic arterial buffer response revisited. *World J. Gastroenterol.* **16**, 6046–57 (2010).

3. Benhamouche, S. *et al.* Apc Tumor Suppressor Gene Is the "Zonation-Keeper" of Mouse Liver. *Dev. Cell* **10**, 759–770 (2006).

4. Matz-Soja, M., Hovhannisyan, A. & Gebhardt, R. Hedgehog signalling pathway in adult liver: A major new player in hepatocyte metabolism and zonation? *Med. Hypotheses* **80**, 589–594 (2013).

5. Stanulović, V. S. *et al.* Hepatic HNF4α deficiency induces periportal expression of glutamine synthetase and other pericentral enzymes. *Hepatology* **45**, 433–444 (2007).

6. Kietzmann, T., Kietzmann & Thomas. Liver Zonation in Health and Disease: Hypoxia and Hypoxia-Inducible Transcription Factors as Concert Masters. *Int. J. Mol. Sci.* **20**, 2347 (2019).

7. Gebhardt, R. & Matz-Soja, M. Liver zonation: Novel aspects of its regulation and its impact on homeostasis. *World J. Gastroenterol.* **20**, 8491 (2014).

8. Birchmeier, W. Orchestrating Wnt signalling for metabolic liver zonation. *Nat. Cell Biol.* **18**, 463–465 (2016).

9. LeCluyse, E. L., Witek, R. P., Andersen, M. E. & Powers, M. J. Organotypic liver culture models: meeting current challenges in toxicity testing. *Crit. Rev. Toxicol.* **42**, 501–48 (2012).

10. Tachikawa, M. *et al.* Liver Zonation Index of Drug Transporter and Metabolizing Enzyme Protein Expressions in Mouse Liver Acinus. *Drug Metab. Dispos.* **46**, 610–618 (2018).

11. Overi, D. *et al.* Contribution of Resident Stem Cells to Liver and Biliary Tree Regeneration in Human Diseases. *Int. J. Mol. Sci.* **19**, (2018).

12. Kmieć, Z. Cooperation of liver cells in health and disease. *Adv. Anat. Embryol. Cell Biol.* **161**, III–XIII, 1–151 (2001).

13. Racanelli, V. & Rehermann, B. The liver as an immunological organ. *Hepatology* **43**, S54–S62 (2006).

14. Poisson, J. *et al.* Liver sinusoidal endothelial cells: Physiology and role in liver diseases. *J. Hepatol.* **66**, 212–227 (2017).

15. Tu, Z., Bozorgzadeh, A., Crispe, I. N. & Orloff, M. S. The activation state of human intrahepatic lymphocytes. *Clin. Exp. Immunol.* **149**, 186–93 (2007).

16. Bilzer, M., Roggel, F. & Gerbes, A. L. Role of Kupffer cells in host defense and liver disease. *Liver Int.* **26**, 1175–1186 (2006).

17. Tsuchida, T. & Friedman, S. L. Mechanisms of hepatic stellate cell activation. *Nat. Rev. Gastroenterol. Hepatol.* **14**, 397–411 (2017).

18. Devi, S. S. Structure and Function of Hepatic Parenchymal Cells. in *Comprehensive Toxicology* 10–28 (Elsevier, 2018). doi:10.1016/B978-0-12-801238-3.64335-0

19. Gauldie, J., Lamontagne, L., Horsewood, P. & Jenkins, E.

Immunohistochemical localization of alpha 1-antitrypsin in normal mouse liver and pancreas. *Am. J. Pathol.* **101**, 723–36 (1980).

20. Koenig, S. *et al.* Zonal expression of hepatocytic marker enzymes during liver repopulation. *Histochem. Cell Biol.* **128**, 105–114 (2007).

21. Carpentier, R. *et al.* Embryonic Ductal Plate Cells Give Rise to Cholangiocytes, Periportal Hepatocytes, and Adult Liver Progenitor Cells. *Gastroenterology* **141**, 1432-U902 (2011).

22. Lee, W. M. Drug-Induced Hepatotoxicity. *N. Engl. J. Med.* **349**, 474–485 (2003).

23. Roskams, T. A. *et al.* Nomenclature of the finer branches of the biliary tree: Canals, ductules, and ductular reactions in human livers. *Hepatology* **39**, 1739–1745 (2004).

24. Alpini, G. *et al.* Morphological, molecular, and functional heterogeneity of cholangiocytes from normal rat liver. *Gastroenterology* **110**, 1636–1643 (1996).

25. Marzioni, M. *et al.* Functional heterogeneity of cholangiocytes. *Semin. Liver Dis.* **22**, 227–240 (2002).

26. Benedetti, A., Bassotti, C., Rapino, K., Marucci, L. & Jezequel, A. M. A morphometric study of the epithelium lining the rat intrahepatic biliary tree. *J. Hepatol.* **24**, 335–342 (1996).

27. Tabibian, J. H., Masyuk, A. I., Masyuk, T. V, O'Hara, S. P. & LaRusso, N. F. Physiology of Cholangiocytes. *Compr. Physiol.* **3**, 541–565 (2013).

28. Kanz, M. F. Anatomy and Physiology of the Biliary Epithelium. *Compr. Toxicol. Vol 9 Hepatic Toxicol. 2nd Ed.* 43–108 (2010).

29. Strazzabosco, M. & Fabris, L. Functional anatomy of normal bile ducts. *Anat. Rec. Integr. Anat. Evol. Biol.* **291**, 653–660 (2008).

30. Mancinelli, R. *et al.* After Damage of Large Bile Ducts by Gamma-Aminobutyric Acid, Small Ducts Replenish the Biliary Tree by Amplification of Calcium-Dependent Signaling and de Novo Acquisition of Large Cholangiocyte Phenotypes. *Am. J. Pathol.* **176**, 1790–1800 (2010).

31. LaRusso, N. F. & Masyuk, T. V. The Role of Cilia in the Regulation of Bile Flow. *Dig. Dis.* **29**, 6–12 (2011).

32. Strazzabosco, M. Transport systems in cholangiocytes: Their role in bile formation and cholestasis. *Yale J. Biol. Med.* **70**, 427–434 (1997).

33. Hohenester, S. *et al.* A biliary HCO3- umbrella constitutes a protective mechanism against bile acid-induced injury in human cholangiocytes. *Hepatology* **55**, 173–183 (2012).

34. Xia, X. F., Francis, H., Glaser, S., Alpini, G. & LeSage, G. Bile acid interactions with cholangiocytes. *World J. Gastroenterol.* **12**, 3553–3563 (2006).

35. Marin, J. J. G., Macias, R. I. R., Briz, O., Banales, J. M. & Monte, M. J. Bile Acids in Physiology, Pathology and Pharmacology. *Curr. Drug Metab.* **17**, 4–29 (2016).

36. Wang, B., Zhao, L., Fish, M., Logan, C. Y. & Nusse, R. Self-renewing diploid Axin2+ cells fuel homeostatic renewal of the liver. *Nature* **524**, 180–185 (2015).

37. Carpino, G. *et al.* Biliary tree stem/progenitor cells in glands of extrahepatic and intraheptic bile ducts: an anatomical in situ study yielding evidence of maturational lineages. *J. Anat.* **220**, 186–199 (2012).

38. Cardinale, V. *et al.* The biliary tree—a reservoir of multipotent stem cells. *Nat. Rev. Gastroenterol. Hepatol.* **9**, 231–240 (2012).

39. Okabe, M. *et al.* Potential hepatic stem cells reside in EpCAM(+) cells of normal and injured mouse liver. *Development* **136**, 1951–1960 (2009).

40. Sackett, S. D. *et al.* Foxl1 is a marker of bipotential hepatic progenitor cells in mice. *Hepatology* **49**, 920–929 (2009).

41. Huch, M. *et al.* In vitro expansion of single Lgr5+ liver stem cells induced by Wnt-driven regeneration. *Nature* **494**, 247–50 (2013).

42. Tanaka, M. & Miyajima, A. Identification and Isolation of Adult Liver Stem/Progenitor Cells. in *Methods in molecular biology (Clifton, N.J.)* **826**, 25–32 (2012).

43. Rountree, C. B. *et al.* A CD133-expressing murine liver oval cell population with bilineage potential. *Stem Cells* **25**, 2419–2429 (2007).

44. Cardinale, V. *et al.* The biliary tree—a reservoir of multipotent stem cells. *Nat. Rev. Gastroenterol. Hepatol.* **9**, 231–240 (2012).

45. Sato, K. *et al.* Ductular Reaction in Liver Diseases: Pathological Mechanisms and Translational Significances. *Hepatology* **69**, 420–430 (2019).

46. Lowes, K. N., Brennan, B. A., Yeoh, G. C. & Olynyk, J. K. Oval cell numbers in human chronic liver diseases are directly related to disease severity. *Am. J. Pathol.* **154**, 537–541 (1999).

47. Miyajima, A., Tanaka, M. & Itoh, T. Stem/Progenitor Cells in Liver Development, Homeostasis, Regeneration, and Reprogramming. *Cell Stem Cell* **14**, 561–574 (2014).

48. Davies, R. A., Knight, B., Tian, Y. W., Yeoh, G. C. T. & Olynyk, J. K. Hepatic oval cell response to the choline-deficient, ethionine supplemented model of murine liver injury is attenuated by the administration of a cyclo-oxygenase 2 inhibitor. *Carcinogenesis* **27**, 1607–1616 (2006).

49. Kim, S. *et al.* Streptozotocin-induced diabetes can be reversed by hepatic oval cell activation through hepatic transdifferentiation and pancreatic islet regeneration. *Lab. Investig.* **87**, 702–712 (2007).

50. Zheng, D., Oh, S., Jung, Y. & Petersen, B. E. Oval cell response in 2-acetylaminofluorene/partial hepatectomy rat is attenuated by short interfering RNA targeted to stromal cell-derived factor-1. *Am. J. Pathol.* **169**, 2066–2074 (2006).

51. Petersen, B. E., Zajac, V. F. & Michalopoulos, G. K. Hepatic oval cell activation in response to injury following chemically induced periportal or pericentral damage in rats. *Hepatology* **27**, 1030–1038 (1998).

52. Endo, Y., Zhang, M. J., Yamaji, S. & Cang, Y. Genetic Abolishment of Hepatocyte Proliferation Activates Hepatic Stem Cells. *PLoS One* **7**, 11 (2012).

53. Lu, W.-Y. *et al.* Hepatic progenitor cells of biliary origin with liver repopulation capacity. *Nat. Cell Biol.* **17**, 971-U43 (2015).

54. Tarlow, B. D., Finegold, M. J. & Grompe, M. Clonal tracing of Sox9+ liver progenitors in mouse oval cell injury. *Hepatology* **60**, 278–89 (2014).

55. Rodrigo-Torres, D. *et al.* The biliary epithelium gives rise to liver progenitor cells. *Hepatology* **60**, 1367–1377 (2014).

56. Yanger, K. *et al.* Adult Hepatocytes Are Generated by Self-Duplication Rather than Stem Cell Differentiation. *Cell Stem Cell* **15**, 340–349 (2014).

57. Schaub, J. R., Malato, Y., Gormond, C. & Willenbring, H. Evidence against a Stem Cell Origin of New Hepatocytes in a Common Mouse Model of Chronic Liver Injury. *Cell Rep.* **8**, 933–939 (2014).

58. Raven, A. *et al.* Cholangiocytes act as facultative liver stem cells during impaired hepatocyte regeneration. *Nature* **547**, 350–354 (2017).

59. Hu, H. *et al.* Long-Term Expansion of Functional Mouse and Human Hepatocytes as 3D Organoids. *Cell* **175**, 1591-1606.e19 (2018).

60. Alfirevic, A. & Pirmohamed, M. Genomics of Adverse Drug Reactions. *Trends Pharmacol. Sci.* **38**, 100–109 (2017).

61. Davies, E. C. *et al.* Adverse drug reactions in hospital in-patients: a prospective analysis of 3695 patient-episodes. *PLoS One* **4**, e4439 (2009).

62. Lazarou, J., Pomeranz, B. H. & Corey, P. N. Incidence of Adverse Drug Reactions in Hospitalized Patients. *JAMA* **279**, 1200 (1998).

63. Giardina, C. *et al.* Adverse Drug Reactions in Hospitalized Patients: Results of the FORWARD (Facilitation of Reporting in Hospital Ward) Study. *Front. Pharmacol.* **9**, 350 (2018).

64. Farcas, A. *et al.* Adverse drug reactions detected by stimulated spontaneous reporting in an internal medicine department in Romania. *Eur. J. Intern. Med.* **21**, 453–457 (2010).

65. Hakkarainen, K. M., Hedna, K., Petzold, M. & Hägg, S. Percentage of Patients with Preventable Adverse Drug Reactions and Preventability of Adverse Drug Reactions – A Meta-Analysis. *PLoS One* **7**, e33236 (2012).

66. Bell, L. N. & Chalasani, N. Epidemiology of idiosyncratic drug-induced liver injury. *Semin. Liver Dis.* **29**, 337–47 (2009).

67. Björnsson, E. S., Bergmann, O. M., Björnsson, H. K., Kvaran, R. B. & Olafsson, S. Incidence, Presentation, and Outcomes in Patients With Drug-Induced Liver Injury in the General Population of Iceland. *Gastroenterology* **144**, 1419-1425.e3 (2013).

68. Andrade, R. J. *et al.* Drug-Induced Liver Injury: An Analysis of 461 Incidences Submitted to the Spanish Registry Over a 10-Year Period. *Gastroenterology* **129**, 512–521 (2005).

69. Sgro, C. *et al.* Incidence of drug-induced hepatic injuries: A French population-based study. *Hepatology* **36**, 451–455 (2002).

70. Singanayagam, A. & Bernal, W. Update on acute liver failure. *Curr. Opin. Crit. Care* **21**, 134–141 (2015).

71. Fontana, R. J. *et al.* Idiosyncratic Drug-Induced Liver Injury Is Associated With Substantial Morbidity and Mortality Within 6 Months From Onset. *Gastroenterology* **147**, 96-U189 (2014).

72. Chen, M. J., Suzuki, A., Borlak, J., Andrade, R. J. & Lucena, M. I. Drug-induced liver injury: Interactions between drug properties and host factors. *J. Hepatol.* **63**, 503–514 (2015).

73. Onakpoya, I. J., Heneghan, C. J. & Aronson, J. K. Post-marketing withdrawal of 462 medicinal products because of adverse drug reactions: a systematic review of the world literature. *Bmc Med.* **14**, (2016).

74. Grant, L. M. & Rockey, D. C. Drug-induced liver injury. *Curr. Opin. Gastroenterol.* **28**, 198–202 (2012).

75. Idilman, R. *et al.* The characteristics and clinical outcome of drug-induced liver injury: a single-center experience. *J. Clin. Gastroenterol.* **44**, e128-32 (2010).

76. Petronijevic, M., Ilic, K. & Suzuki, A. Drug induced hepatotoxicity: data from the Serbian pharmacovigilance database. *Pharmacoepidemiol. Drug Saf.* **20**, 416–423 (2011).

77. Suzuki, A. *et al.* Drugs Associated with Hepatotoxicity and their Reporting Frequency of Liver Adverse Events in VigiBase™. *Drug Saf.* **33**, 503–522 (2010).

78. Chalasani, N. *et al.* Features and Outcomes of 899 Patients With Drug-Induced Liver Injury: The DILIN Prospective Study. *Gastroenterology* **148**, 1340-+ (2015).

79. Medina-Caliz, I. *et al.* Herbal and Dietary Supplement-Induced Liver Injuries in the Spanish DILI Registry. *Clin. Gastroenterol. Hepatol.* **16**, 1495–1502 (2018).

80. Chalasani, N. *et al.* Causes, Clinical Features, and Outcomes From a Prospective Study of Drug-Induced Liver Injury in the United States. **135**, 1924–1934 (2008).

81. Fontana, R. J. Pathogenesis of Idiosyncratic Drug-Induced Liver Injury and Clinical Perspectives. *Gastroenterology* **146**, 914-U437 (2014).

82. Roth, R. A. & Ganey, P. E. Intrinsic versus Idiosyncratic Drug-Induced Hepatotoxicity-Two Villains or One? *J. Pharmacol. Exp. Ther.* **332**, 692–697 (2010).

83. Yu, Y.-C. *et al.* CSH guidelines for the diagnosis and treatment of drug-induced liver injury. *Hepatol. Int.* **11**, 221–241 (2017).

84. Aithal, G. P. *et al.* Case Definition and Phenotype Standardization in Drug-Induced Liver Injury. *Clin. Pharmacol. Ther.* **89**, 806–815 (2011).

85. Bjornsson, E. & Olsson, R. Outcome and prognostic markers in severe drug-induced liver disease. *Hepatology* **42**, 481–489 (2005).

86. DE VALLE, M. B., AV KLINTEBERG, V., ALEM, N., OLSSON, R. & BJÖRNSSON, E. Drug-induced liver injury in a Swedish University hospital out-patient hepatology clinic. *Aliment. Pharmacol. Ther.* **24**, 1187–1195 (2006).

87. David, S. & Hamilton, J. P. Drug-induced Liver Injury. *US Gastroenterol. Hepatol. Rev.* **6**, 73–80 (2010).

88. Reau, N. S. & Jensen, D. M. Vanishing Bile Duct Syndrome. *Clin. Liver Dis.* **12**, 203-+ (2008).

89. Parola, M., Cheeseman, K. H., Biocca, M. E., Dianzani, M. U. & Slater, T. F. BIOCHEMICAL-STUDIES ON BILE-DUCT EPITHELIAL-CELLS ISOLATED

FROM RAT-LIVER. *J. Hepatol.* **10**, 341–345 (1990).

90. Liu, X. & Green, R. M. Endoplasmic reticulum stress and liver diseases. *Liver Res.* **3**, 55–64 (2019).

91. Santa Cruz, V., Liu, H., Kaphalia, L. & Kanz, M. F. Effects of methylenedianiline on tight junction permeability of biliary epithelial cells in vivo and in vitro. *Toxicol. Lett.* **169**, 13–25 (2007).

92. Carpenter-Deyo, L., Marchand, D. H., Jean, P. A., Roth, R. A. & Reed, D. J. Involvement of glutathione in 1-naphthylisothiocyanate (ANIT) metabolism and toxicity to isolated hepatocytes. *Biochem. Pharmacol.* **42**, 2171–2180 (1991).

93. Jean, P. A. & Roth, R. A. Naphthylisothiocyanate disposition in bile and its relationship to liver glutathione and toxicity. *Biochem. Pharmacol.* **50**, 1469–1474 (1995).

94. Dietrich, C. G., Ottenhoff, R., de Waart, D. R. & Elferink, R. Role of MRP2 and GSH in intrahepatic cycling of toxins. *Toxicology* **167**, 73–81 (2001).

95. Hill, D. A., Jean, P. A. & Roth, R. A. Bile duct epithelial cells exposed to alpha-naphthylisothiocyanate produce a factor that causes neutrophil-dependent hepatocellular injury in vitro. *Toxicol. Sci.* **47**, 118–25 (1999).

96. Faiola, B., Peterson, R. A., Kimbrough, C. L., Jordan, H. L. & Cullen, J. M. Acute ANIT toxicity in male IL-10 knockout and wild-type mice. *Toxicol. Pathol.* **38**, 745–755 (2010).

97. Kanz, M. F., Wang, A. X. & Campbell, G. A. INFUSION OF BILE FROM METHYLENE DIANILINE-TREATED RATS INTO THE COMMON BILE-DUCT INJURES BILIARY EPITHELIAL-CELLS OF RECIPIENT RATS. *Toxicol. Lett.* **78**, 165–171 (1995).

98. Cruz, V. S., Dugas, T. R. & Kanz, M. F. Mitochondrial dysfunction occurs before transport or tight junction deficits in biliary epithelial cells exposed to bile from methylenedianiline-treated rats. *Toxicol. Sci.* **84**, 129–138 (2005).

99. Chen, K. *et al.* Characterization of biliary conjugates of 4,4 ’-methylenedianiline in male versus female rats. *Toxicol. Appl. Pharmacol.* **232**, 190–202 (2008).

100. Davila, J. C., Reddy, C. G., Davis, P. J. & Acosta, D. Toxicity assessment of paraverine hydrochloride and papaverine-derived metabolites in primary cultures of rat hepatocytes. *Vitr. Cell. Dev. Biol.* **26**, 515–524 (1990).

101. Shi, Q., Yang, X., Greenhaw, J. & Salminen, W. F. Hepatic Cytochrome P450s Attenuate the Cytotoxicity Induced by Leflunomide and Its Active Metabolite A77 1726 in Primary Cultured Rat Hepatocytes. *Toxicol. Sci.* **122**, 579–586 (2011).

102. Jaeschke, H. Acetaminophen: Dose-Dependent Drug Hepatotoxicity and Acute Liver Failure in Patients. *Dig. Dis.* **33**, 464–471 (2015).

103. LeSage, G. D. *et al.* Acute carbon tetrachloride feeding selectively damages large, but not small, cholangiocytes from normal rat liver. *Hepatology* **29**, 307–319 (1999).

104. Lakehal, F. *et al.* Indirect cytotoxicity of flucloxacillin toward human biliary epithelium via metabolite formation in hepatocytes. *Chem. Res. Toxicol.* **14**, 694–701 (2001).

105. Martin, S., Lenz, E. M., Keene, W. & Clench, M. R. Identification of the Reactive

Metabolites of Fenclozic Acid in Bile Duct Cannulated Rats. *Anal. Chem.* **86**, 11281–11289 (2014).

106. Iverson, S. L. & Uetrecht, J. P. Identification of a reactive metabolite of terbinafine: Insights into terbinafine-induced hepatotoxicity. *Chem. Res. Toxicol.* **14**, 175–181 (2001).

107. Atkinson, A. J. *et al.* Biomarkers and surrogate endpoints: Preferred definitions and conceptual framework. *Clin. Pharmacol. Ther.* **69**, 89–95 (2001).

108. Rockey, D. C. *et al.* Causality Assessment in Drug-Induced Liver Injury Using a Structured Expert Opinion Process: Comparison to the Roussel-Uclaf Causality Assessment Method. *Hepatology* **51**, 2117–2126 (2010).

109. Giannini, E. G., Testa, R. & Savarino, V. Liver enzyme alteration: a guide for clinicians. *Can. Med. Assoc. J.* **172**, 367–379 (2005).

110. Padda, M. S., Sanchez, M., Akhtar, A. J. & Boyer, J. L. Drug-Induced Cholestasis. *Hepatology* **53**, 1377–1387 (2011).

111. Bénichou, C. Criteria of drug-induced liver disorders. Report of an international consensus meeting. *J. Hepatol.* **11**, 272–6 (1990).

112. Regev, A. & Bjornsson, E. S. Drug-Induced Liver Injury: Morbidity, Mortality, and Hy's Law. *Gastroenterology* **147**, 20–24 (2014).

113. Nathwani, R. A., Pais, S., Reynolds, T. B. & Kaplowitz, N. Serum alanine aminotransferase in skeletal muscle diseases. *Hepatology* **41**, 380–382 (2005).

114. Thulin, P. *et al.* Keratin-18 and microRNA-122 complement alanine aminotransferase as novel safety biomarkers for drug-induced liver injury in two human cohorts. *Liver Int.* **34**, 367–378 (2014).

115. Sarac, F. & Saygili, F. Causes of high bone alkaline phosphatase. *Biotechnol. Biotechnol. Equip.* **21**, 194–197 (2007).

116. Mukaiyama, K. *et al.* Elevation of serum alkaline phosphatase (ALP) level in postmenopausal women is caused by high bone turnover. *Aging Clin. Exp. Res.* **27**, 413–418 (2015).

117. Church, R. J. & Watkins, P. B. The transformation in biomarker detection and management of drug-induced liver injury. *Liver Int* (2017). doi:10.1111/liv.13441

118. Robles-Diaz, M., Medina-Caliz, I., Stephens, C., Andrade, R. J. & Lucena, M. I. Biomarkers in DILI: One More Step Forward. *Front. Pharmacol.* **7**, (2016).

119. Longo, D. M. *et al.* Refining Liver Safety Risk Assessment: Application of Mechanistic Modeling and Serum Biomarkers to Cimaglermin Alfa (GGF2) Clinical Trials. *Clin Pharmacol Ther* (2017). doi:10.1002/cpt.711

120. Knopp, R. H. *et al.* COMPARATIVE EFFICACY AND SAFETY OF PRAVASTATIN AND CHOLESTYRAMINE ALONE AND COMBINED IN PATIENTS WITH HYPERCHOLESTEROLEMIA. *Arch. Intern. Med.* **153**, 1321–1329 (1993).

121. Dukes, G. E. *et al.* TRANSAMINASE ELEVATIONS IN PATIENTS RECEIVING BOVINE OR PORCINE HEPARIN. *Ann. Intern. Med.* **100**, 646–650 (1984).

122. Church, R. J. & Watkins, P. B. The transformation in biomarker detection and management of drug-induced liver injury. *Liver Int.* **37**, 1582–1590 (2017).

123. Antoine, D. J., Harrill, A. H., Watkins, P. B. & Park, B. K. Safety biomarkers for drug-induced liver injury-current status and future perspectives. *Toxicology Research* **3**, 75–85 (2014).

124. Howell, L. S., Ireland, L., Park, B. K. & Goldring, C. E. MiR-122 and other microRNAs as potential circulating biomarkers of drug-induced liver injury. *Expert Rev. Mol. Diagn.* **18**, 47–54 (2018).

125. Wang, J., Chen, J. & Sen, S. MicroRNA as Biomarkers and Diagnostics. *J. Cell. Physiol.* **231**, 25–30 (2016).

126. Kim, Y. K., Kim, B. & Kim, V. N. Re-evaluation of the roles of DROSHA, Exportin 5, and DICER in microRNA biogenesis. *Proc. Natl. Acad. Sci. U. S. A.* **113**, E1881–E1889 (2016).

127. Huntzinger, E. & Izaurralde, E. Gene silencing by microRNAs: contributions of translational repression and mRNA decay. *Nat. Rev. Genet.* **12**, 99–110 (2011).

128. Cortez, M. A. *et al.* MicroRNAs in body fluids-the mix of hormones and biomarkers. *Nat. Rev. Clin. Oncol.* **8**, 467–477 (2011).

129. Meunier, J. *et al.* Birth and expression evolution of mammalian microRNA genes. *Genome Res.* **23**, 34–45 (2013).

130. Bala, S. *et al.* Circulating microRNAs in exosomes indicate hepatocyte injury and inflammation in alcoholic, drug-induced, and inflammatory liver diseases. *Hepatology* **56**, 1946–1957 (2012).

131. Yamaura, Y. *et al.* Changes in the expression of miRNAs at the pericentral and periportal regions of the rat liver in response to hepatocellular injury: Comparison with the changes in the expression of plasma miRNAs. *Toxicology* **322**, 89–98 (2014).

132. Castro, R. E. *et al.* Identification of microRNAs during rat liver regeneration after partial hepatectomy and modulation by ursodeoxycholic acid. *Am. J. Physiol. Liver Physiol.* **299**, G887–G897 (2010).

133. Chen, X. Y. *et al.* MicroRNA-21 Contributes to Liver Regeneration by Targeting PTEN. *Med. Sci. Monit.* **22**, 83–91 (2016).

134. Bandiera, S., Pfeffer, S., Baumert, T. F. & Zeisel, M. B. miR-122-A key factor and therapeutic target in liver disease. *J. Hepatol.* **62**, 448–457 (2015).

135. Esau, C. *et al.* miR-122 regulation of lipid metabolism revealed by in vivo antisense targeting. *Cell Metab.* **3**, 87–98 (2006).

136. Boix, L., Lopez-Oliva, J. M., Rhodes, A. C. & Bruix, J. Restoring miR122 in human stem-like hepatocarcinoma cells, prompts tumor dormancy through Smad-independent TGF-beta pathway. *Oncotarget* **7**, 71309–71329 (2016).

137. Gatfield, D. *et al.* Integration of microRNA miR-122 in hepatic circadian gene expression. *Genes Dev.* **23**, 1313–1326 (2009).

138. Wang, K. *et al.* Circulating microRNAs, potential biomarkers for drug-induced liver injury. *Proc. Natl. Acad. Sci. U. S. A.* **106**, 4402–4407 (2009).

139. Starkey Lewis, P. J. *et al.* Circulating microRNAs as potential markers of

human drug-induced liver injury. *Hepatology* **54**, 1767–1776 (2011).

140. Tamai, S. *et al.* A monkey model of acetaminophen-induced hepatotoxicity; phenotypic similarity to human. *J. Toxicol. Sci.* **42**, 73–84 (2017).

141. Vliegenthart, A. D. B. *et al.* Retro-Orbital Blood Acquisition Facilitates Circulating microRNA Measurement in Zebrafish with Paracetamol Hepatotoxicity. *Zebrafish* **11**, 219–226 (2014).

142. Lopez-Riera, M. *et al.* New microRNA Biomarkers for Drug-Induced Steatosis and Their Potential to Predict the Contribution of Drugs to Non-alcoholic Fatty Liver Disease. *Front. Pharmacol.* **8**, (2017).

143. Dear, J. W., Antoine, D. J., Starkey-Lewis, P., Goldring, C. E. & Park, B. K. Early detection of paracetamol toxicity using circulating liver microRNA and markers of cell necrosis. *Br. J. Clin. Pharmacol.* **77**, 904–905 (2014).

144. Vliegenthart, A. D. B. *et al.* Comprehensive microRNA profiling in acetaminophen toxicity identifies novel circulating biomarkers for human liver and kidney injury. *Sci. Rep.* **5**, (2015).

145. Coulouarn, C., Factor, V. M., Andersen, J. B., Durkin, M. E. & Thorgeirsson, S. S. Loss of miR-122 expression in liver cancer correlates with suppression of the hepatic phenotype and gain of metastatic properties. *Oncogene* **28**, 3526–3536 (2009).

146. Woolbright, B. L. *et al.* Plasma biomarkers of liver injury and inflammation demonstrate a lack of apoptosis during obstructive cholestasis in mice. *Toxicol. Appl. Pharmacol.* **273**, 524–531 (2013).

147. Farid, W. R. R. *et al.* Hepatocyte-derived microRNAs as serum biomarkers of hepatic injury and rejection after liver transplantation. *Liver Transplant.* **18**, 290–297 (2012).

148. Pirola, C. J. *et al.* Circulating microRNA signature in non-alcoholic fatty liver disease: from serum non-coding RNAs to liver histology and disease pathogenesis. *Gut* **64**, 800–812 (2015).

149. Ward, J. *et al.* Circulating microRNA profiles in human patients with acetaminophen hepatotoxicity or ischemic hepatitis. *Proc. Natl. Acad. Sci. U. S. A.* **111**, 12169–12174 (2014).

150. Krauskopf, J. *et al.* Serum microRNA signatures as 'liquid biopsies' for interrogating hepatotoxic mechanisms and liver pathogenesis in human. *PLoS One* **12**, (2017).

151. Sekine, S., Ogawa, R., McManus, M. T., Kanai, Y. & Hebrok, M. Dicer is required for proper liver zonation. *J. Pathol.* **219**, 365–372 (2009).

152. Lindros, K. O. Zonation of cytochrome P450 expression, drug metabolism and toxicity in liver. *Gen. Pharmacol.* **28**, 191–196 (1997).

153. Yamaura, Y. *et al.* Plasma MicroRNA Profiles in Rat Models of Hepatocellular Injury, Cholestasis, and Steatosis. *PLoS One* **7**, (2012).

154. Church, R. J. *et al.* Beyond miR-122: Identification of MicroRNA Alterations in Blood During a Time Course of Hepatobiliary Injury and Biliary Hyperplasia in Rats. *Toxicol. Sci.* **150**, 3–14 (2016).

155. Oda, S. *et al.* miRNA in Rat Liver Sinusoidal Endothelial Cells and Hepatocytes and Application to Circulating Biomarkers that Discern Pathogenesis of Liver

Injuries. *Am. J. Pathol.* **188**, 916–928 (2018).

156. Badyal, D. K. & Desai, C. Animal use in pharmacology education and research: the changing scenario. *Indian J. Pharmacol.* **46**, 257–65 (2014).

157. Nelson, D. R. *et al.* Comparison of cytochrome P450 (CYP) genes from the mouse and human genomes, including nomenclature recommendations for genes, pseudogenes and alternative-splice variants. *Pharmacogenetics* **14**, 1–18 (2004).

158. Olson, H. *et al.* Concordance of the Toxicity of Pharmaceuticals in Humans and in Animals. *Regul. Toxicol. Pharmacol.* **32**, 56–67 (2000).

159. Schiano, T., Dolehide, K., Hart, J. & Baker, A. L. Severe but reversible hepatitis induced by troglitazone. *Dig. Dis. Sci.* **45**, 1039–42 (2000).

160. Singer, J. B. *et al.* A genome-wide study identifies HLA alleles associated with lumiracoxib-related liver injury. *Nat. Genet.* **42**, 711–714 (2010).

161. Fontana, R. J. *et al. Acute Liver Failure Associated With Prolonged Use of Bromfenac Leading to Liver Transplantation*. (1999).

162. Foster, A. J. *et al.* Integrated in vitro models for hepatic safety and metabolism: evaluation of a human Liver-Chip and liver spheroid. *Arch. Toxicol.* **93**, 1021–1037 (2019).

163. Soldatow, V. Y., Lecluyse, E. L., Griffith, L. G. & Rusyn, I. In vitro models for liver toxicity testing. *Toxicol. Res. (Camb).* **2**, 23–39 (2013).

164. Guguen-Guillouzo, C. & Guillouzo, A. General Review on In Vitro Hepatocyte Models and Their Applications. in *Methods in molecular biology (Clifton, N.J.)* **640**, 1–40 (2010).

165. Kitamura, H. & Motohashi, H. NRF2 addiction in cancer cells. *Cancer Sci.* **109**, 900–911 (2018).

166. Guo, L. *et al.* Similarities and differences in the expression of drug-metabolizing enzymes between human hepatic cell lines and primary human hepatocytes. *Drug Metab. Dispos.* **39**, 528–38 (2011).

167. Rambhatla, L., Chiu, C.-P., Kundu, P., Peng, Y. & Carpenter, M. K. Generation of Hepatocyte-Like Cells from Human Embryonic Stem Cells. *Cell Transplant.* **12**, 1–11 (2003).

168. Liu, H., Ye, Z., Kim, Y., Sharkis, S. & Jang, Y.-Y. Generation of endoderm-derived human induced pluripotent stem cells from primary hepatocytes. *Hepatology* **51**, 1810–1819 (2010).

169. Du, Y. *et al.* Human Hepatocytes with Drug Metabolic Function Induced from Fibroblasts by Lineage Reprogramming. *Cell Stem Cell* **14**, 394–403 (2014).

170. Sirenko, O., Hesley, J., Rusyn, I. & Cromwell, E. F. High-Content Assays for Hepatotoxicity Using Induced Pluripotent Stem Cell–Derived Cells. *Assay Drug Dev. Technol.* **12**, 43 (2014).

171. Schwartz, R. E., Bram, Y. & Frankel, A. Pluripotent Stem Cell-Derived Hepatocyte-like Cells: A Tool to Study Infectious Disease. *Curr. Pathobiol. Rep.* **4**, 147–156 (2016).

172. Taylor, C. J., Peacock, S., Chaudhry, A. N., Bradley, J. A. & Bolton, E. M. Generating an iPSC Bank for HLA-Matched Tissue Transplantation Based on

Known Donor and Recipient HLA Types. *Cell Stem Cell* **11**, 147–152 (2012).

173. Turinetto, V., Orlando, L. & Giachino, C. Induced Pluripotent Stem Cells: Advances in the Quest for Genetic Stability during Reprogramming Process. *Int. J. Mol. Sci.* **18**, 1952 (2017).

174. Method of the Year 2017: Organoids. *Nat. Methods 2018 151* **15**, 1 (2018).

175. Clevers, H. Modeling Development and Disease with Organoids. *Cell* **165**, 1586–1597 (2016).

176. Li, B. *et al.* Adult Mouse Liver Contains Two Distinct Populations of Cholangiocytes. *Stem Cell Reports* **9**, 478–489 (2017).

177. Dorrell, C. *et al.* The organoid-initiating cells in mouse pancreas and liver are phenotypically and functionally similar. *Stem Cell Res.* **13**, 275–283 (2014).

178. Huch, M. *et al.* In vitro expansion of single Lgr5+ liver stem cells induced by Wnt-driven regeneration. *Nature* **494**, 247–250 (2013).

179. Huch, M. *et al.* Long-term culture of genome-stable bipotent stem cells from adult human liver. *Cell* **160**, 299–312 (2015).

180. Broutier, L. *et al.* Culture and establishment of self-renewing human and mouse adult liver and pancreas 3D organoids and their genetic manipulation. *Nat. Protoc.* **11**, 1724–1743 (2016).

181. Nantasanti, S. *et al.* Disease Modeling and Gene Therapy of Copper Storage Disease in Canine Hepatic Organoids. *Stem Cell Reports* **5**, 895–907 (2015).

182. Sanz-Rubio, D. *et al.* Stability of Circulating Exosomal miRNAs in Healthy Subjects. *Sci. Rep.* **8**, 10306 (2018).

183. Warnefors, M., Liechti, A., Halbert, J., Valloton, D. & Kaessmann, H. Conserved microRNA editing in mammalian evolution, development and disease. *Genome Biol.* **15**, R83 (2014).

184. Jopling, C. Liver-specific microRNA-122: Biogenesis and function. *RNA Biol.* **9**, 137–42 (2012).

185. Ishii, M., Vroman, B. & LaRusso, N. F. Isolation and morphologic characterization of bile duct epithelial cells from normal rat liver. *Gastroenterology* **97**, 1236–47 (1989).

186. Li, W.-C., Ralphs, K. L. & Tosh, D. Isolation and Culture of Adult Mouse Hepatocytes. in *Mouse Cell Culture: Methods and Protocols* (eds. Ward, A. & Tosh, D.) 185–196 (Humana Press, 2010). doi:10.1007/978-1-59745-019-5_13

187. López-Romero, P. Pre-processing and differential expression analysis of Agilent microRNA arrays using the AgiMicroRna Bioconductor library. *BMC Genomics* **12**, 64 (2011).

188. Meng, J. *et al.* MicroRNA-196a/b Mitigate Renal Fibrosis by Targeting TGF- *β* Receptor 2. *J. Am. Soc. Nephrol.* **27**, 3006–3021 (2016).

189. Schmittgen, T. D. & Livak, K. J. Analyzing real-time PCR data by the comparative C(T) method. *Nat. Protoc.* **3**, 1101–8 (2008).

190. Kozomara, A., Birgaoanu, M. & Griffiths-Jones, S. miRBase: from microRNA sequences to function. *Nucleic Acids Res.* **47**, D155–D162 (2019).

191. Cho, Y.-E., Kim, S.-H., Lee, B.-H. & Baek, M.-C. Circulating Plasma and Exosomal microRNAs as Indicators of Drug-Induced Organ Injury in Rodent Models. *Biomol. Ther. (Seoul).* **25**, 367–373 (2017).

192. Shifeng, H. *et al.* Circulating Liver-Specific miR-122 as a Novel Potential Biomarker for Diagnosis of Cholestatic Liver Injury. *PLoS One* **8**, e73133 (2013).

193. Heslop, J. A. *et al.* Mechanistic evaluation of primary human hepatocyte culture using global proteomic analysis reveals a selective dedifferentiation profile. *Arch. Toxicol.* **91**, 439–452 (2017).

194. Ogese, M. O. *et al.* Characterization of Drug-Specific Signaling Between Primary Human Hepatocytes and Immune Cells. *Toxicol. Sci.* **158**, 76–89 (2017).

195. Gordillo, M., Evans, T. & Gouon-Evans, V. Orchestrating liver development. *Development* **142**, 2094–2108 (2015).

196. Franchitto, A. *et al.* Recent advances on the mechanisms regulating cholangiocyte proliferation and the significance of the neuroendocrine regulation of cholangiocyte pathophysiology. *Ann. Transl. Med.* **1**, 27 (2013).

197. Chang, J. *et al.* miR-122, a mammalian liver-specific microRNA, is processed from hcr mRNA and may downregulate the high affinity cationic amino acid transporter CAT-1. *RNA Biol.* **1**, 106–13 (2004).

198. Hou, J. *et al.* Identification of miRNomes in Human Liver and Hepatocellular Carcinoma Reveals miR-199a/b-3p as Therapeutic Target for Hepatocellular Carcinoma. *Cancer Cell* **19**, 232–243 (2011).

199. Gao, Y., Zhang, S.-G., Wang, Z.-H. & Liao, J.-C. Down-regulation of miR-342-3p in hepatocellular carcinoma tissues and its prognostic significance. *Eur. Rev. Med. Pharmacol. Sci.* **21**, 2098–2102 (2017).

200. KATSURA, A. *et al.* MicroRNA profiles following metformin treatment in a mouse model of non-alcoholic steatohepatitis. *Int. J. Mol. Med.* **35**, 877–884 (2015).

201. Karakatsanis, A. *et al.* Expression of microRNAs, miR-21, miR-31, miR-122, miR-145, miR-146a, miR-200c, miR-221, miR-222, and miR-223 in patients with hepatocellular carcinoma or intrahepatic cholangiocarcinoma and its prognostic significance. *Mol. Carcinog.* **52**, 297–303 (2013).

202. Tan, Y. *et al.* Serum MicroRNAs as Potential Biomarkers of Primary Biliary Cirrhosis. *PLoS One* **9**, (2014).

203. Kim, J., Ryu, J. K., Lee, S. H. & Kim, Y.-T. MicroRNA 141 Expression Is a Potential Prognostic Marker of Biliary Tract Cancers. *Gut Liver* **10**, 836–41 (2016).

204. Meng, F. *et al.* Involvement of Human Micro-RNA in Growth and Response to Chemotherapy in Human Cholangiocarcinoma Cell Lines. *Gastroenterology* **130**, 2113–2129 (2006).

205. Zou, Y. *et al.* MicroRNA-146a-5p attenuates liver fibrosis by suppressing profibrogenic effects of TGFβ1 and lipopolysaccharide. *Cell. Signal.* **39**, 1–8 (2017).

206. Du, J. *et al.* MiR-146a-5p suppresses activation and proliferation of hepatic

stellate cells in nonalcoholic fibrosing steatohepatitis through directly targeting Wnt1 and Wnt5a. *Sci. Rep.* **5**, 16163 (2015).

207. McNally, M. E. *et al.* Concomitant dysregulation of microRNAs miR-151-3p and miR-126 correlates with improved survival in resected cholangiocarcinoma. *HPB* **15**, 260–264 (2013).

208. Hai-Ying Liu, Yi-Hao Chen, Shu-Yin Pang, Feng-Hua Wang, Xiao-Fang Peng, Li-Yuan Yang, Z.-R. C. & Yi Chen, B. Z. MiR-200a/ZEB1 Pathway in Liver Fibrogenesis of Biliary Atresia. *Int. J. Med. Heal. Sci.* **11**, (2017).

209. Zahm, A. M., Hand, N. J., Boateng, L. A. & Friedman, J. R. Circulating microRNA is a biomarker of biliary atresia. *J. Pediatr. Gastroenterol. Nutr.* **55**, 366–9 (2012).

210. Fuentes, N., Roy, A., Mishra, V., Cabello, N. & Silveyra, P. Sex-specific microRNA expression networks in an acute mouse model of ozone-induced lung inflammation. *Biol. Sex Differ.* **9**, 18 (2018).

211. Björnsson, E. & Olsson, R. Outcome and prognostic markers in severe drug-induced liver disease. *Hepatology* **42**, 481–489 (2005).

212. Visentin, M., Lenggenhager, D., Gai, Z. & Kullak-Ublick, G. A. Drug-induced bile duct injury. *Biochim. Biophys. Acta - Mol. Basis Dis.* **1864**, 1498–1506 (2018).

213. Danan, G. & Teschke, R. RUCAM in Drug and Herb Induced Liver Injury: The Update. *Int. J. Mol. Sci.* **17**, (2015).

214. Kullak-Ublick, G. A. *et al.* Drug-induced liver injury: recent advances in diagnosis and risk assessment. *Gut* **66**, 1154–1164 (2017).

215. Alvaro, D. *et al.* The function of alkaline phosphatase in the liver: Regulation of intrahepatic biliary epithelium secretory activities in the rat. *Hepatology* **32**, 174–184 (2000).

216. Poupon, R. Liver alkaline phosphatase: A missing link between choleresis and biliary inflammation. *Hepatology* **61**, 2080–2090 (2015).

217. Sotil, E. U. & Jensen, D. M. Serum enzymes associated with cholestasis. *Clin. Liver Dis.* **8**, 41–54 (2004).

218. Iguchi, T., Sakurai, K., Tamai, S. & Mori, K. Circulating liver-specific microRNAs in cynomolgus monkeys. *J. Toxicol. Pathol.* **31**, 3–13 (2018).

219. deLemos, A. S. *et al.* Amoxicillin–Clavulanate-Induced Liver Injury. *Dig. Dis. Sci.* **61**, 2406–2416 (2016).

220. Hara, O. Cholangiocytes and the environment in primary sclerosing cholangitis: where is the link? *Gut Mon.* **0**, (2017).

221. Zaccara, G., Franciotta, D. & Perucca, E. Idiosyncratic adverse reactions to antiepileptic drugs. *Epilepsia* **48**, 1223–1244 (2007).

222. Ju, C. & Reilly, T. Role of immune reactions in drug-induced liver injury (DILI). *Drug Metab. Rev.* **44**, 107–115 (2012).

223. Uetrecht, J. & Naisbitt, D. J. Idiosyncratic Adverse Drug Reactions: Current Concepts. *Pharmacol. Rev.* **65**, 779–808 (2013).

224. Mariotti, V., Strazzabosco, M., Fabris, L. & Calvisi, D. F. Animal models of

biliary injury and altered bile acid metabolism. *Biochim. Biophys. acta. Mol. basis Dis.* **1864**, 1254–1261 (2018).

225. Connolly, A. K., Price, S. C., Connelly, J. C. & Hinton, R. H. Early changes in bile duct lining cells and hepatocytes in rats treated with α-naphthylisothiocyanate. *Toxicol. Appl. Pharmacol.* **93**, 208–219 (1988).

226. Kanz, M. F., Dugas, T. R., Liu, H. & Santa Cruz, V. Glutathione Depletion Exacerbates Methylenedianiline Toxicity to Biliary Epithelial Cells and Hepatocytes in Rats. *Toxicol. Sci.* **74**, 447–456 (2003).

227. Calcamuggi, G., Lanzio, M., Dughera, L., Babini, G. & Emanuelli, G. Endotoxin tolerance and polymyxin B modify liver damage and cholestasis induced by a single dose of α-naphthylisothiocyanate in the rat. *Arch. Toxicol.* **66**, 126–130 (1992).

228. Bothe, M. K. *et al.* Characterization of a rat model of moderate liver dysfunction based on alpha-naphthylisothiocyanate-induced cholestasis. *J. Toxicol. Sci.* **42**, 715–721 (2017).

229. Yu, L. *et al.* SRT1720 Alleviates ANIT-Induced Cholestasis in a Mouse Model. *Front. Pharmacol.* **8**, 256 (2017).

230. Tanimizu, N., Ichinohe, N. & Mitaka, T. Intrahepatic bile ducts guide establishment of the intrahepatic nerve network in developing and regenerating mouse liver. *Development* **145**, dev159095 (2018).

231. Tanaka, Y., Aleksunes, L. M., Cui, Y. J. & Klaassen, C. D. ANIT-Induced Intrahepatic Cholestasis Alters Hepatobiliary Transporter Expression via Nrf2-Dependent and Independent Signaling. *Toxicol. Sci.* **108**, 247–257 (2009).

232. Kwon, S.-B. *et al.* Time- and Dose-based Gene Expression Profiles Produced by a Bile-duct–damaging Chemical, 4,4′-methylene Dianiline, in Mouse Liver in an Acute Phase. *Toxicol. Pathol.* **36**, 660–673 (2008).

233. Kossor, D. C. *et al.* Biliary epithelial cell proliferation following alpha-naphthylisothiocyanate (ANIT) treatment: relationship to bile duct obstruction. *Fundam. Appl. Toxicol.* **26**, 51–62 (1995).

234. Yang, Q. *et al.* Sweroside ameliorates α-naphthylisothiocyanate-induced cholestatic liver injury in mice by regulating bile acids and suppressing pro-inflammatory responses. *Acta Pharmacol. Sin.* **37**, 1218–1228 (2016).

235. Kast, A. & Nishikawa, J. The effect of fasting on oral acute toxicity of drugs in rats and mice. *Lab. Anim.* **15**, 359–364 (1981).

236. Gad, S. C. Rodents model for toxicity testing and biomarkers. *Biomarkers Toxicol.* 7–69 (2014). doi:10.1016/B978-0-12-404630-6.00002-6

237. Clarke, J. I. *et al.* Circulating levels of miR-122 increase post-mortem, particularly following lethal dosing with pentobarbital sodium: implications for pre-clinical liver injury studies. *Toxicol. Res. (Camb).* **6**, 406–411 (2017).

238. Dear FRCP, J. W. *et al.* Risk stratification after paracetamol overdose using mechanistic biomarkers: results from two prospective cohort studies. *Artic. Lancet Gastroenterol Hepatol* **3**, 104–117 (2018).

239. Yang, F. *et al.* Curcumin protects ANIT-induced cholestasis through signaling pathway of FXR-regulated bile acid and inflammation. *Sci. Rep.* **6**, 33052 (2016).

240. Cullen, J. M. *et al.* Time Course Gene Expression Using Laser Capture Microscopy-Extracted Bile Ducts, but Not Hepatic Parenchyma, Reveals Acute Alpha-Naphthylisothiocyanate Toxicity. *Toxicol. Pathol.* **38**, 715–729 (2010).

241. Cullen, J. M. *et al.* Acute Alpha-Naphthylisothiocyanate-induced Liver Toxicity in Germfree and Conventional Male Rats. doi:10.1177/0192623316662360

242. Starckx, S. *et al.* Evaluation of miR-122 and Other Biomarkers in Distinct Acute Liver Injury in Rats. doi:10.1177/0192623312464436

243. Harrill, A. H. *et al.* Mouse population-guided resequencing reveals that variants in CD44 contribute to acetaminophen-induced liver injury in humans. *Genome Res.* **19**, 1507 (2009).

244. Sokolović, M. *et al.* The transcriptomic signature of fasting murine liver. *BMC Genomics* **9**, 528 (2008).

245. Tran, M., Lee, S.-M., Shin, D.-J. & Wang, L. Loss of miR-141/200c ameliorates hepatic steatosis and inflammation by reprogramming multiple signaling pathways in NASH. *JCI Insight* **2**, (2017).

246. Senfter, D., Madlener, S., Krupitza, G. & Mader, R. M. The microRNA-200 family: still much to discover. *Biomol. Concepts* **7**, (2016).

247. Sharapova, T. *et al.* Pharmaceutical Pathobiology-Original Article. doi:10.1177/0300985815591076

248. Murakami, Y. *et al.* The Progression of Liver Fibrosis Is Related with Overexpression of the miR-199 and 200 Families. doi:10.1371/journal.pone.0016081

249. Meltzer, S. *et al.* Circulating Exosomal miR-141-3p and miR-375 in Metastatic Progression of Rectal Cancer. *Transl. Oncol.* **12**, 1038–1044 (2019).

250. Kagawa, T., Shirai, Y., Oda, S. & Yokoi, T. Identification of Specific MicroRNA Biomarkers in Early Stages of Hepatocellular Injury, Cholestasis, and Steatosis in Rats. *Toxicol. Sci.* **166**, 228–239 (2018).

251. Nakamura, T. *et al.* Protective Effect of Brazilian Propolis against Liver Damage with Cholestasis in Rats Treated with α-Naphthylisothiocyanate. *Evid. Based. Complement. Alternat. Med.* **2013**, 302720 (2013).

252. Hughes, J. D. *et al.* Physiochemical drug properties associated with in vivo toxicological outcomes. *Bioorg. Med. Chem. Lett.* **18**, 4872–5 (2008).

253. Dashiell, O. L. & Kennedy, G. L. The effects of fasting on the acute oral toxicity of nine chemicals in the rat. *J. Appl. Toxicol.* **4**, 320–325 (1984).

254. Fickert, P. *et al.* A new xenobiotic-induced mouse model of sclerosing cholangitis and biliary fibrosis. *Am. J. Pathol.* **171**, 525–536 (2007).

255. López-Riera, M., Conde, I., Castell, J. V & Jover, R. A Novel MicroRNA Signature for Cholestatic Drugs in Human Hepatocytes and Its Translation into Novel Circulating Biomarkers for Drug-Induced Liver Injury Patients. *Toxicol. Sci.* (2019). doi:10.1093/toxsci/kfz138

256. Hall, P. & Cash, J. What is the real function of the liver 'function' tests? *Ulster Med. J.* **81**, 30–6 (2012).

257. Weaver, R. J. *et al.* Test systems in drug discovery for hazard identification and risk assessment of human drug-induced liver injury. *Expert Opin. Drug*

Metab. Toxicol. **13**, 767–782 (2017).

258. Hughes, P., Marshall, D., Reid, Y., Parkes, H. & Gelber, C. The costs of using unauthenticated, over-passaged cell lines: how much more data do we need? *Biotechniques* **43**, 575–586 (2007).

259. Gerets, H. H. J. *et al.* Characterization of primary human hepatocytes, HepG2 cells, and HepaRG cells at the mRNA level and CYP activity in response to inducers and their predictivity for the detection of human hepatotoxins. *Cell Biol. Toxicol.* **28**, 69–87 (2012).

260. Rogue, A., Lambert, C., Spire, C., Claude, N. & Guillouzo, A. Interindividual Variability in Gene Expression Profiles in Human Hepatocytes and Comparison with HepaRG Cells. *Drug Metab. Dispos.* **40**, 151–158 (2012).

261. Choi, J. M. *et al.* HepG2 cells as an in vitro model for evaluation of cytochrome P450 induction by xenobiotics. *Arch. Pharm. Res.* **38**, 691–704 (2015).

262. Shibata, T. *et al.* Cancer related mutations in NRF2 impair its recognition by Keap1-Cul3 E3 ligase and promote malignancy. *Proc. Natl. Acad. Sci.* **105**, 13568–13573 (2008).

263. Ishii, T. & Mann, G. E. Redox status in mammalian cells and stem cells during culture in vitro: Critical roles of Nrf2 and cystine transporter activity in the maintenance of redox balance. *Redox Biol.* **2**, 786–794 (2014).

264. Wang, Y., Wang, L., Guo, Y., Zhu, Y. & Qin, J. Engineering stem cell-derived 3D brain organoids in a perfusable organ-on-a-chip system. *RSC Adv.* **8**, 1677–1685 (2018).

265. Kim, Y. K., Nam, S. A. & Yang, C. W. Applications of kidney organoids derived from human pluripotent stem cells. *Korean J. Intern. Med.* **33**, 649–659 (2018).

266. Miller, A. J. *et al.* Generation of lung organoids from human pluripotent stem cells in vitro. *Nat. Protoc.* **14**, 518–540 (2019).

267. Moreira, L. *et al.* Pancreas 3D Organoids: Current and Future Aspects as a Research Platform for Personalized Medicine in Pancreatic Cancer. *Cell. Mol. Gastroenterol. Hepatol.* **5**, 289 (2018).

268. Mahe, M. M. *et al.* Establishment of Gastrointestinal Epithelial Organoids. *Curr. Protoc. Mouse Biol.* **3**, 217–40 (2013).

269. Boj, S. F. *et al.* Organoid Models of Human and Mouse Ductal Pancreatic Cancer. *Cell* **160**, 324–338 (2015).

270. Xu, H. *et al.* Organoid technology in disease modelling, drug development, personalized treatment and regeneration medicine. *Exp. Hematol. Oncol.* **7**, 30 (2018).

271. Huang, D. W., Sherman, B. T. & Lempicki, R. A. Bioinformatics enrichment tools: paths toward the comprehensive functional analysis of large gene lists. *Nucleic Acids Res.* **37**, 1–13 (2009).

272. Huang, D. W., Sherman, B. T. & Lempicki, R. A. Systematic and integrative analysis of large gene lists using DAVID bioinformatics resources. *Nat. Protoc.* **4**, 44–57 (2009).

273. Lorent, K. *et al.* Inhibition of Jagged-mediated Notch signaling disrupts zebrafish biliary development and generates multi-organ defects compatible with an Alagille syndrome phenocopy. *Development* **131**, 5753–5766 (2004).

274. Lu, C. & Li, A. P. Species comparison in P450 induction: effects of dexamethasone, omeprazole, and rifampin on P450 isoforms 1A and 3A in primary cultured hepatocytes from man, Sprague-Dawley rat, minipig, and beagle dog. *Chem. Biol. Interact.* **134**, 271–81 (2001).

275. Hayes, J. D. & Dinkova-Kostova, A. T. The Nrf2 regulatory network provides an interface between redox and intermediary metabolism. *Trends Biochem. Sci.* **39**, 199–218 (2014).

276. Church, R. J. *et al.* Candidate biomarkers for the diagnosis and prognosis of drug-induced liver injury: An international collaborative effort. *Hepatology* **69**, 760–773 (2019).

277. Levy, G. *et al.* Long-term culture and expansion of primary human hepatocytes. *Nat. Biotechnol.* **33**, 1264–1271 (2015).

278. Peng, W. C. *et al.* Inflammatory Cytokine TNFα Promotes the Long-Term Expansion of Primary Hepatocytes in 3D Culture. *Cell* **175**, 1607-1619.e15 (2018).

279. HE, Y. *et al.* Comparison of proliferation and differentiation potential between mouse primary hepatocytes and embryonic hepatic progenitor cells in vitro. *Int. J. Mol. Med.* **32**, 476–484 (2013).

280. Burden, N., Chapman, K., Sewell, F. & Robinson, V. Pioneering better science through the 3Rs: an introduction to the national centre for the replacement, refinement, and reduction of animals in research (NC3Rs). *J. Am. Assoc. Lab. Anim. Sci.* **54**, 198–208 (2015).

281. Stéphenne, X., Najimi, M. & Sokal, E. M. Hepatocyte cryopreservation: is it time to change the strategy? *World J. Gastroenterol.* **16**, 1–14 (2010).

282. Li, J. *et al.* Human hepatic progenitor cells express hematopoietic cell markers CD45 and CD109. *Int. J. Med. Sci.* **11**, 65–79 (2014).

283. Zanger, U. M., Turpeinen, M., Klein, K. & Schwab, M. Functional pharmacogenetics/genomics of human cytochromes P450 involved in drug biotransformation. *Anal. Bioanal. Chem.* **392**, 1093–1108 (2008).

284. Arellano, C., Philibert, C., Vachoux, C., Woodley, J. & Houin, G. The metabolism of midazolam and comparison with other CYP enzyme substrates during intestinal absorption: in vitro studies with rat everted gut sacs. *J. Pharm. Pharm. Sci.* **10**, 26–36 (2007).

285. Majumdar, A. K. *et al.* Effects of aprepitant on cytochrome P450 3A4 activity using midazolam as a probe. *Clin. Pharmacol. Ther.* **74**, 150–6 (2003).

286. Matoulková, P., Pávek, P., Malý, J. & Vlček, J. Cytochrome P450 enzyme regulation by glucocorticoids and consequences in terms of drug interaction. *Expert Opin. Drug Metab. Toxicol.* **10**, 425–435 (2014).

287. Down, M. J., Arkle, S. & Mills, J. J. Regulation and induction of CYP3A11, CYP3A13 and CYP3A25 in C57BL/6J mouse liver. *Arch. Biochem. Biophys.* **457**, 105–110 (2007).

288. WANDEL, C. *et al.* Midazolam is metabolized by at least three different cytochrome P450 enzymes. *Br. J. Anaesth.* **73**, 658–661 (1994).

289. van Waterschoot, R. A. B. *et al.* Midazolam Metabolism in Cytochrome P450 3A Knockout Mice Can Be Attributed to Up-Regulated CYP2C Enzymes. *Mol.*

Pharmacol. **73**, 1029–1036 (2007).

290. Saarikoski, S. T., Rivera, S. P. & Hankinson, O. CYP2S1: A short review. *Toxicol. Appl. Pharmacol.* **207**, 62–69 (2005).

291. Wilkening, S., Stahl, F. & Bader, A. COMPARISON OF PRIMARY HUMAN HEPATOCYTES AND HEPATOMA CELL LINE HEPG2 WITH REGARD TO THEIR BIOTRANSFORMATION PROPERTIES. *Drug Metab. Dispos.* **31**, 1035–1042 (2003).

292. Poloznikov, A. *et al.* In vitro and in silico liver models: Current trends, challenges and opportunities 1. *ALTEX* (2018). doi:10.14573/altex.1803221

293. Marion, M.-J., Hantz, O. & Durantel, D. The HepaRG Cell Line: Biological Properties and Relevance as a Tool for Cell Biology, Drug Metabolism, and Virology Studies. in *Methods in molecular biology (Clifton, N.J.)* **640**, 261–272 (2010).

294. Bellanti, F. *et al.* Nuclear factor (erythroid-derived-2)-like 2 (Nrf2) signalling is involved in transdifferentiation of hepatocyte-like cells. *Free Radic. Biol. Med.* **108**, S85 (2017).

295. Ekhart, C. *et al.* Polymorphisms of drug-metabolizing enzymes (GST, CYP2B6 and CYP3A) affect the pharmacokinetics of thiotepa and tepa. *Br. J. Clin. Pharmacol.* **67**, 50–60 (2009).

296. Vinken, M. In vitro prediction of drug-induced cholestatic liver injury: a challenge for the toxicologist. *Arch. Toxicol.* **92**, 1909–1912 (2018).

297. Tsai, S. *et al.* Development of primary human pancreatic cancer organoids, matched stromal and immune cells and 3D tumor microenvironment models. *BMC Cancer* **18**, 335 (2018).

298. Zhou, T. *et al.* Direct and indirect coculture of mouse hepatic progenitor cells with mouse embryonic fibroblasts for the generation of hepatocytes and cholangiocytes. *Cytotechnology* **71**, 267–275 (2019).

299. Sison-Young, R. L. C. *et al.* Comparative Proteomic Characterization of 4 Human Liver-Derived Single Cell Culture Models Reveals Significant Variation in the Capacity for Drug Disposition, Bioactivation, and Detoxication. *Toxicol. Sci.* **147**, 412–24 (2015).

300. Marroquin, L. D., Hynes, J., Dykens, J. A., Jamieson, J. D. & Will, Y. Circumventing the crabtree effect: Replacing media glucose with galactose increases susceptibility of HepG2 cells to mitochondrial toxicants. *Toxicol. Sci.* **97**, 539–547 (2007).

301. Kuna, L. *et al.* Models of Drug Induced Liver Injury (DILI) – Current Issues and Future Perspectives. *Curr. Drug Metab.* **19**, 830–838 (2018).

302. Jensen, T., Kiersgaard, M., Sørensen, D. & Mikkelsen, L. Fasting of mice: a review. *Lab. Anim.* **47**, 225–240 (2013).

303. Ramos, A. M. O. *et al.* Reversible vanishing bile duct syndrome induced by carbamazepine. *Eur. J. Gastroenterol. Hepatol.* **14**, 1019–22 (2002).

304. Lok, A. S. & Ng, I. O. Prochlorperazine-induced chronic cholestasis. *J. Hepatol.* **6**, 369–73 (1988).

305. Richardet, J. P. *et al.* Prolonged cholestasis with ductopenia after administration of amoxicillin/clavulanic acid. *Dig. Dis. Sci.* **44**, 1997–2000

(1999).

306. Moradpour, D. *et al.* Chlorpromazine-induced vanishing bile duct syndrome leading to biliary cirrhosis. *Hepatology* **20**, 1437–1441 (1994).

307. Masè, M. *et al.* Selection of reference genes is critical for miRNA expression analysis in human cardiac tissue. A focus on atrial fibrillation. *Sci. Rep.* **7**, 41127 (2017).

308. Yang, X. *et al.* Potential of extracellular microRNAs as biomarkers of acetaminophen toxicity in children. *Toxicol. Appl. Pharmacol.* **284**, 180–187 (2015).

309. Pinkerton, M. *et al.* Differential expression of microRNAs in exhaled breath condensates of patients with asthma, patients with chronic obstructive pulmonary disease, and healthy adults. *J. Allergy Clin. Immunol.* **132**, 217-219.e2 (2013).

310. Vliegenthart, A. D., Berends, C., Potter, C. M., Kersaudy-Kerhoas, M. & Dear, J. W. MicroRNA-122 can be measured in capillary blood which facilitates point-of-care testing for drug-induced liver injury. *Br J Clin Pharmacol* (2017). doi:10.1111/bcp.13282

311. An, Y. *et al.* Novel serum microRNAs panel on the diagnostic and prognostic implications of hepatocellular carcinoma. *World J. Gastroenterol.* **24**, 2596–2604 (2018).

312. Messner, C. J., Mauch, L. & Suter-Dick, L. Bile salts regulate CYP7A1 expression and elicit a fibrotic response and abnormal lipid production in 3D liver microtissues. *Toxicol. Vitr.* **60**, 261–271 (2019).

313. Schwarzenbach, H., da Silva, A. M., Calin, G. & Pantel, K. Data Normalization Strategies for MicroRNA Quantification. *Clin. Chem.* **61**, 1333–42 (2015).

314. Holman, N. S., Mosedale, M., Wolf, K. K., LeCluyse, E. L. & Watkins, P. B. Subtoxic Alterations in Hepatocyte-Derived Exosomes: An Early Step in Drug-Induced Liver Injury? *Toxicol. Sci.* **151**, 365–375 (2016).